

WJ-25 DESIGN PRPOSAL

Proposal for the next generation of Single-Engine Turboprop aircraft

In Response to AIAA 2016-2017 Undergraduate Team Design Competition Request for Proposal

Team Leader: Zhang Yingao

Team Member: Wen Mengyang & Wang Haonan

Faculty Advisor: Dr. Chih-Jen Sung

SIGNATURE PAGE

Design Team:

Zhang Yingao: 张英傲
#762521 ZHANG Yingao

Wen Mengyang: 温孟阳
#774336 WEN Mengyang

Wang Haonan: 王浩楠
#774661 WANG Haonan

Acknowledgements

*The authors would like to thank the following individuals who were instrumental
in the success of this engine design:*

Dr. Chih-Jen Sung for his tremendous help in completing this proposal.

Dr. Xin Hui for his comprehensive support and supervision

Dr. Xi Wang for his advice on off-design and transient performance

Our colleague Wang Xinyao for his assistance on combustion system design

Our senior Yang Shubo for his instructions on MATLAB

All the teachers, students and facilities who have aided.

WJ-25 Design Proposal

Proposal for The Next Generation of Single-Engine Turbo-prop Aircraft

Abstract

More 50 years of the PT6A engine lifespan has witnessed only limited technology advancements. However, this is about to change. In this proposal, a brand-new design of a dual spool, reverse-flow, high performance turboprop engine WJ-25 is presented. This engine draws together advanced, proven technologies from the latest institutional researches and industrial practices. This will bring a revolutionary improvement in performance, a ground-breaking enhancement of customer satisfaction, and a game-changing influence in market distribution.

The upgraded compressor features a fully optimized 3D aerodynamic design, with a class-leading 18.9:1 overall pressure ratio, an innovative axial-diagonal-up centrifugal stage, and an industrial-leading bling architecture. The highly compact two-stage gas generator turbine utilizes uncooled CMC material with a working temperature exceeding 2500 °R. Three stages of free power turbine incorporate advanced super alloy for maximum power extraction and full-range peak efficiency. A reverse-flow RQL combustion chamber lowers emission with reduced liner temperature through transpiration cooling. A state-of-art full authority digital engine control unit facilitates unrestricted power lever movement with significant saving of engine weight.

In essence, WJ-25 provides extraordinary performance over its competitors, enables unprecedented cost-saving for its operators, and guarantees unshakable in-service reliability.

Key Analyses



Major analyses done in this proposal includes:

- Structure Selection & Turbomachinery Conceptual Design
- Aero-Thermodynamic Cycle Analysis
- Constraint Analysis & Engine Sizing
- Aerodynamic Design of Turbomachinery
- Duct Design
- Combustion Chamber Design
- Engine Component Test
- Off-Design and Transient Performance
- Control Logic Design
- Mission Analyses
- Miscellaneous Structural Analysis

Performance	
Maximum speed	370KEAS
Cruise speed	337KTAS
Mission Fuel Burn	1410.233501 lb.
Cruise BSFC	0.415085047
Takeoff BSFC	0.443762418
Engine Weight	No more than 543.4lb
Engine Diameter	19 Inch
Required Trade Studies	
Engine Cycle Design Space Carpet Plots Page #	20
In-Depth Cycle Summary Page #	31
Final engine flow path (Page #)	89
Final cycle study using chosen cycle program (Page #)	79
Detailed stage-by-stage turbomachinery design information (page # for each component)	HPT: 33, LPT: 40, AC: 50, CC: 54
Detailed design of velocity triangles for first stage of each component (list page #'s and component)	HPT: 39, LPT: 47 AC: 53, CC: 58

Table RFP-1 Compliance Matrix

Summary Data	
Design MN	0
Design Altitude	0
Design Shaft Horsepower	2087.642072
Design BSFC	0.449675766
Design Overall Pressure Ratio	18.9
Design T4.1	2654.986132
Design Engine Pressure Ratio	18.9
Design Chargeable Cooling Flow (% @25)	0
Design Non-Chargeable Cooling Flow (% @25)	0
Design Adiabatic Efficiency for Each Turbine	0.907495807@HPT 0.808984908@FPT
Design Polytropic Efficiency for Each Compressor	AC: 0.8676, CC: 0.8990
Design Shaft Power Loss	0.5%
Design HP/IP/LP/PT Shaft RPM	41093.59326@HP 21041.2598@LP

Flow Station Data (List for Each Engine Component at Design Condition)	
Inflow	Refer to: Table 11-2 Off-Design Summary: Cycle Design Point
Corrected Inflow	
Inflow Total Pressure	
Inflow Total Temperature	
Inflow Fuel-air-Ratio	
Inflow Mach #	
Inflow Area	
Pressure Loss/Rise Across Component	
Additional Information	
Design HP/LP Shaft Off-Take Power	16.5566hp @ HP
Design Customer Bleed Flow	7% Inlet Corrected Mass Flow Rate

Table RFP-2 Engine Summary Table

Compressor		Turbine	
Lieblein Diffusion Factor	Refer to: Table 7-6 Centrifugal Compressor Detailed Information	Zweifel Coefficient	Refer to: Table 7-8 GGT Detailed Information Refer to: Table 7-9 FPT Detailed Information
De Haller Number		Taper Ratio	
Stage Loading		Stage Work	
Flow Coefficient		Stage Pressure Ratio	
Hub-to-Tip Ratio		Degree of Reaction	
Number of Blades (Rotor & Stator)		Velocity Triangles (Hub, Mean, & Tip)	
Solidity		Aspect Ratio	
Pitch		AN2	
Chord (Axial & Blade)		Number of Blades (Rotor & Stator)	
Aspect Ratio		Chord (Axial & Blade)	
Taper Ratio		Blade Metal Angles	
Tip Speed		Mach numbers (absolute and relative)	
Stagger Angle		Tip speed	
Blade metal angles		Flow Coefficient	
Velocity Triangles (hub, mean, & tip)		Stage Work Split	
Blade chord		Pitch	
Degree of Reaction		Cooling Flow Details	
Mach Numbers (absolute & relative)			

Table RFP-3: Required Detailed Stage and Component Information

Table of Contents

1. Introduction	8
1.1. Architecture of This Proposal	8
1.2. Customer Requirements, Market Research & Potential Technology Advancements	9
2. Nomenclature & Station Numbering	10
2.1. Station Numbers.....	10
2.2. Nomenclature	11
3. Structure Selection & Turbomachinery Conceptual Design.....	11
4. Aero-Thermodynamic Cycle Analysis.....	13
4.1. Design Point Selection.....	13
4.2. Input Setup.....	13
4.2.1. Ambient Condition.....	13
4.2.2. Axial-Centrifugal Compressor	14
4.2.3. Combustion Chamber.....	14
4.2.4. Turbines.....	15
4.2.5. Ducts	16
4.2.6. Engine Fuel	18
4.2.7. Secondary Air System.....	18
4.2.8. Mechanical Losses	18
4.2.9. Station Mach Number.....	18
4.2.10. Input Summary	19
4.3. Carpet Plotting, Diagramming & Cycle Optimization.....	20
4.4. Summary of PR and COT Selections	25

5.	Constraint Analysis & Engine Sizing.....	25
5.1.	Drag Polar Estimation.....	25
5.2.	Takeoff Constraints.....	26
5.3.	Cruise Constraints.....	27
5.4.	Maximum Speed Constraints.....	27
5.5.	Climb Rate & Service Ceiling Constraints.....	27
5.6.	Constraint Analysis Conclusion.....	28
5.7.	Engine Sizing.....	29
6.	Cycle Summary.....	31
7.	Aerodynamic Design of Turbomachinery.....	33
7.1.	Gas Generator Turbine Design.....	33
7.1.1.	GGT Preliminary Design.....	33
7.1.2.	GGT Design Space.....	35
7.1.3.	Manual Adjustment of Meridional Flow Path.....	36
7.1.4.	GGT S1 Optimization.....	36
7.1.5.	GGT Blade Twist Factors.....	37
7.1.6.	GGT Streamline Analysis.....	37
7.1.7.	GGT Blade Profiling & 3D Design.....	39
7.2.	Free Power Turbine Design.....	40
7.2.1.	FPT Preliminary Design.....	40
7.2.2.	FPT Design Space.....	43
7.2.3.	Manual Adjustment of Meridional Flow Path.....	43
7.2.4.	FPT S1 Optimization.....	43

7.2.5.	FPT Blade Twist Factors	44
7.2.6.	FPT Streamline Analysis	45
7.2.7.	FPT Blade Profiling & 3D Design	49
7.3.	Pressure Ratio Separation Between Axial and Centrifugal Compressors.....	49
7.4.	Axial Compressor Design	50
7.4.1.	Axial Compressor Preliminary Design.....	50
7.4.2.	Axial Compressor Design Space.....	52
7.4.3.	Axial Compressor Streamline Analysis	53
7.4.4.	Axial Compressor Profiling & 3D Design	54
7.5.	Centrifugal Compressor Design.....	54
7.5.1.	Centrifugal Compressor Architecture	54
7.5.2.	Centrifugal Compressor Preliminary Design	55
7.5.3.	Centrifugal Compressor Design Space.....	55
7.5.4.	Centrifugal Compressor Streamline Analysis	56
7.5.5.	Centrifugal Compressor Profiling & 3D Design	58
7.6.	Hand Calculation of Velocity Triangle.....	59
7.7.	Detailed Component Information	60
8.	Duct Design.....	64
8.1.	Intake Design.....	64
8.1.1.	Intake Sizing.....	64
8.1.2.	Inlet Pressure Loss Estimation	66
8.1.3.	Anti-Icing System.....	67
8.2.	Inter-Compressor and Inter-Turbine Duct	68

9.	Combustion Chamber Design	68
9.1.	Design Point Selection.....	69
9.2.	Pre-Diffuser Design.....	69
9.3.	RQL Combustor Configuration.....	70
9.4.	Air Flow Distribution	71
9.4.1.	Fuel Atomizing Flow	71
9.4.2.	Swirler Flow.....	71
9.4.3.	Dome Cooling Flow	72
9.4.4.	Passage Air Flow, Dilution Flow and Liner Cooling Flow.....	72
9.5.	Combustion Chamber Sizing.....	72
9.5.1.	Reference Area Calculation.....	72
9.5.2.	Dome and Passage Height.....	73
9.5.3.	Number of Fuel Injectors and Length of Combustor.....	73
9.5.4.	3D Geometry of Combustion Chamber.....	73
10.	Engine Component Test.....	73
10.1.	Compressor Test.....	73
10.2.	Turbine Test.....	74
10.3.	Intake Map	75
10.4.	Burner Lean Flame Out Limit	75
11.	Off-Design and Transient Performance.....	76
11.1.	Steady-State Model Building and Verifications.....	76
11.1.1.	Steady-State Model Overview	76
11.1.2.	Main Corrections and Modifications	76

11.1.3.	Steady-State Model Verification	78
11.1.4.	Critical Off-Design Points	78
11.2.	Controller Design.....	81
11.2.1.	Steady State Controller Design	81
11.2.2.	Transient Controller Design	82
11.2.3.	Control System Integration.....	83
11.3.	Transient Performance on Map.....	83
11.4.	Mission Analyses.....	85
11.4.1.	Mission Profile	85
11.4.2.	Mission Analysis.....	86
12.	Miscellaneous Structural Issues.....	88
12.1.	Bearing Supports.....	88
12.2.	Main Shaft Reduction Gearbox.....	89
12.3.	Implementation of the Control Logic.....	89
13.	2D Engine Meridional Section View.....	89
14.	References.....	91

1.2. Customer Requirements, Market Research & Potential Technology Advancements

To update the current frontrunner PT6A-68B, while simultaneously meeting the customer requirements, a comprehensive market research has been performed, with latest technology potentials being regarded. One of the major competitors with PT6 series is the new emerging GE Advanced Turboprop (GE93) announced in 2015, which possesses “highest power to weight ratio in its class”, “20% lower fuel burn than same size class competitors”, and “an industry-best 16:1 overall pressure ratio” (GE Business & General Aviation, 2017). Therefore, performance parameters of both PT6A-68B and GE93 as well as the customer requirements are listed in Table 1-1 Current & Advanced Engine Technologies in accordance with corresponding propulsion development goals.

Advanced propulsion development goals	Propulsion changes to achieve goals (Younghans, Johnson, & Csonka, 1994)	Current engines in service		Customer requirements (AIAA, 2016)
		PT6A-68B	GE93	
Reduced SFC	<ul style="list-style-type: none"> • Increased propulsive efficiency • Increased thermal efficiency <ul style="list-style-type: none"> - Improved component efficiency - Higher cycle pressure ratio • Reduced cycle parasitic cooling air <ul style="list-style-type: none"> - Higher temperature materials 	<ul style="list-style-type: none"> • BSFC: 0.566 <i>lb/hr/SHP</i> 	20% lower fuel burn	<ul style="list-style-type: none"> • 20% less fuel burn • Extended payload and/or the range
Reduced ownership cost	<ul style="list-style-type: none"> • Smaller engines <ul style="list-style-type: none"> - Increased specific power • Reduced parts count <ul style="list-style-type: none"> - Higher stage loading • Reduced manufacturing costs • Reduced maintenance costs • More affordable advanced materials • Improved installation integration 	\$855,000 (Kasper & Balle, 2016)		
Increased power to weight ratio	<ul style="list-style-type: none"> • Reduced weight <ul style="list-style-type: none"> - Higher stage loadings - Improved strength to density materials • Increased thrust <ul style="list-style-type: none"> - Higher turbine temperatures - Improve component efficiencies 	<ul style="list-style-type: none"> • Power to weight ratio: 2.185 <i>SHP/lb</i> • Maximum power at sea level: 1250 <i>SHP</i> • Dry weight less tailpipe: 572 <i>lb</i> 	Highest power to weight ratio in its class	<ul style="list-style-type: none"> • 25% greater power output • 5% lighter
Higher power per pound of airflow	<ul style="list-style-type: none"> • Increased cycle energy <ul style="list-style-type: none"> - Higher turbine temperatures • Reduced cycle parasitic cooling air 	<ul style="list-style-type: none"> • Power/pound of airflow: 235.8 <i>hp · s/lb</i> • Air mass flow: 5.3 <i>lb/second</i> • Maximum power at sea level: 1,250 <i>shp</i> 		
Reduced emissions	<ul style="list-style-type: none"> • More efficient combustors 	<ul style="list-style-type: none"> • Burner Eff: 0.99 		

Table 1-1 Current & Advanced Engine Technologies

After a quick scantling of technology emergence during recent years, following features are incorporated into WJ-25:

- Ceramic-Matrix Composite in engine hot section components. (Gardiner, 2015)
 - Improved high-temp capability
 - Reduced material density
- Carbon fiber reinforced polymer in engine casing (Gardiner, 2015)
 - Less component weight
 - Increased material strength
 - Better damping characteristics
- Axial-Diagonal-Up Centrifugal Compressor
- Bling and blisk stages
- RQL Combustor
- Transpiration combustor liner cooling
- Full authority digital engine control (FADEC)

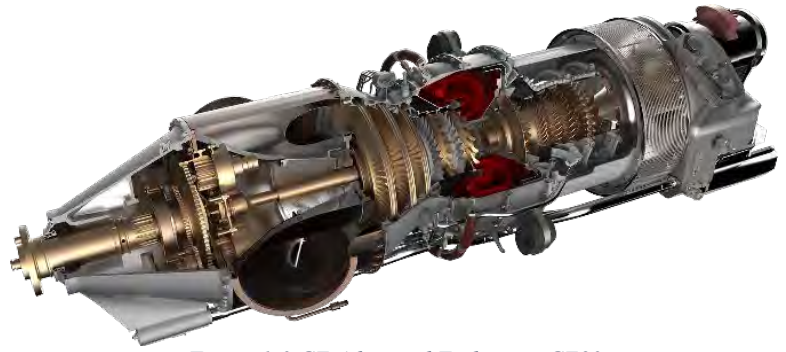


Figure 1-3 GE Advanced Turboprop GE93 (GE Business & General Aviation, 2017)



Figure 1-3 PT6A-68B (Pilatus, 2002)

The corresponding benefits of utilizing the above listed technologies are conspicuous when referring to Table 1-1 Current & Advanced Engine Technologies.

2. Nomenclature & Station Numbering

This section provides the standard of engine station numbering and nomenclature used for WJ-25. The general naming rule is adapted from ARP 755A (SAE, 1974) with occasional reference towards AS681 Rev. E (SAE, 1989), ARP 1211A (SAE, 1974), ARP 1210A (SAE, 1996), and ARP 1257 (SAE, 1989). Briefly, the basis of station numbering and engine nomenclature is described below, which enables the reader to comprehend analyses throughout this proposal without referring to the standards listed above.

2.1. Station Numbers

1	Engine intake front flange, or leading edge
2	Axial compressor front face
24	Axial compressor exit face
25	Centrifugal compressor front face
3	Centrifugal compressor exit face
31	Compressor outlet diffuser exit/combustor inlet
4	Combustor exit plane
44	Gas generator turbine exit
45	Free power turbine nozzle guide vane leading edge
5	Free power turbine exit face
6	Turbine exit duct outlet face
8	Propelling nozzle throat

2.2. Nomenclature

The symbols for mass flow, pressures and other quantities are defined as follows:

A	Area	HPT	High pressure turbine	RQL	Rich burn-quick mix-lean burn
alt	Altitude	ISA	International standard atmosphere	RFP	Request for Proposal
amb	Ambient	LDI	Lean Direct Inject	RNI	Reynolds number index
ax	Axial	LP	Low-pressure	s	Static
Bld	Bleed	Lk	Leakage	SD	Shaft, delivered
corr	Corrected	LPP	Lean Premixed-Prevaporized	SFC	Specific fuel consumption
C	Constant value, coefficient	LPT	Low-pressure turbine	SiC	Silicon Carbide
CFG	Thrust coefficient	MN	Mach number	SLS	See level static
Cl	Cooling	n	Spool speed	SOT	Stator outlet temperature
CMC	Ceramic matrix composite	NGV	Nozzle guide vane (of turbine)	t	Tip (blade)
COT	Combustor outlet temperature	NOx	Nitrogen Oxides	t	Time
d	Diameter	OTDF	Overall temperature distribution factor	T	Total temperature
dH	Enthalpy difference	P	Total pressure	TAS	True airspeed
dp	Design point	PLA	Pilot Lever Angle	TRQ	Torque
f	Fuel	PR	Pressure ratio	U	Blade (tip) velocity
F	Thrust	PS	Static pressure	V	Velocity
FAR	Fuel-air-ratio	prop	Propulsion	VSV	Variable Stator Vane
FPT	Free power turbine	PW	Shaft power	W	Mass flow
FHV	Lower Heating Value of Fuel	R	Gas constant	XN	Relative spool speed
GGT	Gas Generator Turbine	rel	Relative		
H	Enthalpy				
HP	High-pressure				

3. Structure Selection & Turbomachinery Conceptual Design

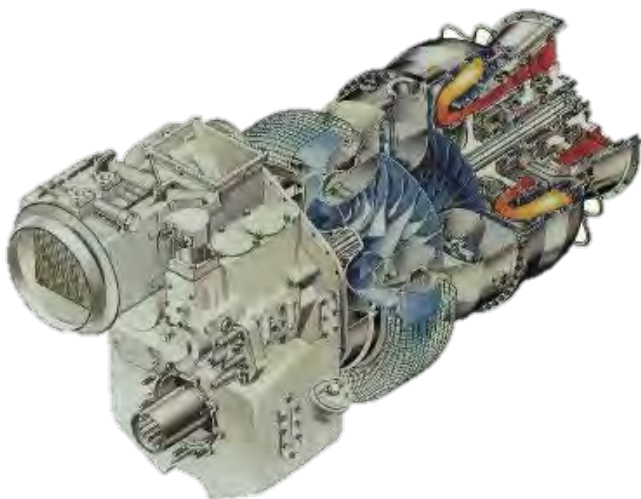


Figure 3-1 Structure of MTR390 (IPT, 2017)

To select the ideal structure for the new engine design, several different and innovative engine concepts are discussed. Pros and cons of each concept was analyzed, from which the most suitable structure for WJ-25 was decided. The first concept to be discussed is the dual stage centrifugal compressor architecture, which was incorporated into MTR390, developed cooperatively by MTU, Turbomeca, and Rolls-Royce. The structure of MTR390 is showed in Figure 3-1 Structure of MTR390. If utilizing this concept to update the original PT6A, the axial-centrifugal compressor with four axial and one centrifugal stages will be replaced by two centrifugal stages in sequence. Obviously, this construction could possibly reduce the engine weight, and decrease the overall length of the engine. However, due to the structural difficulty of inter-compressor ducting, not only

is it unusual to use more than two centrifugal stages in series, but the highest PR achievable from two centrifugal stages is also limited to 15:1, since the pressure ratio of the second stage is likely designed conservatively to compensate the extensive inter-stage flow turning for avoiding massive separation (Walsh & Fletcher, 2004, p. 182).

A second possibility is the full-axial compressor architecture, which is widely used in large turboprop engines, such as Europrop TP400. The structure of Europrop TP400 is showed in Figure 3-2 Structure of Europrop TP400. With all axial compressor stages, the overall

pressure ratio of the engine can reach a very high level, up to 25 or more. Higher overall pressure ratio enables higher cycle efficiency, which in turn increases the aircraft flight range. However, to maintain a relatively satisfying compressor efficiency, more stages are needed in a fully axial compression system in comparison with structural alternatives resembling PT6A. Due to the inverse relationship between polytropic efficiency and stage loading (Glassman J. , 1992), stage work must be lowered to attain a higher polytropic efficiency when a certain threshold for isentropic efficiency needs to be guaranteed. Thus, the disadvantage of increased engine weight and length might be compromised by high overall PR. Additionally, axial compressors are predominantly favorable for turbomachinery of mass flow rate larger than 10kg/s for aerospace applications (Walsh & Fletcher, 2004, p. 185). Small mass flow rate poses efficiency challenges, such as the increased percentage tip clearance from the small blade size under constant manufacturing limits.

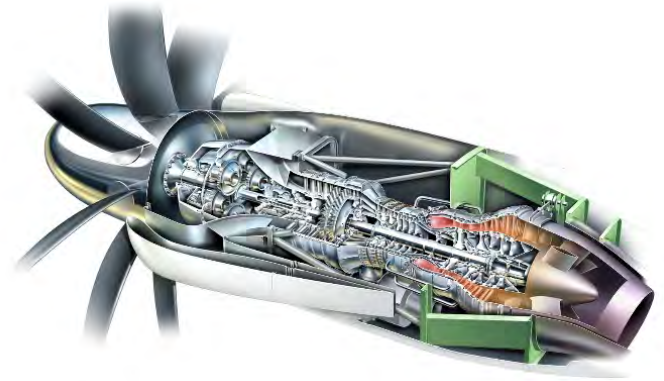


Figure 3-2 Structure of Europrop TP400 (Europrop, 2017)

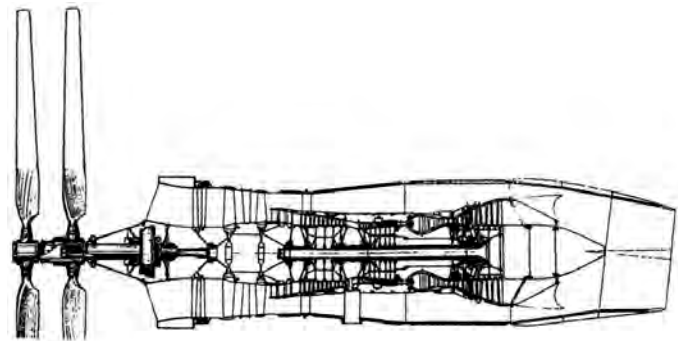


Figure 3-3 Structure of Kuznetsov NK-62 (Авиабаза, 2017)

Coaxial contra-rotating is yet another concept proposed in the discussion. Contra-rotation is realized through a mechanism where two mechanically independent rotors spin around a common axis, however, in opposite directions aiming for minimization of gyroscopic effect. A typical structure of coaxial counterrotating turboprop engine is Kuznetsov NK-62 shown in Figure 3-3 Structure of Kuznetsov NK-62 (Авиабаза, 2017). In coaxial counterrotating engines, the propeller efficiency is increased by recovering tangential (rotational) momentum from the leading propeller in its downstream

stage. Tangential velocity gradient in the downstream air doesn't contribute to the thrust. Hence, conversion of airflow momentum from tangential to axial increases both propeller efficiency and overall system effectiveness. But in engines of this kind, complex mechanical structure and sophisticated bearing systems are mandatory supplements for coaxial counterrotating spool configuration, which are expensive in both fabrication and maintenance. Besides, the noise level of the engine is also dramatically increased by the coaxial contra-rotating propeller. Therefore, synthesizing considerations on reliability and noise, the concept of NK-62 is not adopted.

After careful comparison and discussion, the original axial-centrifugal compressor with axial turbine and reverse-flow combustor structure is finally chosen, whose feasibility has been validated in not only more than 30 years of PT6 development, but also in the new emerging GE93 market disruptor. For WJ-25, this is the best combination for suitable overall pressure ratio, acceptable total weight, and attainable technology readiness, regarding its mass flow rate, power level, and customer's cost expectations.

4. Aero-Thermodynamic Cycle Analysis

4.1. Design Point Selection

The 0-D engine model used for Design Point calculation is depicted in Figure 4-2 0-D Engine Model:

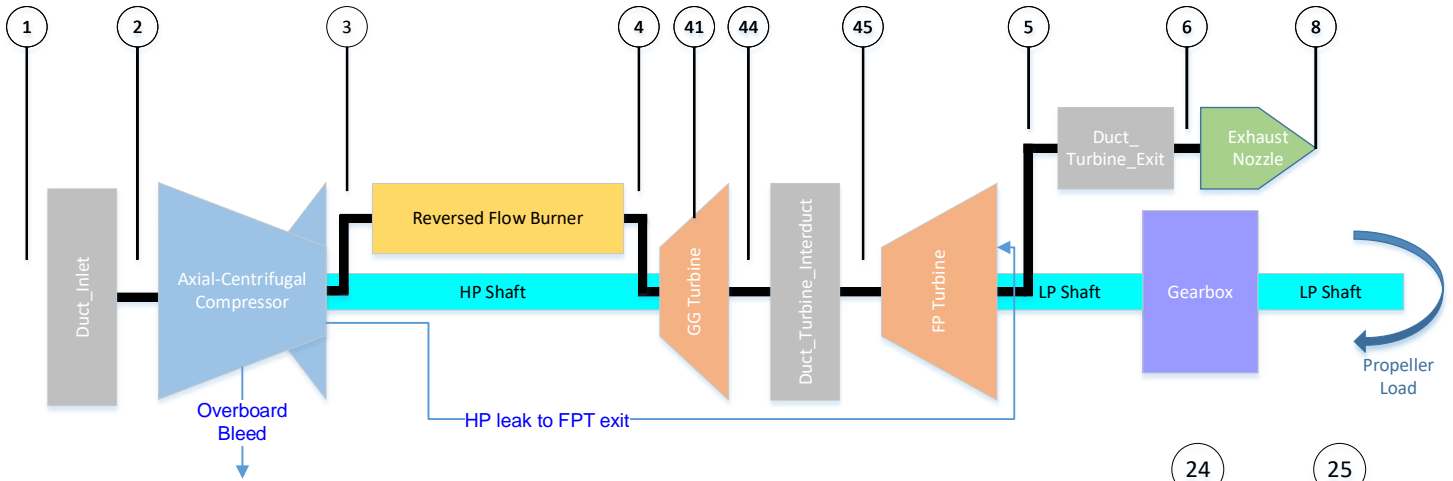


Figure 4-2 0-D Engine Model

In the first cycle model, the Axial-Centrifugal Compressor is regarded as a single unit. Thus, overall efficiency and PR values are used in the calculation. After that, a second model is established with axial and centrifugal compressors discussed separately, as shown in Figure 4-1 Axial-Centrifugal Compressor. An inter-compressor duct component is added to model the duct loss in detail.

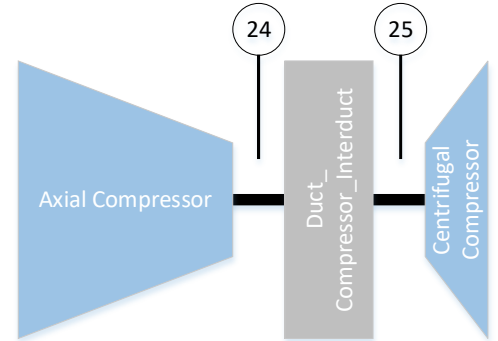


Figure 4-1 Axial-Centrifugal Compressor

4.2. Input Setup

In this section, all input variables will be discussed, including component efficiencies and certain losses. It is presented following the sequence of front to rear. Remarks on how each value is determined are also included.

4.2.1. Ambient Condition

As per *Principles of Turbomachinery in Air-Breathing Engines* (BASKHARONE, 2006, p. 65), The design point for turboprop engines is traditionally the sea-level takeoff, since they are categorically tailored for significantly short missions. Combined takeoff-climb phases would naturally constitute a heavy segment of the entire mission. Therefore, the design point of WJ-25 is set at 0 km in altitude and 0 knot in TAS. The ambient temperature and humidity is chosen per ISA (ISO, 1975).

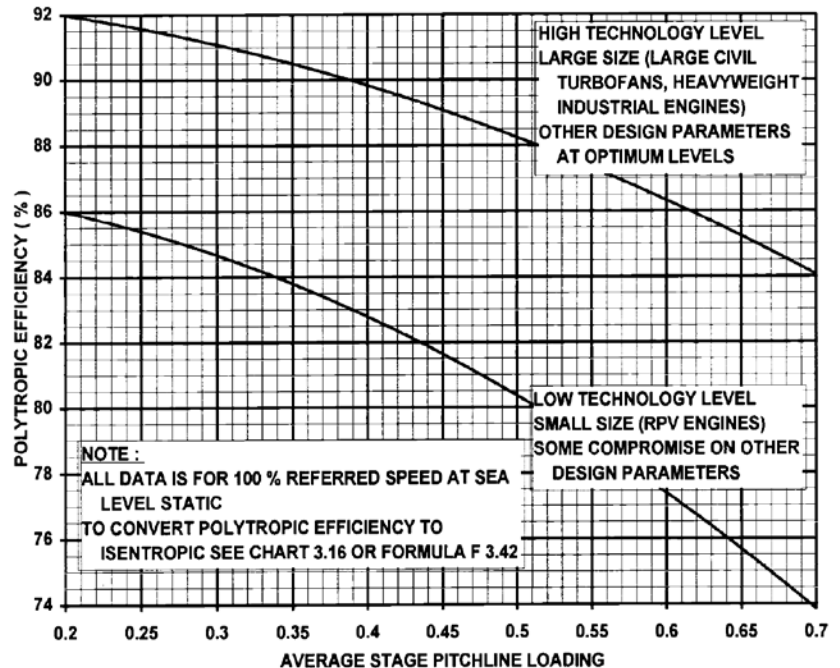


Figure 4-3 Axial Compressor Polytropic Efficiency Versus Stage Loading (*Gas Turbine Performance*, p. 273)

4.2.2. Axial-Centrifugal Compressor

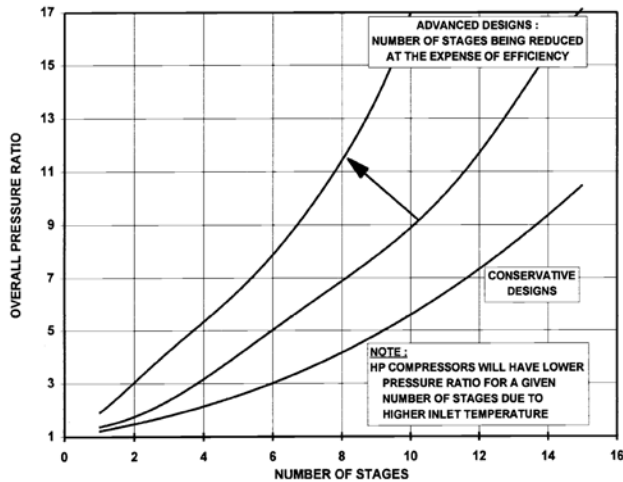


Figure 4-5 Axial Compressors: Pressure Ratio Versus Number of Stages (Gas Turbine Performance, 2004, p. 273)

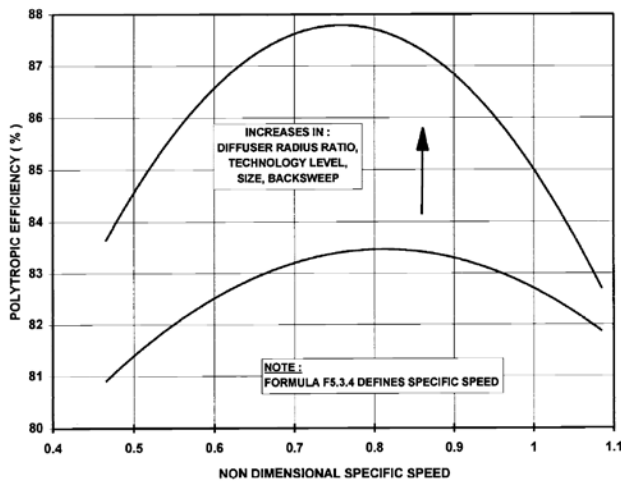


Figure 4-4 Centrifugal Compressor: Polytrropic Efficiency Versus Specific Speed (Gas Turbine Performance, p. 274)

As per *Gas Turbine Theory* (Saravanamuttoo, Rogers, Cohen, & Straznicky, 2009, p. 62), when performing calculations over a range of pressure ratio, it is reasonable to assume constant polytrropic efficiency. Therefore, the polytrropic efficiency of Axial-Centrifugal Compressor is selected per Figure 4-3 Axial Compressor Polytrropic Efficiency Versus Stage Loading (Gas Turbine Performance, p. 273) and Figure 4-4 Centrifugal Compressor: Polytrropic Efficiency Versus Specific Speed (Gas Turbine Performance, p. 274). For axial compressors, apart from supersonic aero-engines, loading along the pitch line should be between 0.25 and 0.5 for all stages (Walsh & Fletcher, 2004, p. 163). Hence, the polytrropic efficiency for axial compressor is chosen as 0.89 per Figure 4-3 Axial Compressor Polytrropic Efficiency Versus Stage Loading (Gas Turbine Performance, p. 273). For centrifugal compressor, non-dimensional specific speed is preliminarily considered to fall between 0.57 and 0.95. Thus, the polytrropic efficiency for centrifugal compressor is chosen as 0.87, which will be rechecked in Section 10.1 Compressor Test after detailed design of blade geometry. Additionally, the ratio of pressure rises in axial compressor and in centrifugal compressor is assumed similar as per baseline engine (AIAA, 2016), i.e. slightly larger pressure ratio in axial compressor than in centrifugal compressor. Therefore, the overall polytrropic efficiency throughout Axial-Centrifugal Compressor is presumed as 0.88, which will be rechecked after cycle analysis in Section 10.1 Compressor Test.

The pressure ratio of Axial-Centrifugal Compressor will be studied in section 4.3 Carpet Plotting, Diagramming & Cycle Optimization. However, constraints on its upper and lower limits are presented here. For centrifugal compressor, the highest PR possible from a single stage is approximately 9:1, and from two stages up to 15:1 (Walsh & Fletcher, 2004, p. 182), while for axial compressors, Figure 4-5 Axial Compressors: Pressure Ratio Versus Number of Stages provides a first order estimation of the relationship between number of stages and the PR achievable. Regarding the compatibility with existing nacelle envelop (AIAA, 2016), number of stages for axial compressor will be kept unaltered as 4 to maintain a comparable engine length as the baseline engine.

4.2.3. Combustion Chamber

Figure 4-6 Combustion efficiency versus loading (Gas Turbine Performance, p. 275) presents guideline for combustion chamber efficiency selection. Combustor loading at SLS should be less than $10 \text{ kg/s} \cdot \text{atm}^{-1.8} \text{m}^3$, and preferably less than

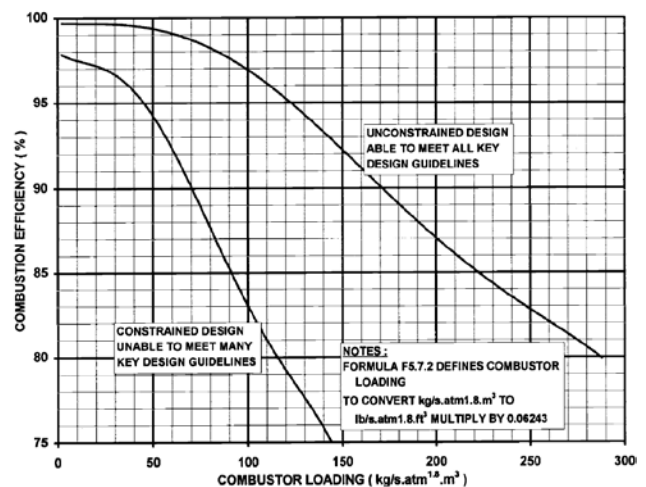


Figure 4-6 Combustion efficiency versus loading (Gas Turbine Performance, p. 275)

$5\text{ kg/s} \cdot \text{atm}^{1.8}\text{m}^3$ (Walsh & Fletcher, 2004, p. 195). Therefore, combustor efficiency is chosen as 0.995. The combustor cold pressure loss is usually between 2 and 4% of total pressure at the design point, while fundamental loss around 0.05% and 0.15% (Walsh & Fletcher, 2004, p. 194). Thus, combustor pressure ratio is chosen as 0.975, which counts for 4% of losses. Combustor exit temperature is mainly restricted by the material of turbine stators and rotors. With new emergence of CMC, this design incorporates CMC for all turbine nozzles, blades, and discs. The use of CMC in engine hot section greatly improves COT, reduces weight, and eliminates the need for sophisticated turbine cooling. The SiC CMC with a highest working temperature of $2400^\circ\text{F}/1316^\circ\text{C}$ (Wood, 2013) has already been made into engine service by GE Aviation (Norris, 2015), while other types of CMC with more aggressive high-temp capabilities are still under research and development. Additionally, a combustor exit temperature profile parameter, OTDF, should be controlled to less than 50% and ideally less than 20% (Walsh & Fletcher, 2004, p. 198). Thus, to tolerate reasonable level of combustor outlet temperature unevenness, i.e. a no less than 20% OTDF, the combustor exit temperature, i.e. COT, should be lower than the highest material capability to ease the design challenge of

combustor exit mixing, and will be studied in detail in section 4.3 Carpet Plotting, Diagramming & Cycle Optimization.

4.2.4. Turbines

Turbine pressure ratio and rotational speed are limited by power requirements of its corresponding compressors (GGT) or outputs (FPT), as well as the mechanical stressing of blades or discs respectively. Academically, the standard practice is to

make carpet plots with constant turbine polytropic efficiency. However, it is unrealistic to omit considerations on turbine stages during preliminary design per Kurzke (1995). Since practically the turbine efficiency jumps with the number of

stages, stage numbers for both GGT and FPT need to be estimated. Per Figure 4-8 Small Turboshaft Engine Performance (Philpot, 1992), dual stages of GGT promises a significant reduction in SFC based on statistics for engine performances of past designs. Therefore, the GGT for WJ-25 will also be chosen with 2 stages, the same as GE93, Meanwhile, GE93 also incorporates 3 stages of FPT. Thus, stage number of FPT for WJ-25 will be determined as the same to maintain the state of art. This configuration results in relative small size of turbine blades, which imposes additional challenges on impinge cooling. This serves as a second reason for using uncooled turbine rotors and stators. The turbine efficiency estimation process utilizes symmetrical diagrams mode of a NASA code described in NASA-CR-189171 (Glassman J., 1972). With geometrical dimensions measured from Figure 4-7 PT6 Engine Meridional Section View (Badger, et al., 1994). Following parameters are given as input:

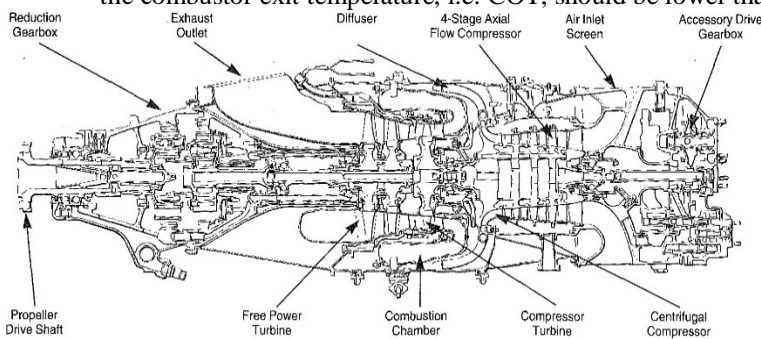


Figure 4-7 PT6 Engine Meridional Section View (Badger, et al., 1994)

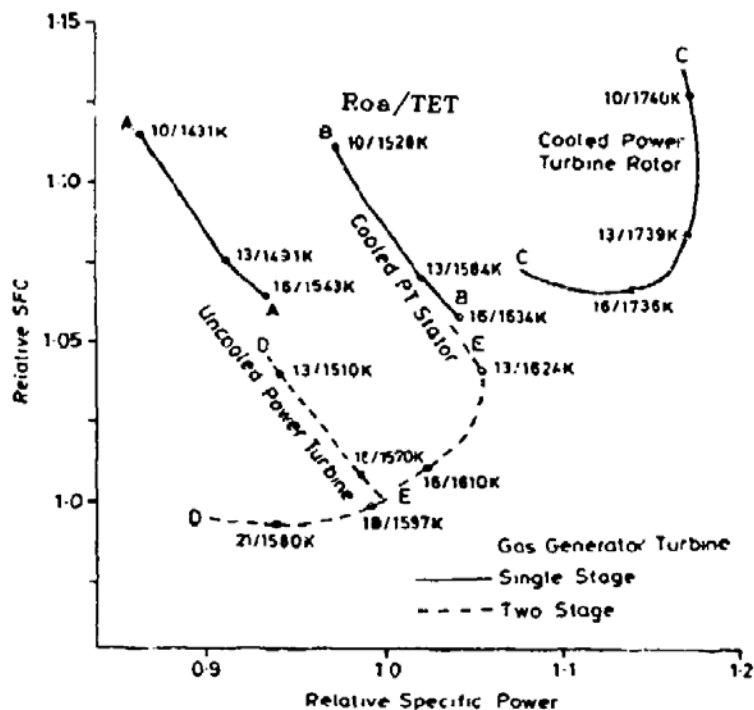


Figure 4-8 Small Turboshaft Engine Performance (Philpot, 1992)

- 1st GGT Rotor Inlet Mean Diameter = 8 in
- Last GGT Rotor Exit Mean Diameter = 8.5 in

- GGT Exit Radius Ratio = 0.8
- $\text{GGT} \frac{\text{Exit Axial Velocity}}{\text{Average Axial Velocity}} = 1.05$

- GGT Loss Factor = 0.3
- Number of GGT Stages = 2
- 1st FPT Rotor Inlet Mean Diameter = 9 in
- Last FPT Rotor Exit Mean Diameter = 9.5 in
- FPT Exit Radius Ratio = 0.5

- $FPT \frac{Exit\ Axial\ Velocity}{Average\ Axial\ Velocity} = 1$
- FPT Loss Factor = 0.3
- Number of FPT Stages = 3

Besides turbine 2D meridional geometries, the design code also calls for the mechanical spool speed. Hence, material

strength of CMC was referred to as per Figure 4-9 Mechanical Properties of CMC (Kurtz, 1992). From the picture, SiC CMCs manufactured using chemical vapor infiltration(CVI) provides best tensile strength of 310MPa, while possessing a density of $2.1g/cm^3$. This corresponds to an allowable turbine AN^2 of $84.35 \times 10^6 rpm^2 m^2$. However, simple calculation shows that this value is high enough to permit even zero exit swirl of GGT. On the other hand, to lower the manufacturing cost of the engine, super alloy will be used on FPT due the reduced working temperature and RPM. Mechanical properties for common Ni-based and Co-based high-temperature alloys are well-known. With the assistance of thermal barrier coating, these classes of alloy can well sustain a working temperature of around $850^\circ C / 2021.67^\circ R$ (Superalloy, n.d.) and an AN^2 up to $45 \times 10^6 rpm^2 m^2$ (Walsh & Fletcher, 2004, p. 206). Thus, after applying constraint on FPT temperature and AN^2 , both GGT and FPT will be optimized for zero exit swirl, which yields highest turbine component efficiency as well as minimum duct loss. Spool speed will be determined correspondingly.

Additionally, to demonstrate the difference between using turbine design code and using turbine polytropic efficiency, a traditional carpet plot with 0.91 and 0.89 respectively for FPT and GGT polytropic efficiencies will be presented next to the carpet plot using turbine design code in section 4.3 Carpet Plotting, Diagramming & Cycle Optimization. To estimate tip

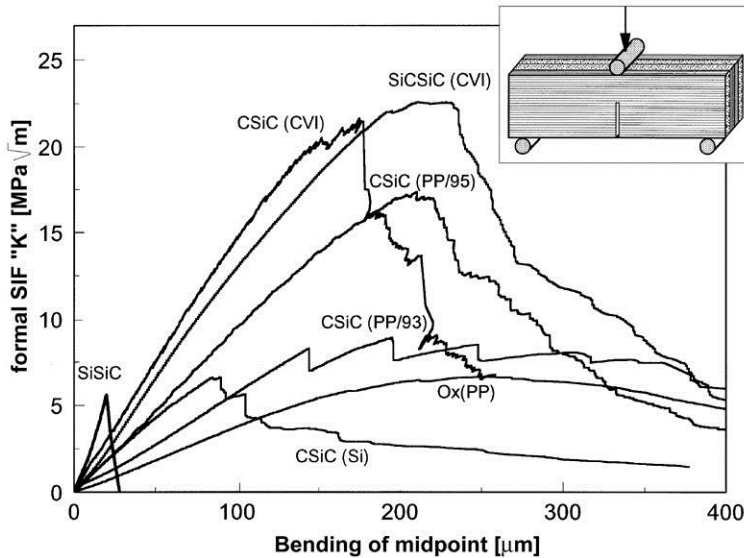


Figure 4-9 Mechanical Properties of CMC (Kurtz, 1992)

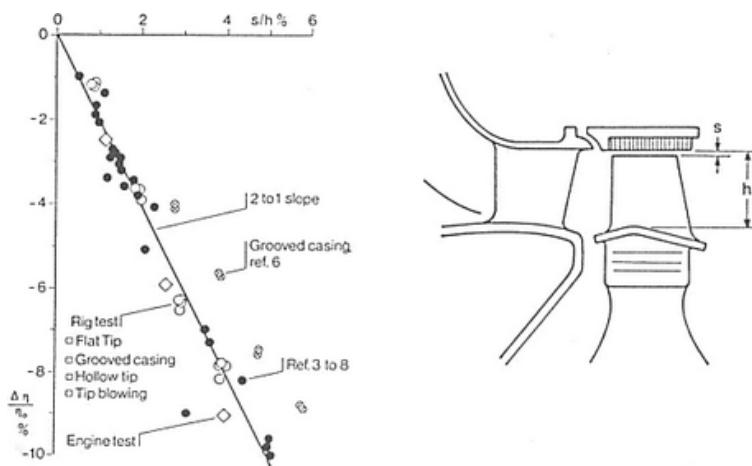


Figure 4-10 Effects of Tip Clearance on the Efficiency of Single Stage Shroudless Turbines (Kurzke J. , 1992)

clearance effects, GGT is assumed unshrouded and has 0.5% of tip clearance. The exchange rate between tip clearance and efficiency degradation is approximated using relationships provided in Figure 4-10 Effects of Tip Clearance on the Efficiency of Single Stage Shroudless Turbines (Kurzke J. , 1992). This picture shows a 2% degradation of efficiency on every 1% of tip clearance increase. On the contrary, FPT is considered shrouded per gas turbine legacy.

4.2.5. Ducts

Duct pressure losses are calculated per Formula 4-1 Pressure Loss Coefficient (Gas Turbine Performance, p. 254), usually called λ parameter (Walsh & Fletcher, 2004, p. 221):

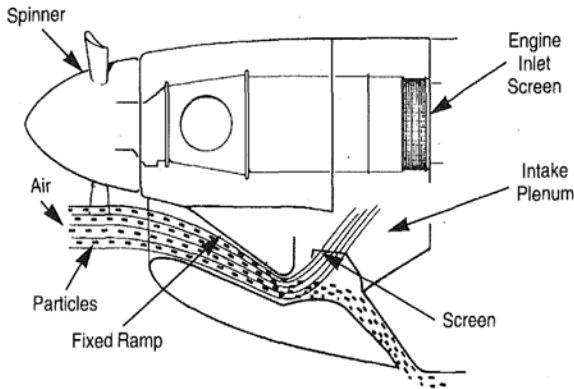


Figure 4-11 Inlet Duct (Badger, et al., 1994)

$$\lambda = \frac{P_{in} - P_{out}}{P_{in} - P_{S_{in}}}$$

Formula 4-1 Pressure Loss Coefficient (Gas Turbine Performance, p. 254)

$$\text{Lambda} = F \times L / Dh$$

- F — Friction factor, A typical value for friction factor is 0.04. Other details may be found from the “Moody chart”.
- L (m) — Length of pipe.
- Dh (m) — Hydraulic diameter.

Formula 4-2 Total Pressure Loss Coefficient Due to Friction in A Pipe (Gas Turbine Performance, p. 255)

Formula 4-2 Total Pressure Loss Coefficient Due to Friction in A Pipe (Gas Turbine Performance, p. 255) and Figure 4-12 Inter-Turbine Duct Lambda (Gas Turbine Performance, p. 219) provide guideline respectively for inlet and turbine inter-duct λ value selections, while Figure 4-11 Inlet Duct (Badger, et al., 1994) depicts the real world geometry of inlet. For combustor entry diffuser, however, a set of hand calculation following the same mathematical model generates results of less than 0.1% of pressure loss. Therefore, its effect is neglected as per baseline engine (AIAA, 2016). Thus, the following chosen input parameters are summarized with explanations on how the corresponding values are determined following each parameter entry.

- Inlet friction factor $F = 0.04$, As per Formula 4-2 Total Pressure Loss Coefficient Due to Friction in A Pipe (Gas Turbine Performance, p. 255).
- Inlet duct length $L = 2$ m, As per nacelle length 71.3 inch (AIAA, 2016).
- Inlet hydraulic diameter $Dh = 0.608$ m. As per baseline engine inlet area (AIAA, 2016).
- Inter-turbine duct $\text{Lambda} = 0.05$. As per Figure 4-12 Inter-Turbine Duct Lambda (Gas Turbine Performance, p. 219).

Nonetheless, when Turbine design is performed, inter-turbine duct loss can be estimated using a more sophisticated model (Kurzke J., 2015). The calculation employs the loss coefficient ζ , which is defined as:

$$\zeta = \left(1 - \frac{P_2}{P_1}\right) \cdot \left(1 + \frac{\gamma - 1}{2} \cdot M_{ref}^2\right)^{\frac{\gamma}{\gamma - 1}} \cdot \frac{1}{M_{ref}^2}$$

Where,

- P_2 and P_1 — Downstream and upstream total pressure of the duct.
- γ — Heat capacity ratio.
- M_{ref} — Reference Mach number.

The actual pressure ratio for the duct inlet Mach number M is then

INTER-TURBINE DUCT



LAMBDA = 0.05 TO 0.2

Figure 4-12 Inter-Turbine Duct Lambda (Gas Turbine Performance, p. 219)

$$\frac{P_2}{P_1} = 1 - \xi \cdot M^2 \cdot \left(1 + \frac{\gamma - 1}{2} \cdot M^2\right)^{-\frac{\gamma}{\gamma - 1}}$$

Per *Gas Turbine Performance* (Walsh & Fletcher, 2004, p. 219), inter-turbine duct Mach number ranges from 0.3 to 0.55. Thus, M_{ref} is chosen as the middle value 0.4.

Since compatibility with original aircraft needs to be maintained, new engine proposal tends to remain the exhaust system unaltered. Therefore, pressure recovery of Turbine Exit Duct is chosen as 0.98, Nozzle Thrust Coefficient as 0.975, and Nozzle Discharge Coefficient as 0.96, all per baseline engine (AIAA, 2016). Furthermore, since the design of propeller isn't solicited in the RFP, it is preliminarily assumed that new propeller will inherit similar performance level with the baseline engine. Thus, the value of nozzle pressure ratio from the baseline engine is taken as "already being optimized" in the contemporary design. Therefore, the nozzle pressure ratio of WJ-25 is chosen as 1.13, the same as PT6A-68B (AIAA, 2016).

4.2.6. Engine Fuel

JP4, Jet B, Avgas, Jet A, A-1, and JP5 are all available fuel types for baseline engine (EASA, 2016). In this proposal, analyses are done on JP4, which is the most common fuel available. Therefore, the FHV is set to 43.323 MJ/kg or 18552.4 Btu/lb in US customary unit. (MIL-DTL-5624U, 1998).

4.2.7. Secondary Air System

Due to the use of CMC in engine hot section, both turbine nozzle vanes and rotor blades are uncooled. This designates the same value of COT and SOT, and only leakages from HP compressor to FPT are counted as 1% per GasTurb 12 (Kurzke J. , 2015). The customer bleed requirement of 7% inlet corrected airflow at 32 psi at cruise is regarded as part of the installation effect, and will not be discussed until later in Section 5 Constraint Analysis & Engine Sizing.

4.2.8. Mechanical Losses

As per *Gas Turbine Performance*, if ball and roller bearings are utilized mechanical efficiency may range from 99% to 99.9%, increasing with engine size (Walsh & Fletcher, 2004, p. 230). Typically, 0.5% of shaft power will be required for a small engine at the design point, and less than 0.1% for a large engine. Moreover, design point gearbox efficiency is usually between 97.5% and 99% (Walsh & Fletcher, 2004, p. 231). Therefore, the HP/LP spool mechanical efficiency, shaft power extraction, as well as gearbox efficiency are chosen as 0.995, 0.5%, and 0.985 respectively.

4.2.9. Station Mach Number

In addition to the aforementioned inputs, following station Mach numbers are pre-estimated per engineering practice and will be used for flow area calculation as well as turbomachinery design. Note that these Mach numbers are only preliminary assumptions, and results may differ slightly after detailed aerodynamic analysis.

- | | | | |
|------------------------------|-----|-------------------------|-----|
| • Station 2 Compressor Inlet | 0.5 | • Station 4 Burner Exit | 0.2 |
| • Station 3 Compressor Exit | 0.2 | • Station 45 FPT Inlet | 0.4 |

4.2.10. Input Summary

Type	Parameters	Value	Type	Parameters	Value
Compressors	Compressor overall polytropic efficiency	0.88	Combusator	Combusator Efficiency	0.995
	Centrifugal compressor polytropic efficiency	0.87		Combusator Pressure ratio	0.975
	Axial compressor polytropic efficiency	0.89		Ducts	Inlet friction factor ¹
GGT polytropic efficiency ²	0.89	Inlet duct length (m)	2		
1st GGT Rotor Inlet Mean Diameter	8	Inlet hydraulic diameter (m)	0.608		
Last GGT Rotor Exit Mean Diameter (in)	8.5	Inter-turbine duct λ	0.05		
GGT Exit Radius Ratio	0.8	Turbine exit duct pressure ratio	0.98		
GGT $\frac{\text{Exit Axial Velocity}}{\text{Average Axial Velocity}}$	1.05	Nozzle thrust coefficient	0.975		
GGT Loss Factor	0.3	Nozzle pressure ratio	1.13		
Number of GGT Stages	2	Nozzle discharge coefficient	0.96		
GGT Exit Swirl (°)	0	Inter-turbine duct M_{ref}	0.4		
GGT percentage tip clearance (%)	0.5	Engine	FHV (MJ/kg)		43.323
FPT polytropic efficiency	0.91	Fuel	FHV (Btu/lb)	18552.4	
1st FPT Rotor Inlet Mean Diameter (in)	9	Secondary	leakages from HP compressor to FPT	1%	
Last FPT Rotor Exit Mean Diameter (in)	9.5	Air System	HP Mechanical efficiency	0.995	
FPT Exit Radius Ratio (in)	0.5	Mechanical losses	LP Mechanical efficiency	0.995	
FPT $\frac{\text{Exit Axial Velocity}}{\text{Average Axial Velocity}}$	1		Shaft power extraction	0.5%	
FPT Loss Factor	0.3		Gearbox efficiency	0.985	
Number of FPT Stages	3		Station Mach Number	Station 2 Compressor Inlet	0.5
FPT Exit Swirl (°)	0	Station 3 Compressor Exit		0.2	
% Efficiency change/% Tip clearance	2	Station 4 Burner Exit		0.2	
Ambient	Altitude (km/ft.)	0		Station 45 FPT Inlet	0.4
	TAS (knot/Mach)	0		Station 6 Turbine Exit Duct Exit	0.2
	Conditions	ISA			

Table 4-1 Summary of Fixed Input Parameters

Table 4-1 Summary of Fixed Input Parameters provides a tabular view of all constant inputs for design point aero-thermodynamic calculation. Parameters proprietary to Axial-Centrifugal Compressor only, to Installation Effects only, and to carpet plot without turbine design only are highlighted in orange, green, and blue respectively. Effects of small variation of these parameters on engine performance will be discussed in Section 6 Cycle Summary.

¹ Parameters marked green are for Installation Effects only.

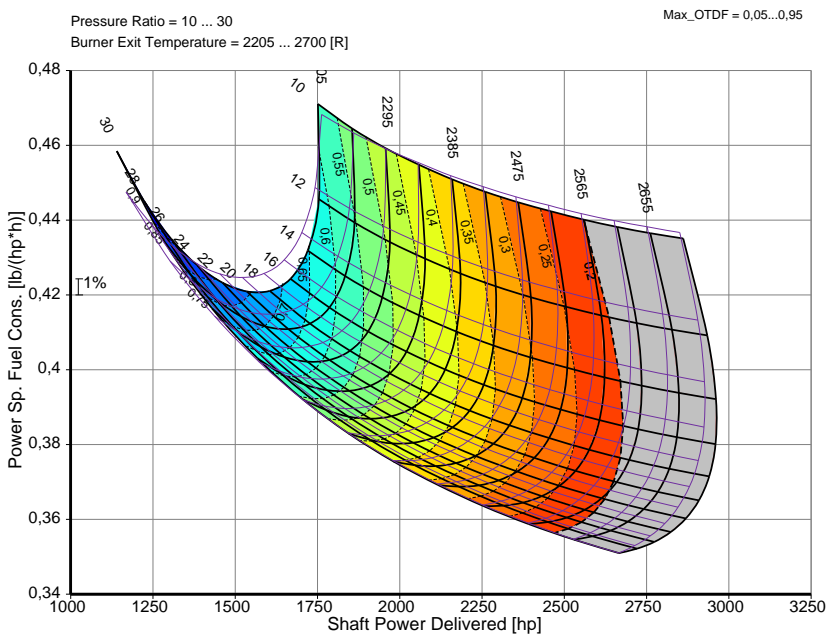
² Parameters marked blue are for conventional carpet plot without turbine design only.

Parameters to be studied in following sections as well as their constraints include:

- | | |
|-----------------------------------|--|
| 1. Overall PR | Constraints: engine length and weight |
| 2. Axial Compressor PR | Per Figure 4-5 Axial Compressors: Pressure Ratio Versus Number of Stages |
| 3. Centrifugal Compressor PR | Constraints: no more than 9:1 for a single stage |
| 4. T4, namely COT | Constraints: OTDF larger than 20% |
| 5. Inlet corrected mass flow rate | To be calculated per power requirements in Section 5.7 Engine Sizing. |

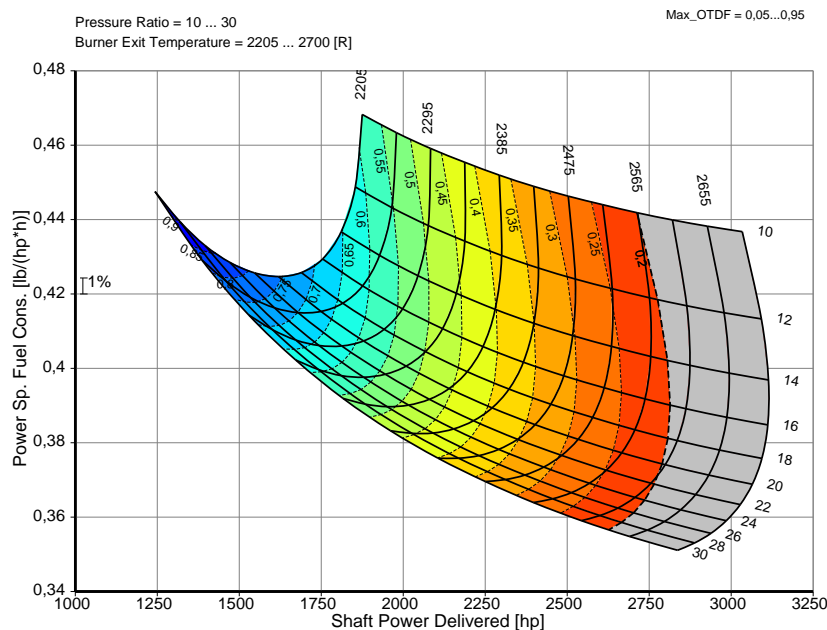
4.3. Carpet Plotting, Diagramming & Cycle Optimization

In this section, critical cycle parameters are studied through carpet plot, diagramming and other optimization methodologies. During this process, no installation effects are included, since the baseline engine performance summary at design point didn't covered the



Carpet Plot 1 (Maximum OTDF) Metadata

- The plot above is using turbine design code, while the plot below is using turbine polytropic efficiency
- Variable 1 = Overall PR
Start: Step: End = 10:2:30
- Variable 2 = COT
Start: Step: End =
2205°R:45°R:2700°R
- Contour: Maximum OTDF¹ allowed
- Constraint: Maximum OTDF ≥ 0.2
- The carpet plot below is overlaid in magenta on top of the carpet plot above



¹ Maximum OTDF is calculated as

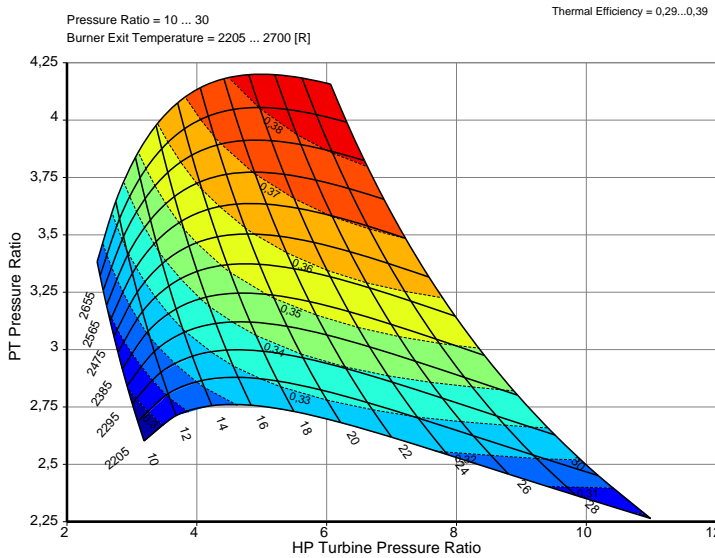
$$Max_OTDF = \frac{1316^{\circ}C - T4}{T4 - T3}$$

$$Max_OTDF = \frac{2400^{\circ}F - T4}{T4 - T3}$$

Where, 1316°C/2400°F is the highest working temperature of turbine material

Figure 4-13 Carpet Plot 1 (Maximum OTDF)

airframe influences when provided in the RFP. Therefore, zero inlet loss, no power offtake, and absence of customer bleed are considered when carpet plotting for design point analysis, as were in the engine summary table from Request for Proposal (AIAA, 2016).



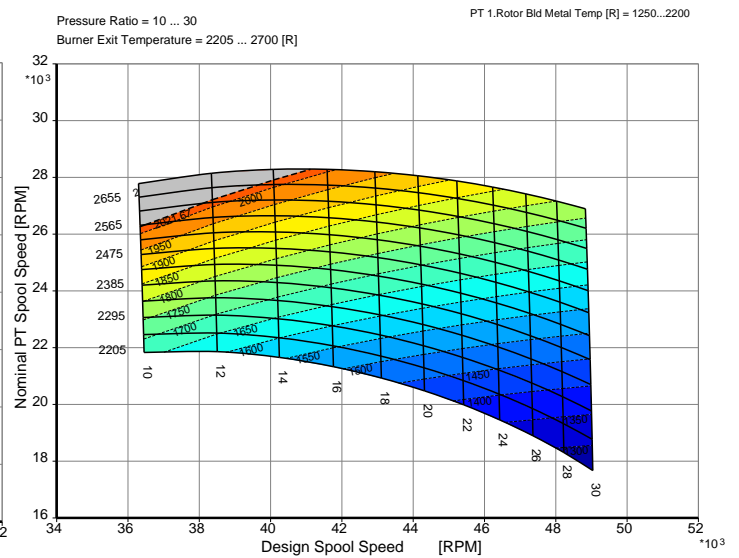
Carpet Plot 2 (Thermal Efficiency) has same variables and ranges as Figure 4-13. Contour: Thermal Efficiency. No constraint is applied when plotting.

Figure 4-15 Carpet Plot 2 (Thermal Efficiency)

From Figure 4-13 Carpet Plot 1 (Maximum OTDF), it is easy to detect the limiting effect of OTDF on COT. When acceptable OTDF is necessary at all operating conditions of various engine PRs, the highest COT usable is restricted to around 1425K/2565°R, which provides reasonable tolerance to manufacturing errors and engine deterioration. In the retrospect, Figure 4-15 Carpet Plot 2 (Thermal Efficiency) provides the insight that, when pursuing higher engine thermal efficiency, designers should push the operating point as much as possible to the top right corner, where both elevated COT and increased PR are being indicated. Furthermore, this carplot plot also demonstrate that GGT PR is more directly affected by the compressor PR and less sensitive to COT, while FPT PR is a function of both variables. Commonly, the PR upper limit of a highly loaded single-stage turbine is around 4. Thus, the highest PRs on the plot, around 4.2 and 11 for GGT and FPT respectively, are both achievable from 2 stages of GGT and 3 stages of FPT.

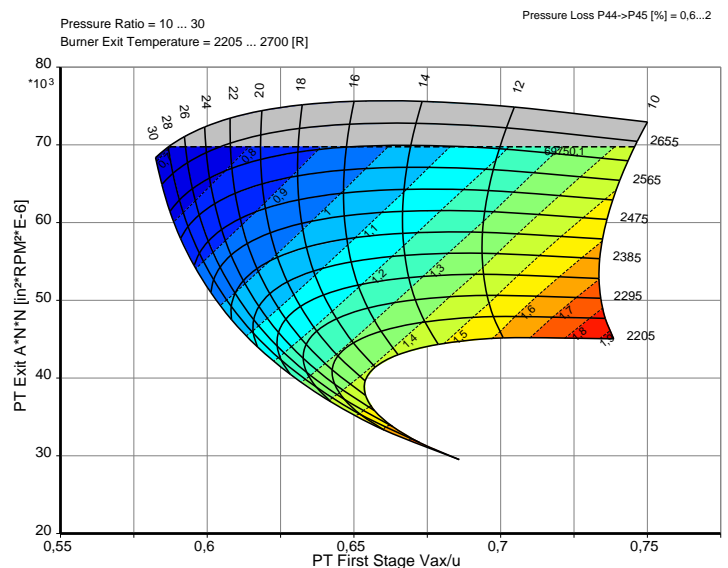
Figure 4-16 Carpet Plot 3 (FPT 1st Rotor Metal Temperature)

presents variations of GGT spool speed, FPT spool speed, and FPT 1st Rotor Metal Temperature with PR and COT. This plot shows no correlation between GGT spool speed and COT. Although FPT spool speed changes with both PR and COT, GGT spool speed is purely a function of PR. Moreover, the constraint on FPT metal temperature only limits a small area of design space at the upper left



Carpet Plot 3 (FPT 1st Rotor Metal Temperature) has same variables and ranges as Figure 4-13. Contour: FPT 1st Rotor Metal Temperature. Constraint: FPT 1st Rotor Metal Temperature $\leq 850^{\circ}\text{C}$.

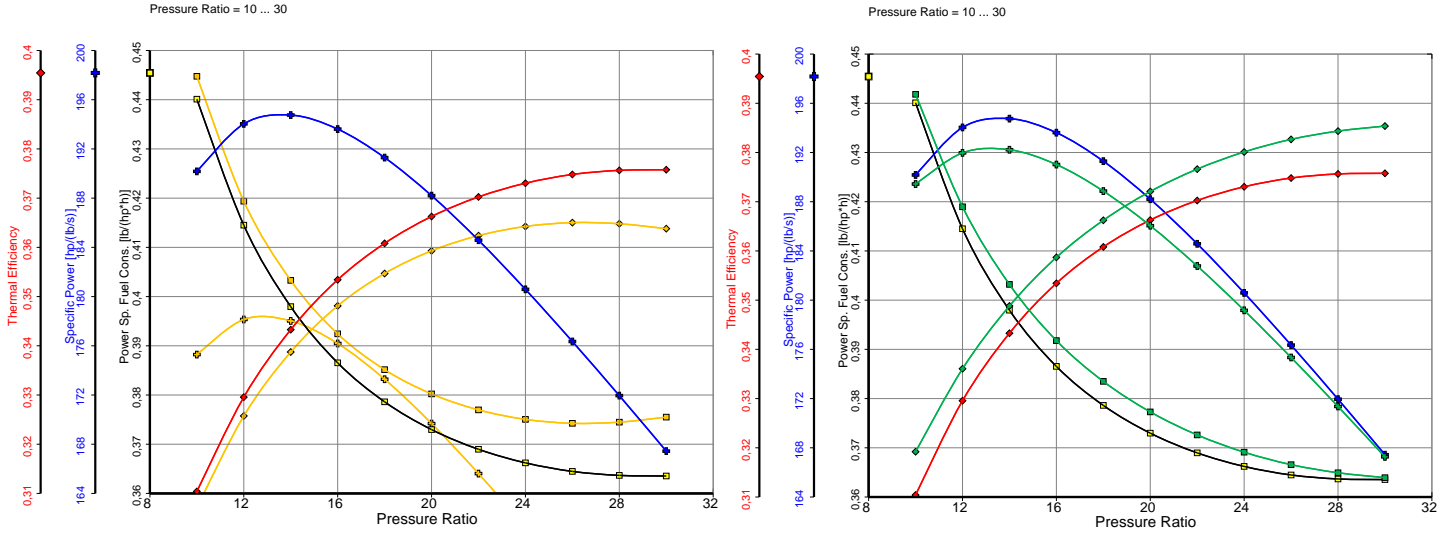
Figure 4-16 Carpet Plot 3 (FPT 1st Rotor Metal Temperature)



Carpet Plot 4 (Turbine Inter-Duct Pressure Loss) has same variables and ranges as Figure 4-13. Contour: Turbine Inter-Duct Percentage Pressure Loss. Constraint: Last Stage FPT $AN^2 \leq 45 \times 10^6 \text{rpm}^2 \text{m}^2$.

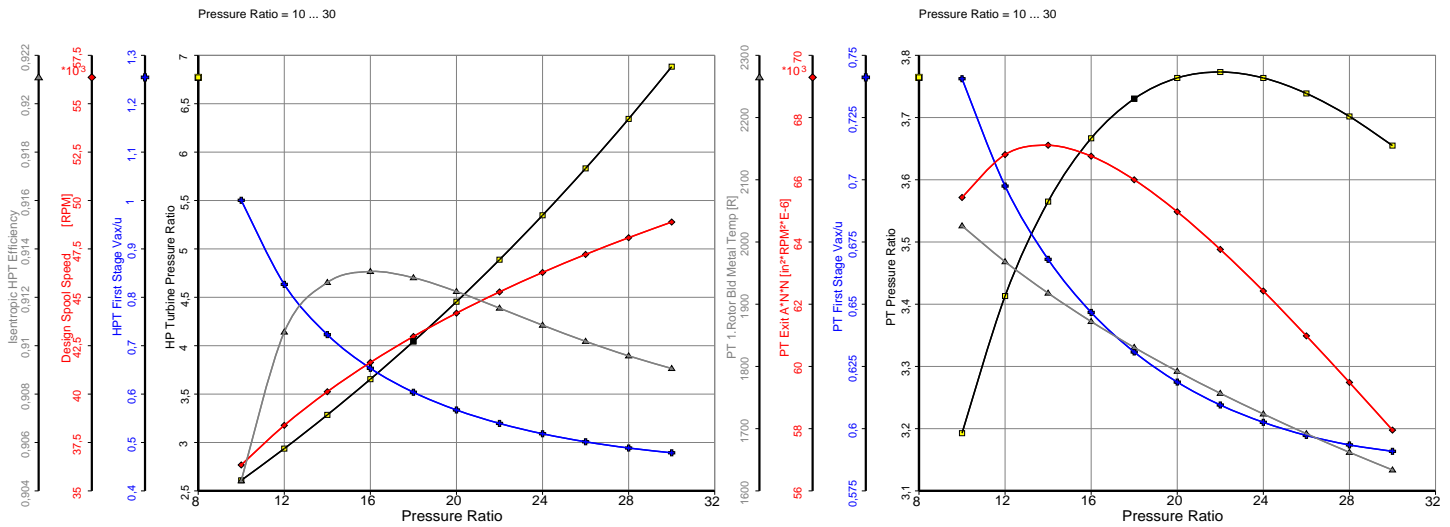
Figure 4-14 Carpet Plot 4 (Turbine Inter-Duct Pressure Loss)

corner. On the other hand, Figure 4-14 Carpet Plot 4 (Turbine Inter-Duct Pressure Loss) demonstrates the relationship between, FPT first stage flow coefficient, FPT last stage AN^2 , inter-turbine duct pressure loss and PR, COT. FPT last stage AN^2 is purely a function of FPT spool speed, while inter-turbine duct pressure loss is only related to duct Mach number. From the plot, both FPT first stage flow coefficient (below 0.75) and inter-turbine duct pressure loss (below 2%) are satisfactory on all design spaces. Thus, no constraints were applied to them. Nevertheless, the highest value for FPT last stage AN^2 approaches $50 \times 10^6 rpm^2 m^2$ on the high COT end. Therefore, a constraint was put on to limit its blade stress.



- Red, blue, green, and black lines are plotted for $COT = 1425K/2565^\circ R$; Overall PR: Start: Step: End=10:2:30
- Orange lines are plotted for $COT = 1375K$. Green lines are plotted for not using turbine design. They are overlaid for comparative purpose.

Figure 4-17 Variation of Pressure Ratio on Overall Performance



- $COT = 1425K/2565^\circ R$; Overall PR: Start: Step: End=10:2:30. Left Plot is for GGT, while the right plot is for FPT.

Figure 4-18 Variation of Pressure Ratio on Turbine Performance

Synthesizing all considerations and constraints above, the COT is preliminarily selected as $2565^\circ R/1425K$, the highest available. Under this COT, the effect of PR variation is studied in Figure 4-17 Variation of Pressure Ratio on Overall Performance. Here, at a constant COT of $2565^\circ R$, PRs ranging from 10 to 30 are studied versus Power SFC, Specific Power, and Thermal Efficiency. In parallel with the main plotting using turbine design code for $COT=2565^\circ R$, a secondary plot for $COT=2475^\circ R/1375K$ is overlaid on top in orange, as well as a third plot without turbine design overlaid in green. Conspicuously from the plotting, $90^\circ R$ of decrease in COT has a detrimental effect on specific power, as evidenced by the dramatic downward shifting of blue line when COT lowered slightly from

2565°R to 2475°R. Additionally, higher COT also gently improves SFC and Thermal Efficiency, since with increased cycle energy, percentage loss decreases when absolute losses remain relatively unchanged.

Besides the study on engine overall performance, effect of overall PR on turbine performance is also plotted in Figure 4-18 Variation of Pressure Ratio on Turbine Performance. Evidently from the diagram, flow coefficients for both GGT and FPT decrease with overall PR, though only the spool speed and PR for GGT is positively correlated with it. For FPT, the higher the PR, the lower the blade metal temperature. Although, the GGT isentropic efficiency reaches top as PR is around 16, this is the region where undesired FPT AN^2 is encountered. Furthermore, the FPT PR approaches the highest at overall PR of around 22. However, plot on the turbine performance does not provide insight into engine cycle. Thus, for determination of PR, Figure 4-17 Variation of Pressure Ratio on Overall Performance needs to be again referred to.

A second phenomenon obvious from Figure 4-17 Variation of Pressure Ratio on Overall Performance is that optimum PR for SFC deviates tremendously from optimum PR for Specific Power. Meanwhile, the usage of turbine design code significantly reduces the optimum PR for minimum SFC, though the optimum PRs for max specific power remains similar for using and not using turbine design code. Therefore, Random Search Methods (Rao, 2009) is exploited for numerically solving the above-mentioned two optimum PRs, and its computation results are presented in tabular form in Table 4-2 Optimum PRs for min SFC & max Specific Power. Clearly, turbine design avoids the overestimated optimum PR of 32.7 for minimum SFC. However, for the turboprop/turboshaft engines, unlike the transport and fighter applications, it is more difficult to focus on any one performance attribute as a design driver. The pursuit of improved fuel consumption has rather more importance and low SFC may be a cardinal point requirement in roles where long endurance is a major factor. But in most applications, endurance and low SFC are not critical issues. Thus, the design will not necessarily be optimized around minimum SFC. (Philpot, 1992)

COT = 1425K/2565°R	Using Turbine Design Code		Without Turbine Design	
	Optimum PR for Minimum SFC	Optimum PR for Max Specific Power	Optimum PR for Minimum SFC	Optimum PR for Max Specific Power
PR	29.3931	13.6592	32.6716	13.2511
Power SFC (kg/(kW · h))	0.221117	0.243523	0.221095	0.248473
Specific Power (kW/(kg/s))	277.538	320.225	265.792	316.194
Power SFC (lb/(hp · h))	0.363513	0.400349	0.363478	0.408486
Specific Power (hp/lb/s)	168.820	194.786	161.675	192.334

Table 4-2 Optimum PRs for min SFC & max Specific Power³

Therefore, flexibility is given to the designer when deciding the PR for turboprop engine under given COT. Final decision should be a compromise between the two PRs listed in Table 4-2 Optimum PRs for min SFC & max Specific Power, which regards both reduction in SFC and improvement in Specific Power. Again, customer requirement is referred to for generating the criteria for PR optimization. As per RFP, candidate engines should have an improved fuel burn of at least 20% and should have a power output 25% greater than the baseline (AIAA, 2016). This means the customer has a slightly higher emphasis on power than on SFC, and the degree of biasing

³ Results in this table are not reproducible because of the use of Random Search Methods.

towards power enhancement over fuel burn lessening is approximately following the mathematical ratio of 25%:20% = 5:4. Consequently, the following mathematical criteria is generated for performing final PR optimization:

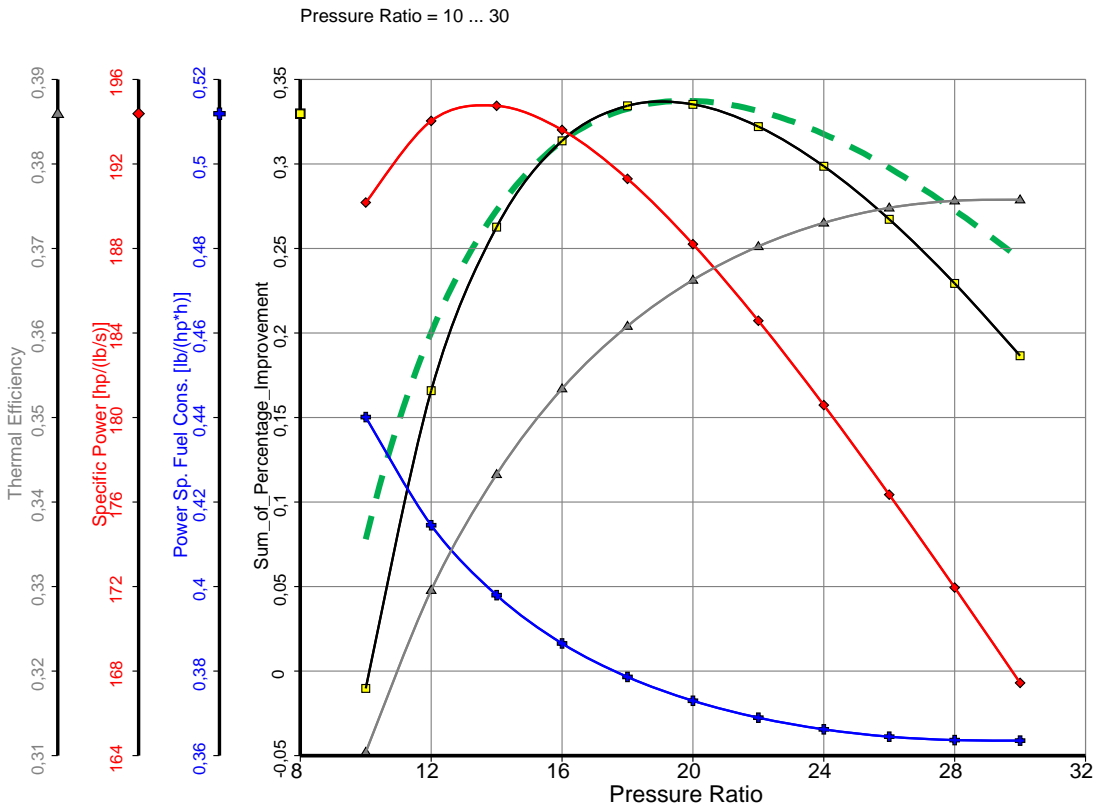


Figure 4-19 Metadata

- $Sum_{\%imp.}$ is labeled as **Sum_of_Percentage_Improvement** along the vertical axis.
- $COT = 1425K/2565^{\circ}R$
- Overall PR range is the same as Figure 4-17.
- $Sum_{\%imp.}$ for not using turbine design code is overlaid in dashed green line on top.

Figure 4-19 Sum of Percentage Improvement

$$Sum_{\%imp.} = 25\% \times \frac{Sp.Pwr_{Tg.PR} - Sp.Pwr_{Opt.PR_{SFC}}}{Sp.Pwr_{Opt.PR_{Sp.Pwr}} - Sp.Pwr_{Opt.PR_{SFC}}} + 20\% \times \frac{SFC_{Tg.PR} - SFC_{Opt.PR_{Sp.Pwr}}}{SFC_{Opt.PR_{SFC}} - SFC_{Opt.PR_{Sp.Pwr}}}$$

Where,

- $Sum_{\%imp.}$ — Sum of percentage improvement.
- $Sp.Pwr$ — Specific Power.
- $Tg.PR$ — Target PR.
- $Opt.PR_{SFC}$ — Optimum PR for Minimum SFC.
- $Opt.PR_{Sp.Pwr}$ — Optimum PR for Max Specific Power.
- To achieve the optimum engine performance, $Sum_{\%imp.}$ should be maximized.

COT = 1425K/2565°R		Result PR	SFC	Specific Power	Thermal Efficiency	$Sum_{\%imp.}$
Using Turbine Design Code	Search Result	19.0718	0.22832kg/(kW · h) 0.37536lb/(hp · h)	311.893kW/kg · s 189,717hp/(lb/s)	0.36394	0.336871
	Exchange Rate	+1	-0.68%	-0.86%	+0.69%	-0.56%
		-1	+0.80%	+0.78%	-0.80%	-0.64%
Not performing Turbine Design	Search Result	19.7858	0.229855 kg/(kW · h) 0.37788 lb/(hp · h)	306.402 kW/kg · s 186.377 hp/(lb/s)	0.36152	0.337439

Table 4-3 Optimum PR for maximum $Sum_{\%imp.}$

Next, the value of $Sum_{\%imp}$ is plotted in Figure 4-19 Sum of Percentage Improvement against Overall PR, where $Sum_{\%imp}$ is detected to have a single peak on the interval of PR 10 to 30. Thus, Random Search Methods was again used for searching the PR for maximum $Sum_{\%imp}$, whose result is demonstrated in Table 4-3 Optimum PR for maximum $Sum_{\%imp}$.

From the Table 4-3 Optimum PR for maximum $Sum_{\%imp}$, the result PR is 18.8. However, ± 1 change in PR causes only around 1% of change in corresponding Figure of Merits. Therefore, cycle PR is preliminarily chosen as 19, and may be altered within ± 1 when this number causes infinite decimal PRs for axial and centrifugal compressors when they are considered separately.

4.4. Summary of PR and COT Selections

In this section, following parameters are decided:

1. Overall PR = 19 ± 1
2. T4, namely COT = $1425K/2565^{\circ}R$

Parameters still need further studies includes: Axial & Centrifugal Compressor PR and Inlet corrected mass flow rate.

5. Constraint Analysis & Engine Sizing

To determine the inlet corrected mass flow rate of the engine, the power requirement of the aircraft need to be studied. Thus, characteristics of the next generation of Single-Engine Turboprop aircraft from RFP is referred to, where aircraft performance will be translated into its power-plant specifications. In addition to the power requirement of $1600hp$ at takeoff and $1300hp$ at cruise (AIAA, 2016), engines are usually also sized to meet airplane performances in the following categories (Roskam, 1985, p. 89):

- Takeoff distance
- Steady level flight speed at required attitude
- Climb rate
- Service ceiling
- Maximum speed

Per *Airplane Design I* (Roskam, 1985, p. 89), analyses to the above-listed performance constraints will result in the determination of power to weight ratio P/W , where value of wing loading W/S at takeoff can be directly calculated per maximum takeoff weight $W = 6,834 \text{ lbm}$ and wing area $S = 168.85 \text{ ft}^2$ (AIAA, 2016).

Configuration	C_{D0}	k	Drag Polar
Clean	0.020	0.073	$C_D = 0.020 + 0.073 \times C_L^2$
Takeoff gear up	0.035	0.077	$C_D = 0.035 + 0.077 \times C_L^2$
Takeoff gear down	0.055	0.083	$C_D = 0.055 + 0.083 \times C_L^2$
Landing gear up	0.080	0.083	$C_D = 0.080 + 0.083 \times C_L^2$
Landing gear down	0.100	0.083	$C_D = 0.100 + 0.083 \times C_L^2$

Table 5-1 Drag polar under different conditions

5.1. Drag Polar Estimation

The drag polar of an aircraft is directly linked to in-service thrust requirements. An accurate estimation of drag polar is essential for later processes. As preliminary approximation, it is sufficient to evaluate the drag polar per equation (Roskam, 1985, p. 118)

$$C_D = C_{D0} + k \times C_L^2$$

Where,

- C_D — Airplane drag polar
- C_{D0} — Zero-lift drag coefficient
- C_L — Lift coefficient

Using the methodologies demonstrated by Roskam (1985), the results of drag polar estimation under different conditions is presented in Table 5-1 Drag polar under different conditions.

Inputs	Values	Comments
l_p	5.75	(Roskam, 1985, p. 102)
N	1	Single Engine
ND_p^2/P_{TO}	30hp/ft ²	(Roskam, 1985, p. 102)
σ	1	ISA at SLS
ρ	0.0765lb/ft ³	1.225kg/m ³
S_{TOG}	1600ft	(Pilatus, 2002)
C_{D0}	0,02	Table 5-1
μ_G	0,025	(MIL-C-005011B, 1977)
C_{LmaxTO}	1.8 – 2.2	(Roskam, 1985, p. 107)

Table 5-2 Takeoff Constraint Parameters Input

5.2. Takeoff Constraints

Adapted from equation 3.9, *Airplane Design* (Roskam, 1985, p. 102), relationship between P/W and W/S during takeoff can be correlated through Formula 5-1 Takeoff Constraints.

$$\left(\frac{P}{W}\right)_{TO} = \frac{0.0376(W/S)_{TO}}{\rho \times S_{TOG} \times k} + \frac{0.72C_{D0}}{kC_{LmaxTO}} + \frac{\mu_G}{k}$$

Formula 5-1 Takeoff Constraints

Where,

- $(P/W)_{TO}$ — Takeoff power to weight ratio
- $k = l_p(\sigma ND_p^2/P_{TO})^{1/3}$, where
 - For constant speed propellers, $l_p = 5.75$ (Roskam, 1985, p. 102)
 - N — Number of engines; D_p — Diameter of propeller
 - Term ND_p^2/P_{TO} — Propeller disk loading
 - σ — Relative density
- $(W/S)_{TO}$ — Takeoff wing loading
- ρ — Density of air
- S_{TOG} — Takeoff ground run distance
- C_{D0} — Zero-lift drag coefficient
- μ_G — Ground friction coefficient
- C_{LmaxTO} — Maximum takeoff lift coefficient

The results with inputs from Table 5-2 Takeoff Constraint Parameters Input are plotted in Figure 5-2 Takeoff Distance Constraints.

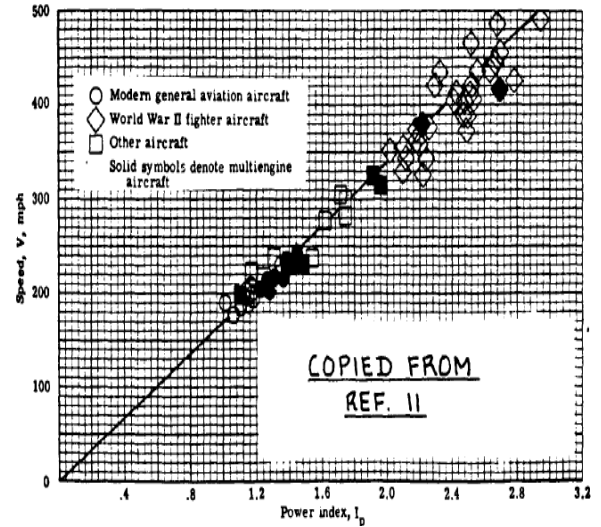


Figure 5-1 Finding Appropriate I_p (Roskam, 1985, p. 163)

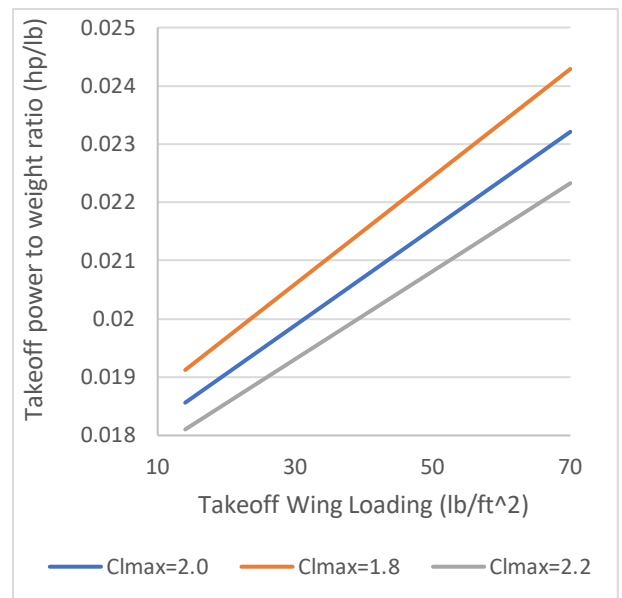


Figure 5-2 Takeoff Distance Constraints

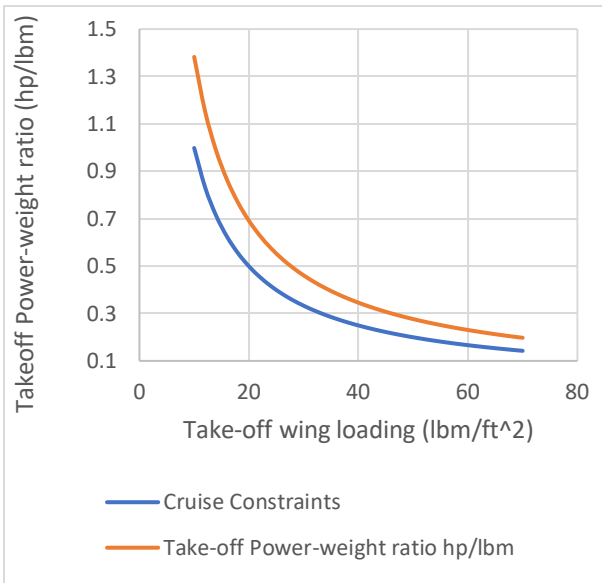


Figure 5-3 Cruise Constraints

5.3. Cruise Constraints

Under cruise condition, induced drag is relatively small comparing to profile drag. Therefore, the cruise speed can be assumed to be proportional to the Power Index $I_p = ((W/S)/\sigma(W/P))^{1/3}$. without much loss in accuracy (Loftin, 1980). Regression estimation of the relation between Power Index I_p and speed V during level flight is demonstrated in Figure 5-1 Finding Appropriate I_p . With the cruise condition set at 337 KTAS, 10,000ft (AIAA, 2016), relationship between $(P/W)_{TO}$ and $(W/S)_{TO}$ can be determined as presented in Figure 5-3 Cruise Constraints. Assumption was taken that for propeller driven airplanes, cruise power setting is at around 75 to 80 percent. (Roskam, 1985, p. 162) Thus, the altitude P/W to W/S relationship was subsequently converted into ground takeoff situation, and plotted in orange together with the 10,000ft condition in blue.

5.4. Maximum Speed Constraints

Maximum speed constraints can be interpreted as power capability at specific ambient condition. As per *Aircraft Engine Design* (Mattingly, 2002, p. 25), the relation between takeoff thrust to weight ratio and wing loading can be obtained from Formula 5-2 Relation Between Takeoff Thrust to Weight Ratio and Wing Loading.

$$\frac{T_{SL}}{W_{TO}} = \frac{\beta}{\alpha} \left\{ K_1 \frac{\beta}{\alpha} \left(\frac{W_{TO}}{S} \right) + K_2 + \frac{C_{D0} + C_{DR}}{\beta/q(W_{TO}/S)} \right\}$$

Formula 5-2 Relation Between Takeoff Thrust to Weight Ratio and Wing Loading

Where,

- α — Installed full throttle thrust lapse
- β — Remaining weight fraction
- K_1 & K_2 — Two coefficients in drag polar definition $C_D = K_1 C_L^2 + K_2 C_L + C_{D0}$
- q — Dynamic pressure

With the maximum speed given as 370KEAS in the RFP (AIAA, 2016), which represents 370knots at sea level, the result is presented in Figure 5-4 Maximum Speed Constraints with assumption of constant propulsion efficiency.

5.5. Climb Rate & Service Ceiling Constraints

In *Airplane Design Part I* (Roskam, 1985), service ceiling constraints and climb rate constraints are calculated interchangeably. Thus, necessary formulas for performing these calculations are summarized in Table 5-3 Formulas for Climb Rate & Service Ceiling Con-

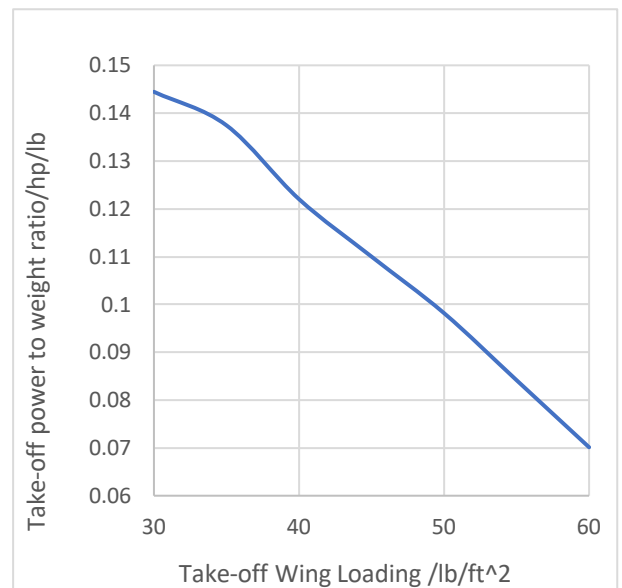


Figure 5-4 Maximum Speed Constraints

straints Calculation. Takeoff power to weight ratio W/P can be resolved through equating two RC_h values from the 2nd and 4th formulas respectively. This originates from the self-explanatory nature that climb rate at any given height h shouldn't have dual values. Therefore, different physical approaches ought to result in same mathematical outcome.

The current flight performance level of Pilatus PC-21 is that the aircraft can reach 10,000ft from sea level within 2min 35s. (Pilatus, 2002), while the service ceiling of next generation turboprop trainer is expected to achieve 38,000ft as stated in RFP (AIAA, 2016). Therefore, the constraints analysis results for both aspects are presented in Figure 5-5 Climb Rate & Service Ceiling Constraints.

Formula description	Formula	Remarks
1. Define Climb rate at sea level RC_0	$RC_0 = \left(\frac{h_{abs}}{t_{cl}}\right) \times \ln(1 - h/h_{abs})^{-1}$	RC_h : climb rate at any height h h_{abs} : absolute ceiling t_{cl} : time needed to climb to h from sea level
2. Calculate RC_h from RC_0	$RC_h = RC_0 \times \left(1 - \frac{h}{h_{abs}}\right)$	
3. Define rate of climb parameter RCP	$RCP = \eta_P / (W/P) - \left(\frac{(W/S)^{0.5}}{19\sigma^{0.5}(C_L^{1.5}/C_D)}\right)$	
4. Calculate RC_h from RCP	$RC_h = 33,000RCP$	

Table 5-3 Formulas for Climb Rate & Service Ceiling Constraints Calculation

5.6. Constraint Analysis Conclusion

The minimum $(P/W)_{TO}$ can be found by synthesizing all the constraints together as depicted in Figure 5-6 Constraint Analysis. The $(W/S)_{TO}$ has already been given in the RFP as $\frac{6,834 \text{ lb}}{168.85 \text{ ft}^2} = 40.47 \text{ lb/ft}^2$. Thus, the minimum aircraft $(P/W)_{TO}$ is chosen as 0.32, which matches to the black dot shown in the figure. This means a maximum power capability at sea level ISA of 2186.88hp which corresponds to a flat rating temperature of around 55°C/590°R, comparable to the flat rating temperature 62.8°C of the baseline PT6 engine family (Saravanamuttoo, Rogers, Cohen, & Straznicky, 2009, p. 523).

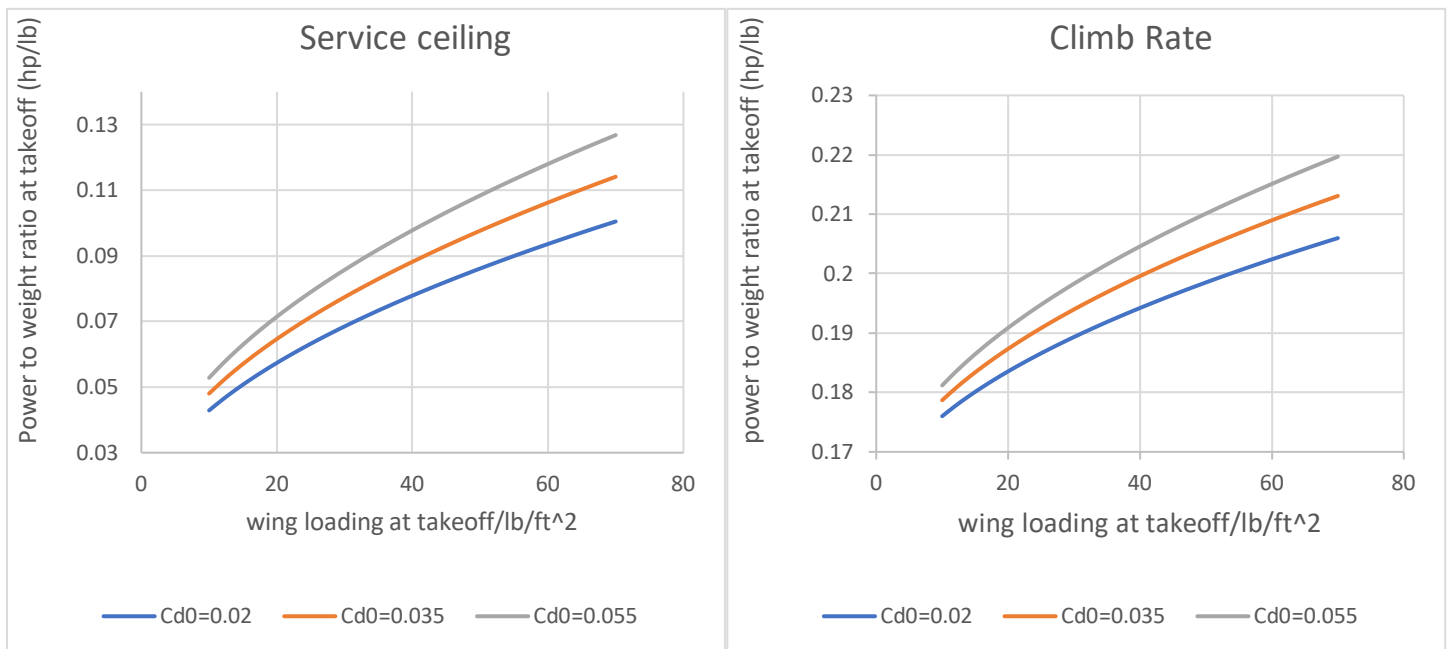


Figure 5-5 Climb Rate & Service Ceiling Constraints

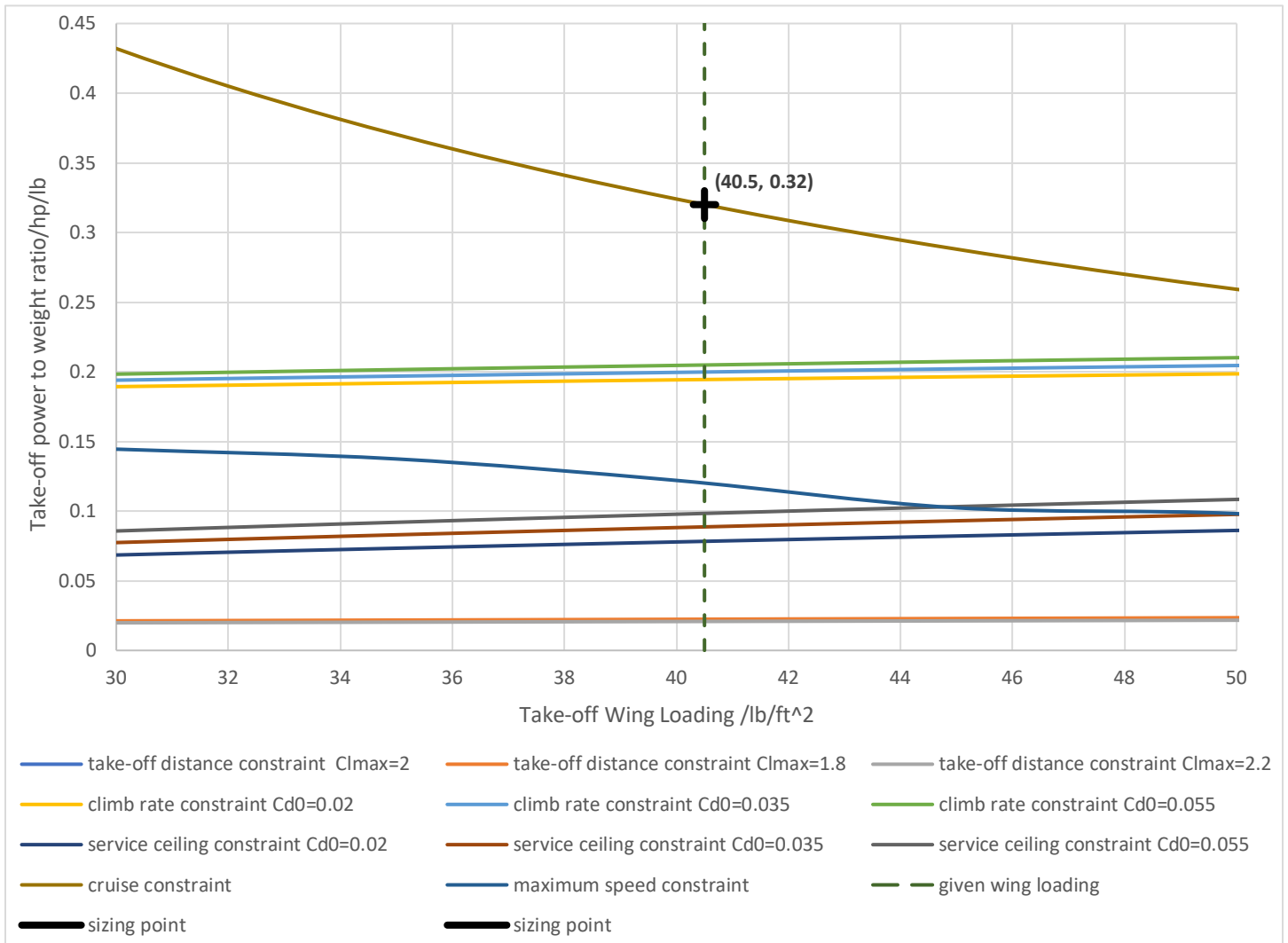


Figure 5-6 Constraint Analysis

5.7. Engine Sizing

With the ISA SLS power requirement determined, the inlet corrected mass flow rate of the engine can be calculated. During this phase of analysis, it is necessary to take all installation effects into consideration, including inlet pressure loss, shaft power offtake, and customer bleed. However, instead of being the same as engine design point, the customer bleed requirements are given as 7% of the inlet corrected flow under cruise condition. To solve the discrepancy of two different flight conditions between sea level takeoff and 10,000ft, 337KTAS, a proprietary algorithm as depicted in Figure 5-7 Algorithm for Determining Relative Bleed Air Enthalpy is employed for iteratively solving the relative enthalpy of bleeding air such that a bleed pressure of 32psi can be met in altitude.

During the computation, sample maps from NASA-SP-36 (Bullock & Johnsen, 1965, p. 366), NASA-TM-83655 (Stabe, Whitney, & Moffitt, 1984, p. 18), and ASME 96-GT-164 (Kurzke J. , 1996) was loaded for compressor, GGT, and FPT respectively. Maps are scaled using methods presented in *How to Get Component Maps for Aircraft Gas Turbine Performance Calculations* (Kurzke J. , 1996) with design point chosen at relative corrected spool speed $N_{corr,rel} = 1$; $\beta = 0.5$ for compressor and GGT, and the same spool speed however $\beta = 0.7$ for FPT (This auxiliary coordinate is named R value in the original NASA report). Under this input condition, the numeration demonstrates following results:

- Inlet Corrected Mass Flow Rate = 13.108lb/s

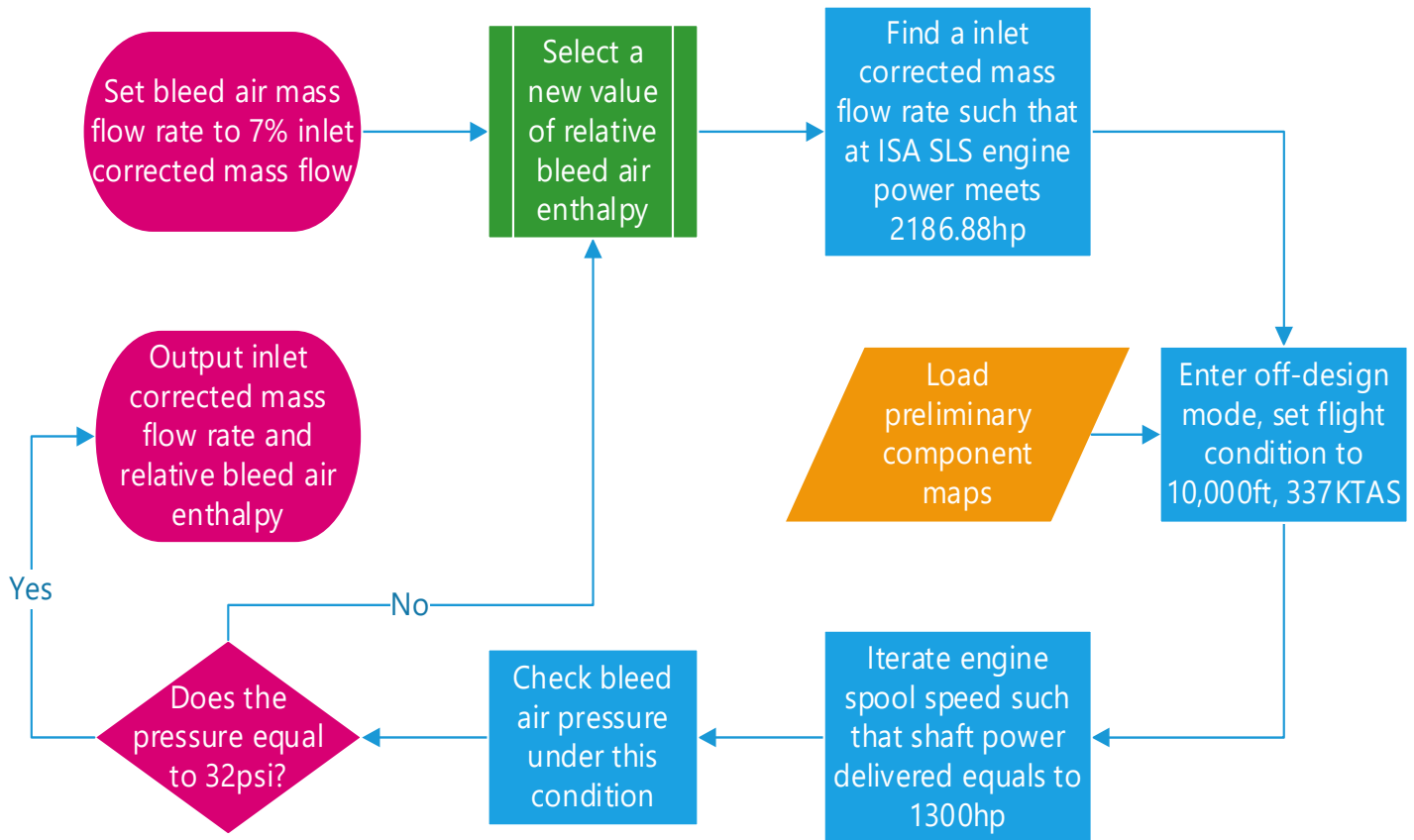


Figure 5-7 Algorithm for Determining Relative Bleed Air Enthalpy

- Corrected Mass Flow Rate at Station 2⁴ $W2_{corr} = 13.384 \text{ lb/s}$
- Relative Enthalpy of Bleed Air = 0.282155
- Relative Pressure of Bleed Air = 0.158586

This results in a relative gas generator spool speed equaling 0.8763, to produce a shaft power of 1300hp at 10,000ft, 337KTAS.

However, in real design, bleed valve can only be located in the vacant space between stages, and bleeding from mid-stage, either rotor or stator, is unrealistic. Thus, instead of having an infinite number of choices between 0 and 1 for relative bleed enthalpy, it could only have 4 to 5 inter-stage locations to choose from. Therefore, slightly larger parameters are chosen as follows for cycle summary table as well as detailed aerodynamic design.

- Relative Pressure of Bleed Air = 0.175
- Relative Enthalpy of Bleed Air = 0.311923
- Corrected Mass Flow Rate at Station 2 $W2_{corr} = 13.5 \text{ lb/s}$
- Inlet Corrected Mass Flow Rate = 13.221 lb/s

Next, engine cycle summary table is to be provided. This cluster of tables and diagrams cover information on GGT Velocity Triangle, GGT Geometry Data, FPT Velocity Triangle, FPT Geometry Data, Flow Station Summary Table, and Overall Engine Performance.

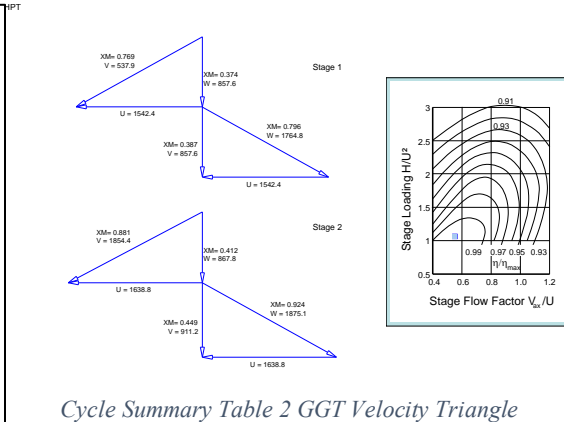
⁴ Refer to Figure 4-2 0-D Engine Model

Station	W lb/s	T R	P psia	WRstd lb/s	PWSD	=	2198,8 hp
amb		518,67	14,696				
1	13,221	518,67	14,696		PSFC =	0,39836	lb/(hp*h)
2	13,221	518,67	14,392	13,500	Heat Rate =	7427,6	BTU/(hp*h)
3	12,296	1318,02	273,454	1,053	V0 =	0,00	ft/s
31	12,163	1318,02	273,454		FN res =	289,64	lb
4	12,407	2565,00	266,618	1,521	WF =	0,24331	lb/s
41	12,407	2565,00	266,618	1,521	Therm Eff =	0,34293	
43	12,407	1869,60	59,657		P2/P1 =	0,97934	
44	12,407	1869,60	59,657		TRQ =	100,0	%
45	12,407	1869,60	59,197	5,848	P45/P44 =	0,99230	
49	12,407	1407,02	16,945		Incidence =	0,00000	°
5	12,539	1406,11	16,945	17,906	P6/P5 =	0,98000	
6	12,539	1406,11	16,606		PWX =	11	hp
8	12,539	1406,11	16,606	18,271	P8/Pamb =	1,13000	
Bleed	0,925	774,29	47,855		WBld/W2 =	0,07000	
					A8 =	81,39	in ²
					WCHN/W2 =	0,00000	
					WCHR/W2 =	0,00000	
					Loading =	100,00	%
					WCLN/W2 =	0,00000	
					WCLR/W2 =	0,00000	
					PW_gen =	2198,8	hp
					eta t-s =	0,84568	
Efficiencies:	isentrp	polytr	RNI	P/P			
Compressor	0,8260	0,8800	0,979	19,000			
Burner	0,9950		0,975				
HP Turbine	0,9107	0,8948	2,800	4,469			
LP Turbine	0,9261	0,9144	0,893	3,493			
Generator	1,0000						
HP Spool mech Eff	0,9950	Nom Spd	44188	rpm			
PT Spool mech Eff	0,9801	Nom Spd	25566	rpm			
hum [%]	war0	PHV	Fuel				
	0,0	0,00000	18638,0	JP-4			

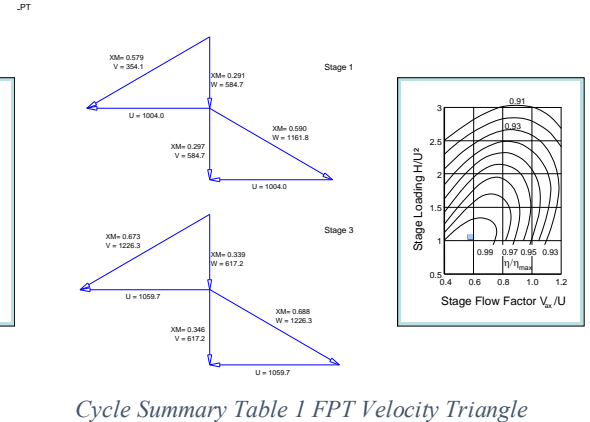
Cycle Summary Table 6 Overall Engine Performance

6. Cycle Summary

Four tables and two diagrams are presented as the cycle summary, including Cycle Summary Table 3 GGT Geometry Data, Cycle Summary Table 4 FPT Geometry Data, Cycle Summary Table 5 Flow Station Summary Table, Cycle Summary Table 1 FPT Velocity Triangle, Cycle Summary Table 2 GGT Velocity Triangle, Cycle Summary Table 6 Overall Engine Performance. Nomenclature on major outputs are provided in Table 6-2 Design Point Output Nomenclature. These data will serve as the cornerstone for turbomachinery aerodynamic detailed design in succeeding chapters. Note that turbine efficiencies, flow coefficients, and other outputs are grounded on the model of Stewart (1962), which is the theoretical base for NASA's preliminary turbine design code (Glassman J., 1972). During detailed aerodynamic design, different models are used. Thus, results may not be the same, however, won't deviate significantly.



Cycle Summary Table 2 GGT Velocity Triangle



Cycle Summary Table 1 FPT Velocity Triangle

Input:			
Number of Stages		2	
1. HPT Rotor Inlet Dia	in	8,00000	
Last HPT Rotor Exit Dia	in	8,50000	
HPT Exit Radius Ratio		0,80000	
HPT Vax.exit / Vax.average		1,05000	
HPT Loss Factor [0.3...0.4]		0,30000	
Interduct Reference Mach No.		0,40000	
Output:			
Isentropic HPT Efficiency		0,91075	
Polytropic HPT Efficiency		0,89478	
Thermodyn. HPT Efficiency		0,91075	
HPT Inlet Radius Ratio		0,92689	
HPT 1. Stator Exit Angle		62,09665	
HPT Exit Mach Number		0,45163	
HPT Exit Angle		-1,4091E-9	
HPT Last Rotor abs Inl Temp	R	2237,97	
HPT 1. Rotor rel Inl Temp	R	2401,49	
HPT First Stage H/T	BTU/(lb*R)	0,03946	
HPT First Stage Loading		1,06445	
HPT First Stage Vax/u		0,55602	
HPT Exit Tip Speed	ft/s	1820,94	
HPT Exit A*N*N	in ² *RPM ² *E-6	49243,44	
HPT 1.Rotor Bld Metal Temp	R	2401,49	

Cycle Summary Table 3 GGT Geometry Data

Input:			
Number of Stages		3	
With Exit Guide Vanes [0/1]		0,00000	
1. PT Rotor Inlet Dia	in	9,00000	
Last PT Rotor Exit Dia	in	9,50000	
PT Exit Radius Ratio		0,50000	
PT Vax.exit / Vax.average		1,00000	
PT Loss Factor [0.3...0.4]		0,30000	
Output:			
Ps5 / Pamb		1,06404	
Total-Static Efficiency		0,87891	
PT Inlet Radius Ratio		0,74968	
PT 1. Stator Exit Angle		59,78453	
PT Exit Mach Number		0,34767	
PT Exit Angle		-2,7716E-6	
PT Last Rotor abs Inl Temp	R	1568,53	
PT 1. Rotor rel Inl Temp	R	1796,39	
PT First Stage H/T	BTU/(lb*R)	0,00000	
PT First Stage Loading		1,05684	
PT First Stage Vax/u		0,58238	
PT Exit Tip Speed	ft/s	1338,61	
PT Exit A*N*N	in ² *RPM ² *E-6	61770,97	
PT 1.Rotor Bld Metal Temp	R	1796,39	
PT Torque	lb*ft	460,28603	

Cycle Summary Table 4 FPT Geometry Data

	Units	St 2	St 3	St 4	St 44	St 45	St 5	St 6	St 8
Mass Flow	lb/s	13,2211	12,2956	12,4067	12,4067	12,4067	12,5389	12,5389	12,5389
Total Temperature	R	518,67	1318,02	2565	1869,6	1869,6	1406,11	1406,11	1406,11
Static Temperature	R	493,933	1308,61	2549,77	1810,52	1822,95	1377,34	1396,47	1362,63
Total Pressure	psia	14,3923	273,454	266,618	59,6567	59,1972	16,9453	16,6064	16,6064
Static Pressure	psia	12,1326	266,137	259,792	52,2416	53,3268	15,6356	16,1676	14,6959
Velocity	ft/s	544,798	349,752	477,228	915,903	813,83	620,057	359,005	762,258
Area	in ²	52,7104	9,22246	13,6147	25,0495	27,8073	95,0518	160,972	81,3851
Mach Number		0,5	0,2	0,2	0,451629	0,4	0,347673	0,2	0,429567
Density	lb/ft ³	0,066298	0,548916	0,274969	0,07787	0,078946	0,030636	0,031244	0,029106
Spec Heat @ T	BTU/(lb*R)	0,240085	0,258741	0,29794	0,283153	0,283153	0,268956	0,268956	0,268956
Spec Heat @ Ts	BTU/(lb*R)	0,240006	0,258444	0,297694	0,28159	0,281919	0,267965	0,268624	0,267458
Enthalpy @ T	BTU/lb	-4,31598	193,647	552,342	349,907	349,907	221,712	221,712	221,712
Enthalpy @ Ts	BTU/lb	-10,2473	191,202	547,791	333,143	336,672	214,029	219,137	210,101
Entropy Function @ T		-0,11924	3,22671	6,0378	4,69813	4,69813	3,55095	3,55095	3,55095
Entropy Function @ Ts		-0,290041	3,19959	6,01187	4,5654	4,59369	3,47051	3,52417	3,42873
Exergy	BTU/lb	-0,742845	182,932	440,684	232,643	232,368	100,482	99,7628	99,7628
Isentropic Exponent		1,40007	1,36085	1,3004	1,32088	1,32088	1,34342	1,34342	1,34342
Gas Constant	BTU/(lb*R)	0,068607	0,068607	0,068615	0,068615	0,068615	0,068615	0,068615	0,068615
Fuel-Air-Ratio		0	0	0,020004	0,020004	0,020004	0,019788	0,019788	0,019788
Water-Air-Ratio		0	0	0	0	0	0	0	0

Cycle Summary Table 5 Flow Station Summary Table

		PWSD	SFC	PWSDq2	FN_res	eta_ther	eta_core	V8	PWeq	SFCeq	WF	e444isc	e444polc	Nrpm_GG	NPTrpm	P44d45q	PWX	t_c_T	
	UnitBasis	Delta %	%	%	%	%	%	%	%	%	%	%	%	%	%	%	%	%	
Polytr.Compr.Efficiency	0,88	-0,01	-2,94	+1,98	-2,94	-0,01	-1,94	-1,70	+0,01	-2,94	+1,98	-1,01	+0,02	-0,02	+0,88	-1,47	+14,1	-2,94	-3,11
1. HPT Rotor Inlet Dia	in 8	0,5	-0,27	+0,27	-0,27	+0,05	-0,27	-0,24	+0,05	-0,27	+0,27	+0,00	-0,21	-0,26	+0,00	+0,00	+1,2	+0,00	+0,00
Last HPT Rotor Exit Dia	in 8,5	-0,5	+0,04	-0,04	+0,04	-0,01	+0,04	+0,04	-0,01	+0,04	-0,04	+0,00	+0,03	+0,04	+2,97	+0,02	-0,27	+0,04	+13,6
HPT Exit Radius Ratio	0,8	0,5	-0,06	+0,06	-0,06	+0,01	-0,06	-0,05	+0,01	-0,06	+0,06	+0,00	-0,14	-0,17	+0,00	+0,00	-21,6	+0,00	+0,00
HPT Vax.exit / Vax.average	1,05	-0,5	-0,28	+0,29	-0,28	+0,05	-0,28	-0,25	+0,05	-0,28	+0,29	+0,00	+0,10	+0,12	+3,17	-0,14	+77,38	-0,28	-19,1
HPT Loss Factor [0.3...0.4]	0,3	0,01	-0,08	+0,08	-0,08	+0,01	-0,08	-0,07	+0,01	-0,08	+0,08	+0,00	+0,06	+0,08	+0,00	-0,04	+30,0	-0,08	-6,79
Number of HP Turbine Stages	2	-0,01	-0,01	+0,01	-0,01	+0,00	-0,01	-0,01	+0,00	-0,01	+0,01	+0,00	-0,10	-0,12	+0,00	-0,01	-21,43	-0,01	+6,6
Percentage HPT Tip Clearance	0,5	0,05	-0,14	+0,14	-0,14	+0,02	-0,14	-0,12	+0,02	-0,14	+0,14	+0,00	-0,11	-0,13	+0,00	+0,00	+0,45	+0,00	+0,00
1. PT Rotor Inlet Dia	in 9	0,5	-0,32	+0,32	-0,32	+0,05	-0,32	-0,28	+0,05	-0,32	+0,32	+0,00	-0,25	-0,30	+0,00	-0,16	+2,13	-0,32	-0,56
Last PT Rotor Exit Dia	in 9,5	1	+0,35	-0,35	+0,35	-0,06	+0,35	+0,31	-0,06	+0,35	-0,35	+0,00	+0,28	+0,34	-18,3	+0,18	-2,33	+0,35	-0,08
PT Exit Radius Ratio	0,5	0,5	-1,64	+1,67	-1,64	+0,28	-1,64	-1,46	+0,28	-1,64	+1,67	+0,00	-1,29	-1,55	+0,00	-0,82	+11,6	-1,64	+94,2
PT Vax.exit / Vax.average	1	0,5	-0,05	+0,05	-0,05	+0,01	-0,05	+0,00	+0,01	-0,05	+0,05	+0,00	+0,00	+0,00	+0,00	+0,00	+0,00	+0,00	+0,00
PT Loss Factor [0.3...0.4]	0,3	-0,5	+0,04	-0,04	+0,04	-0,01	+0,04	+0,00	-0,01	+0,04	-0,04	+0,00	+0,00	+0,00	+0,00	+2,72	+0,00	+0,04	+0,0
Number of PT Stages	3	0,5	-0,24	+0,24	-0,24	+0,04	-0,24	+0,00	+0,04	-0,24	+0,24	+0,00	+0,00	+0,00	+0,00	+0,00	+0,00	+0,00	+0,00
Burner Design Efficiency	0,995	-0,5	+0,09	-0,09	+0,09	-0,01	+0,09	+0,00	-0,01	+0,09	-0,09	+0,00	+0,00	+0,00	+0,00	+2,85	+0,00	+0,09	+0,0
Burner Pressure Ratio	0,975	0,1	-0,10	+0,10	-0,10	+0,02	-0,10	+0,00	+0,02	-0,10	+0,10	+0,00	+0,00	+0,00	+0,00	+0,00	+0,00	+0,00	+0,00
Intake Pressure Ratio	0,979341	-0,01	-0,04	+0,04	-0,04	+0,01	-0,04	+0,00	+0,01	-0,04	+0,04	+0,00	+0,00	+0,00	+0,00	-0,02	+0,00	-0,04	+0,0
Turbine Interduct Lambda	0,05	0,1	-0,16	+0,17	-0,16	+0,03	-0,16	+0,00	+0,03	-0,16	+0,17	+0,00	+0,00	+0,00	+0,00	-0,08	+0,00	-0,16	+0,00
Turbine Exit Duct Press Ratio	0,98	0,01	-0,24	+0,24	-0,24	+0,04	-0,24	+0,00	+0,04	-0,24	+0,24	+0,00	+0,00	+0,00	+0,00	-0,12	-0,01	-0,24	+0,00
Nozzle Thrust Coefficient	0,975	3	-1	-0,43	+0,43	-0,43	+0,07	-0,43	+0,00	+0,07	-0,43	+0,43	+0,00	+0,00	+0,00	+22,2	-0,01	-0,43	+0,00
Exhaust Pressure Ratio P8/Pamb	1,13	0,995	-0,01	+0,08	+0,94	+0,08	-0,93	-0,93	+0,01	+0,08	+0,94	+1,02	+0,00	+0,00	-0,01	+0,03	-0,06	+0,08	+0,03
Interduct Reference Mach No.	0,4	0,975	-0,01	-0,70	+0,70	-0,70	+0,12	-0,70	-0,62	+0,12	-0,70	+0,70	+0,00	+0,01	+0,02	+0,00	-0,35	+4,77	-0,70
Rel. HP Leakage to PT exit	0,01	0,979341	-0,01	-1,75	+0,74	-0,74	-0,90	-0,74	-0,63	+0,12	-1,75	+0,74	-1,02	-0,02	+0,00	-0,37	+0,11	-1,75	-0,03
HP Spool Mechanical Efficiency	0,995	0,05	-0,52	+0,53	-0,52	+0,09	-0,52	-0,46	+0,09	-0,52	+0,53	+0,00	+0,00	+0,00	+0,00	-0,26	+99,9	-0,52	+0,00
LP Spool Mechanical Efficiency	0,980075	0,98	-0,01	-0,70	+0,71	-0,70	+0,12	-0,70	+0,00	+0,12	-0,70	+0,71	+0,00	+0,00	+0,00	-0,35	-0,02	-0,70	+0,00
Percentage Power Extraction	0,005	0,975	0,01	+0,00	+0,00	+0,00	+1,03	+0,00	+0,00	+0,00	+0,00	+0,00	+0,00	+0,00	+0,00	+0,00	+0,00	+0,00	+0,00
Burner Exit Temperature	R 2565	1,13	0,01	-0,60	+0,61	-0,60	+3,59	-0,60	+0,00	+3,59	-0,60	+0,61	+0,00	+0,00	+0,00	-0,30	-0,01	-0,60	+0,00
Pressure Ratio	19	0,4	0,05	+0,10	-0,10	+0,10	-0,02	+0,10	+0,09	-0,02	+0,10	-0,10	+0,00	+0,00	+0,00	+0,05	-18,8	+0,10	+0,00
Relative Bleed Air Pressure	0,175	0,01	0,01	-2,88	+1,85	-2,88	-0,04	-1,82	-1,82	-0,02	-2,88	+1,85	-1,09	-0,02	-0,05	+0,54	-0,91	+3,34	-2,88
Inlet Corr. Flow W2Rstd	lb/s13,5	0,995	-0,01	-1,65	+1,67	-1,65	+0,01	-1,65	-1,51	+0,01	-1,65	+1,67	+0,00	+0,01	+0,50	-0,82	+7,75	-1,64	-1,78

Table 6-1 Design Point Exchange Rate

Physical Meaning	Term	Units
Shaft Power Delivered	PWSD	Hp
Power Sp. Fuel Cons.	SFC	lb/(hp*h)
Specific Power	PWSDq2	hp/(lb/s)
Residual Thrust	FN_res	lb
Thermal Efficiency	eta_ther	
Core Efficiency	eta_core	
Exhaust Flow Velocity V8	V8	ft/s
Equivalent Shaft Power	PWeq	hp
Equivalent SFC	SFCeq	lb/(hp*h)
Fuel Flow	WF	lb/s
Isentropic HPT Efficiency	e444isc	
Polytropic HPT Efficiency	e444polc	
Design Spool Speed [RPM]	Nrpm_GG	
Nominal PT Spool Speed [RPM]	NPTrpm	
Pressure Loss P44->P45 [%]	P44d45q	
Rel. Enthalpy of Overb. Bleed	h_bld	
Power Offtake	PWX	hp
HPT 1. Stage Tip Clear.	t_c_T	mil

Table 6-2 Design Point Output Nomenclature

Table 6-1 Design Point Exchange Rate provides insights on influence of input variations on engine performance. Critical information from the table includes that, certain amount of variation on turbine geometries, such as 0.5in changes on turbine in- & outlet diameters, produces acceptable level of fluctuation on power output, SFC, and specific power. Therefore, these given flexibilities will be used in turbomachinery preliminary design.

7. Aerodynamic Design of Turbomachinery

Since the shaft power engines are not necessarily optimized around minimum SFC, a consequence of this basic thermodynamics is that the SFC loop does not have the catenary shape of the jet engine. As the engine is throttled back, SFC rises continuously, the minimum normally being at the maximum power. Like the civil turbofan, the turboprop engines spend little time at maximum power and may be well throttled back for most of its duty cycle. Thus, there is advantage to the designer in allowing component efficiency to fall off at top power, in exchange for improved part power performance. This will have the effect of flattening out the curve slightly over the top part of the range. (Philpot, 1992)

Therefore, as relative Spool Speed at cruise is 0.8751 (previously calculated in Section 5.7 Engine Sizing), HP spool turbomachinery will be designed within a spool speed range of 37559.6 rpm (85% relative Spool Speed) to 39768.9 rpm (90% relative Spool Speed) based on the criteria of best isentropic total-to-total efficiency. Nominal FPT Spool Speed will be re-optimized for this part load condition after HPT design. During the selection process of various design possibilities, Cycle Design Point mass flow rate and pressure ratio will be rechecked using streamline calculation. The AxSTREAM code from SoftInWay Inc. is utilized for turbomachinery development. Since its core algorithm and standard profile are not published in its user manual, accuracy and precision of the design outcome will only be guaranteed by SoftInWay Inc. itself. In the following context, the condition of 100% spool speed will be called Cycle Design Point, while the condition of 87.51% spool speed will be called Turbine/Compressor/Turbomachinery Design Point.

7.1. Gas Generator Turbine Design

7.1.1. GGT Preliminary Design

During preliminary solution generation, AxSTREAM uses a quasi-random method to generate design points per boundary conditions. Therefore, following parameters are chosen as inputs, while parameters not mentioned are using AxSTREAM default:

- Working Fluid: Ideal Gas
 - Isentropic Exponent = 1.31957 Per off design cycle calculation
 - Gas Constant = 53.357597 Per off design cycle calculation
- Boundary Conditions:
 - Inlet total pressure = 200.663 psi Per off design cycle calculation
 - Inlet total temperature = 2301.41 °R Per off design cycle calculation
 - Total Pressure at outlet = 45.818 psi Per off design cycle calculation
 - Mass flow rate = 9.890 lb./s Per off design cycle calculation
 - Inlet flow angle = 0 axial degree No inlet pre-swirl
 - 37,559.6 rpm ≤ Shaft rotational speed ≤ 39,768.9 rpm 80% to 85% relative spool speed
- Constraints

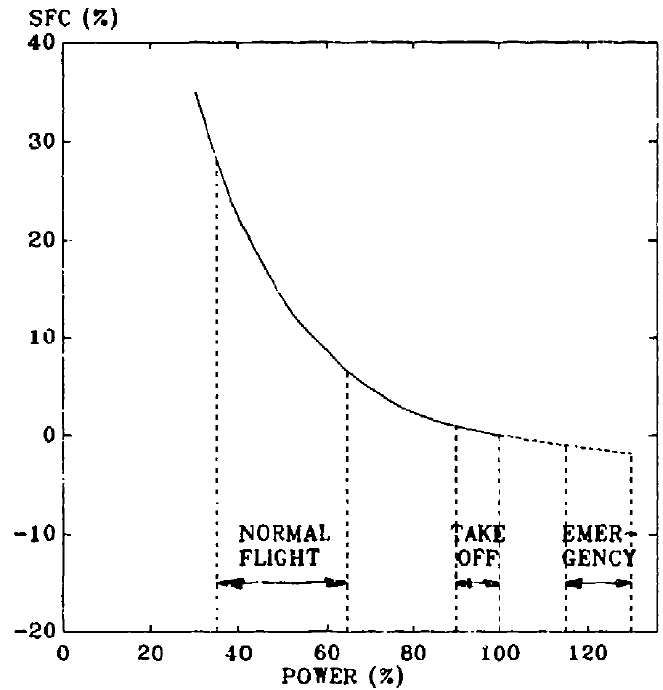


Figure 6-1 Typical Propeller Engine SFC Loop (Philpot, 1992)

- Number of Stages = 2
Per design point cycle calculation

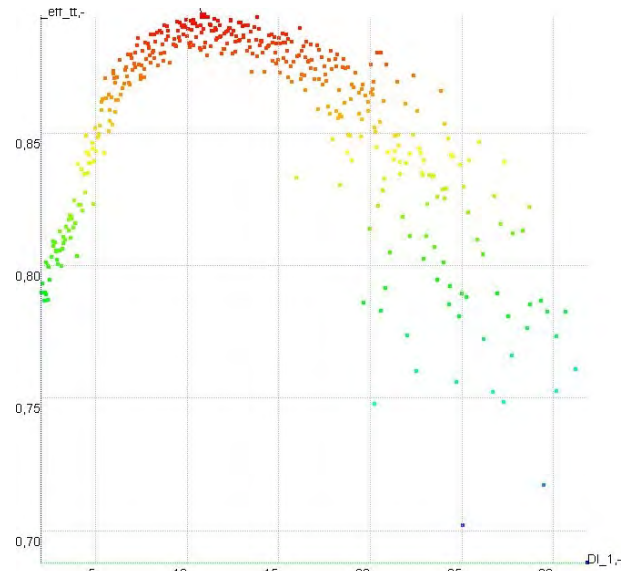
- Parameters

- $7.5 \leq \text{Mean Inlet Diameter} \leq 8.5$ in
The design point mean diameter is 8in, and the Cycle Exchange Table shows that ± 0.5 in of variation provides acceptable level of change in performance.
- $1 \leq \text{Rotor Mean Diameter Ratio (D2/D1)} \leq 1.2$
The largest GGT outlet diameter in the Cycle Exchange Table is 9in, while the minimum inlet diameter is 7.5in. this yields a Rotor Diameter Ratio of 1.2. Additionally, the outlet mean diameter should be no smaller than the inlet, or else extra difficulty will be posed on inter-turbine duct design.
- $5 \leq 1^{\text{st}} \text{ Stage Mean Diameter/Blade Height Ratio D/I1} \leq 25$

D/I1 is the Russian convention of describing blade hub-tip ratio. As per Figure 7-2 GGT Relationship between D/I1 and Efficiency, the D/I1 range of 5 to 25 yields highest concentration of high efficiency design options. In Cycle Summary Table, the hub-tip ratio of 0.92689 calculated from NASA's turbine design code corresponds to a D/I1 of 26.3563, and lower D/I1

represents lower hub-tip ratio, which is in turn satisfactory for increased flow capacity needed at Cycle Design Point.

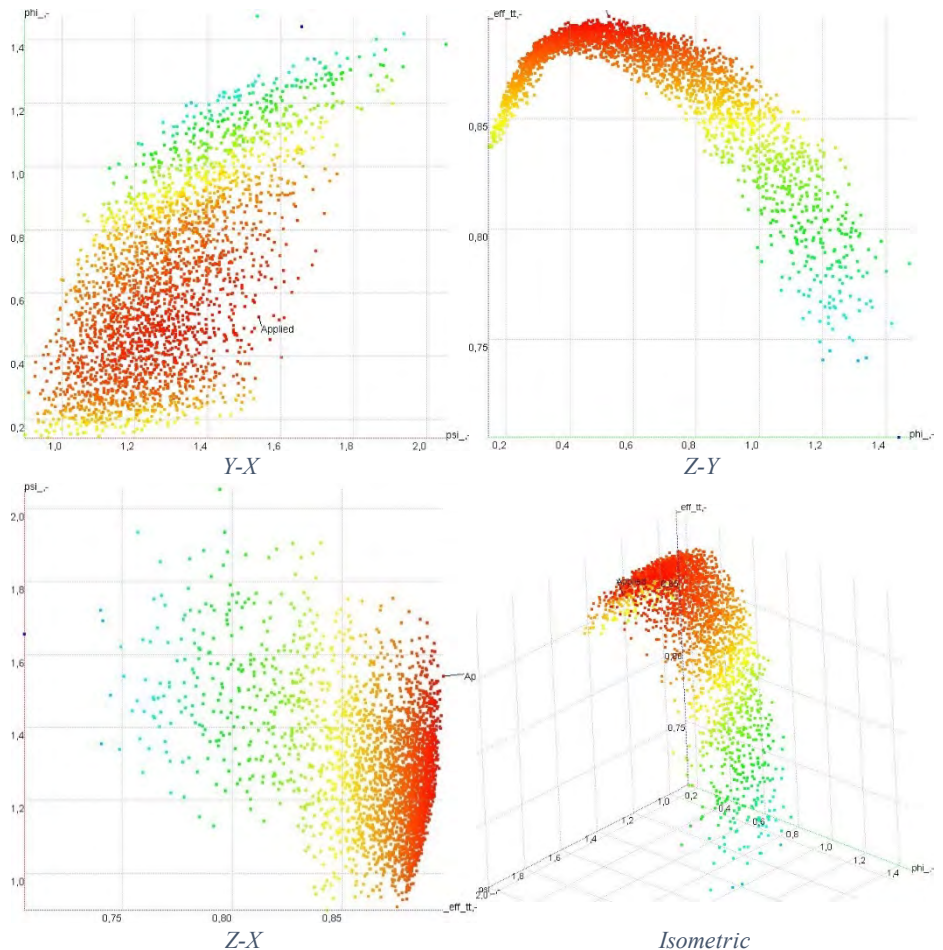
- $0.2 \leq \text{Hub Reaction} \leq 0.4$
The hub reaction for reaction turbines usually lies in the range of 20% - 40%. (SoftInWay)
- $0.45 \leq \text{Isentropic Velocity Ratio (u/C0)} \leq 0.7$
The isentropic velocities ratio range for reaction-type turbines usually is 0.45-0.7. (SoftInWay)
- Heat drop gradient $(H_z/H_1) = 1$
The heat drop gradient is used to control the heat drops distribution by stage. By default, the inverse task



Horizontal Axis: 1st Stage Mean Diameter/Blade Height Ratio D/I1

Vertical Axis: Internal Total-to-total Efficiency
Contour: Internal Total-to-total Efficiency

Figure 7-2 GGT Relationship between D/I1 and Efficiency



X — Stage Loading (psi); Y — Flow Coefficient (phi); Z — Total-to-total Efficiency

Figure 7-3 GGT Design Space

solver divides the overall heat drop equally between the stages (SoftInWay). Since the turbine to be designed has only two stages and the inlet and outlet blade height do not deviate too much, this default value is not changed.

- o $1.4 \leq \text{Meridional Velocity Gradient } (Cm_z/Cm_1) \leq 2.4$

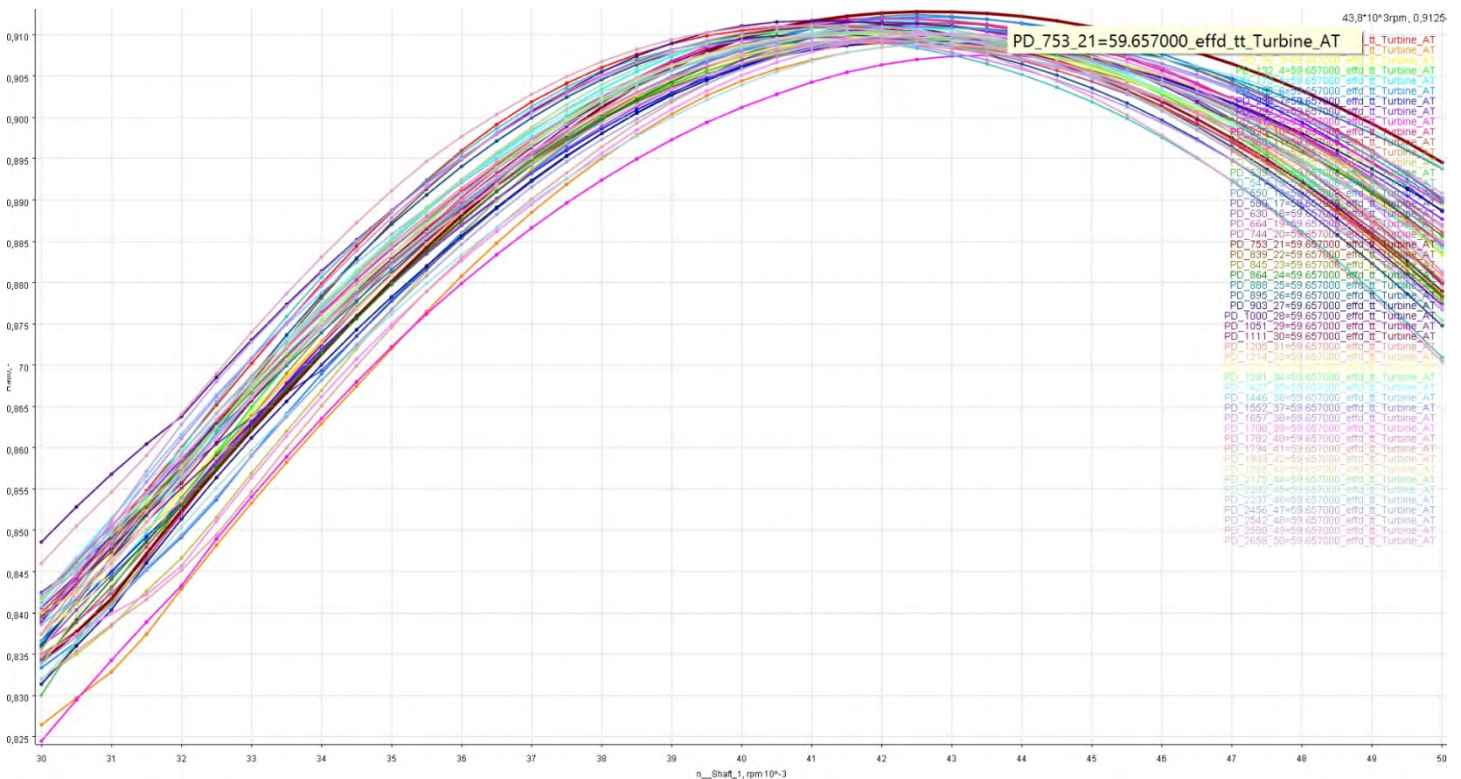
From the Cycle Summary Table the velocity ratio of Station 44 to Station 4 is 1.8830. Thus, around a flexibility of 0.5 for the meridional velocity gradient was given. This corresponds to a Mach number fluctuation of approximately 0.1 at Station 2.

Rotors and Stators are profiled using SoftInWay standard profiles SIW_R7N and SIW_R5B respectively.

7.1.2. GGT Design Space

Using the corresponding inputs, a design space with totally 2747 design options is generated as presented in Figure 7-3 GGT Design Space, where phi stands for average flow coefficient, psi represents average work coefficient, and eff_tt means isentropic total-to-total efficiency. Obviously from the diagram, both flow and work coefficient have optimum values for highest efficiency, while these two aerodynamics parameters are positively correlated themselves. The optimum value for flow coefficient matches the result of 0.55602 from NASA's preliminary turbine design code as listed in Cycle Summary Table.

After using Direct Problem Solver in AxSTREAM to validate all available solutions in the design space, a filtration for top 50 designs of highest internal total-to-total efficiency is applied. These 50 design points are imported to PD Map for streamline calculation of operational performance under Cycle Design Point, which is different from the condition that GGT is designed under. A plot of the efficiency versus spool speed for all 50 designs at Cycle Design Point is presented in Figure 7-4 GGT Efficiency versus Spool Speed



Shaft Speed (Horizontal Axis): 30,000rpm-50,000rpm; GGT Total-to-total Efficiency (Vertical Axis): 0.825-0.915

Figure 7-4 GGT Efficiency versus Spool Speed for 50 Optional Designs

for 50 Optional Designs. From the plot, it can be detected that Design Option 753, which corresponds to the highest blue line, provides optimum performance under Cycle Design Condition. Thus, this design point is chosen for S1 optimization and profiling.

7.1.3. Manual Adjustment of Meridional Flow Path

To ease the design of inter-turbine duct, certain level of increase of the mean diameter needs to be guaranteed, so that the outlet diameter of GGT and inlet diameter of FPT won't deviate significantly. Therefore, the flow path mean diameter is aligned using a straight line, such that the GGT outlet mean diameter is 0.5in larger than the inlet.

7.1.4. GGT S1 Optimization

To perform S1 Optimization in AxSTREAM, material properties are solicited by the software. Therefore, CMC mechanical characteristics listed in Table 7-1 CMC Mechanical Properties are taken from open literature and input into the AxSTREAM project grid.

Temperature (°C)	Elasticity modulus (GPa)	Linear expansion coefficient (10^{-6})	Yield strength limit (MPa)	Creep strength limit (MPa)	Long time strength limit (MPa)
20	410	1.4	250	220	215
600	400	5.3	250	160	215
1000	380	6.0	250	120	215
1200	350	6.0	250	100	215
Source	A. Michaux, C. Sauder, G. Camus, R. Pailler (2007)	A. Michaux, C. Sauder, G. Camus, R. Pailler (2007)	NASA Glenn Research Center (Bansal, 2005)	Vinayak Pandey (2000)	NASA Glenn Research Center (Bansal, 2005)

Table 7-1 CMC Mechanical Properties

Various safety factors are all using the AxSTREAM default, namely, 2 for blade yield strength Design Safety Factor, 2 for blade long-time Design Safety Factor, and 1.5 for blade creep strength Design Safety Factor. Target of optimization is set to minimizing chord length while maintaining a constant solidity of 1.333 for stators and 1.429 for rotors. This solidity value for stators and rotors is selected per SoftInWay recommendation (SoftInWay). During the optimization, vibration and structural constraints are also considered.

The optimization yields satisfactory results for both performance improvement and Margin Safety Factor Values. Blade numbers for all four rows of blades are 41, 88, 43, and 90 respectively from front to rear, while design spool speed is 39129.1955 rpm. This combination of blade numbers exhibits satisfaction in vibrational considerations.

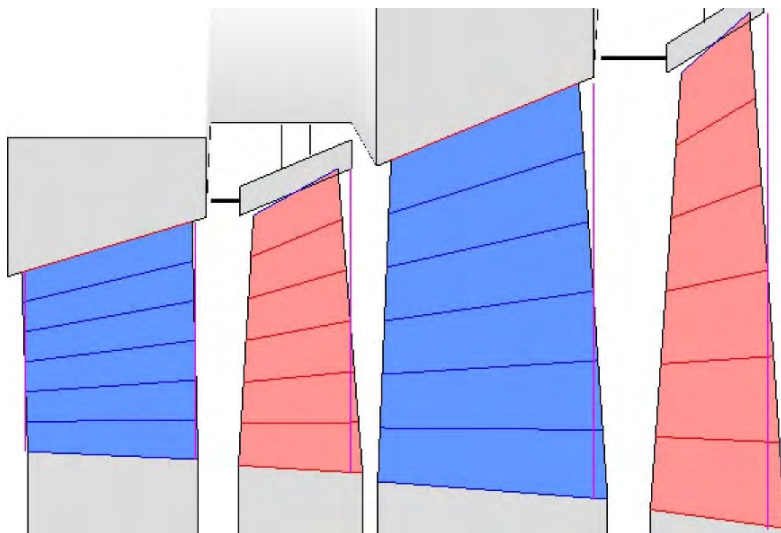


Figure 7-5 GGT Meridional Flow Path

Thus, the meridional flow path of the machine is frozen and presented as in Figure 7-5 GGT Meridional Flow Path. Additionally, information about temperature, pressure, Mach number, entropy, velocity, and flow path dimensions are provided in Figure 7-9 Miscellaneous GGT Meridional Flow Path Info. Note that these colored plots are generated purely using 7 sectional 2D streamline calculations. Thus, they are not as accurate as 3D CFD analyses due to the physical nature of streamline calculation method.

7.1.5. GGT Blade Twist Factors

After the determination of 2D meridional flow path geometry, it is necessary to set up the staking mode for nozzle and rotor profiles in the radial direction. Per SoftInWay recommendation (SoftInWay), both stators and rotating blades use profile centroid mode for staking, while Custom Side Profile mode is used. Next, discussions on twist factors are carried out. Twist Factor is defined in $B2g_i = \tan^{-1}(B2g_{\text{mean}}/r_i^m)$, where m — Twist factor; r_i — Section radius at tailing edge; $B2g_i$ — Gauging angle of i^{th} -section; $B2g_{\text{mean}}$ — Gauging angle of mean line (pitch) section (SoftInWay). In *Gas Turbine Theory*, a further description on effects of twist factors is provided, where a twist factor of -1 corresponds Free Vortex Blading, 0 corresponds Exponential, and 1 corresponds First Power (Saravanamuttoo, Rogers, Cohen, & Straznicky, 2009, p. 211). Therefore, an AxPLAN DoE test is made to study the influence of twist factors on overall total-to-total efficiency. During test, “minimized incidence” option in AxSTREAM direct problem solver is turned on. Results are plotted in Figure 7-6 Stage 1&2 Twist Factors versus GGT Efficiency.

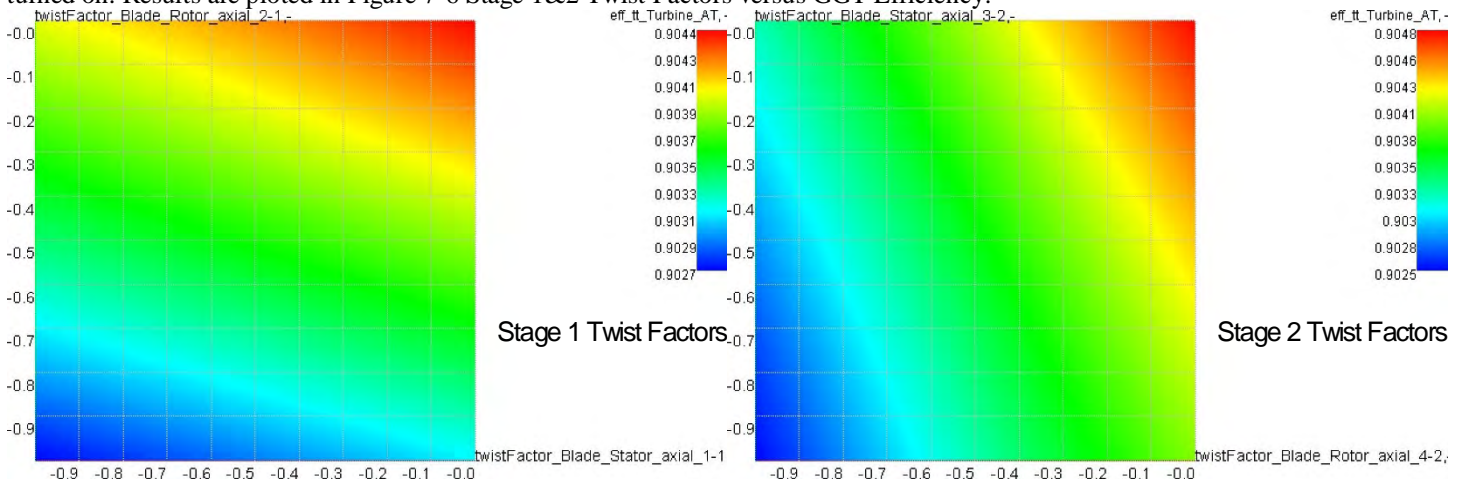


Figure 7-6 Stage 1&2 Twist Factors versus GGT Efficiency

For both stages, selecting twist factor as 0 for both rotor and stator provides the optimal outcome of total-to-total efficiency. Thus, values of twist factors of all 4 rows of blades is determined for further analysis.

7.1.6. GGT Streamline Analysis

Calculations of stream curves are evenly placed on 7 sections along the blade height, and the discrete numerical results are fitted using NURBS curves as illustrated in Figure 7-7 GGT Stream Curves. Moreover, the shapes of the velocity triangles at 3 different blade

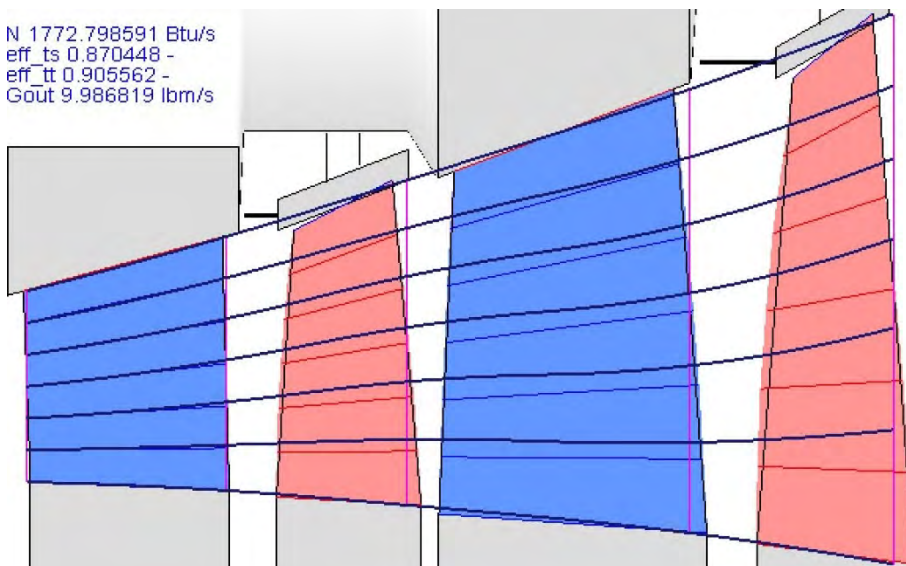
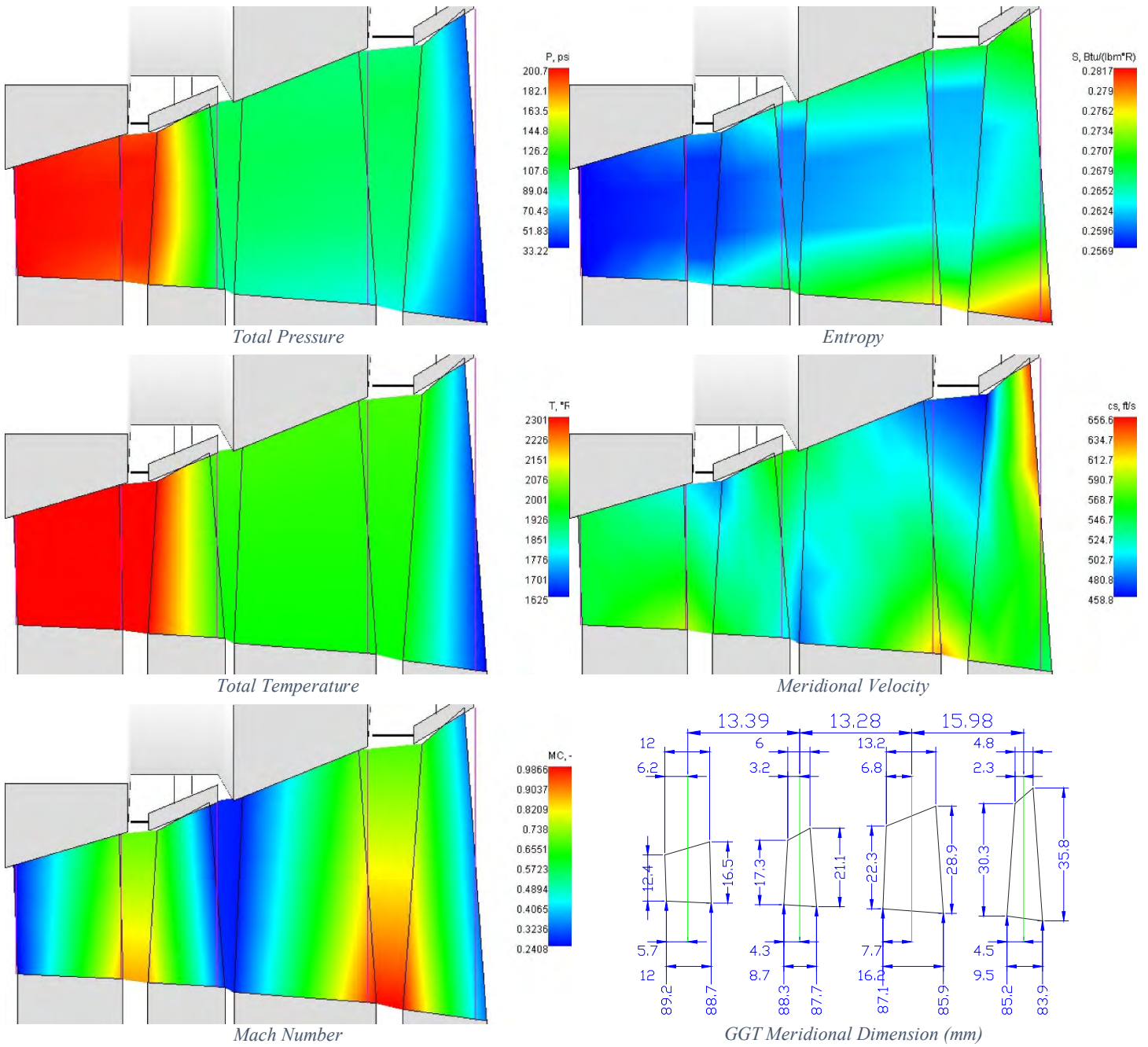


Figure 7-7 GGT Stream Curves

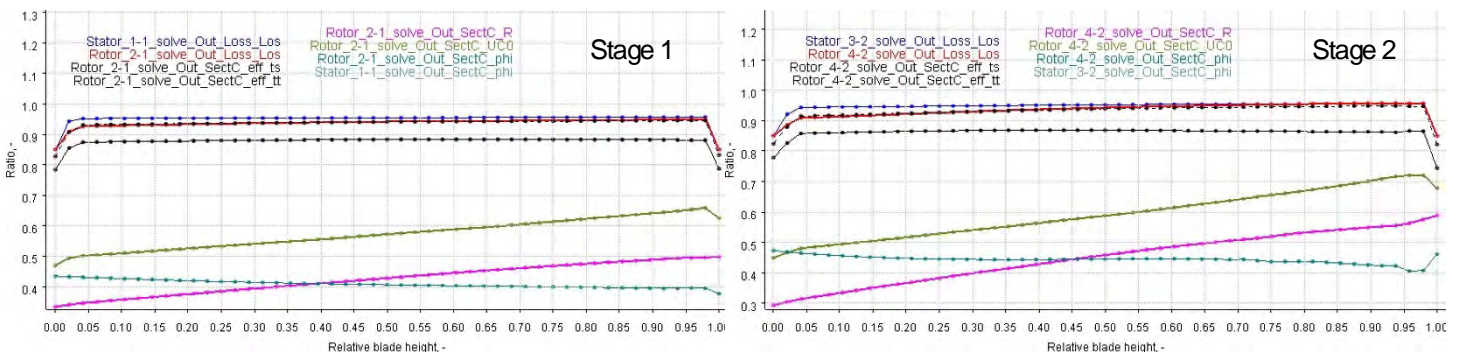
sections are provided in Figure 7-10 GGT Velocity Triangle at Hub, Mid, and Tip, while the variations of local efficiencies, degree of reaction, losses, and flow coefficient along the blade height for both stages are presented in Figure 7-8 Variation of Physical Properties along the Blade Height. From the plot, velocity triangles at all 3 sections demonstrate satisfactory shape with minimum outlet swirl, while the curve of loss variations along the blade height validates a less than 5% thickness of boundary layer for both locations near hub and



Results purely using Streamline Method. Difference between Streamline Method and CFD see Cumpsty (2004, pp. 93-131).

Figure 7-9 Miscellaneous GGT Meridional Flow Path Info

near casing. Degree of reaction along the blade increases from around 0.37 to 0.5 for both stages. Lowest reaction at the hub also lies within the recommended range of 0.2-0.4. Flow Coefficients for both stages are no larger than 0.6, which is also within the suggestion.



Nomenclature on the graph: R = Degree of Reaction; UC0 = Velocity Ratio; phi = Flow Coefficient; Los = losses; eff_ts =GGT Total-to-static Efficiency; eff_tt =GGT Total-to-total Efficiency

Figure 7-8 Variation of Physical Properties along the Blade Height

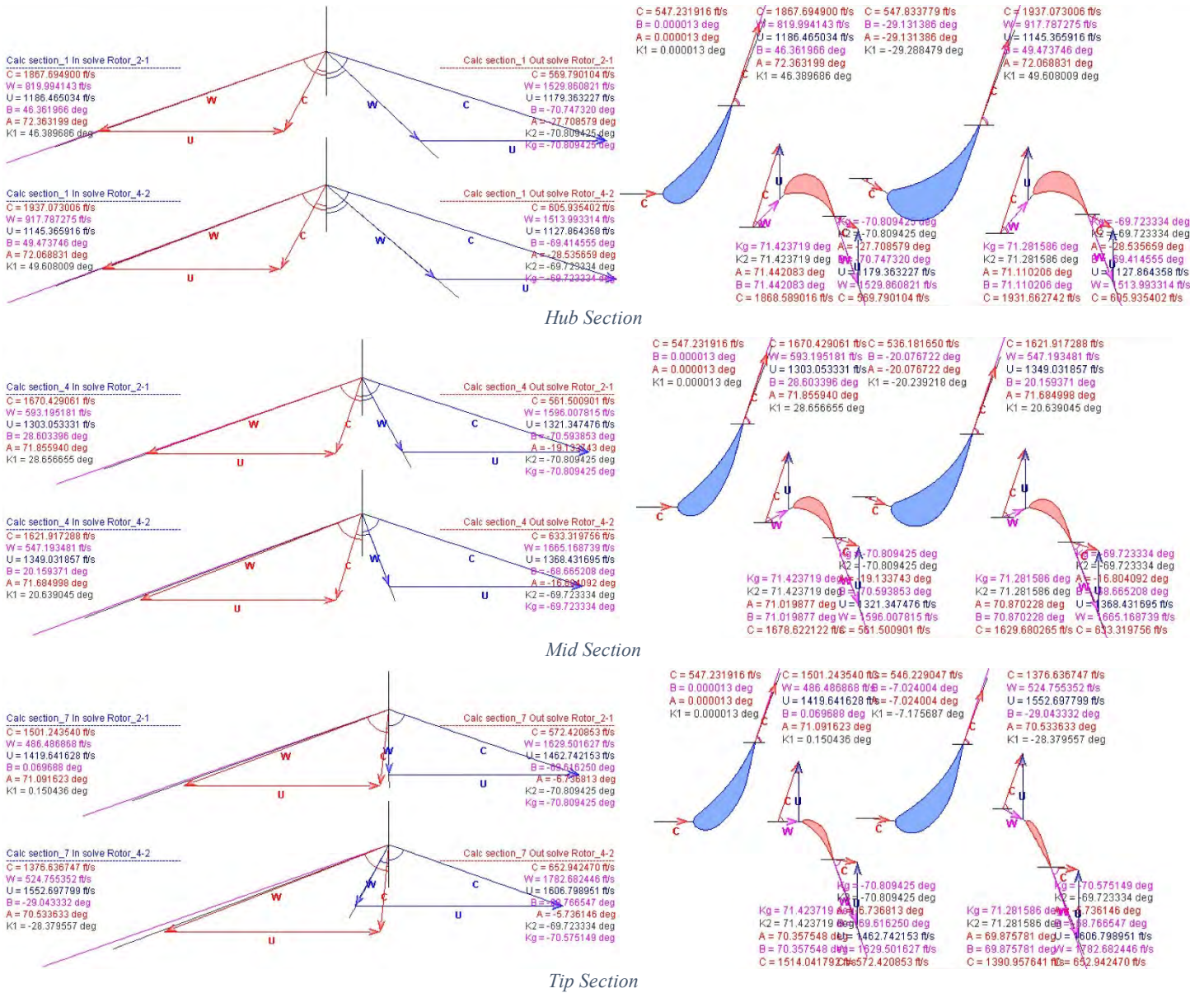


Figure 7-10 GGT Velocity Triangle at Hub, Mid, and Tip

Meanwhile, a H-S diagram of the thermodynamic properties across these two stages of GGT is also provided in Figure 7-11 GGT Enthalpy-Entropy Diagram. Blue lines correspond to the processes in stators, while red lines stand for processes across rotors. Solid and dash lines represent static and total enthalpy respectively.

7.1.7. GGT Blade Profiling & 3D Design

During the 3D Design of turbine stators and rotors, SoftInWay standard profiles SIW_R7N and SIW_R5B are used respectively for vanes and blades, the same as in the Preliminary Design. Profiling mode has been set to Custom Side Profiling for root and mid sections and Custom Camber Profiling for tip sections, per recommendation by SoftInWay in

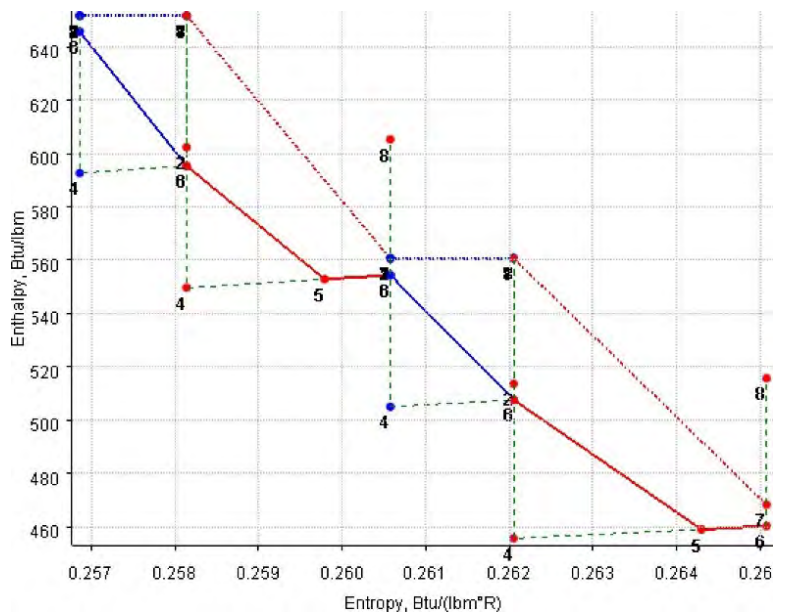
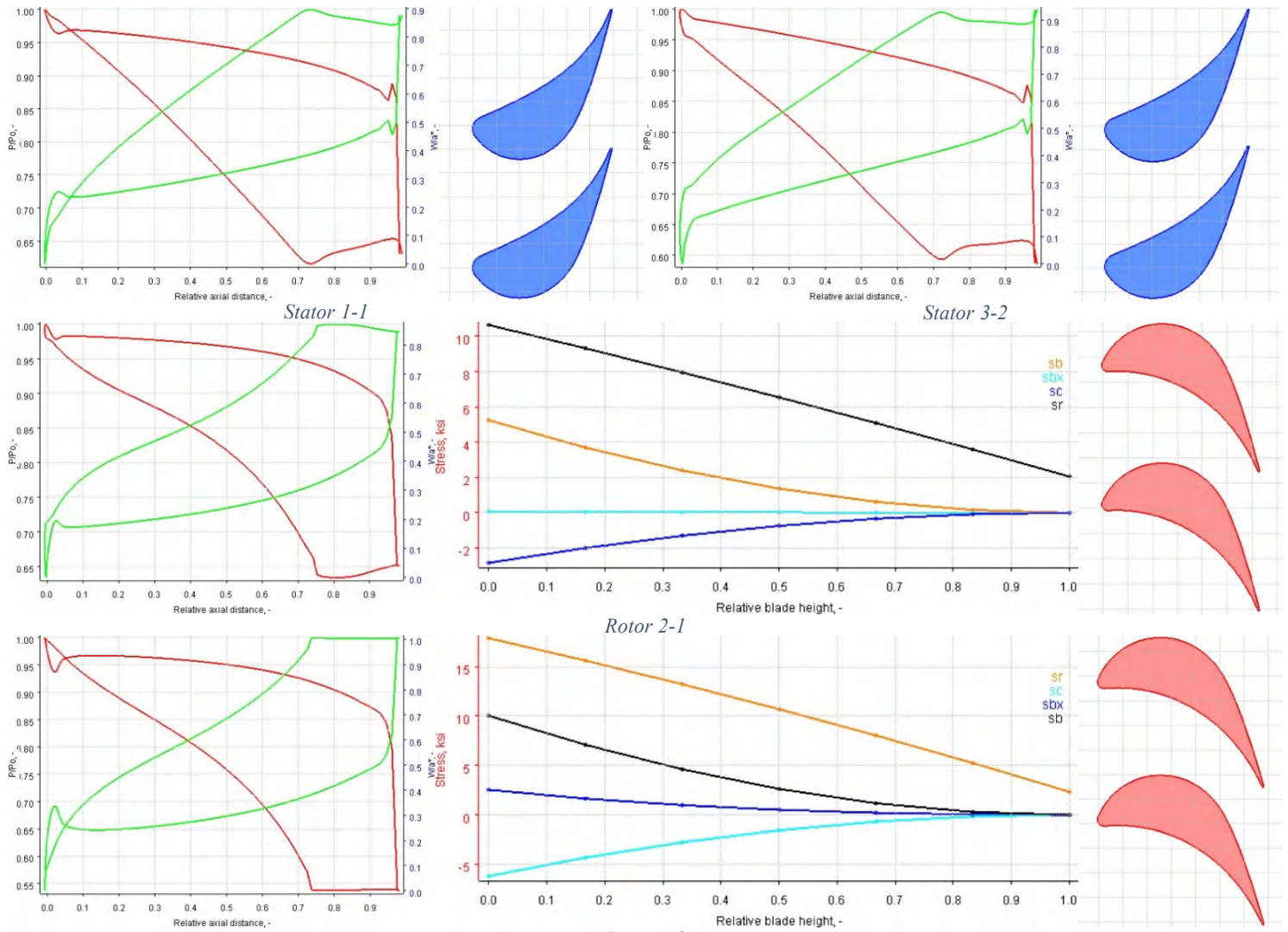


Figure 7-11 GGT Enthalpy-Entropy Diagram



Green Lines — Relative Mach Number on Pressure and Suction Sides; Red Lines — Relative Pressure on Pressure and Suction Sides; Orange Lines — Blade Tensile Stress; Cyan Lines — Stress at Suction Side; Blue Lines — Stress at Trailing Edges; Black Lines — Stress at Leading Edges. Stresses are calculated using purely analytical methods described in *Gas Turbine Theory* (Saravanamuttoo, Rogers, Cohen, & Straznicky, 2009, p. 418), thus they may differ from 3D FEA analysis.

Figure 7-12 Profile Cascade Performance

their user manual (SoftInWay). Since standard profile has been used, no optimization on the profile shape will be made, and only performance data of the profile cascade at mid-sections are provided in Figure 7-12 Profile Cascade Performance for illustrative purpose. After the profile, 3D blade shape is automatically generated by AxSTREAM as shown in Figure 7-13 3D GGT Blade Geometry. Throat area is also highlighted in the figure.

7.2. Free Power Turbine Design

7.2.1. FPT Preliminary Design

Like GGT design, following parameters are specified as inputs, while parameters not mentioned are using AxSTREAM default:

- Working Fluid: Ideal Gas
 - Isentropic Exponent = 1.34055 Per off design cycle calculation
 - Gas Constant = 53.357597 Per off design cycle calculation

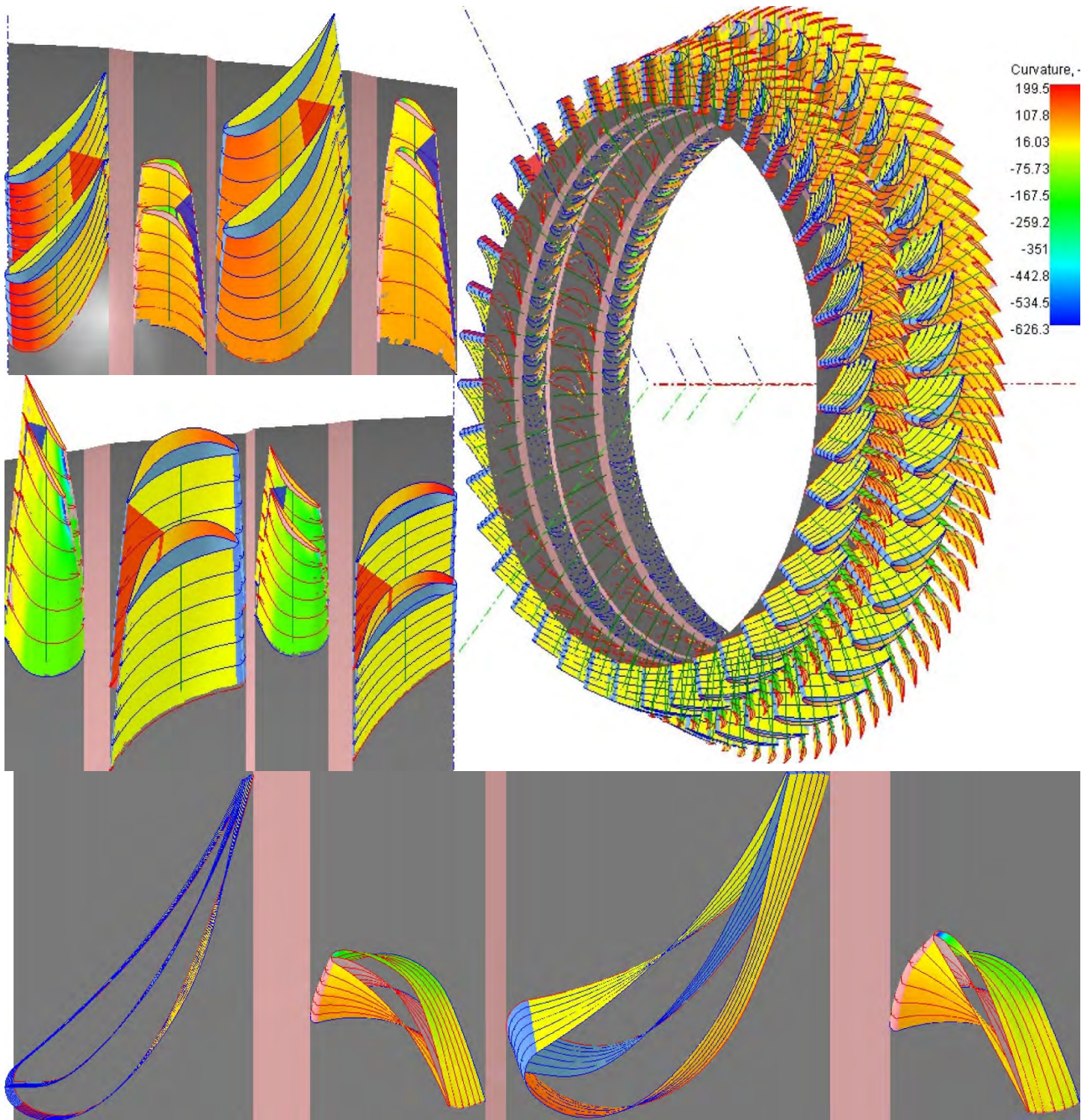


Figure 7-13 3D GGT Blade Geometry

- **Boundary Conditions:**

- Inlet total pressure = 45.475 psi
- Inlet total temperature = 1686.77 °R
- Total Pressure at outlet = 16.039 psi
- Mass flow rate = 9.89 lb./s
- Inlet flow angle = 0 axial degree
- 20,000 rpm ≤ Shaft rotational speed ≤ 30,000 rpm

- Per off design cycle calculation
- No inlet pre-swirl
- Design spool speed ± 5,000 rpm

- **Constraints**

- Number of Stages = 3
Per design point cycle calculation

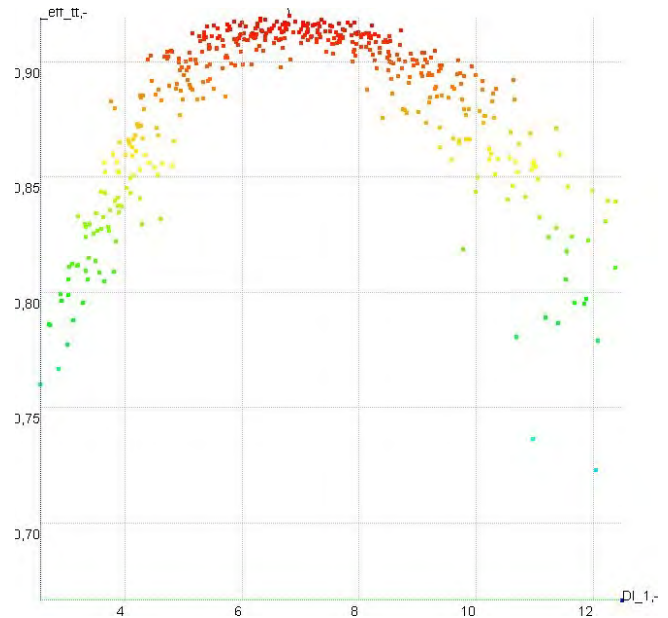
- Parameters

- $7.25 \leq \text{Inlet Hub Diameter} \leq 8.25$ in
The design point hub diameter is 7,7124 in, and the Cycle Exchange Table shows that ± 0.5 in of variation provides acceptable level of change in performance.
- $0.7034 \leq \text{Rotor Hub Diameter Ratio } (D2/D1) \leq 0.9801$
Same calculation mechanism as GGT yields a mean diameter ratio of $0.94737 \leq \text{Mean Diameter Ratio} \leq 1.17647$, which corresponds to a hub diameter ratio of $0.7034 \leq \text{Rotor Hub Diameter Ratio } (D2/D1) \leq 0.9801$.

- $4 \leq 1^{\text{st}} \text{ Stage Mean Diameter/Blade Height Ratio } D/H \leq 10$

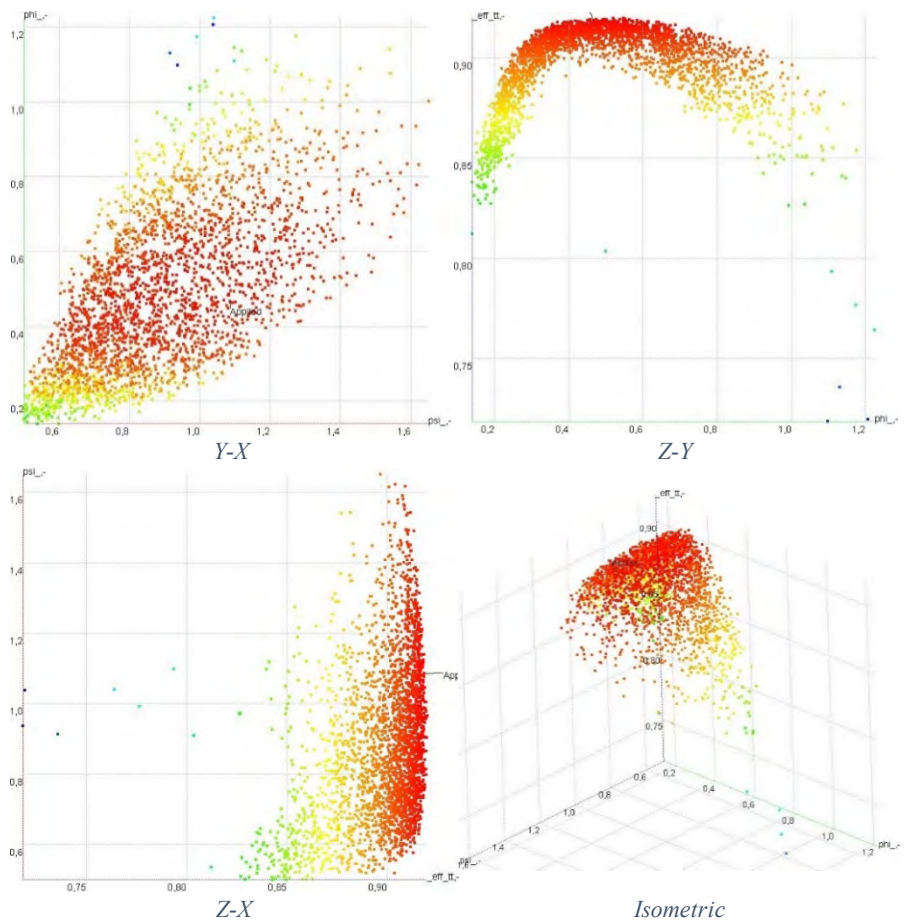
As per Figure 7-14 FPT Relationship between D/H and Efficiency, the D/H range of 4 to 10 yields highest concentration of high efficiency design options. In Cycle Summary Table, the hub-tip ratio of 0.74968 calculated from NASA's turbine design code corresponds to a D/H of 6.9898.

- $0.2 \leq \text{Hub Reaction} \leq 0.4$
Same as GGT
- $0.45 \leq \text{Isentropic Velocity Ratio } (u/C0) \leq 0.7$
Same as GGT
- Heat drop gradient $(H_z/H_1) = 1$
Same as GGT
- $0.5 \leq \text{Meridional Velocity Gradient } (Cm_z/Cm_1) \leq 0.8$
From the Cycle Summary Table the velocity ratio of Station 5 to Station 45 is 0.63. Thus, around a flexibility of 0.15 was given. This corresponds to a Mach number fluctuation of approximately 0.1 at Station 45.



Horizontal Axis: 1st Stage Mean Diameter/Blade Height Ratio D/H
Vertical Axis: Internal Total-to-total Efficiency
Contour: Internal Total-to-total Efficiency

Figure 7-14 FPT Relationship between D/H and Efficiency



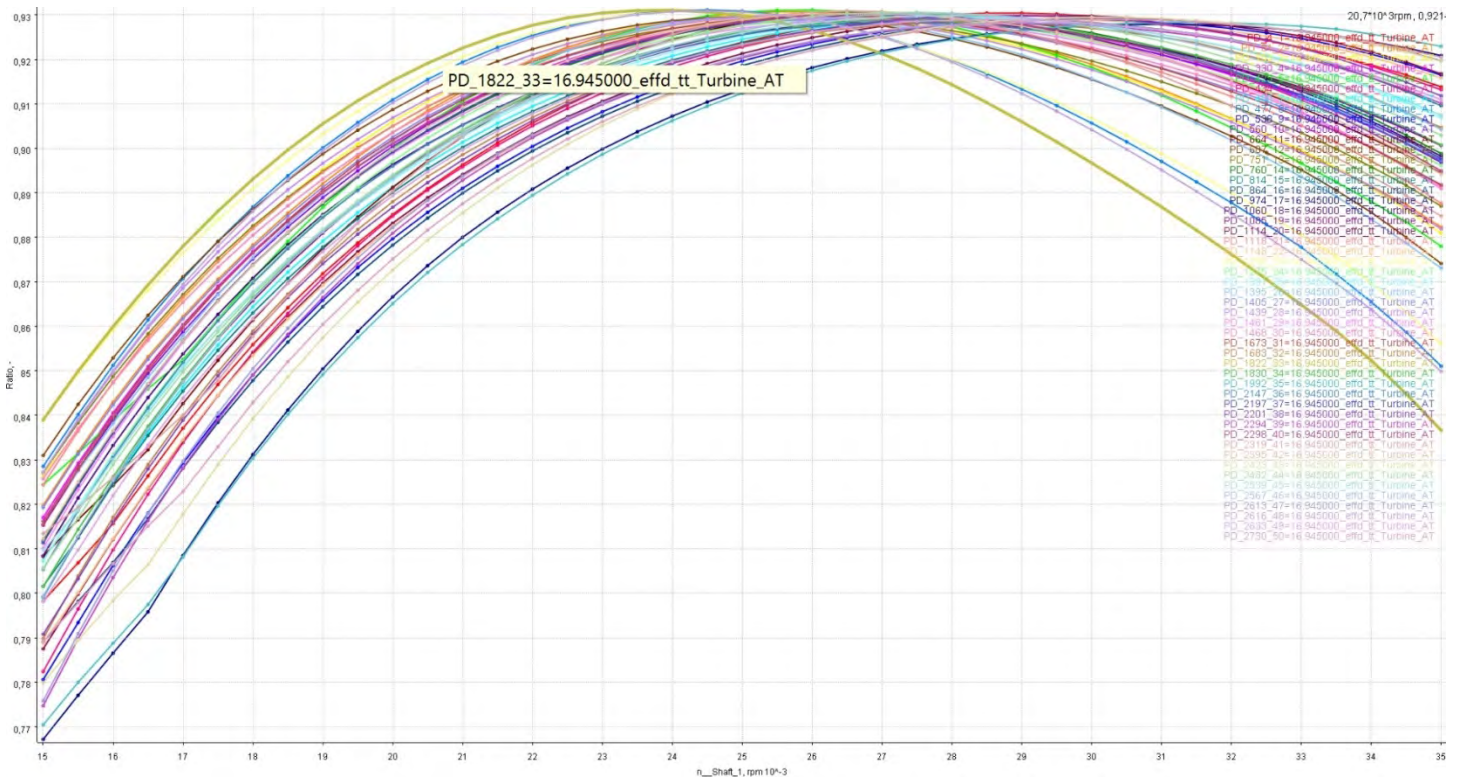
X — Stage Loading (psi); Y — Flow Coefficient (phi); Z — Total-to-total Efficiency
Figure 7-15 FPT Design Space

Rotors and Stators are profiled using SoftInWay standard profiles SIW_R7N and SIW_R5B respectively.

7.2.2. FPT Design Space

Using the corresponding inputs, a design space with totally 2781 design options is generated as presented in Figure 7-15 FPT Design Space. Nomenclature in the figure are the same as in Figure 7-3 GGT Design Space. Optimum value for flow coefficient also matches the result from NASA’s preliminary turbine design code.

Comparable to the procedure for GGT design, top 50 designs of highest internal total-to-total efficiency are imported to PD Map for performance calculation under Cycle Design Point. Results are presented in Figure 7-16 FPT Efficiency versus Spool Speed for 50 Optional Designs. Different from GGT, there’s no single option standing out over the others in efficiency. Thus, the selection criterion is switched to lowest spool speed, since at the same level of efficiency, lower RPM can reduce the weight of corresponding gear box. The leftist line in the diagram corresponds Design Option 1822. Thus, this design is selected for S1 optimization and profiling.



Shaft Speed (Horizontal Axis): 15,000rpm-35,000rpm; FPT Total-to-total Efficiency (Vertical Axis): 0.825-0.915

Figure 7-16 FPT Efficiency versus Spool Speed for 50 Optional Designs

7.2.3. Manual Adjustment of Meridional Flow Path

To keep the diameter of the last stage FPT rotor tip within the nacelle diameter limit of 19 inches, the flow path hub diameter is aligned using a straight line, such that the FPT outlet hub diameter is 0.5in smaller than the inlet. This results in an outlet tip diameter of 13.029in, which is highly acceptable for a 19in engine diameter limit.

7.2.4. FPT S1 Optimization

Same as for GGT, S1 Optimization module in AxSTREAM requires exact material properties to perform numeration. Per *Advances in Gas Turbine Technology*, nickel-based cast super alloys are extensively used for turbine blades and vanes (Muktinutalapati, 2016). Therefore, UNS N07718 and Rene 80 are chosen respectively for nozzles and blades, and their properties are presented in Table 7-2 UNS N07718 Mechanical Properties and Table 7-3 Rene 80 Mechanical Properties.

Temperature (°C)	Elasticity modulus (GPa)	Linear expansion coefficient (10 ⁻⁶)	Yield strength limit (MPa)	Creep strength limit (MPa)	Long time strength limit (MPa)
20	200	1.8e-005	1175	1075	1015
650	163	1.8e-005	995	985	975
760	153	1.8e-005	750	740	730
870	139	1.8e-005	420	410	400
980	120	1.8e-005	90	89	88

Table 7-2 UNS N07718 Mechanical Properties

Temperature (°C)	Elasticity modulus (GPa)	Linear expansion coefficient (10 ⁻⁶)	Yield strength limit (MPa)	Creep strength limit (MPa)	Long time strength limit (MPa)
20	210	1.8e-005	920	870	820
600	169	1.8e-005	790	780	770
700	156	1.8e-005	780	770	760
800	141	1.8e-005	790	780	770
1000	125	1.8e-005	450	440	430
1100	118	1.8e-005	200	190	180

Table 7-3 Rene 80 Mechanical Properties

Same optimization targets and safety factors are adopted for FPT as for GGT. Blade numbers after the optimization are 79, 108, 89, 112, 91, and 114 respectively for blade rows from front to rear, which also show acceptance in avoiding detrimental vibration issues.

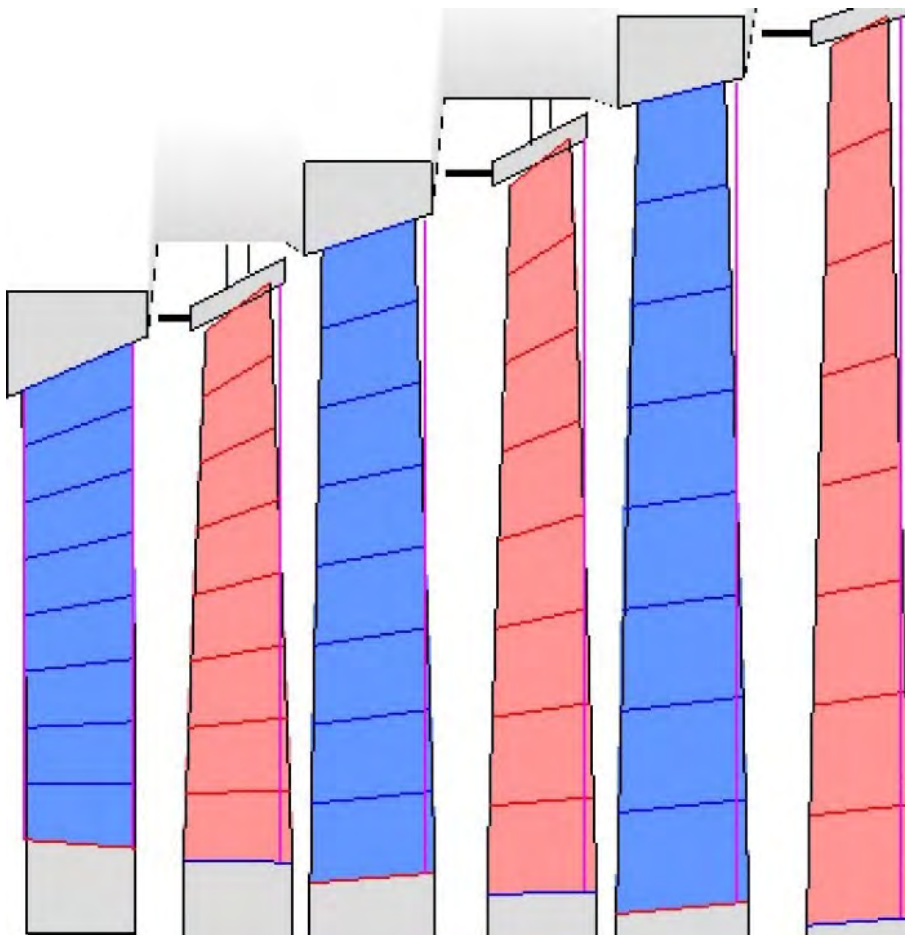


Figure 7-17 FPT Meridional Flow Path

Design spool speed is 21041.2598 rpm. Therefore, the meridional flow path of the machine is frozen and presented in Figure 7-17 FPT Meridional Flow Path. Additional information about flow path is presented in Figure 7-21 Miscellaneous FPT Meridional Flow Path Info.

7.2.5. FPT Blade Twist Factors

Like GGT, an AxPLAN DoE test with all settings being the same as for GGT is carried out to study the effect of twist factor on overall total-to-total efficiency. Results are plotted in Figure 7-19 Stage 1, 2, & 3 Twist Factors versus FPT Efficiency. From the plot, it is easy to detect that 0 is the optimal twist factor for all 6 rows of rotor and stator blades, as validated by the red color at upper corners on all three vertically stacking plots. Therefore, this number is determined for FPT to carry on further streamline analysis.

7.2.6. FPT Streamline Analysis

For FPT, stream curves are calculated on 9 sections along the blade height. Other settings are the same as GGT. Results of the stream curves are again fitted by NURBS curves and depicted in Figure 7-19 FPT Stream Curves. From the stream curve plot, result stream curves exhibit a wavy shape. This demonstrates the existence of radial centrifugal effect of rotating blades on the working fluid. Similar waving phenomenon of stream curves have been published by various authors, including Cumpsty (Compressor Aerodynamics, 2004, p. 100). Other meridional flow path properties exhibit similarity with GGT, such as the comparatively significant increase of entropy at last stage hub, and the total pressure/temperature drop in rotor blades. However, maximum Mach number is conspicuously lower than its front predecessor. With a highest value of 0.65 at the upstream area of rotor hub, GGT is in comparison obviously heavier loaded.

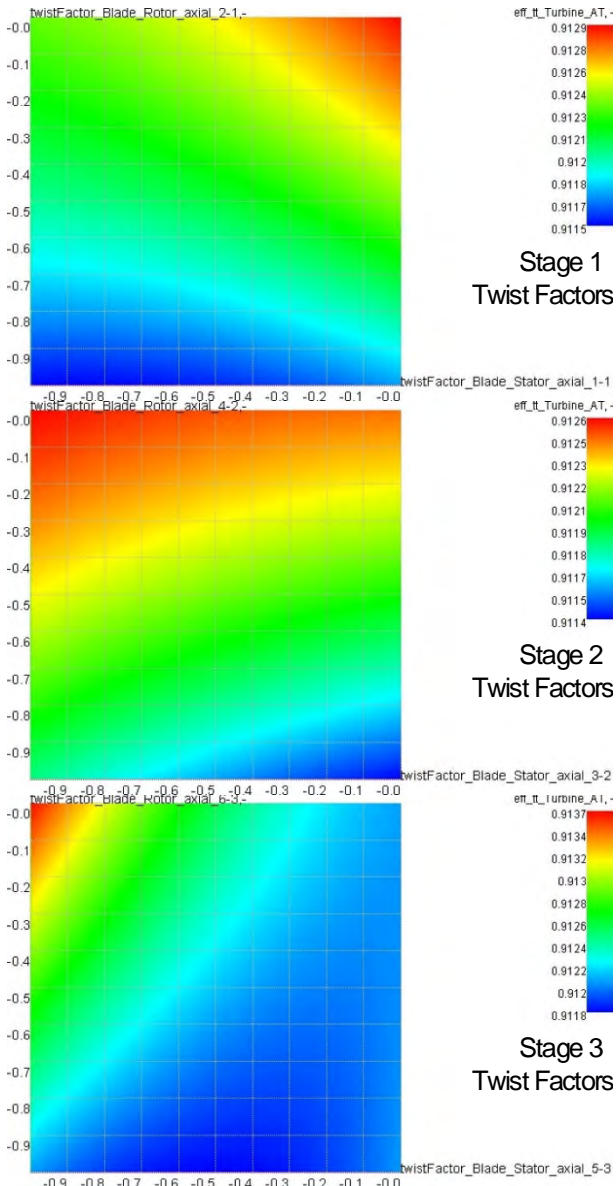


Figure 7-19 Stage 1, 2, & 3 Twist Factors versus FPT Effi-

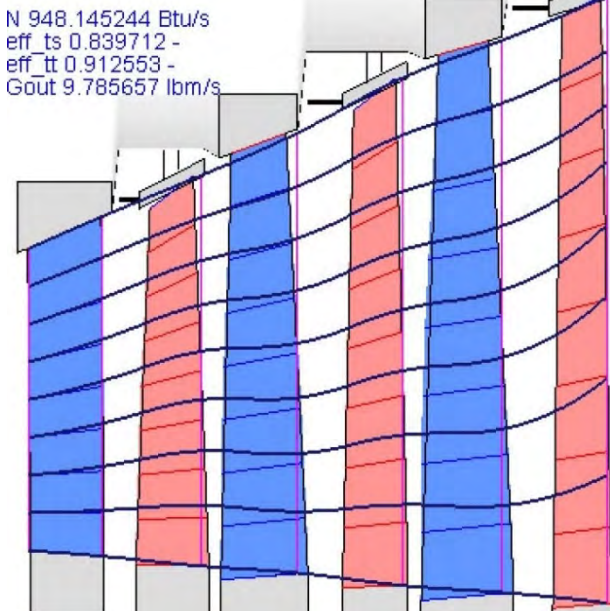
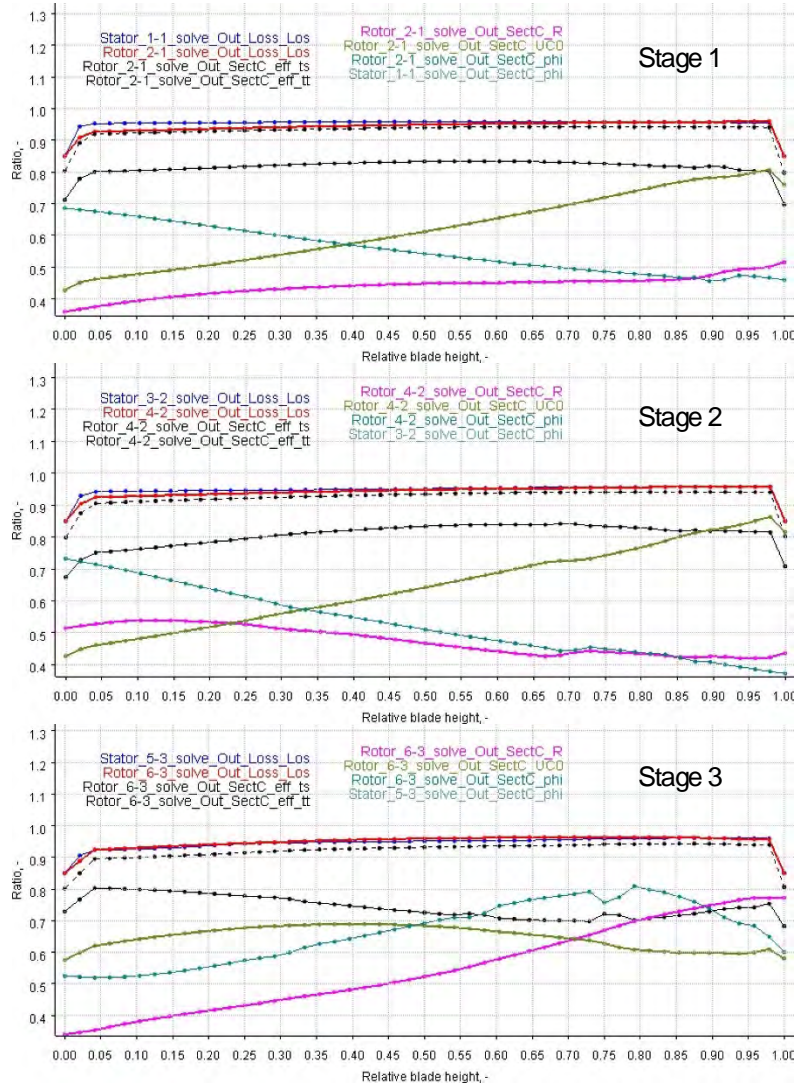
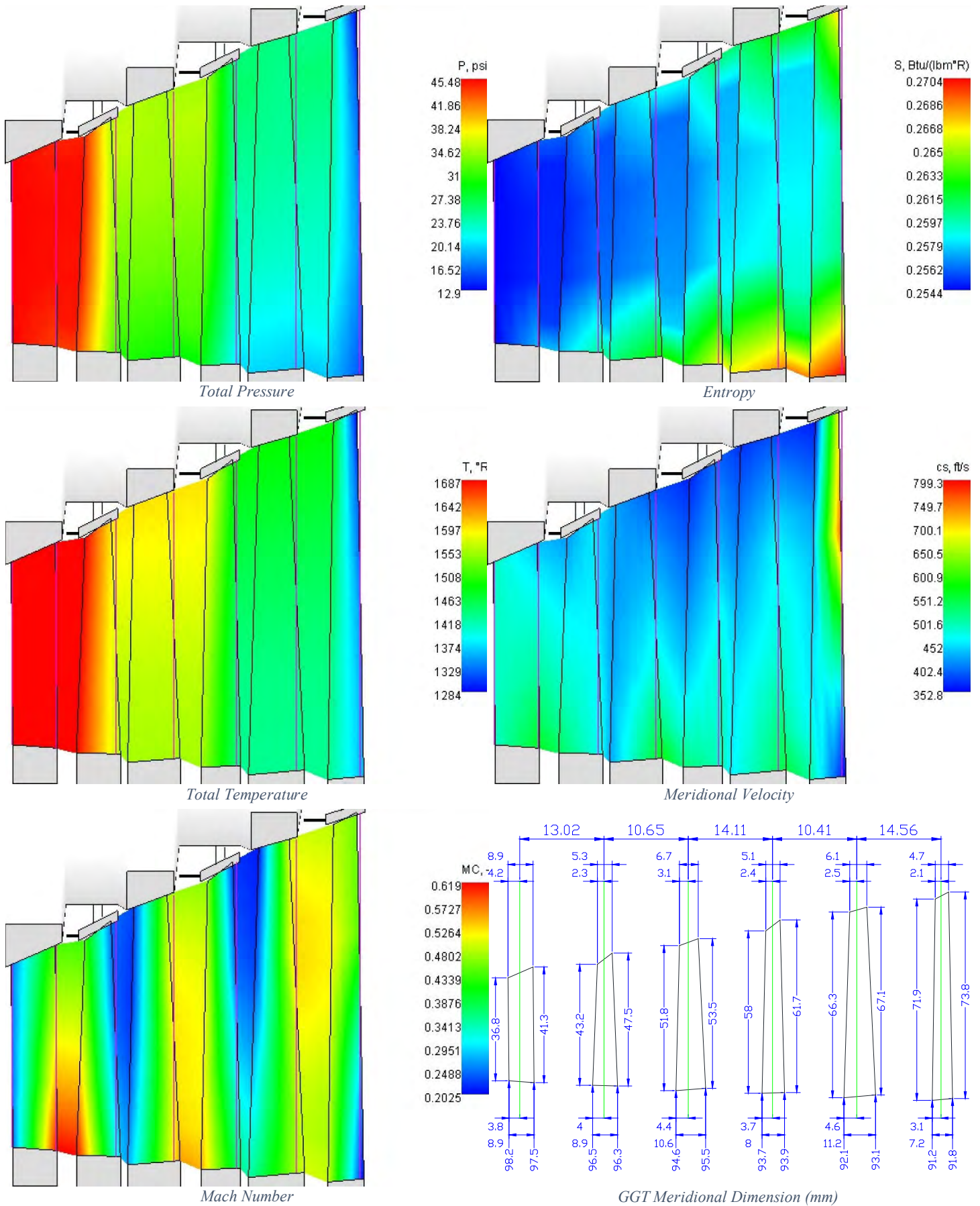


Figure 7-19 FPT Stream Curves



Nomenclature on the graph: R = Degree of Reaction; UCO = Velocity Ratio; phi = Flow Coefficient; Los = losses; eff_ts =GGT Total-to-static
Figure 7-20 Variation of Physical Properties along the Blade Height



Results purely using Streamline Method. Difference between Streamline Method and CFD see Cumpsty (2004, pp. 93-131).

Figure 7-21 Miscellaneous FPT Meridional Flow Path Info

Variations of local efficiencies, degree of reaction, losses, and flow coefficients along the blade height for all stages are presented in

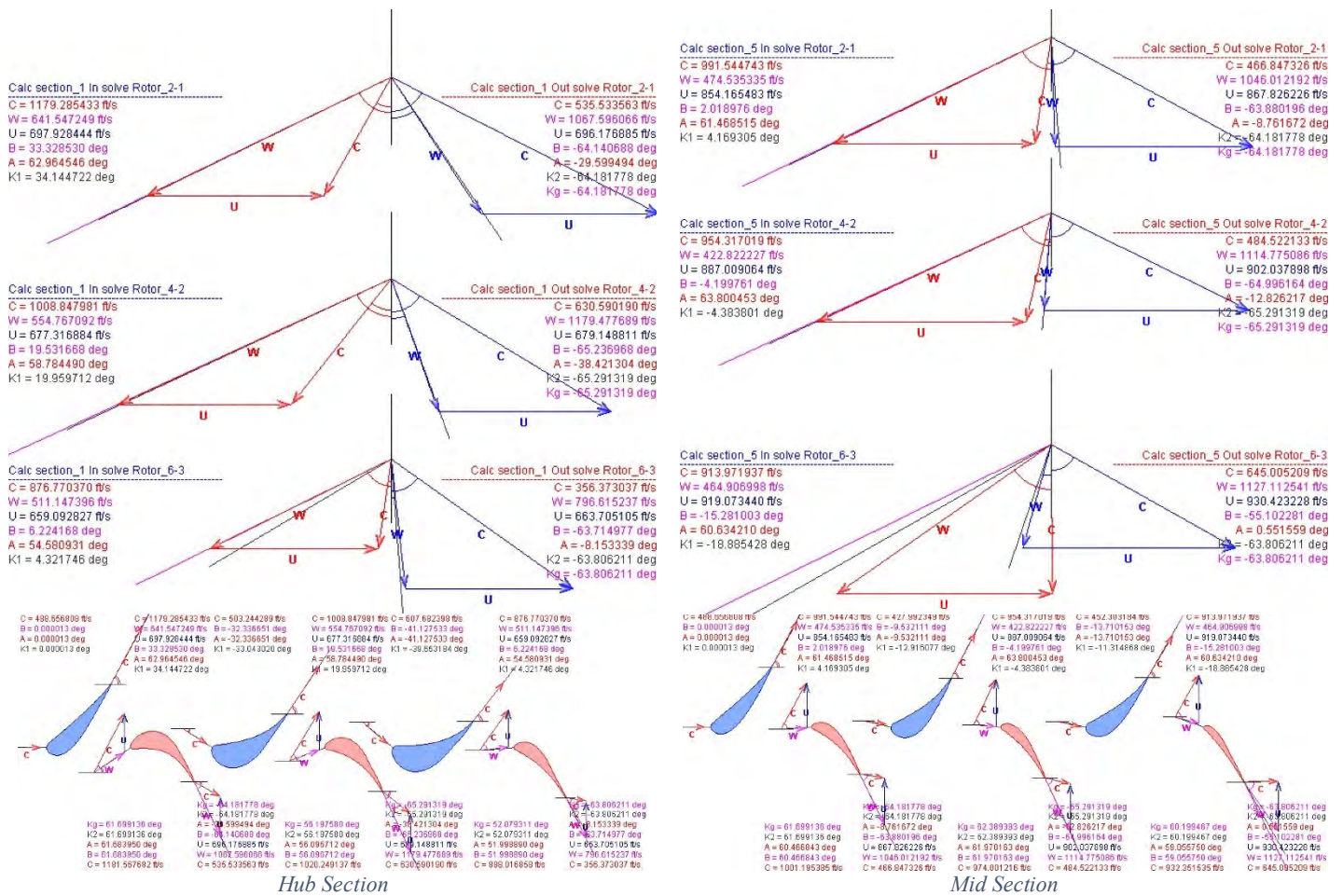


Figure 7-22 FPT Velocity Triangle at Hub, Mid, and Tip

Figure 7-20 Variation of Physical Properties along the Blade Height. Peculiarity on the plot is that the second stage has a degree of reaction decreasing in the upper majority of the blade height. This is because the tapering shape of the rotor due to mechanical constraints results in constantly reducing length of the cord, which limits the fluid bending capacity of the rotor cascade geometry in the upper part around tip. With smaller cord length, local solidity is even further minimized, which forces a mediocre camber angle to become the only design choice left over. However, the extent of decreasing in degree of reaction is only moderate, and a value larger than 0.4 is nonetheless promised at the tip. A second phenomenon is the distortion of property curves at upper part of the blade height, while an increasing extent of unevenness at rear stages is witnessed. This is because of the switch of profiling modes from Custom Side Profiling to Custom Camber Profiling when the Custom Side Profiling, which is more suitable for hub and mid sections, causes peculiar cascade geometry at tip. Although the rapid switch of profiling mode isn't detected from

the curvature of blade surface, it's indeed visible from the plot of physical properties along the blade height.

Meanwhile, the velocity triangle at 3 different blade sections are provided in Figure 7-22 FPT Velocity Triangle at Hub, Mid, and Tip. Noting that the particularly large deviation angle of stage 2&3 at the tip section also serves as a second evidence of low solidity, which also causes the decreasing trend of reaction along the blade height for stage 2. Finally, a H-S diagram of the thermodynamic properties across these three stages of FPT is provided in Figure 7-24 FPT Enthalpy-Entropy Diagram. Same as for GGT, blue lines correspond the processes in stators, while red lines stand for processes across rotors. Solid and dash lines represent static and total enthalpy respectively.

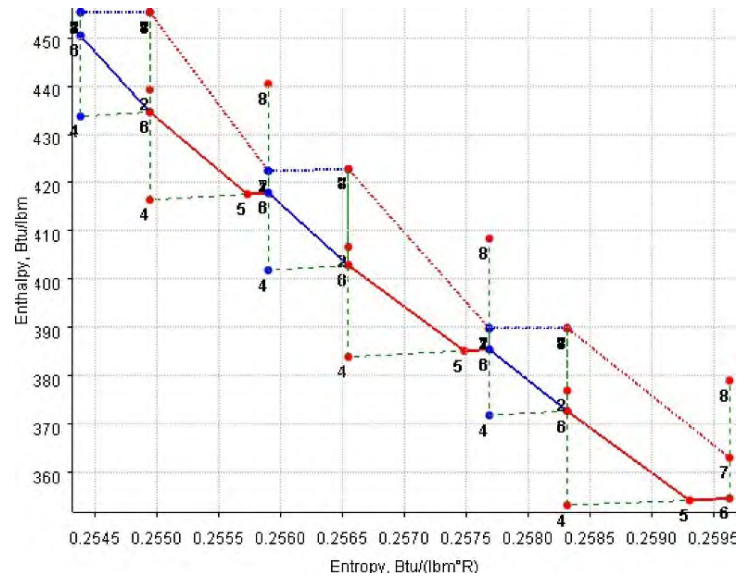


Figure 7-24 FPT Enthalpy-Entropy Diagram

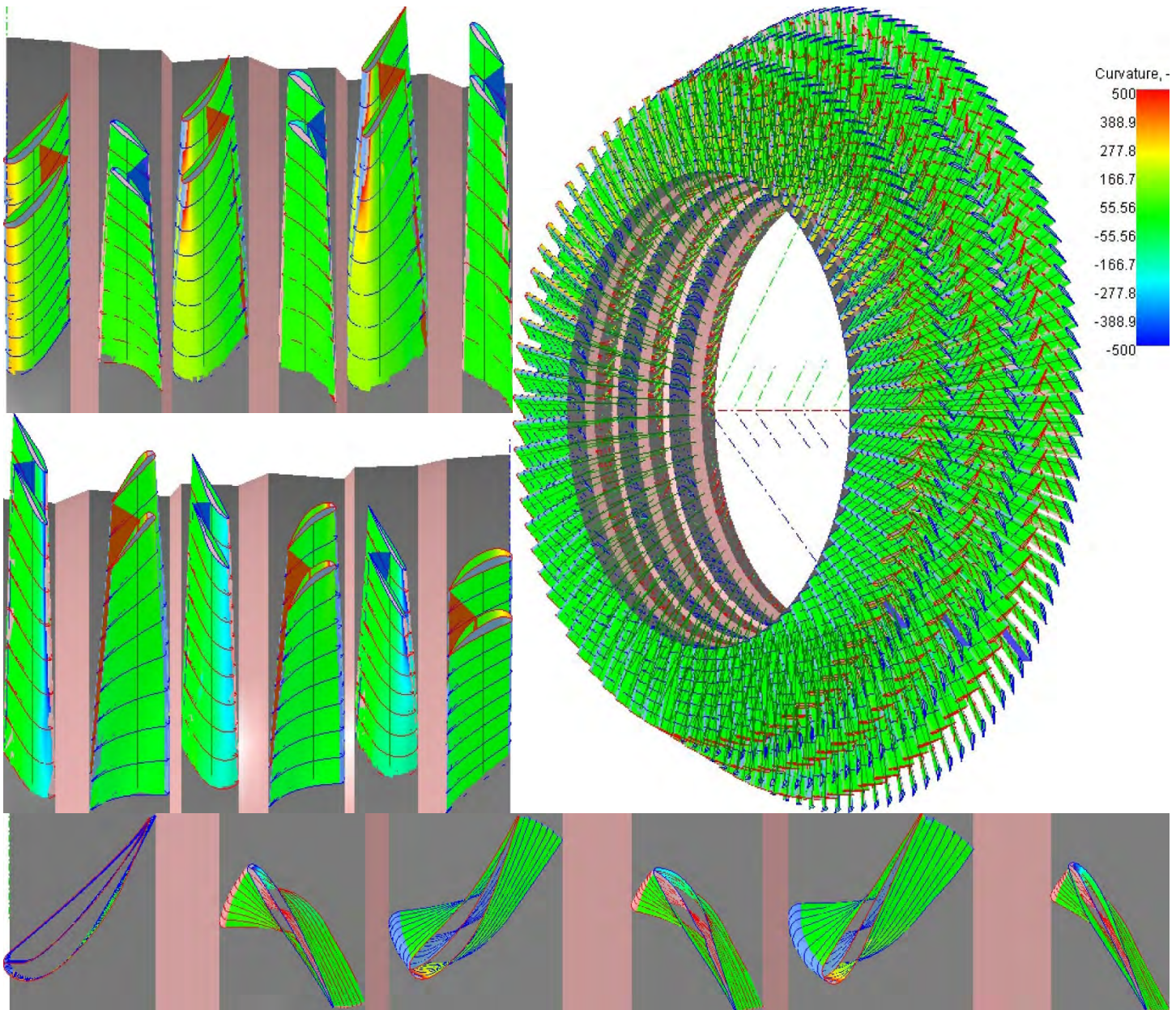


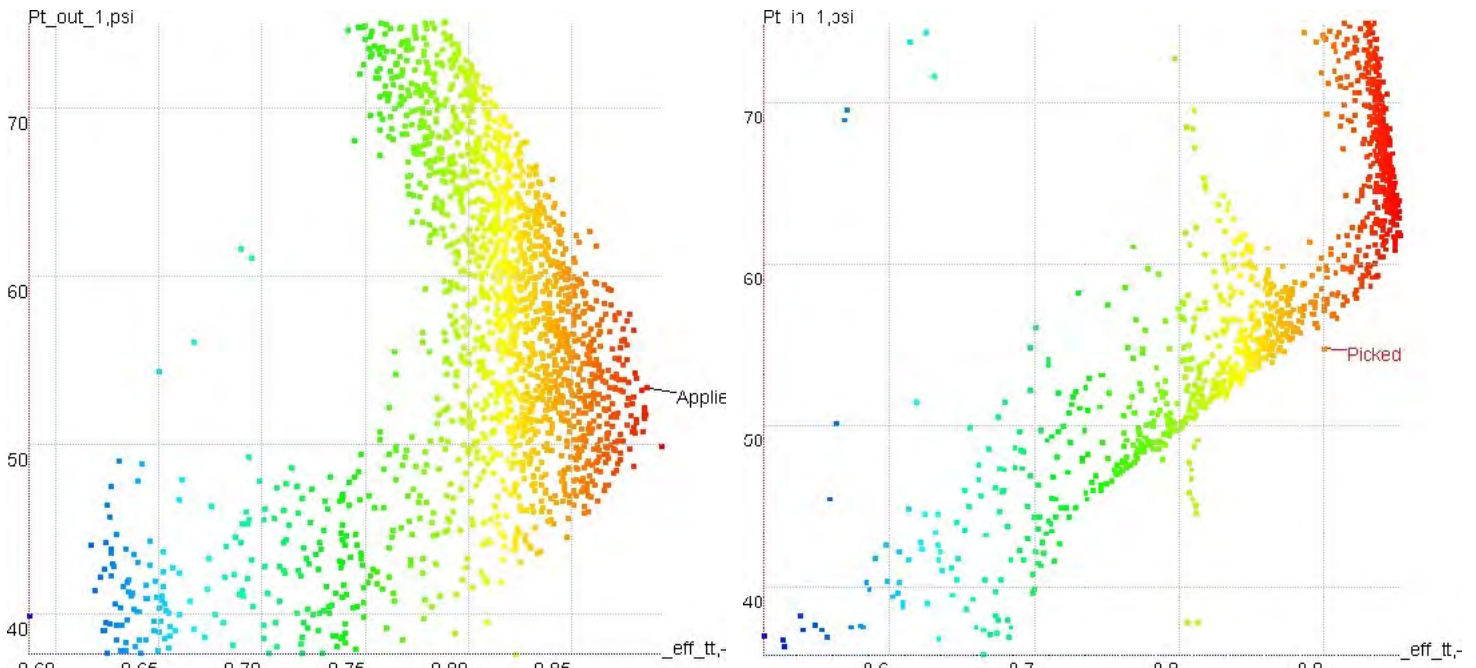
Figure 7-25 3D FPT Blade Geometry

7.2.7. FPT Blade Profiling & 3D Design

Like GGT, during the 3D Design of turbine blades and vanes, SoftInWay standard profiles SIW_R7N and SIW_R5B are used respectively for stators and rotors. Profiling mode has also been set to the same as GGT, namely Custom Side Profiling for hub and mid sections and Custom Camber Profiling for tip sections. Again, no optimization on the profile shape will be made, since standard profile has been used. 3D blade geometry is shown in Figure 7-25 3D FPT Blade Geometry with throat area being highlighted.

7.3. Pressure Ratio Separation Between Axial and Centrifugal Compressors

Before designing the blade geometry of each individual compressor, the pressure rises of axial and centrifugal compressors must be determined respectively to enable the use of the 2D design algorithm imbedded in AxSTREAM. Per Section 4.3 Carpet Plotting, Diagramming & Cycle Optimization, Cycle Design Point PR has been chosen as 19 ± 1 . Scaling this range of Cycle Design Point PR down to Compressor Design Point, a PR range of 14.313 ± 0.87 can be obtained. Therefore, the product of Axial Compressor PR and Centrifugal Compressor PR should fall within this range. Two main principles are considered in the process of determining the value of each individual PR. On one hand, the chosen PR should not exceed the achievability in the engineering level, e.g. per Figure 4-5



Horizontal Axis: Axial Compressor (Left) & Centrifugal Compressor (Right) Internal Total-to-total Efficiency
 Vertical Axis: Axial Compressor Outlet Pressure (Left) & Centrifugal Compressor Inlet Pressure (Right)
 Contour: Axial Compressor (Left) & Centrifugal Compressor (Right) Internal Total-to-total Efficiency

Figure 7-26 Axial Compressor Outlet Pressure vs. Efficiency

Figure 7-27 Centrifugal Compressor Inlet Pressure vs. Efficiency

Axial Compressors: Pressure Ratio Versus Number of Stages (Gas Turbine Performance, 2004, p. 273). On the other hand, the selected turbomachinery structure should lie within the feasibility of the AxSTREAM design code. Thus, with the number of stages for the axial and centrifugal compressors fixed to 4 and 1 respectively and the spool speed fixed to the same as GGT design spool speed, relationships between the PR and total-to-total efficiency for both compressor types are studied in the AxSTREAM PD module and presented in Figure 7-26 Axial Compressor Outlet Pressure vs. Efficiency and Figure 7-27 Centrifugal Compressor Inlet Pressure vs. Efficiency. During the plotting, axial and centrifugal compressors are connected in chain, with the overall inlet pressure equaling the ambient condition and the overall outlet pressure corresponding an overall PR of 14.313. Only the inter-compressor pressure is being varied, which represents a change of PR distribution.

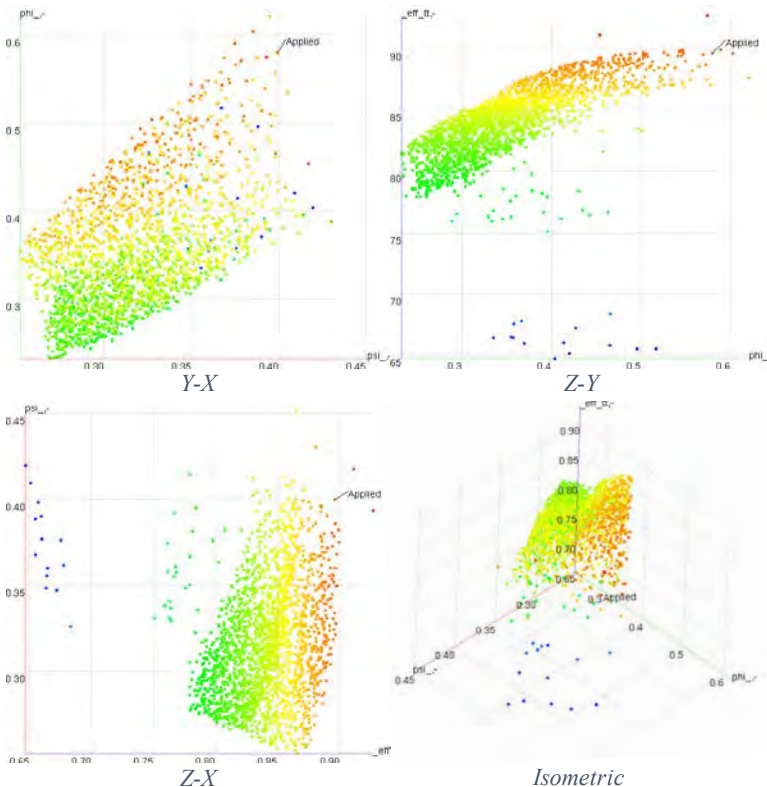
From both graphs, it's conspicuous to detect that, the highest efficiency is achieved with an outlet pressure of 52 psi for the axial compressor, while an inlet pressure of 60 psi for the centrifugal compressor. Therefore, the final inter-compressor pressure is set to 55 regarding the optimum range of peak efficiency for both compressor types. This results in PRs of 4.5 and 4.2 individually for axial and centrifugal types at Cycle Design Point.

7.4. Axial Compressor Design

7.4.1. Axial Compressor Preliminary Design

Like GGT and FPT, following parameters are chosen as inputs, while parameters not mentioned are using AxSTREAM default:

- Working Fluid: Ideal Gas
 - Isentropic Exponent = 1.38324
 - Gas Constant = 53.34997
- Boundary Conditions:
 - Inlet total pressure = 14.696 psi
 - Inlet total temperature = 518.67 °R
 - Total Pressure at outlet = 55 psi
 - Mass flow rate = 10.569 lb./s
 - Inlet flow angle = 0 axial degree



X — Stage Loading (psi); Y — Flow Coefficient (phi); Z — Total-to-total Efficiency
Figure 7-29 Axial Compressor Design Space

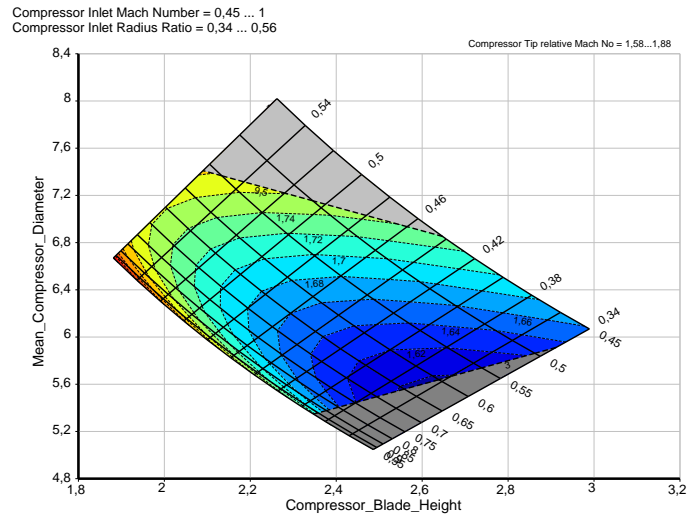


Figure 7-28 Axial Compressor Inlet Geometry

Per off design cycle calculation

Per pressure ratio separation

Per off design cycle calculation

No inlet pre-swirl

- Shaft rotational speed = 39,129.1995 rpm

Per GGT design

- Constraints

- Number of Stages = 4

Per design point cycle calculation

- Parameters

- $5 \leq \text{Mean Inlet Diameter} \leq 7.5$ in

- $2 \leq 1^{\text{st}} \text{ stage blade height} \leq 3$

According to GasTurb user manual, a good first estimate for the high-pressure compressor inlet tip diameter is the mean high pressure turbine inlet diameter (Kurzke J., 2015). And per gas turbine engineering practice, lower tip Mach number usually represents a comparatively lower loss. Therefore, a parametric study is being carried out using the equation of mass flow continuity:

$$m = \rho A C_a = \rho \pi r_t^2 \left[1 - \left(\frac{r_r}{r_t} \right)^2 \right]$$

Result of the parametric study is presented in Figure 7-29 Axial Compressor Inlet Geometry. With the varying of

compressor inlet Mach number and radius ratio from 0.45 to 1 and 0.34 to 0.56 respectively, its tip relative Mach number changes from 1.58 to 1.88. After the constraints of tip diameter < 9.5 in, and root diameter > 3 in are added, mean inlet diameter and 1st stage blade height can be seen ranging from 5 to 7.5 inch and 2 to 3 inch correspondingly.

- $0.2 \leq \text{Work Coefficient} \leq 0.4$

The Work Coefficient for axial compressor usually lies in the range of 20% - 40%. (SoftInWay)

- Specific work gradient $(Lu_z/Lu_1) = 1$

The specific work gradient is used to control the work distribution between stages. By default, the inverse task solver divides the overall work input equally between the stages (SoftInWay).

- Meridional Velocity Gradient $(Cm_z/Cm_1) = 1$

This parameter is used for controlling flow path flare, by default it is set to 1.

Rotors and Stators are profiled using SoftInWay Custom Camber Profiling per user manual recommendation (SoftInWay).

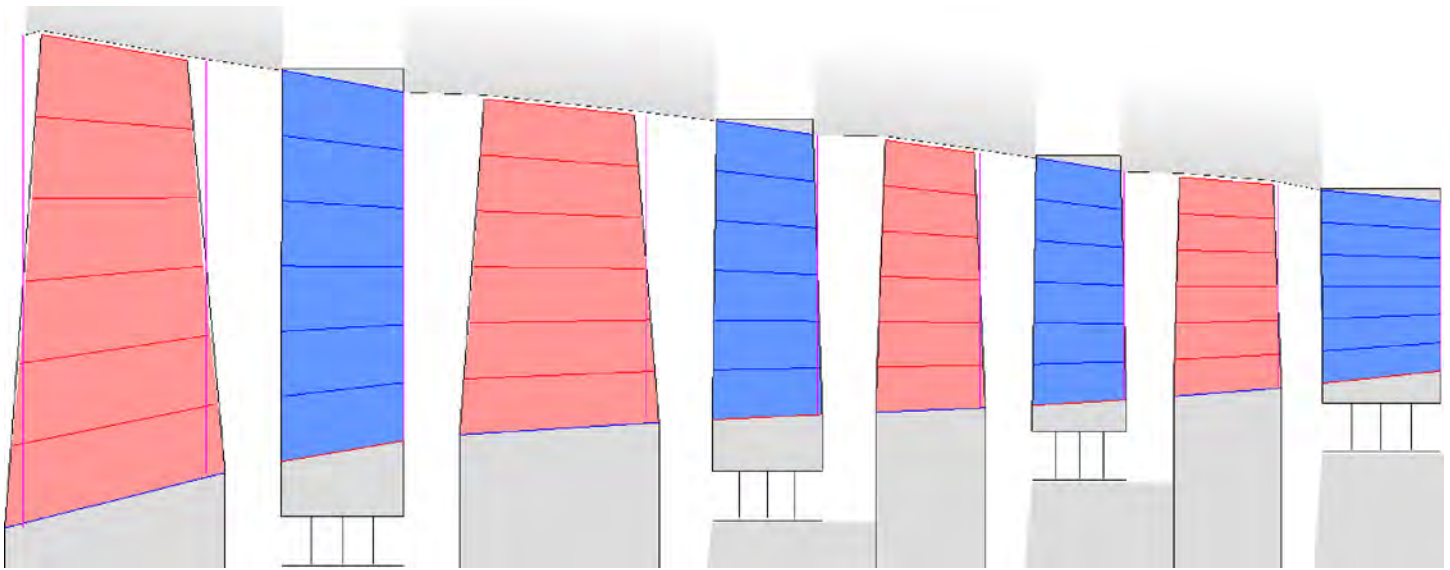


Figure 7-30 Axial Compressor Meridional Flow Path

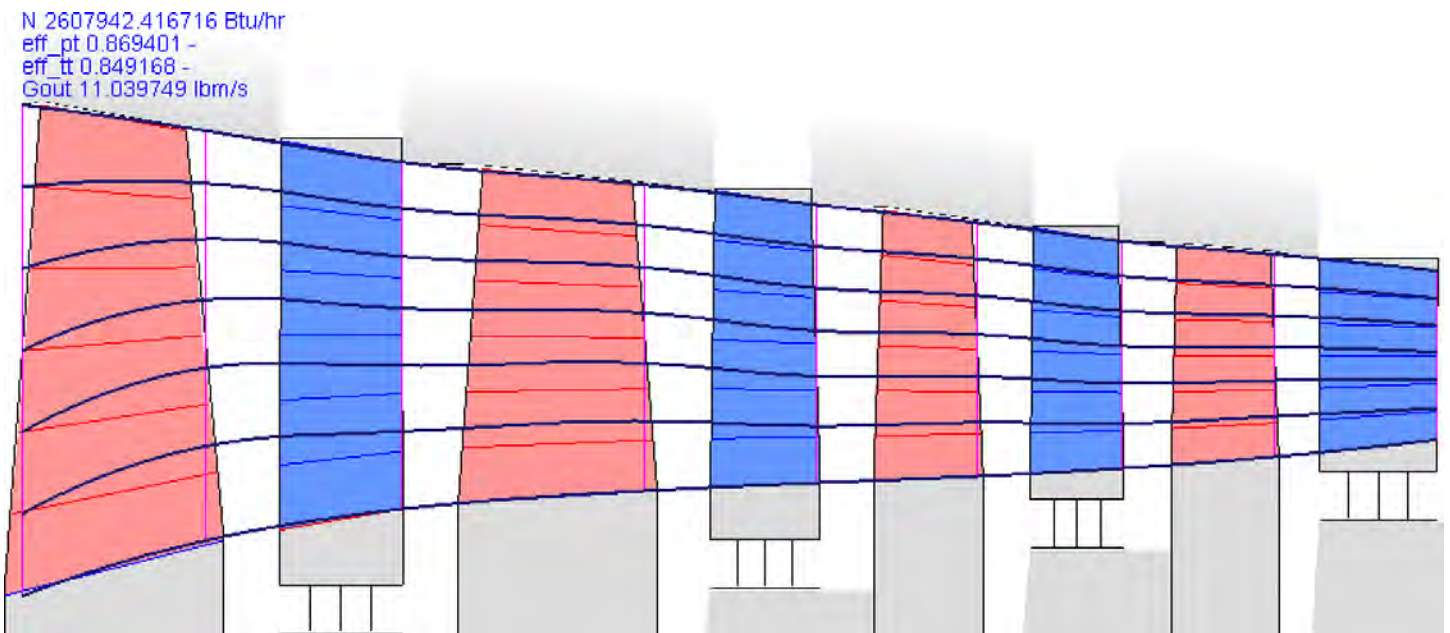


Figure 7-31 Axial Compressor Stream Curves

7.4.2. Axial Compressor Design Space

Using the corresponding inputs, a design space with totally 2134 design options is generated as presented in Figure 7-30 Axial Compressor Design Space. Like the turbine design process, top 50 design options are imported to PD Map for performance calculation under Cycle Design Point. Due to requirement of brevity of this document, PD Map calculation results will not be presented, while only the final select is given as Design Point 758. After the selection of the design option, twist factors of blades are adjusted to -1 for rotors and 0 for stators, which corresponds to the theoretical design approach of Free Vortex (Saravanamuttoo, Rogers, Cohen, & Straznicky, 2009, p. 211). Similar manual adjustments on the flow path, and S1 flow surface optimization are being made. On one hand, according to *Compressor Aerodynamics* (Cumpsty, 2004), slight increase of the blade mean diameter from the front to rear stages is helpful in achieving a higher efficiency. Thus, the meridional flow path was adjusted manually to achieve a higher outlet mean diameter than the inlet. On the other hand, S1 flow surface optimization is carried out regarding both the dependence of optimal solidity on air bending angle as well as outlet metal angle and the constraints on vibrational issues. Blade numbers for all four rows of blades are finally chosen as 18, 23, 24, 29, 30, 37, 36, and 43 respectively from front to rear. Thus, the meridional flow path of the machine is frozen and presented as in Figure 7-31 Axial Compressor Meridional Flow Path.

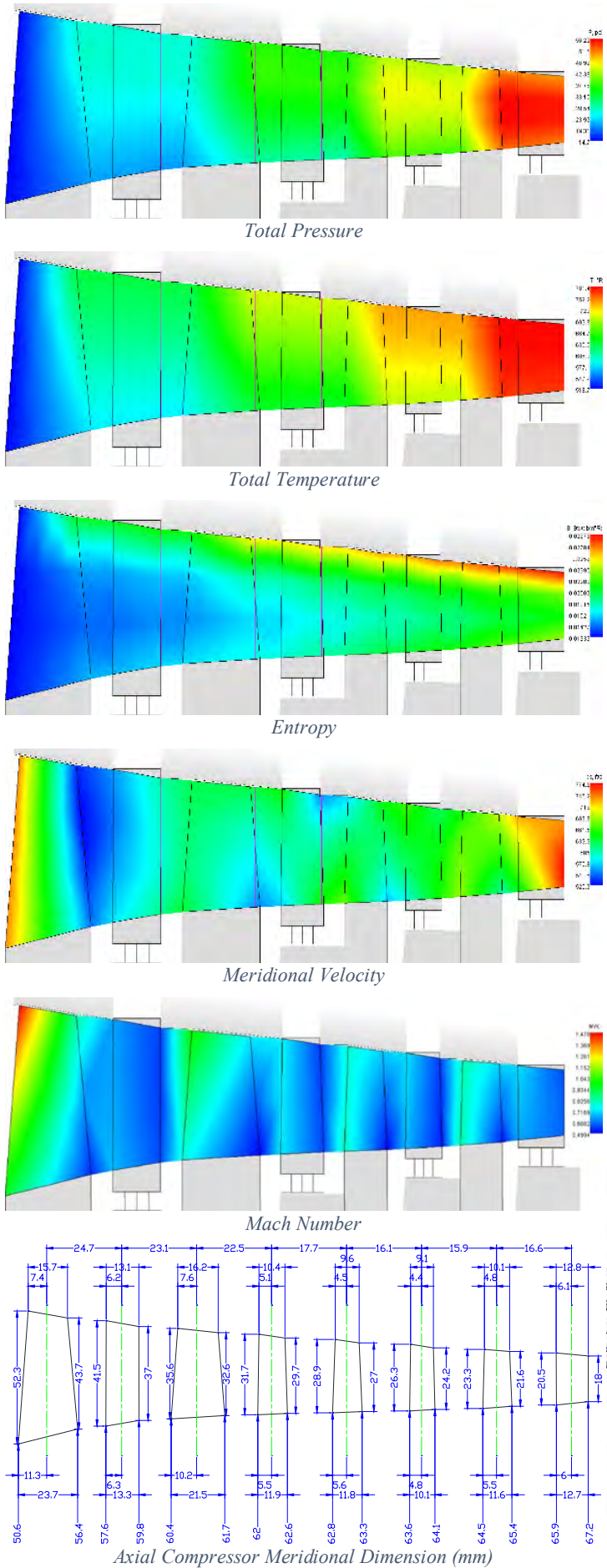


Figure 7-32 Miscellaneous Axial Compressor Meridional Flow Path Info

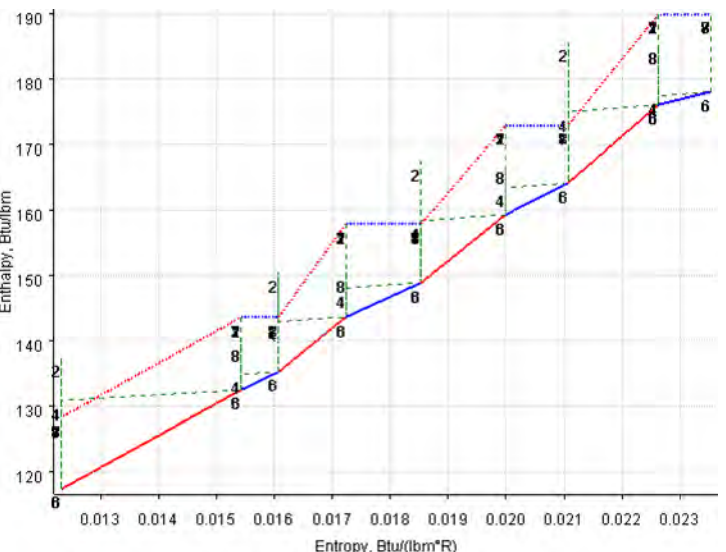


Figure 7-33 Axial Compressor Enthalpy-Entropy Diagram

7.4.3. Axial Compressor Streamline Analysis

Calculations of stream curves are evenly placed on 7 sections along the blade height, and the discrete numerical results are fitted using NURBS curves as illustrated in Figure 7-32 Axial Compressor Stream Curves. Stream Curves again exhibits similarity to those seen in open literatures. Additionally, information about temperature, pressure, Mach number, entropy, velocity, and flow path dimensions are provided in Figure 7-33 Miscellaneous Axial Compressor Meridional Flow Path Info. These results also match the estimation of physical insight, such as the more rapid increase of entropy at tip regions than the root due to existence of tip clearance, and the absence of total pressure rise in stator blade rows.

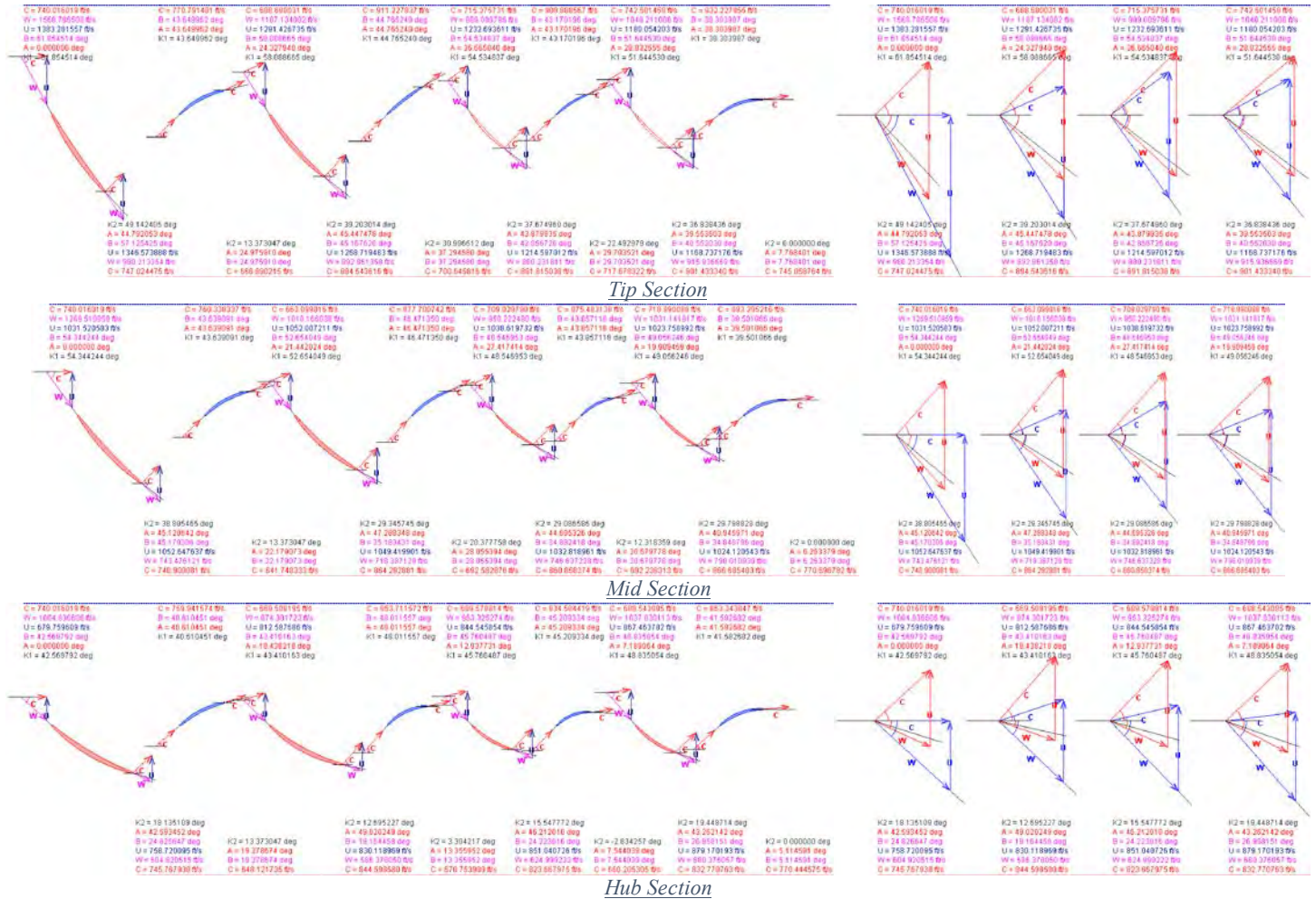


Figure 7-34 Axial Compressor Velocity Triangle at Hub, Mid and Tip

Velocity triangles at 3 different blade sections are provided in Figure 7-35 Axial Compressor Velocity Triangle at Hub, Mid and Tip, and the H-S diagram of the thermodynamic properties across these four stages of axial compressor is presented in Figure 7-34 Axial Compressor Enthalpy-Entropy Diagram.

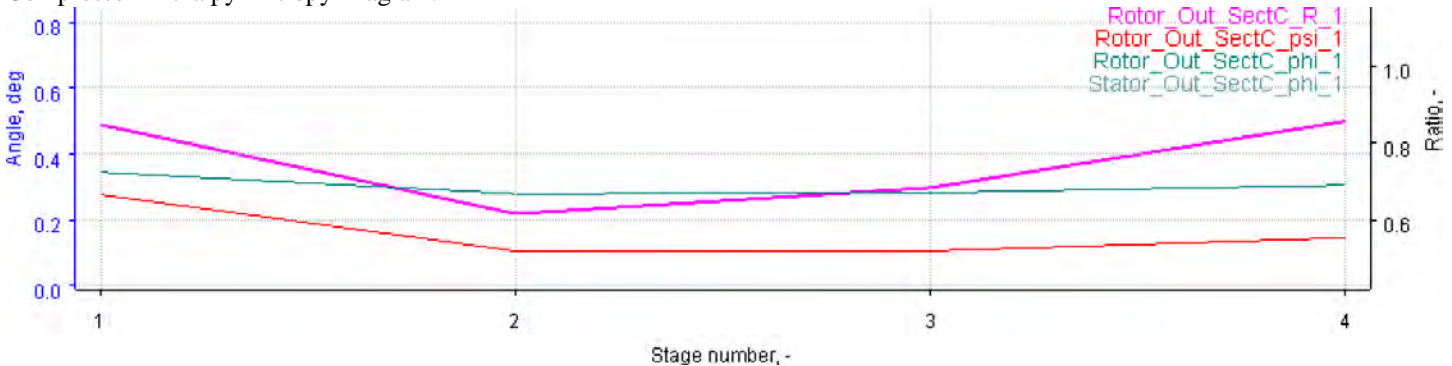


Figure 7-35 Axial Compressor Stage Reaction from Front to Rear

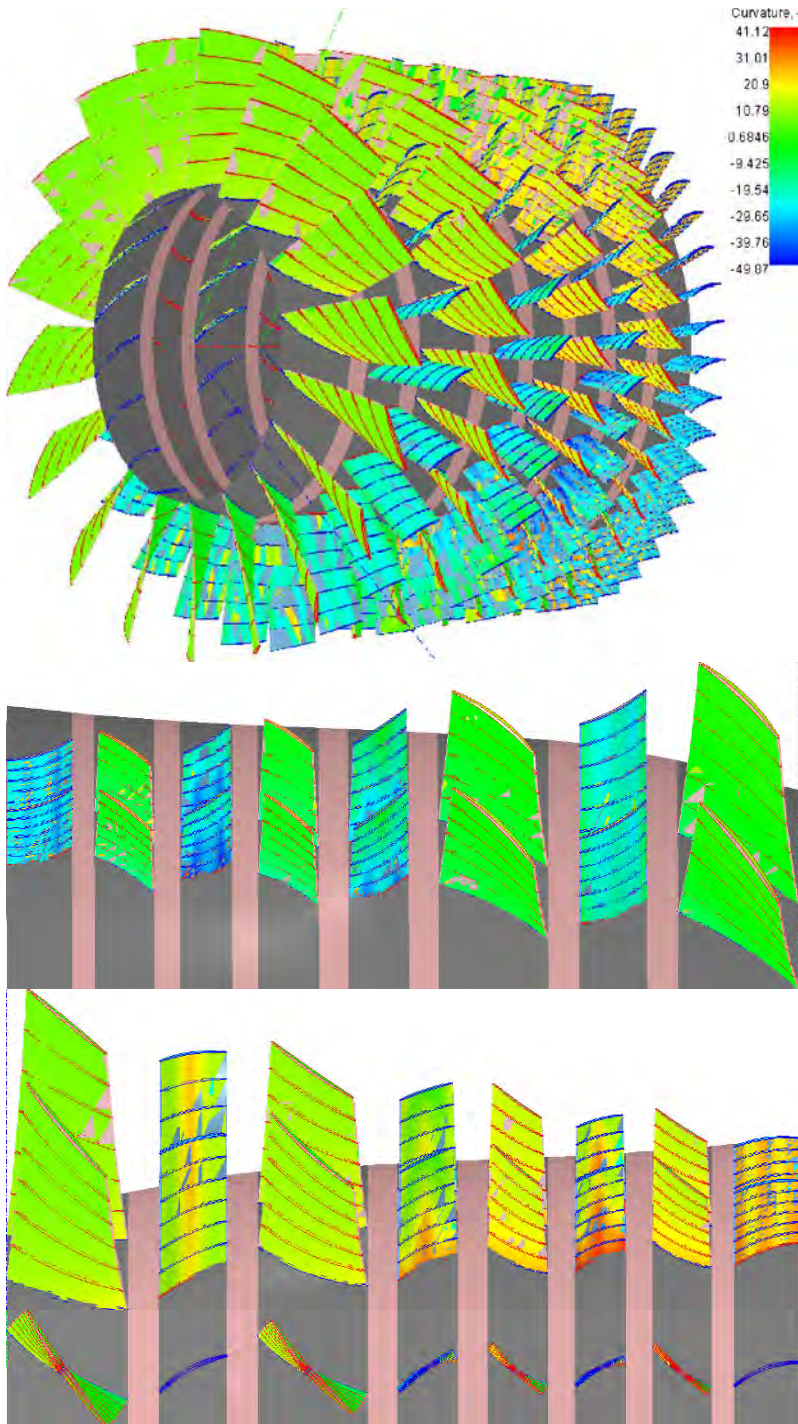


Figure 7-36 3D Axial Compressor Geometry

Finally, the stage reactions from front to rear are shown in Figure 7-36 Axial Compressor Stage Reaction from Front to Rear. Except for the second stage, degree of reaction lies near 0.5. Reason for the obviously lowered level of reaction for all stages is due to the significantly larger rotor blade chord than the stator. Since a larger rotor chord enables a higher level of diffusion within the cascade, rotor blades obviously contribute more to the stage temperature rise. 1st stage also witnesses an elevated degree of reaction than stages coming thereafter. Because no pre-swirl is present for the 1st stage rotor blade, which is typically long and with high tip Mach number, degree of stage work input along the cascade is self-explanatorily stronger than its successors. Similar phenomenon of a higher 1st stage degree of reaction can also be found in *Gas Turbine Theory* (Saravanamuttoo, Rogers, Cohen, & Straznicky, 2009, p. 220).

7.4.4. Axial Compressor Profiling & 3D Design

Per SoftInWay recommendation (SoftInWay), compressor blades are profiled using Custom DCA Profiling, which provides satisfactory transonic performance. Due to the considerable extent of availability of DCA cascade performance information, no cascade performance diagrams will be provided for the compressor. However, similar diagram can be found in *Compressor Aerodynamics* (Cumpsty, 2004, p. 143). Staking mode of the profile along the blade height is set to Profile Centroid, which eases the centrifugal untwisting in rotors. After the automatic profiling processes in AxSTREAM, 3D blade

geometry is provided in Figure 7-37 3D Axial Compressor Geometry with the color contour representing mean curvature.

7.5. Centrifugal Compressor Design

7.5.1. Centrifugal Compressor Architecture

Conventionally, centrifugal compressor has an axial inlet and radial outlet, which fully eliminates the axial fluid momentum at the exit of diffuser. Although this architecture benefits the pursuit of a higher efficiency due to the large loss-free centrifugal contribution to the pressure rise, it limits the maximum adoptable diameter of the stage when coupling together with a reverse flow combustor. Since air needs to be again bended into the axial direction to facilitate the entrance into combustion chamber, a relatively sizable percentage of the radial space needs to be spared for accommodating bending tubes. Thus, instead of the traditional axial-radial architecture, an

axial diagonal-up architecture is adopted, which initiates the air flow bending right at the entrance of diffuser, and when the air reaches the exit of diffuser vanes, only its axial momentum will be left over.

7.5.2. Centrifugal Compressor Preliminary Design

Like Axial Compressor, following parameters are chosen as inputs, while parameters not mentioned are using AxSTREAM default:

- Working Fluid: Ideal Gas
 - Isentropic Exponent = 1.38375 Per off design cycle calculation
 - Gas Constant = 53.349977 Per off design cycle calculation
- Boundary Conditions:
 - Inlet total pressure = 55 psi Per off design cycle calculation
 - Inlet total temperature = 735.2529 °R Per off design cycle calculation
 - Total Pressure at outlet = 205.991 psi Per pressure ratio separation
 - Mass flow rate = 9.83 lb./s Per off design cycle calculation
 - Inlet flow angle = 0 axial degree No inlet pre-swirl
 - Shaft rotational speed = 39,129.1995 rpm Per GGT design
- Constraints
 - Number of Stages = 1 To avoid high-loss inter-compressor duct
- Parameters

- $3 \leq \text{Inlet mean Diameter} \leq 8 \text{ in}$

To achieve higher compressor efficiency, a lower inlet mean diameter than the axial compressor outlet is needed.

This fact is validated by Figure 7-38 Centrifugal Compressor Relationship between specD_1 and Efficiency. As the diameter goes down, efficiency goes up. However, considering the problem of structure design, a lower limitation is selected according to the baseline engine.

- $1.5 \leq \text{Rotor Diameter Ratio } (D2/D1) \leq 3$
Chosen per SoftInWay recommendation (SoftInWay).

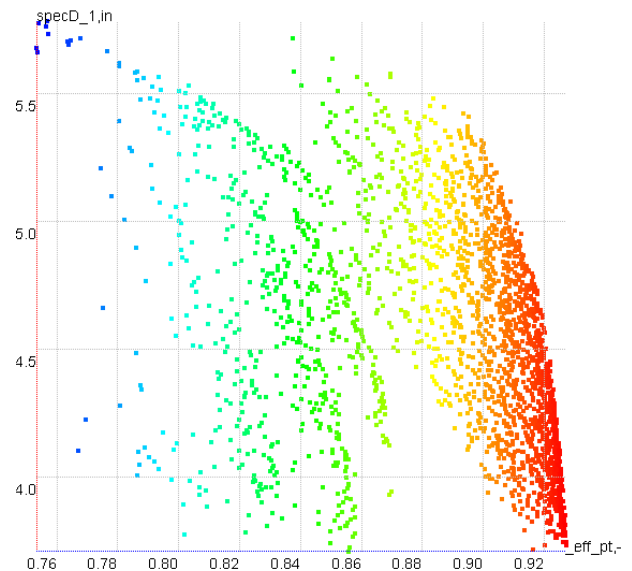
- $0.4 \leq \text{Flow Factor } (c1z/u1) \leq 1.2$
Chosen per SoftInWay recommendation (SoftInWay).

- Meridional Velocity Gradient $(Cm_z/Cm_1) = 1$
Meridional velocity gradient reflects meridional velocity distribution between stages. As for 1-stage compressor, this parameter is meaningless and set to 1 per Ax-STREAM default.

Rotors and Stators are profiled using SoftInWay Custom Camber Profiling per user manual recommendation (SoftInWay).

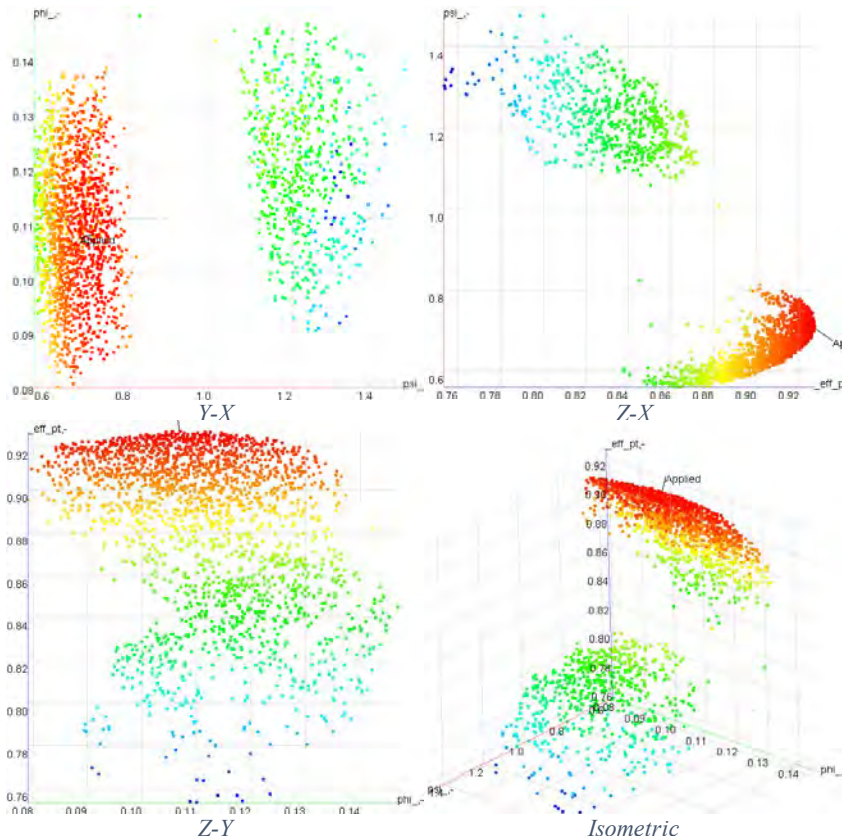
7.5.3. Centrifugal Compressor Design Space

Using the corresponding inputs, a design space with totally 2196 design points is generated as presented in Figure 7-39 Centrifugal Compressor



Horizontal Axis: Polytypic Efficiency
Vertical Axis: Inlet Mean Diameter specD_1
Contour: Polytypic Efficiency

Figure 7-37 Centrifugal Compressor Relationship between specD_1 and Efficiency



X — Stage Loading (psi); Y — Flow Coefficient (phi); Z — Total-to-total Efficiency
 Figure 7-38 Centrifugal Compressor Design Space

thus increase the likelihood of surging. For this reason, the number of diffuser vanes is usually less than the number of impeller vanes. (Saravanamuttoo, Rogers, Cohen, & Straznicky, 2009, p. 182). Next, the meridional flow path of the machine is frozen and presented in Figure 7-40 Centrifugal Compressor Meridional Flow Path.

7.5.4. Centrifugal Compressor Streamline Analysis

Due to the module constraints of centrifugal compressor, AxSTREAM is unable to fit the calculation results using curves. However, streamline calculation still provides insight on temperature, pressure, Mach number, entropy, and velocity. Accordingly, these physical properties are shown together with centrifugal compressor meridional dimensions in Figure 7-41 Miscellaneous Centrifugal Compressor Flow Path Info. Due to the convex shape of the casing at the tip vicinity of rotor inlet, Mach number at this region exhibits the highest value because of the acceleration.

Velocity triangles at 3 blade sections are provided in Figure 7-42 Centrifugal

Compressor Velocity Triangle at Hub, Mid and Tip. Lastly, a h-S diagram of thermodynamic properties across this single stage of centrifugal compressor is provided in Figure 7-43 Centrifugal Compressor Enthalpy-Entropy Diagram. Same as for axial compressor, blue lines correspond the processes in stators, while red lines stand for processes across rotors. Solid and dash lines represent static and total enthalpy respectively. Owing to restricted increase of diameter, the differ is the largest resource for entropy increment. Since the stator vanes can only bend the air from tangential to axial, relatively longer duct is need for the same amount of diffusion, which results in prominent level of friction loss. However, the absence of an end-diffuser bending tube permits a larger rotor size.

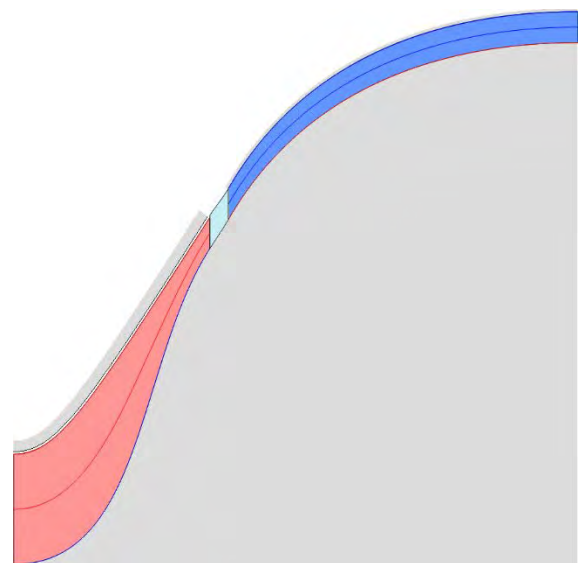
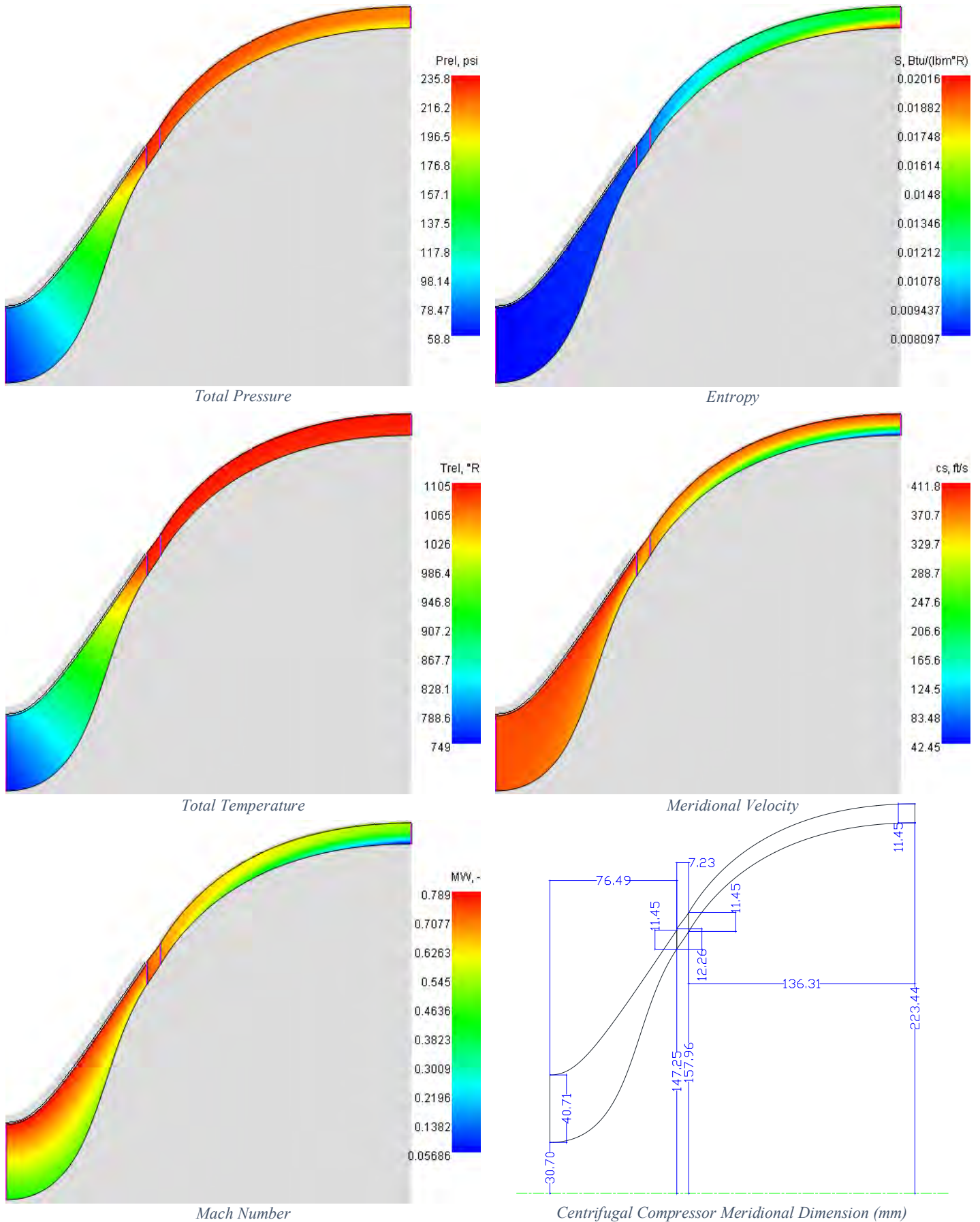


Figure 7-39 Centrifugal Compressor Meridional Flow Path

Design Space. Nomenclature in the figure are the same as in axial compressor design process. Like the axial compressor, top 50 design options are imported to PD Map for performance calculation under Cycle Design Point. Finally, Design Point 462 is selected. After similar manual adjustments on flow path and S1 flow surface optimizations, blade numbers are confirmed as 12 and 11 respectively for rotor and stator. Stator vanes are less than rotor blades, which presents good avoidance to surge and vibrational issues. The tendency to surge appears to increase with the number of diffuser vanes. This is because it is very difficult to split the flow of air so that the mass flow is the same in each passage. When there are several diffuser channels to every impeller channel, and these deliver into a common outlet pipe, there is a tendency for the air to flow up one channel and down another when the conditions are conducive to surging. If this occurs in only one pair of channels, the delivery pressure will fall, and



Results purely using Streamline Method. Difference between Streamline Method and CFD see Cumpsty (2004, pp. 93-131).

Figure 7-40 Miscellaneous Centrifugal Compressor Flow Path Info

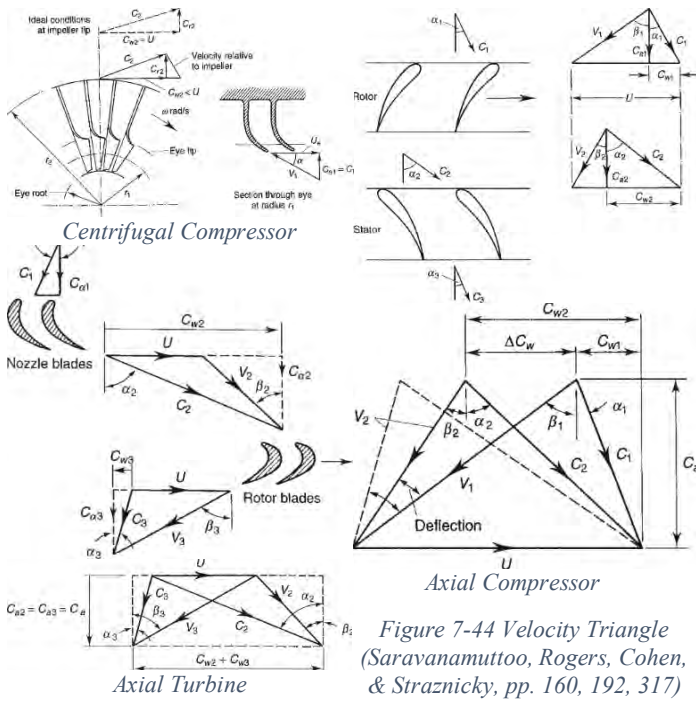


Figure 7-44 Velocity Triangle (Saravanamuttoo, Rogers, Cohen, & Straznicky, pp. 160, 192, 317)

7.6. Hand Calculation of Velocity Triangle

According to the requirement of AIAA RFP (AIAA, 2016), one set of hand calculations showing velocity triangle for the first stage of each component needs to be provided. To facilitate the presentation of hand calculation process, nomenclature and simplifications on the velocity triangle is provided in Figure 7-45 Velocity Triangle (Saravanamuttoo, Rogers, Cohen, & Straznicky, pp. 160, 192, 317). Due to the purely academic nature of this hand calculation requirement, the common assumption of same velocity into and out of an axial stage is being adopted, which is widely used as the main method for students training by major turbomachinery texts (Saravanamuttoo, Rogers, Cohen, & Straznicky, 2009). Calculation will be performed on the pitch line, while the angle of incidence for all turbomachinery components is assumed zero. For inlet velocity triangle, spool speed ω , pitch line radius r , absolute incoming air velocity C , and incoming air angle α are read from previously mentioned velocity diagrams Figure 7-10, Figure 7-22, Figure 7-35, and Figure 7-42. Thus, blade metal tangential speed $U = \omega \times r$, and $C_a = C \cos \alpha$, $C_w = C \sin \alpha$. Therefore, relative incoming air angle $\beta = \tan^{-1} \frac{|U - C_w|}{C_a}$, and relative incoming air velocity $V = \frac{C_a}{\cos \beta}$. Follow these processes, all 5 parameters, U , V , C , α , and β , for the inlet velocity triangle can be determined. This repetitive calculation is done in a batch mode presented in Table 7-4 Inlet Velocity Triangle Hand Calculation. As for the calculation of outlet velocity triangle, a similar presentation of the repetitive calculation process is given. Except for the centrifugal component, same C_a and r values as the inlet are assumed for the outlet. Calculation result is shown in Table 7-5 Outlet Velocity Triangle Hand Calculation.

inlet velocity triangle can be determined. This repetitive calculation is done in a batch mode presented in Table 7-4 Inlet Velocity Triangle Hand Calculation. As for the calculation of outlet velocity triangle, a similar presentation of the repetitive calculation process is given. Except for the centrifugal component, same C_a and r values as the inlet are assumed for the outlet. Calculation result is shown in Table 7-5 Outlet Velocity Triangle Hand Calculation.

	Axial Compressor		Centrifugal Compressor		GGT		FPT	
Read ω, r	ω (rpm)	r (in)	ω (rpm)	r (in)	ω (rpm)	r (in)	ω (rpm)	r (in)
	39,129.2	6.0417	39,129.2	4.01983	39,129.2	7.5151	21,041.3	9.17676
Calculate U	1031.5 (ft/s)		686.3 (ft/s)		1283.1 (ft/s)		842.5 (ft/s)	
Read C, α	C (ft/s)	α (deg)	C (ft/s)	α (deg)	C (ft/s)	α (deg)	C (ft/s)	α (deg)
	740.0	0	384.8	0	1670.4	71.9	991.5	61.5
Calculate C_a, C_w	C_a (ft/s)	C_w (ft/s)	C_a (ft/s)	C_w (ft/s)	C_a (ft/s)	C_w (ft/s)	C_a (ft/s)	C_w (ft/s)
	740.0	0	384.8	0	520.2	1587.4	473.6	871.2
Calculate β	54.3 (deg)		60.7 (deg)		30.3 (deg)		3.5 (deg)	
Calculate V	1269.5 (ft/s)		786.8 (ft/s)		602.6 (ft/s)		474.5 (ft/s)	

Table 7-4 Inlet Velocity Triangle Hand Calculation

	Axial Compressor		Centrifugal Compressor		GGT		FPT	
Read ω, r	ω (rpm)	r (in)	ω (rpm)	r (in)	ω (rpm)	r (in)	ω (rpm)	r (in)
	39,129.2	6.0417	39,129.2	4.01983	39,129.2	7.5151	21,041.3	9.17676
Calculate U	1031.5 (ft/s)		1028.3 (ft/s)		1283.1 (ft/s)		842.5 (ft/s)	
Read β and C_a or V	β (deg)	C_a (ft/s)	β (deg)	V (ft/s)	β (deg)	C_a (ft/s)	β (deg)	C_a (ft/s)
	45.2	740.0	69.7	1060.0	70.8	520.2	64.2	473.6
Calculate V_ω and V or C_a	V (ft/s)	V_ω (ft/s)	C_a (ft/s)	V_ω (ft/s)	V (ft/s)	V_ω (ft/s)	V (ft/s)	V_ω (ft/s)
	1049.7	744.4	368.0	994.1	1582.5	1494.6	1087.4	978.9
Calculate α	21.2 (deg)		1.8 (deg)		22.1 (deg)		16.1 (deg)	
Calculate C	793.8 (ft/s)		368.2 (ft/s)		561.5 (ft/s)		492.8 (ft/s)	

Table 7-5 Outlet Velocity Triangle Hand Calculation

Note that the hand calculation of the outlet velocity triangle shows a very small value of α for centrifugal compressor, which corresponds to nearly pure axial outlet air direction and absence of tangential momentum at Turbomachinery Design Point. Since the spatial velocity triangle is not projected on to a plane parallel to the rotation axis, the shape of the hand calculated velocity triangle may differ from that generated by AxSTREAM for the centrifugal compressor.

7.7. Detailed Component Information

Due the extensive number of parameters involved in AxSTREAM for defining the 3D geometry of the turbomachinery design outcome, it is not possible to include all of them in this proposal. Therefore, only those geometrical parameters required by the RFP are presented in Table 7-7 Axial Compressor Detailed Information, Table 7-6 Centrifugal Compressor Detailed Information, Table 7-8 GGT Detailed Information, and Table 7-9 FPT Detailed Information respectively. Angles are defined as Figure 7-45 Velocity Triangle (Saravanamuttoo, Rogers, Cohen, & Straznicky, pp. 160, 192, 317)

RPF Nomenclature	Nomenclature in AxSTREAM	Units	Machine Level	Rotor diagonal 1-1	Stator diagonal 3-1
Lieblein Diffusion Factor	--	--	Not available for centrifugal components		
De Haller Number	--	--	Not available for centrifugal components		
Stage Loading	averaged work coefficient (H/U2^2)	--	0.524864	0.524864	--
Flow Coefficient	averaged flow coefficient (C2s/U2)	--	0.178023	0.178023	--
Hub-to-Tip Ratio	mean diameter to blade height ratio	--	--	26.710898	40.012925
		--	--	0.927826229	0.951234885
Number of Blades (Rotor & Stator)	number of blades	--	--	12	11
Solidity	Solidity	--	Tip	9.111363	1.544967
		--	Mid	12.537166	1.599023
		--	Hub	20.597461	1.656999
Pitch	cascade pitch	in	Tip	1.47196	3.809891
		in	Mid	1.052389	3.681094
		in	Hub	0.632817	3.552297
Chord (Axial & Blade)	chord	in	Tip	13.411565	5.886154
		in	Mid	13.193972	5.886154
		in	Hub	13.034425	5.886154
	profile axial chord length	in	Tip	3.011452	5.36673
		in	Mid	3.011452	5.36673
		in	Hub	3.011452	5.36673
Aspect Ratio	aspect ratio	--	--	0.121468	0.076615
Taper Ratio	--	--	Chord Taper	1.028934149	1
	--	--	Axial Taper	1	1
Tip Speed	tangential velocity @ Section 3	ft./s	--	959.9439428	--
Stagger Angle	--	--	Not available for centrifugal components		
Blade metal angles	inlet metal angle	deg	Tip	69.466527	71.749009
		deg	Mid	62.350925	71.749009
		deg	Hub	48.93692	71.749009
	outlet metal angle	deg	Tip	68.284067	60.360734
		deg	Mid	67.550521	59.749009
		deg	Hub	66.768515	59.114035
Velocity Triangles (hub, mean, & tip)	Figure 7-42 Centrifugal Compressor Velocity Triangle at Hub, Mid and Tip				
Degree of Reaction	reaction		Average	0.807439	
Mach Numbers (absolute & relative)	Mach number	inlet	Average	0.293558	0.678845
		outlet	Average	0.738158	0.38906
	Mach number in rel. frame	inlet	Average	0.605027	--
		outlet	Average	0.688316	--

Table 7-6 Centrifugal Compressor Detailed Information

RFP Nomenclature	Nomenclature in AxSTREAM	Units	Machine Level	Rotor 1-1	Stator 2-1	Rotor 3-2	Stator 4-2	Rotor 5-3	Stator 6-3	Rotor 7-4	Stator 8-4
Lieblein Diffusion Factor	diffusion factor (by NASA)	--	Average	0.555285	0.410298	0.447702	0.450719	0.389683	0.462316	0.372392	0.367174
De Haller Number	diffusion factor by de Haller (w2/w1)	--	Average	0.612132	0.8495	0.712158	0.78104	0.786797	0.788556	0.775019	0.855687
Stage Loading	averaged work coefficient (H/U2^2)	--	0.371519	0.480683	--	0.355192	--	0.252539	--	0.301343	--
Flow Coefficient	averaged flow coefficient (C2s/U2)	--	0.711678	0.492008	--	0.561582	--	0.59488	--	0.642488	--
Hub-to-Tip Ratio	mean diameter to blade height ratio	--	--	3.581322	4.235536	4.785308	5.219834	5.681755	6.293141	7.065301	8.477373
	--	--	--	0.563445	0.617995	0.654297	0.678448	0.700677	0.725770	0.752024	0.788971
Number of Blades	number of blades	--	--	18	23	24	29	30	37	36	43
Solidity	Solidity	--	Tip	1.55379	0.942124	1.532404	0.973463	1.039089	1.001196	1.240335	1.405696
		--	Mid	1.023929	0.692578	1.183653	0.775373	0.844927	0.829755	1.050976	1.216574
		--	Hub	0.763549	0.547547	0.964214	0.64427	0.711903	0.708443	0.911777	1.072306
Pitch	cascade pitch	in	Tip	0.694887	0.619357	0.623004	0.529266	0.518004	0.42489	0.443384	0.379114
		in	Mid	1.054477	0.84252	0.806564	0.664482	0.637041	0.512679	0.523271	0.438049
		in	Hub	1.414066	1.065683	0.990125	0.799698	0.756077	0.600469	0.603157	0.496984
Chord (Axial & Blade)	chord	in	Tip	1.079709	0.583511	0.954693	0.515221	0.538253	0.425398	0.549945	0.532919
		in	Mid	1.079709	0.583511	0.954693	0.515221	0.538253	0.425398	0.549945	0.532919
		in	Hub	1.079709	0.583511	0.954693	0.515221	0.538253	0.425398	0.549945	0.532919
	profile axial chord length	In	Tip	0.934046	0.52168	0.845043	0.466655	0.465095	0.398487	0.457712	0.50011
		in	Mid	0.747642	0.514763	0.724915	0.432124	0.422305	0.377042	0.42814	0.50327
		in	Hub	0.618783	0.514738	0.636841	0.409447	0.377316	0.359194	0.39823	0.505011
Aspect Ratio	aspect ratio	--	--	1.908194	2.799955	1.468852	2.422604	2.111852	2.430516	1.664589	1.51367
Taper Ratio	--	--	Chord Taper	1	1	1	1	1	1	1	1
	--	--	Axial Taper	1.5094888	1.0134865	1.3269293	1.1397202	1.2326405	1.1093921	1.1493659	0.9902953
Tip Speed	tangential velocity @ Section 3	ft./s	--	1383.2815	--	1291.4270	--	1232.6947	--	1180.0535	--
Stagger Angle	stagger angle design	deg	Hub	30.35245	26.991749	28.052695	25.657887	30.65413	21.187538	34.141884	20.791341
		deg	Mid	46.574855	28.506069	40.999897	33.424554	38.816769	28.087739	39.427537	19.750533
		deg	Tip	55.498459	28.511504	48.645839	37.880926	46.104898	32.831587	44.241483	19.151994
Blade metal angles	inlet metal angle	deg	Hub	42.569792	40.610451	43.410163	48.011557	45.760487	45.209334	48.835054	41.582682
		deg	Mid	54.344244	43.639091	52.654049	46.47135	48.546953	43.857118	49.056246	39.501066
		deg	Tip	61.854514	43.649962	58.088665	44.76524	54.534837	43.170196	51.64453	38.303987
	outlet metal angle	deg	Hub	18.135109	13.373047	12.695227	3.304217	15.547772	-2.834257	19.448714	0
		deg	Mid	38.805465	13.373047	29.345745	20.377758	29.086586	12.318359	29.798828	0
		deg	Tip	49.142405	13.373047	39.203014	30.996612	37.67496	22.492979	36.838436	0
		Figure 7-35 Axial Compressor Velocity Triangle at Hub, Mid and Tip									
Velocity Triangles	Figure 7-35 Axial Compressor Velocity Triangle at Hub, Mid and Tip										
Degree of Reaction	reaction		Average	0.890648	0.890648	0.890648	0.63488	0.63488	0.63488	0.63488	
Mach Numbers (absolute & relative)	Mach number	inlet	Average	0.697214	0.659892	0.57388	0.730448	0.574229	0.698691	0.563483	0.686789
		outlet	Average	0.642829	0.555522	0.719278	0.560818	0.687094	0.542608	0.666494	0.581333
	Mach number in rel. frame	inlet	Average	1.203259	--	0.885647	--	0.781571	--	0.812936	--
		outlet	Average	0.674272	--	0.612048	--	0.602968	--	0.616288	--

Table 7-7 Axial Compressor Detailed Information

RFP Nomenclature	Nomenclature in Ax- STREAM	Units	Machine Level	Stator 1-1	Rotor 2-1	Stator 3-2	Rotor 4-2
Zweifel Coefficient	Zweifel Coefficient	--	--	0.761028	0.477893	0.527248	0.572412
Taper Ratio	--	--	Chord Taper	1	1	1	1
	--	--	Axial Taper	1	0.6802955	0.8176782	0.5055325
Stage Work	power	Btu/s	1778.925336	884.04841		894.876926	
Stage Pressure Ratio	total-total pressure ratio	--	4.382996	1.99147		2.240771	
		--		1.018073	1.923846	1.021185	2.200306
Degree of Reaction	reaction	--	Average	0.446557		0.471717	
Velocity Triangle	Figure 7-10 GGT Velocity Triangle at Hub, Mid, and Tip						
Aspect Ratio	aspect ratio	--	--	0.85473	2.198609	1.449293	3.55094
AN2	tip diameter at inlet	in	--	8.004614	8.402466	8.662011	9.267517
	hub diameter at inlet	in	--	7.025586	6.964468	6.904702	6.728763
	tip diameter at outlet	in	--	8.291202	8.559964	9.04353	9.424
	hub diameter at outlet	in	--	7.025586	6.978706	6.912097	6.606
	shaft rotational speed	rpm	39129.1955	--	--	--	--
	--	in ² rpm ²	--	--	--	1.12. E+11	--
Number of Blades	number of blades	--	--	41	88	43	90
Chord (Axial & Blade)	chord	in	Tip	0.767784	0.374752	0.786979	0.396796
		in	Mid	0.767784	0.374752	0.786979	0.396796
		in	Hub	0.767784	0.374752	0.786979	0.396796
	profile axial chord length	in	Tip	0.472817	0.234306	0.521211	0.189602
		in	Mid	0.472817	0.302212	0.588735	0.303754
		in	Hub	0.472817	0.344418	0.637428	0.375054
Blade Metal Angles	inlet metal angle	deg	Tip	0.000013	0.150436	-7.175687	-28.379557
		deg	Mid	0.000013	28.656655	-20.23922	20.639045
		deg	Hub	0.000013	46.389686	-29.28848	49.608009
	outlet metal angle	deg	Tip	71.423719	-70.809425	71.281586	-69.723334
		deg	Mid	71.423719	-70.809425	71.281586	-69.723334
		deg	Hub	71.423719	-70.809425	71.281586	-69.723334
Mach numbers (absolute and relative)	Mach number	inlet	Average	0.242091	0.745659	0.259015	0.790585
		outlet	Average	0.756436	0.274781	0.806982	0.332176
	Mach number in rel. frame	inlet	Average	--	0.262012	--	0.289624
		outlet	Average	--	0.766003	--	0.872249
Tip speed	tangential velocity @ Section 3	ft./s	--	--	1434.575274	--	1267.349103
Flow Coefficient	averaged flow coefficient (C2s/U2)	--	0.409121	--	0.403914	--	0.429251
Stage Work Split	--	--	--	0.496956444494644:0.503043555505356			
Pitch	cascade pitch	in	Tip	0.635307	0.30559	0.660723	0.32896
		in	Mid	0.585022	0.276176	0.577393	0.279776
		in	Hub	0.534738	0.246761	0.494063	0.230593
Cooling Flow Details	GGT Uncooled						

Table 7-8 GGT Detailed Information

RFP Nomenclature	Nomenclature in Ax- STREAM	Units	Machine Level	Stator 1-1	Rotor 2-1	Stator 3-2	Rotor 4-2	Stator 5-3	Rotor 6-3
Zweifel Coefficient	Zweifel Coefficient	--	--	0.90526	0.76800	0.75034	0.84723	0.74328	1.37157
Taper Ratio	--	--	Chord Taper	1	1	1	1	1	1
	--	--	Axial Taper	1	0.59272	0.63229	0.63627	0.54132	0.65735
Stage Work	power	Btu/s	948.145244	300.276597		318.731584		329.137063	
Stage Pressure Ratio	total-total pressure ratio	--	2.844227	1.358658		1.420074		1.49433	
		--		1.00794	1.34889	1.00513	1.41243	1.01057	1.368163
Degree of Reaction	reaction	--	Average	0.442161		0.515542		0.571916	
Velocity Triangles	Figure 7-22 FPT Velocity Triangle at Hub, Mid, and Tip								
Aspect Ratio	aspect ratio	--	--	3.30681	4.76387	4.67707	6.17592	5.76992	7.37842
AN2	tip diameter at inlet	in	--	10.6244	11.0054	11.5321	11.9454	12.4763	12.8423
	hub diameter at inlet	in	--	7.72913	7.60189	7.45145	7.37739	7.25258	7.17889
	tip diameter at outlet	in	--	10.9306	11.3220	11.7272	12.2528	12.6122	13.0394
	hub diameter at outlet	in	--	7.67668	7.58282	7.51683	7.39734	7.33026	7.22913
	shaft rotational speed	rpm	21041.2598	--	--	--	--	--	--
	--	in ² rpm ²	--	--	9.3. E+10	--	1.3. E+11	--	1.6. E+11
Number of Blades	number of blades	--	--	79	108	89	112	91	114
Chord (Axial & Blade)	chord	in	Tip	0.492	0.39245	0.45011	0.39310	0.45772	0.39374
		in	Mid	0.492	0.39245	0.45011	0.39310	0.45772	0.39374
		in	Hub	0.492	0.39245	0.45011	0.39310	0.45772	0.39374
	profile axial chord length	in	Tip	0.35096	0.20699	0.26285	0.20025	0.23972	0.18691
		in	Mid	0.35096	0.28155	0.35155	0.25927	0.35973	0.23400
		in	Hub	0.35096	0.34922	0.41572	0.31473	0.44284	0.28434
Blade Metal Angles	inlet metal angle	deg	Tip	0.00001	-31.2632	15.5790	-32.3875	30.0071	-42.5169
		deg	Mid	0.00001	4.16931	-12.9161	-4.38380	-11.3149	-18.8854
		deg	Hub	0.00001	34.1447	-33.0430	19.9597	-39.6532	4.32175
	outlet metal angle	deg	Tip	61.6991	-64.1818	66.7742	-65.2913	65.6394	-63.8062
		deg	Mid	61.6991	-64.1818	62.3894	-65.2913	60.1995	-63.8062
		deg	Hub	61.6991	-64.1818	56.1976	-65.2913	52.0793	-63.8062
Mach numbers (absolute and relative)	Mach number	inlet	Average	0.24933	0.51803	0.23607	0.50843	0.25699	0.50146
		outlet	Average	0.618957	0.255262	0.51869	0.272607	0.511669	0.386846
	Mach number in rel. frame	inlet	Average	--	0.26660	--	0.24466	--	0.26844
		outlet	Average	--	0.55317	--	0.61792	--	0.73781
Tip speed	tangential velocity @ Section 3	ft./s	--	--	734.313	--	1096.70	--	1179.05
Flow Coefficient	averaged flow coefficient (C2s/U2)	--	0.542675	--	0.52506	--	0.50888	--	0.49874
Stage Work Split	--	--	--	0.31669894343740:0.33616324715752:0.34713780940508					
Pitch	cascade pitch	in	Tip	0.43468	0.32934	0.41396	0.34369	0.43541	0.35934
		in	Mid	0.36998	0.27496	0.33965	0.27559	0.34424	0.27928
		in	Hub	0.30528	0.22058	0.26534	0.20750	0.25306	0.19922
Cooling Flow Details	FPT Uncooled								

Table 7-9 FPT Detailed Information

8. Duct Design

In this part three major ducts, intake, inter-compressor duct, and inter-turbine duct, are designed. Analytical methods of estimating duct performance at design and off-design points are also provided.

8.1. Intake Design

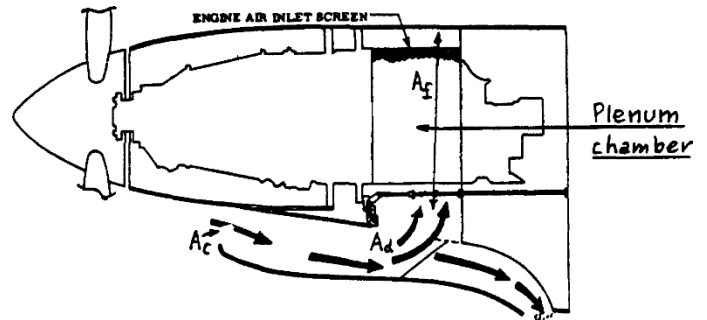


Figure 7-1 Example of Plenum Intake (Roskam, 1985, p. 151)

A plenum inlet is chosen as the inlet of WJ-25 to accommodate the inverse-flow structure of the engine itself. A typical example of a plenum inlet for a turbo-propeller installation was presented in Figure 7-1 Example of Plenum Intake (Roskam, 1985, p. 151). As shown, the plenum inlet consists of a short conventional diffuser in which the air velocity is reduced to almost half its inlet value. Then, the air is “dumped” at the sudden enlargement surrounding the main body of the engine and being sucked into the engine inlet evenly. Design procedures of this plenum inlet for WJ-25 are stated below.

8.1.1. Intake Sizing

Four important section areas are commonly used to define inlet flow properties:

- A_∞ — Stream tube cross section at infinity, also called the inlet capture area.
- A_c — Stream tube cross section at the inlet, also called inlet area or cowl capture area.
- A_f — Stream tube cross section at the engine station, also called internal area.
- A_d — Stream tube cross section at the exit of diffuser, also called the diffuser area.

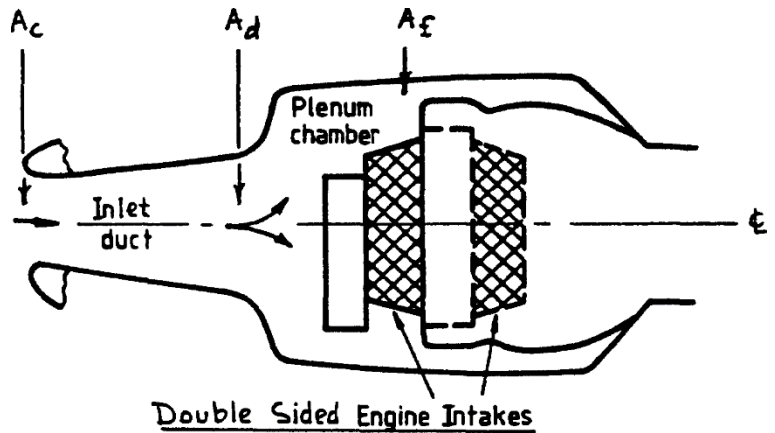


Figure 8-2 Intake Sizing Parameters (Roskam, 1985, p. 151)

A schematic depiction of all 4 sizing parameters is given in Figure 8-2 Intake Sizing Parameters.

8.1.1.1. Capture Area and Inlet Area

According to Roskam (1985, p. 147), the intake of an aircraft is normally working at its peak efficiency at airplane design cruise condition. Thus, the design point of the intake of WJ-25 is set as the cruise point accordingly. Working conditions of the inlet at its design point are listed in Table 8-1 Intake Design Point.

Therefore, inlet capture area can be calculated using equation:

$$A_\infty = \frac{\dot{m}}{\rho_\infty \times v_\infty} = 0.28 ft^2$$

Where,

Parameters	Symbol	Unit	Value	Source
Cruise speed	U_∞	KTAS	337	RFP
Cruise height	H_∞	feet	10000	RFP
Cruise mass flow	m_∞	lb./s	9.01	Cycle Analysis
Cruise air density	ρ_∞	lb./ft ³	0.056456	ISA
Cruise air pressure	P_{s_∞}	psi	10.10647	ISA
Cruise temperature	T_∞	R	483.0084	ISA

Table 8-1 Intake Design Point

- \dot{m} — Air mass flow rate
- ρ_∞ — Air density at infinity
- v_∞ — Air velocity at infinity

Per Roskam (1985, p. 147), inlet operation is often characterized by the inlet flow ratio, A_∞/A_C . If external surface area exists ahead of the inlet, the flow ratio is selected to be closer to 1.0 to prevent inlet separation. If no wetted surface area exists ahead of the inlet, the flow ratio is in the 0.5 - 0.8 range. Consider the extended fuselage structure in front of the inlet of Pylatus PC-21, the flow ratio is set to 0.5. Thus,

$$A_C = \frac{A_\infty}{0.5} = 0.56ft^2$$

8.1.1.2. Diffuser Exit Area and Design

The conventional diffuser between cross section A_C and A_d of WJ-25's new inlet can be simplified as a typical two-dimensional diffuser showed in Figure 8-4 2D Surrogate Diffuser Model (L. R. Reneau, 1967). To accommodate the engine nacelle, the total length N of this diffuser is set to 40 inch, measured from baseline engine. Non-dimensional length N/W_1 can be calculated as 7.7, with height of diffuser entrance W_1 calculated as 5.20 inch using the value of A_C and baseline engine inlet height-width ratio. Therefore, referring to the diffuser effectiveness contour on Figure 8-4 Diffuser Performance (L. R. Reneau, 1967), the area ratio that permits highest diffuser effectiveness $(W_2/W_1)_{MaxEff}$ can be read as around 1.6 for the afore calculated non-dimensional length $N/W_1 = 7.7$. However, the design area ratio $(W_2/W_1)_{des}$ is chosen a little bit conservatively, since real intake diffuser is geometrically bended instead of straight. Too large an angle of flare may result in fluid separation at the location of extensive bending. Finally, based on the value of $(W_2/W_1)_{des} = 1.5$, the diffuser exit area A_d can be calculated as 121.21 in² with diffuser outlet height-width ratio also being the same as baseline engine.

8.1.1.3. Internal Area

Cross section area at the engine inlet is calculated from geometrical dimensions of the compressor design result, when intake for the gas turbine portion is regarded as part of the overall inlet design. Reading the axial compressor 1st stage tip and hub diameters d_{t1} and d_{h1} from its meridional dimensions, internal area A_f can be determined as $A_f = \pi \left(\left(\frac{d_{t1}}{2} \right)^2 - \left(\frac{d_{h1}}{2} \right)^2 \right) \times AR_E = 127.86 in^2$. AR_E is engine inlet area to 1st blade section area ratio measured from baseline engine.

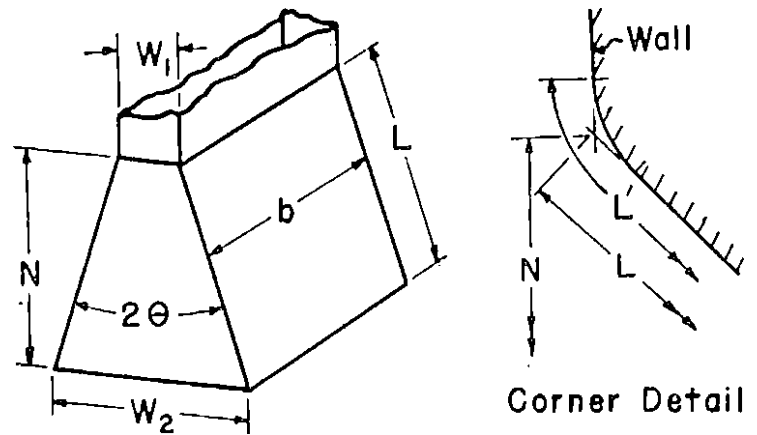


Figure 8-3 2D Surrogate Diffuser Model (L. R. Reneau, 1967)

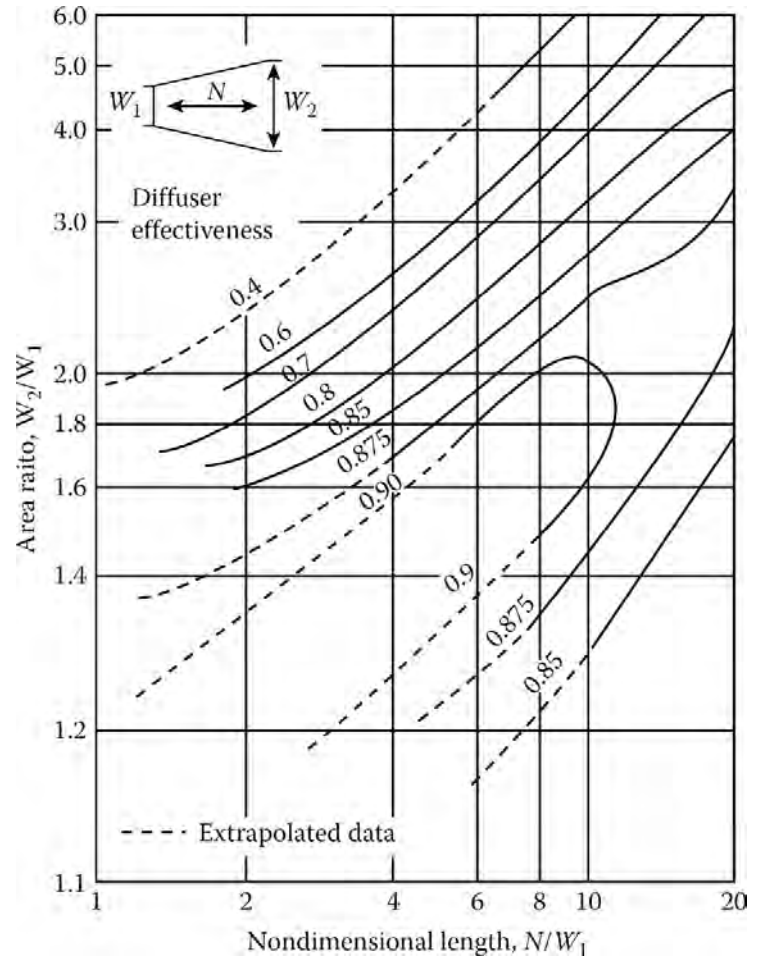


Figure 8-4 Diffuser Performance (L. R. Reneau, 1967)

8.1.2. Inlet Pressure Loss Estimation

According to *Intake Aerodynamics* (J. Seddon, 1999), for turboprop engines with plenum inlets, the pressure loss caused by inlet installation effect is consist of three major parts:

- ΔP_d — Pressure loss caused by the plenum inlet duct, including friction loss and pressure drop in the “sudden enlargement”.
- ΔP_b — Pressure loss caused by propeller in front of engine inlet.
- ΔP_a — Pressure loss caused by approach effect, before air is sucked into inlet.

In the upcoming sessions, method of estimation for each kind of loss will be introduced.

8.1.2.1. ΔP_d Duct Loss

Pressure loss of the inlet duct can be estimated from the method introduced in *Airplane Design VI* (Roskam, 1985, p. 175):

$$\frac{\Delta P_d}{q_c} = \frac{1}{\left(\frac{A_\infty}{A_c}\right)^2} \times \left(\frac{A_c}{A_d}\right)^2 \times \left(1 - \frac{A_d}{A_f}\right)^2$$

Where,

- q_c — Dynamic head of the air flow at the inlet capture section
- A_c, A_d, A_∞ , and A_f — Defined in Section 8.1.1 Intake Sizing

With ram pressure q_c and total pressure p_c at inlet calculated as 1.97psi and 12.08psi respectively from ISA and flight speed, inlet duct pressure loss ΔP_d is finally determined as 0.04psi.

8.1.2.2. ΔP_b Propeller Loss

Wind tunnel tests show that additional loss is attributable to the presence of the propeller blade roots ahead of the intake. Flow over this section is complicate because of the large thickness/chord ratio of the blade root and the action of centrifugal forces on the boundary layer. Pressure loss caused by propeller can be estimated from the method introduced in *Intake Aerodynamics* (J. Seddon, 1999, p. 33):

$$\frac{\Delta P_b}{q_b} = 0.6 \times \frac{Nt}{2\pi r}$$

Where,

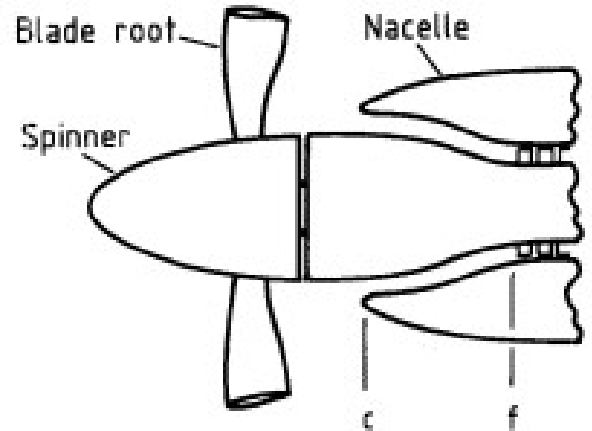


Figure 8-5 Propeller Loss



Figure 8-6 Five Propeller Blades (Pilatus, 2002)

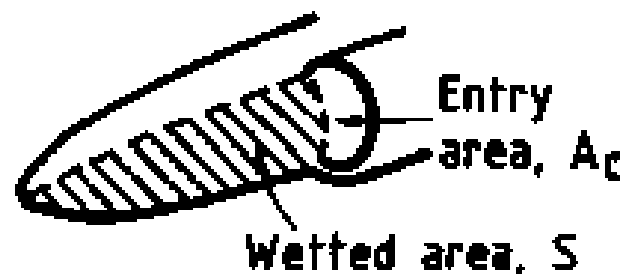


Figure 8-7 Wetted Area (J. Seddon, 1999, p. 18)

- N — Number of the blades; Value: $N = 5$; Source: Figure 8-6 Five Propeller Blades (Pilatus, 2002)
- t and r — Profile thickness and radius of rotation of a representative propeller root section; Value: $t = 0.3$ length unit on screen, $r = 3.5$ length unit on screen; Source: (Pilatus, 2002)
- q_b — Dynamic head at the section of the inlet of blades; Value same as q_c in Section 8.1.2.1 ΔP_d Duct Loss

Based on the equations and parameter value selections above, propeller loss ΔP_b is calculated as 0.08psi.

8.1.2.3. ΔP_a Approach Loss

Approach loss calculated here only include pressure loss caused essentially by friction on the wetted area in front of the inlet of PC-21, namely the wetted area on the fuselage nose. Wetted area means the surface area wetted by the airflow before it enters the inlet duct. This definition is liable to be somewhat imprecise, since streamline patterns ahead of an intake are not usually known with precision. However, for practical purpose, wetted area discussed here can be defined as surface area between generators carried from the ends of the entry where it meets the surface to the foremost point of the fuselage nose, as illustrated in Figure 8-7 Wetted Area. Approach loss can be calculated using the method below (J. Seddon, 1999, p. 21):

$$\frac{\Delta P_a}{q_c} = C_{Fa} \times \left(\frac{A_c}{A_\infty}\right)^3 k \frac{S}{A_c}$$

Where,

- C_{Fa} — The overall friction coefficient of the approach chosen from the Moody Chart
- A_c/A_∞ — Inverse of the inlet flow ratio
- S — Wetted surface area measured and calculated from the official brochure of PC-21 (Pilatus, 2002)
- k — An empirical factor, experience shows that $k = 0.8$ is a sufficiently good approximation for may practical cases

Result for the approach loss at design condition is 0.045psi, with C_{Fa} calculated as 0.002975 and wetted area given as 347.1051761 in².

8.1.2.4. Intake Loss Summary

Combining all three forms of intake losses, namely Duct Loss ΔP_d , Propeller Loss ΔP_b , and Approach Loss ΔP_a , the overall value of pressure loss is 0.266psi, which corresponds to an intake pressure recovery of 0.98626787.

8.1.3. Anti-Icing System

Per Roskam (Roskam, 1985, p. 152), icing of such plenum inlet is a major problem, detailed design of an anti-icing system is required to ensure the feasibility of such

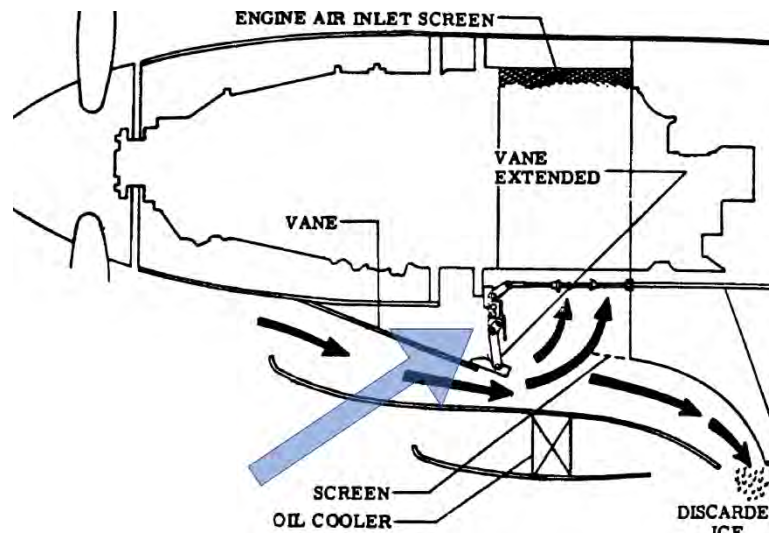


Figure 8-8 Anti-Icing System (Roskam, 1985, p. 368)

INTER-COMPRESSOR DUCT

- AXIAL COMPRESSORS



LAMBDA = 0.15 TO 0.2

INLET MACH NUMBER = 0.3 TO 0.4

DP/P = 1% TO 2%

Figur8-9 Inter-Compressor Duct Loss Estimation (Walsh & Fletcher, 2004, p. 219)

inlet. However, since the overall structure of the inlet remains unchanged, the mechanism of anti-icing system of WJ-25 inlet remains the same as that of other conventional design. A typical example is shown in Figure 8-8 Anti-Icing System (Roskam, 1985, p. 368). When icing problem is encountered, the actuator vane on the top of the inlet duct wall, which is indicated by the arrow, will be extended to increase the velocity of the incoming airflow. Any foreign objects, typically ice and snow, will be rushed to bypass the entrance of the plenum chamber and flow out of the inlet duct from the back exit.

8.2. Inter-Compressor and Inter-Turbine Duct

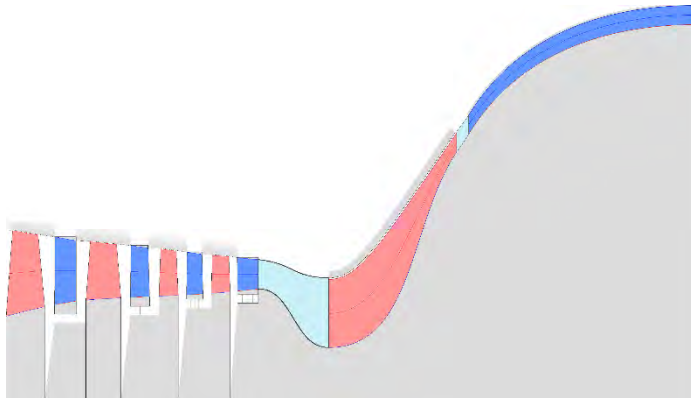


Figure 8-10 Inter-Compressor Duct

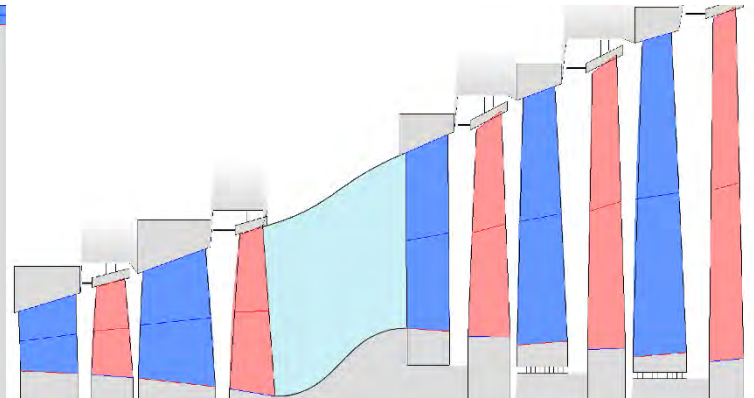


Figure 8-11 Inter-Turbine Duct

Inter-compressor and inter-turbine ducts are designed using the AxSTREAM axial duct module. Since its geometry is automatic generated, no further explanations are given, and the design outcome is presented in Figure 8-10 Inter-Compressor Duct and Figure 8-11 Inter-Turbine Duct. The performance of inter-compressor duct is estimated using the same loss coefficient model as inter-turbine duct, however, with design point pressure loss chosen as 1.5% per Figure 8-9 Inter-Compressor Duct Loss Estimation.

9. Combustion Chamber Design

To accommodate all engine components in limited space and reduce the overall length of gas generator spool, a reverse-flow annular combustion

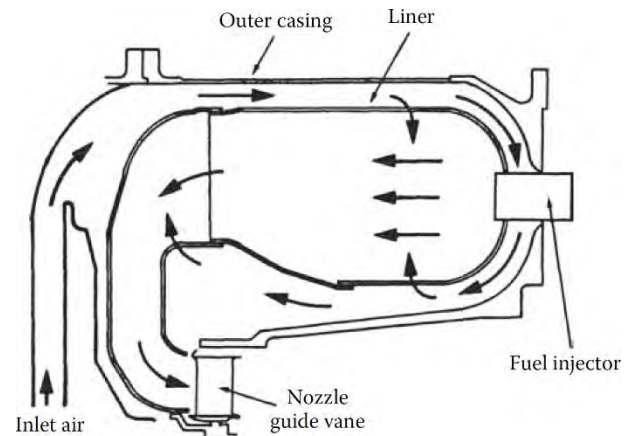


Figure 8-12 Reverse-Flow Combustion Chamber Architecture (Arthur H. Lefebvre, 2010, p. 27)

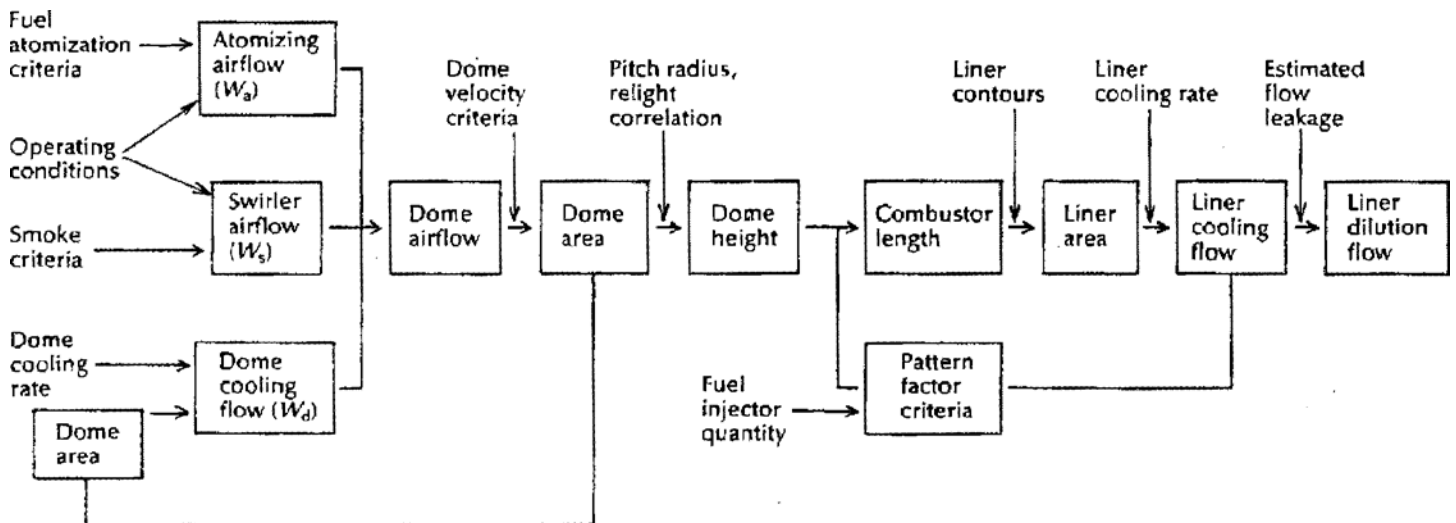


Figure 9-1 Combustion Chamber Flow Path Design Procedure (Mellor, 1990, p. 379)

chamber is utilized in WJ-25. This combustion chamber framework has been widely adopted in turboprop engines in the same class of PT6A, including GE93. Thus, feasibility of reverse-flow annular combustion chamber is already validated. A typical configuration of reverse-flow combustion chamber is shown in Figure 8-12 Reverse-Flow Combustion Chamber Architecture.

In this chapter, combustion chamber of WJ-25 will be designed at the engine cycle design point. Off-design Performance of combustion chamber in other operating conditions will be correlated using publicly available generic models. Generally, combustion chamber of WJ-25 is designed using the method described in *Design of Modern Turbine Combustors* (Mellor, 1990). Overall design procedure is shown in Figure 9-1 Combustion Chamber Flow Path Design Procedure.

9.1. Design Point Selection

According to *Design of Modern Turbine Combustors* (Mellor, 1990, p. 378), the combustion chamber geometry is first specified by determining a single design point, normally a maximum power at standard day sea level operating conditions. The design point of Wj-25 combustion chamber is selected accordingly. Combustor inlet conditions of the design point is quoted from engine cycle calculation and listed in Table 9-1 Combustion Chamber Design Condition.

Parameter	Value	Unit	Source
Total pressure at inlet	273.454	psi	cycle analysis
Total temperature at inlet	1318.02	R	cycle analysis
Static pressure at inlet	250.596	psi	compressor design
Air mass flow rate	12.163	lb./s	cycle analysis
Fuel mass flow rate	0.244	lb./s	cycle analysis
Fuel air ratio	0.02		
Density at inlet	0.5853	lb./ft ³	compressor design
Velocity at inlet	222.4	ft./s	compressor design

Table 9-1 Combustion Chamber Design Condition

9.2. Pre-Diffuser Design

Pre-diffuser is a section in front of the combustor dome aiming to reduce the velocity of compressor exit air and to recover the dynamic head. Normally, a pre-diffuser section consists of two major parts: the standard diffuser region and the step diffuser region. However, in the combustion chamber design of WJ-25, due to the restriction of the engine spacing and the 180° reverse turn at the inlet of the combustion chamber, a high-efficiency standard diffuser is difficult to generate. Thus, all the dynamic head recovery duty will be handled by the step diffuser. Although the pressure recovery capability and the efficiency will be compromised, practical feasibility of this diffuser design can be guaranteed.

The diffuser inlet geometry parameters and flow conditions are inherited from corresponding parameters at the exit of the compressor. One major difficulty in the analysis of dumping performance is to select an appropriate value for the exit cross section of the step diffuser region. According to the method introduced in *Design of Modern Turbine Combustors* (Mellor, 1990, p. 364), the step diffuser ends at the point where flow reattaches to the wall, shown as station 3.2 in Figure 9-3 Step Diffusor Nomenclature (Mellor, 1990, p. 363). In this current design case of WJ-25, considering the configuration of the pre-diffuser part showed in Figure 9-2 Surrogate

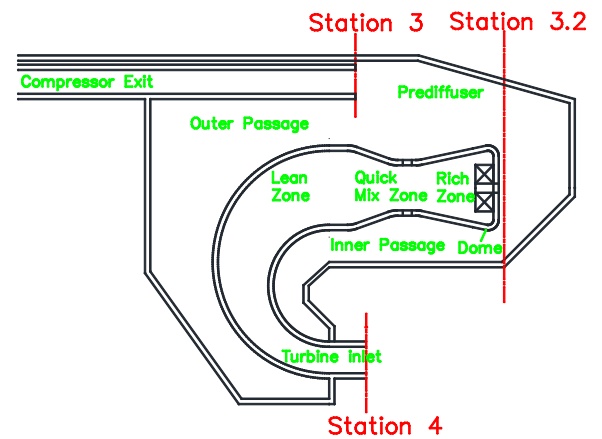


Figure 9-2 Surrogate WJ-25 Combustor Meridional View

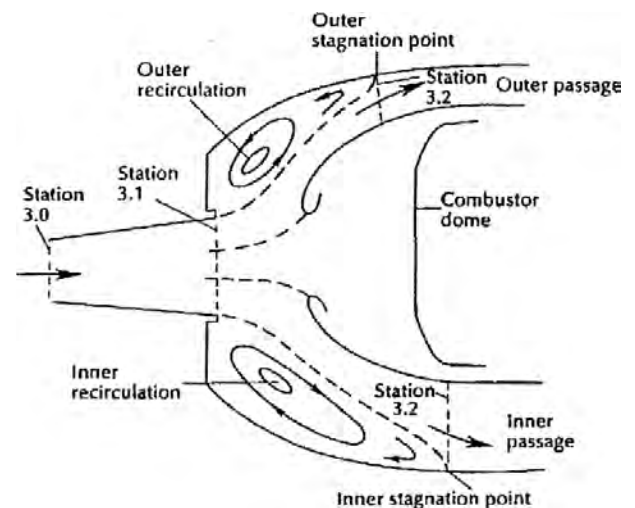


Figure 9-3 Step Diffusor Nomenclature (Mellor, 1990, p. 363)

WJ-25 Combustor Meridional View, the step diffuser exit cross section is selected as the reference cross section of the combustion chamber. This value will first be set according to practical experience and corrected iteratively using the calculated result of the engine sizing part.

Theoretical dumping loss, which is also the total pressure loss of the pre-diffuser section considered here, is obtained by applying the momentum equation with the assumption of uniform, steady, incompressible flow with negligible friction (Mellor, 1990, p. 363):

$$\Delta P_d = P_3 [(P_3 - PS_3)/p_3][1 - A_3/A_{3.2}]^2$$

Where,

- A_3 and $A_{3.2}$ — Cross-section areas at the diffuser inlet and exit
- P_3 and PS_3 — Total and static pressure at diffuser inlet

Parameter	Symbol	Value	Unit	Source
Inlet area of step region	A_3	18.12957481	in ²	compressor design
outlet area of step region 1st selected	$A_{3.2}$	36	in ²	compressor design
Total pressure at step region inlet	P_3	273.454	psi	compressor design
Static pressure at step region inlet	PS_3	250.596	psi	compressor design
Pressure loss in the step region	ΔP_{dsr}	5.632523317	psi	(Mellor, 1990, p. 363)

Table 9-2 Pre-Diffusor Design Calculation

Geometry parameters and calculated results are listed in Table 9-2 Pre-Diffusor Design Calculation.

9.3. RQL Combustor Configuration

Under the pressure of globe warming and climate change, new generation of gas turbine combustion systems are required to implement new means of pollutant reduction. In this design project of WJ-25, to achieve

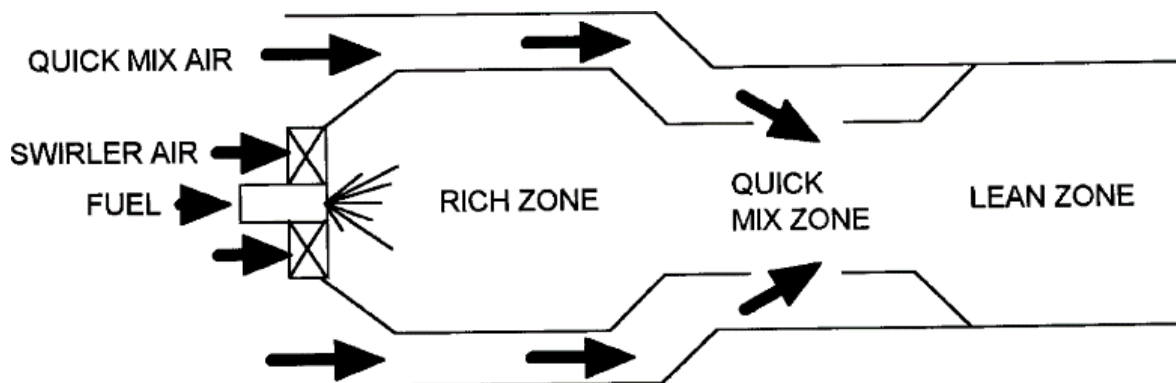


Figure 9-4 RQL Combustor (Christopher O. Peterson, 2002)

the emission reduction target, a promising configuration of three-stage RQL (Rich Burn – Quick Mix – Lean Burn) is conducted. According to NASA (Christopher O. Peterson, 2002), the combustion process is separated into two parts in a RQL combustor. In the primary zone, a fuel-rich burn is conducted, in which all fuel reacts with a fraction of the total air. At the end of the primary zone, via dilution jets, a substantial portion of remaining air is injected and mixed instantaneously with combustion products exiting the primary zone. With the addition of remaining air, the mixture is converted from fuel rich to fuel lean. During the entire process, equivalence ratio of reaction is kept away from the stoichiometric 1, which results in lower flame temperature and limited creation rate of NO_x. A typical architecture of RQL combustion chamber is showed in Figure 9-4 RQL Combustor (Christopher O. Peterson, 2002). Note that chamber wall cooling air is omitted from this figure. Comparing to other low emission combustion concepts, such as LPP and LDI, RQL combustor has the advantage of practical feasibility and all-range reliability. Since the target engine of this RFP is based on the baseline engine PT6A-68B produced by Pratt & Whitney Canada, using a combustor configuration co-developed by NASA and Pratt & Whitney may reduce new technology development and implementation cost. Additionally, unlike LPP and other low emission combustors, the flame stability in the primary zone is highly guaranteed because of the fuel-rich combustion in this area. Thus, the engine may possess a lower lean fuel flame out limit, which permits a faster deceleration in transient performance.

9.4. Air Flow Distribution

Airflow in the burner is distributed to different combustion zones to permit the desired fuel-air ratio. According to *Design of Modern Turbine Combustors* (Mellor, 1990, p. 378), airflow distribution normally does not vary significantly with combustor operating conditions. Exact nomenclature for different airflows discussed in this design process are listed below:

- W_3 — Compressor exit airflow
- W_c — Combustor airflow, Airflow into the combustion section
- W_a — Fuel atomizing airflow admitted through the fuel injector to brake the fuel into small drops
- W_s — Swirler airflow admitted through a swirler around the atomizer to provide a strong, well-mixed recirculation zone within the primary zone
- W_{dc} — Dome cooling flow
- W_d — Combustor dome flow $W_d = W_a + W_s + W_{dc}$
- W_{pas} — Passage flow
- W_{dil} — Dilution air jets downstream of the primary zone to convert fuel-rich burn to fuel-lean burn
- W_{lc} — Liner cooling flow. Cooling flow other than W_{dc}

9.4.1. Fuel Atomizing Flow

An initial estimation of atomizing airflow can be generated using the experience fuel-air ratio provided in *Design of Modern Turbine Combustors* (Mellor, 1990, p. 380). From the text, atomizer airflow should be at least two to three times the atomizer fuel flow, which means that normally 5-7.5% of combustor airflow is used by the atomizer. Lower levels will compromise atomization while higher levels may reduce blowout capability. Fuel atomizing flow and other related parameters are listed in Table 9-3 Fuel Atomizing Flow Calculation.

Parameter	Symbol	Value	Unit	Source
Combustor Airflow	W_c	12.163	lb./s	
Fuel Flow	W_f	0.244	lb./s	
Maximum Atomize Air Fuel Ratio	AFR_{max}	2		(Mellor, 1990, p. 380)
Minimum Atomize Air Fuel Ratio	AFR_{min}	3		(Mellor, 1990, p. 380)
Atomize Air Fuel Ratio Chosen	AFR_{aa}	3		
Fuel Atomizing Flow	W_a	0.732	lb./s	
		60.182521	%	

Table 9-3 Fuel Atomizing Flow Calculation

9.4.2. Swirler Flow

Based on laboratory studies of spray flames, primary zone equivalence ratio should be below about 1.4 to 1.5 to avoid excessive smoke formation. According to method introduced by Mellor (1990, p. 381), it is adequate to set the equivalence ratio at the swirler exit, including both W_a and W_s . Since the fuel atomizing flow has already been calculated, the swirler flow can be generated accordingly. Swirler flow and other related parameters are listed in Table 9-4 Swirler Flow Calculation.

Parameter	Symbol	Value	Unit
Practical equivalence ratio at swirler exit	φ_{se}	2	
Fuel air ratio at swirler exit	FAR_{se}	0.133333333	
Overall air flow at swirler exit	$W_s + W_a$	1.83	lb./s
Swirler flow	W_s	1.098	lb./s
		12.163	%
Guideline of minimum swirler flow	$W_{s,g}$	11	%

Table 9-4 Swirler Flow Calculation

9.4.3. Dome Cooling Flow

Estimation of the dome cooling flow needs to be based on the total area to be cooled. However, at this point, a dome cooling flow can be estimated according to previous experience to carry on the combustor sizing process. An accurate value will be updated after actual dome area has been calculated. Dome cooling flow and other related parameters are listed in Table 9-5 Dome Cooling Flow.

Parameter	Symbol	Value	Unit
Experimental dome cooling rate	CR_d	0.5	kg/(s×m ² ×atm)
		4.83921E-05	lb./(s×in ² ×psi)
Dome cooling flow rate assumed		0.15	
Dome cooling flow assumed	$W_{dc,a}$	1.82445	lb./s
Dome air flow	W_d	3.65445	lb./s
		30.0456302	%

Table 9-5 Dome Cooling Flow

9.4.4. Passage Air Flow, Dilution Flow and Liner Cooling Flow

According to Mellor (1990, p. 389), normally in a RQL combustor, the equivalence ratio in the secondary zone should be between 0.5 and 0.8. Higher levels will increase NOx emission, while lower levels may result in quench, when engine is working at sever part load conditions. Passage air flow, dilution flow, liner cooling flow and related parameters are listed in Table 9-6 Passage Air Flow, Dilution Flow and Liner Cooling Flow.

Parameter	Symbol	Value	Unit
Passage air flow	W_p	8.50855	lb./s
		69.95436981	%
Equivalence ratio selected	φ_p	0.5	
Dilution flow at the primary zone exit	W_{dil}	7.176470588	lb./s
		59.00247133	%
Liner cooling flow	W_{lc}	1.332079412	lb./s
		10.9518985	%

Table 9-6 Passage Air Flow, Dilution Flow and Liner Cooling Flow

9.5. Combustion Chamber Sizing

9.5.1. Reference Area Calculation

Reference areas are calculated using “velocity method” introduced by Mellor (1990, p. 383). According to this method, dome and passage reference velocities are chosen from previous design. In this design project, to simplify the calculation, passage airflow is assumed to be split equally between inner and outer passages. Once reference velocities are selected, dome and passage areas can be easily calculated using equation:

$$A_i = W_i / (\rho_3 V_i)$$

Where,

- A_i , W_i and V_i — Area, airflow and velocity of a section
- ρ_3 — Air density at the combustion chamber inlet

Parameter	Symbol	Value	Unit
Dome reference velocity selected	V_{rdom}	32.80839895	ft/s
Passage reference velocity selected	V_{rpas}	164.0419948	ft/s
Dome reference area	A_{rdom}	0.190308621	ft ²
		27.40444146	in ²
Passage reference area	A_{rdom}	0.088618009	ft ²
		12.76099333	in ²
Reference area	A_{ref}	40.16543478	in ²

Table 9-7 Reference Area Calculation

Reference areas and other parameters calculated are listed in Table 9-7 Reference Area Calculation.

9.5.2. Dome and Passage Height

After dome and passage areas are specified, dome and passage height can be calculated using the method introduced by Mellor (1990, p. 386):

$$H_D = A_{ref} / (\pi D_{mean})$$

Where,

- H_D — Height of the dome
- A_{ref} — Reference area of the combustion chamber
- D_{mean} — Mean diameter of the combustor

Calculated results and other parameters are listed in Table 9-8 Dome and Passage Height Calculation.

Parameter	Symbol	Value	Unit
Combustor tip diameter selected	D_{tcomb}	15.5	in
Combustor hub diameter 1st calculated	D_{hcomb}	11.42270337	in
Combustor mean diameter selected	D_{mcomb}	13	in
Combustor height calculated	H_c	1.96	in
Dome height calculated	H_d	1.1	in
Half passage height	H_p	0.43	in

Table 9-8 Dome and Passage Height Calculation

Parameter	Symbol	Value	Unit
Injector spacing	B	1.1	in
Mean perimeter of combustor	C_m	40.8407	in
Number of fuel injectors calculated	$N_{fi,c}$	37.12791	
Number of fuel injectors selected	N_{fi}	20	
Combustor length to height ratio	L_c/H_d	4	
Combustor length	L_c	4.4	in

Table 9-9 Fuel Injector Number & Burner Length

9.5.3. Number of Fuel Injectors and Length of Combustor

According to Mellor (1990, p. 387), the number of fuel injectors should be selected such that injector spacing B is about the same as the combustor dome height. Number of fuel injectors, length of the chamber and other related parameters are listed in Table 9-9 Fuel Injector Number & Burner Length.

9.5.4. 3D Geometry of Combustion Chamber

After all the above-mentioned calculations, the geometrical parameters are integrated together in a single 3D model of the combustion chamber. Noting that the purpose of this 3D model is demonstrative for the afore calculated areas, length, numbers, etc., its geometry is only representative instead of exact. A picture of the model is presented in Figure 9-6 3D Combustion Chamber Model

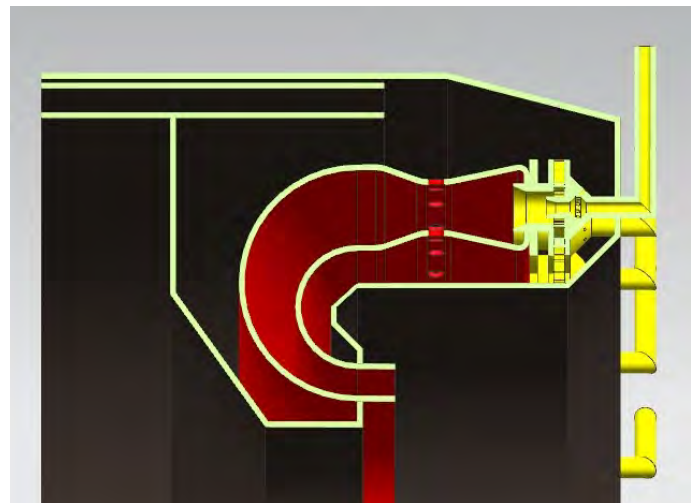


Figure 9-5 3D Combustion Chamber Model

10. Engine Component Test

To facilitate off-design calculation, the component off-design data, such as compressor and turbine map, need to be calculated. In this section, four component types are tested numerically, including compressor, turbine, inlet, and burner.

10.1. Compressor Test

Testbed compressor rig test is usually done with atmospheric inlet condition while outlet being throttled. Thus, the numerical test also follows this legacy. With total temperature and pressure at inlet fixed as ISA SLS values, outlet pressure and mechanical spool speed are chosen as variable. Target values include total-to-total efficiency, inlet corrected mass flow rate, pressure ratio, and corrected spool

speed. Results for both axial and centrifugal compressors are presented in Figure 10-1 Axial Compressor Map and Figure 10-2 Centrifugal Compressor Map. Noting that maps shown here have been manually smoothed to attain a more reasonable illustration.

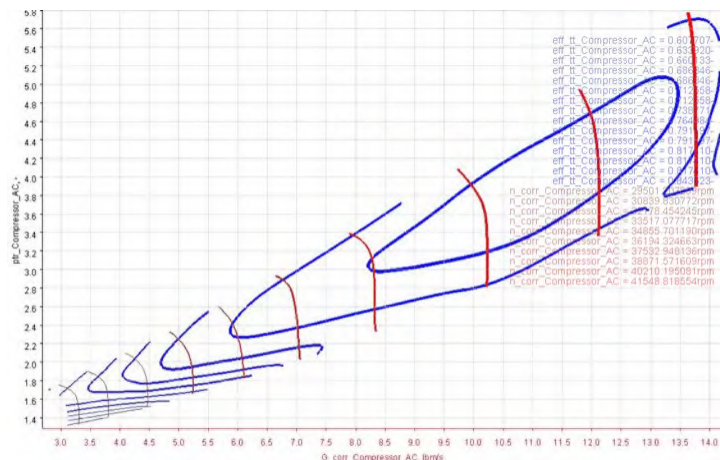


Figure 10-1 Axial Compressor Map

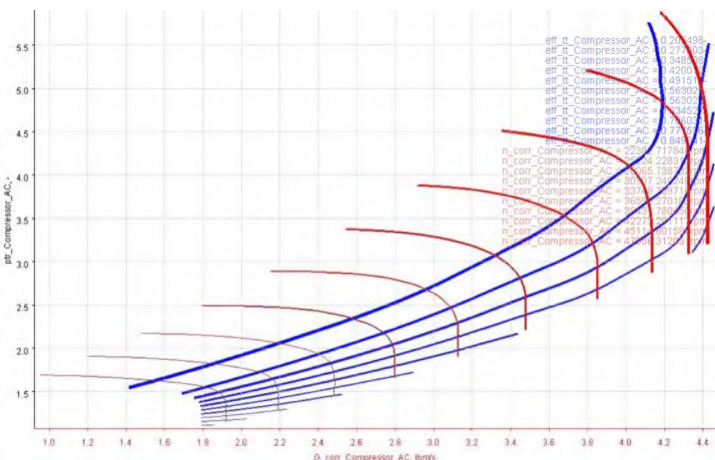


Figure 10-2 Centrifugal Compressor Map

Special note need to be given for axial compressor since a VSV schedule is incorporated with this map test. VSV is well-known for its capability of improving the part load performance. Since it regulates the stagger angle of certain stages of stator vanes, it helps the metal geometry to refit with the varied airflow angle. Therefore, the angle of incidence on the blade cascade is also minimized, which in turn avoids surge and improves efficiency. The only non-satisfying characteristic of VSV is its effect of reducing mass flow rate when flow passage becomes narrow during the re-staggering. However, this fact doesn't manage to limit its popularity in modern compressors, even in advanced turboprop engines, such as GE93. Thus, the axial compressor of WJ-25 also facilitates a 1st stage variable vane, while the staggering schedule of this stage of stator is also tested numerically. For the testing of staggering schedule, SoftIn-Way provided the user with a lengthy and complicated operation tutorial. Physical principle of the numerical test resembles that of the real rig test for VSV schedule. Namely, the operating points on each corrected speed line should firstly be determined. Then the stagger angle is optimized for each operating point on each spool speed line. However, if this procedure is strictly followed, then the off design steady state co-working line must be first calculated. Therefore, a simplification is adopted: due to fact that off design co-working line of a gas turbine engine compressor normally lies within the vicinity of the point of peak efficiency on each corrected spool speed line, the VSV is in fact optimized for the point of peak efficiency instead of off-design working point. A tabular demonstration of the final VSV schedule is presented in Table 10-1 VSV Schedule.

RPM	RA
44000	-2
39600	0
33000	1.5
28600	4.5
22000	6.5

Table 10-1 VSV Schedule

10.2. Turbine Test

Similar as compressor test, the numerical turbine test also follows the legacy of rig test. Namely, the outlet condition is set as atmospheric while the inlet pressure is being varied. With total pressure at outlet fixed as ISA SLS values, inlet pressure and mechanical spool speed are chosen as variable. Target values include total-to-total efficiency, inlet corrected mass flow rate, pressure ratio, and corrected spool speed. Results for both GGT and FPT are presented in Figure 10-4 GGT Map and Figure 10-5 FPT Map respectively.

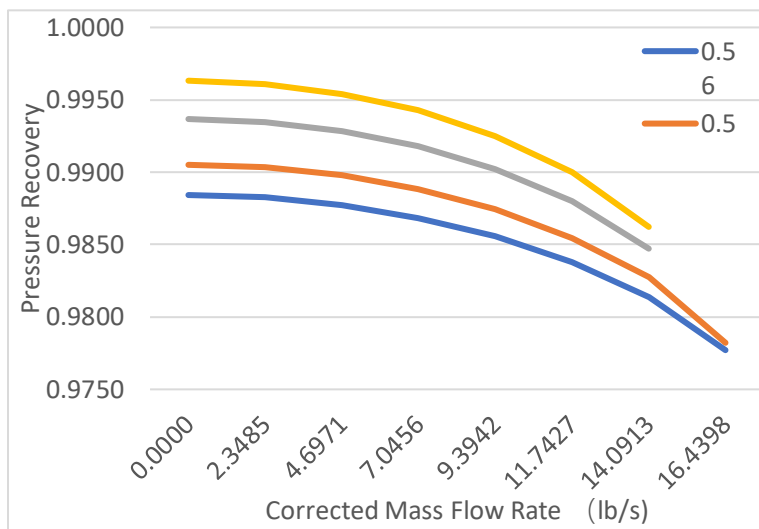


Figure 10-3 Intake Map

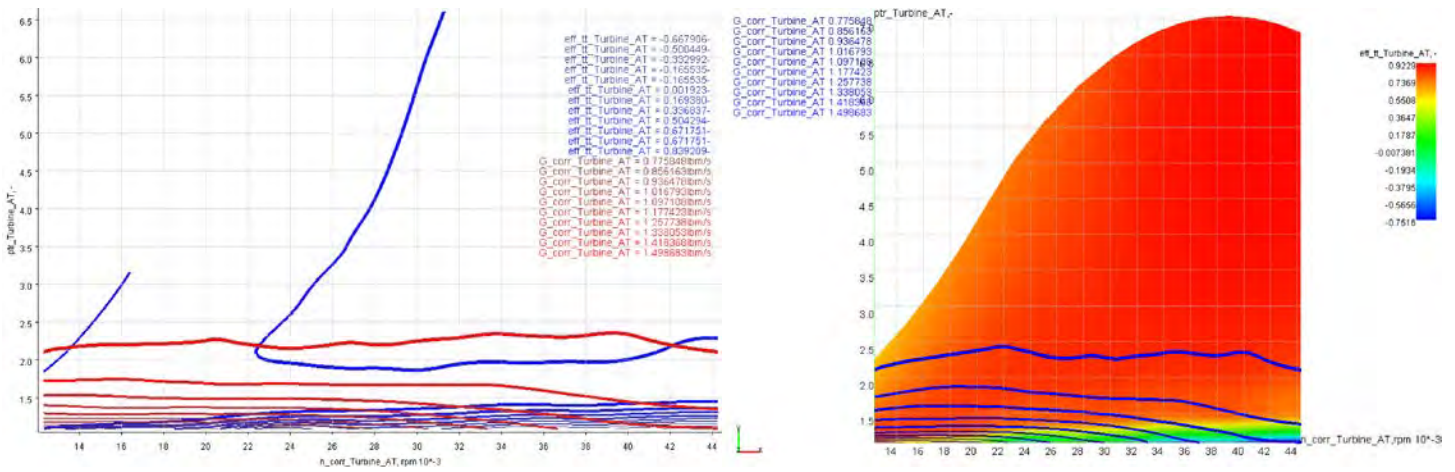


Figure 10-5 GGT Map

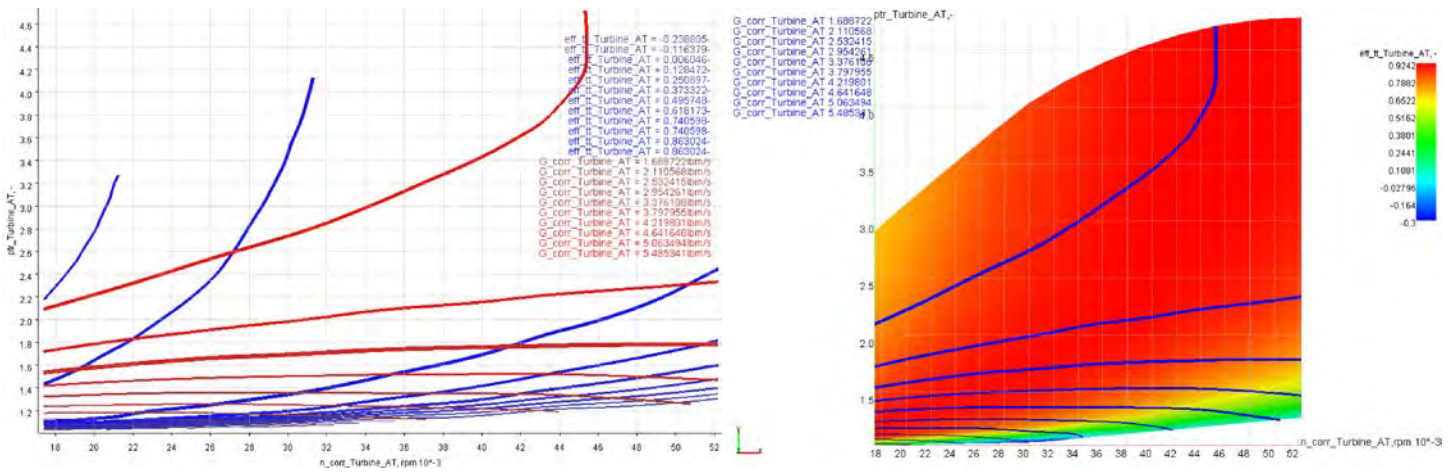


Figure 10-6 FPT Map

10.3. Intake Map

An intake map consists of a single table with the corrected inlet mass flow rate as the argument and flight Mach number as the parameter. This map is tested using the design loss estimation model and presented in Figure 10-3 Intake Map.

Note that with larger corrected mass flow rate or higher Mach number the pressure recovery of the intake map deteriorates. What is shown on the map coincides with the physical instinct.

10.4. Burner Lean Flame Out Limit

To facilitate the generation of transient engine deceleration schedule, the burner lean flame out limit must be tested. However, this process is commonly done experimentally during the development process, and no analytical model has yet been generated to fit all combustion chamber types. Therefore, the burner flame out limit is directly read from a sample pictorial limit line available from open literature. And the result of the flame out limit as well as the original source are presented in Figure 10-5 Combustor Stability Map and Figure 10-5 Combustor Blowout Limit respectively.

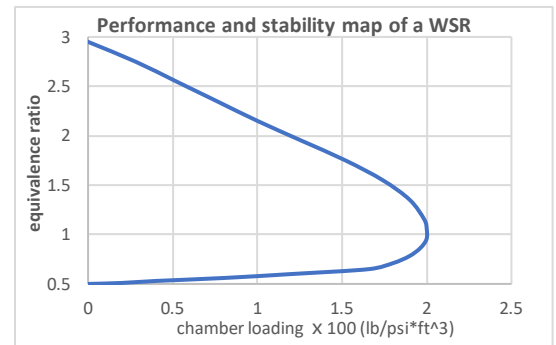


Figure 10-4 Combustor Stability Map

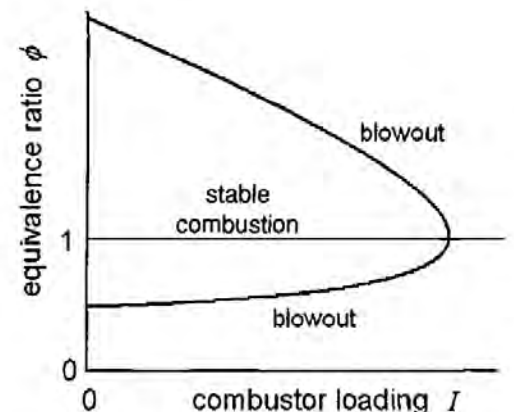


Figure 10-7 Combustor Blowout Limit (Mattingly, 2002, p. 346)

11. Off-Design and Transient Performance

To design the engine controllers with more flexibility and present the off-design and transient performance with higher precision, an open source gas turbine modeling code T-MATS (NASA Glenn Research Center, 2014) from NASA has been utilized as platform for achieving this purpose. However, extensive amount of correction algorithms and modifications have been added to improve the level of fidelity.

11.1. Steady-State Model Building and Verifications

In this section, the modeling process for the steady state is demonstrated. Basic architecture of the model is the same as Figure 4-2 0-D Engine Model, however, with the axial and centrifugal compressor modeled separately as shown in Figure 4-1 Axial-Centrifugal Compressor. Some of the imbedded component model blocks in T-MATS have been modified to obtain a higher compatibility with the model from GasTurb, which will be demonstrated in greater details later in this section.

11.1.1. Steady-State Model Overview

An overview of the steady state MATLAB model is presented in Figure 11-1 Steady-State Model Overview.

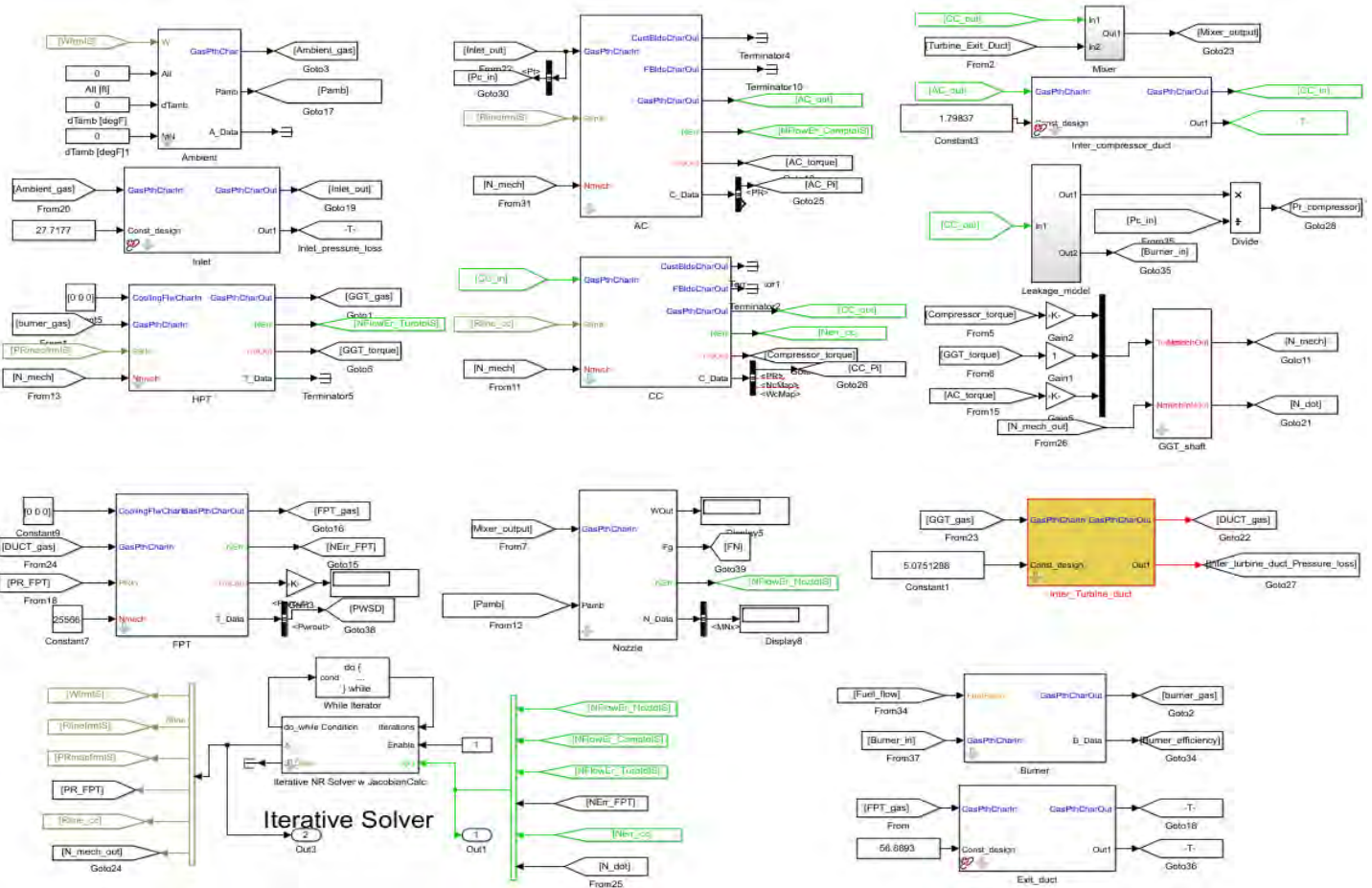


Figure 11-1 Steady-State Model Overview

11.1.2. Main Corrections and Modifications

This section presents correction algorithms proprietary to off design calculations. Design condition model correction are included, however, not mentioned again here.

11.1.2.1. Corrections on Duct Pressure Loss

During off-design and transient calculation, a simplified version of λ pressure loss calculation method demonstrated before in Section 4.2.5 Ducts has been modified to the so-called pseudo loss coefficient, or α coefficient (Walsh & Fletcher, 2004):

$$\frac{\Delta P}{P_{in}} = \alpha \times \left(W_{in} \times \frac{\sqrt{T_{in}}}{P_{in}} \right)^2$$

Except for the inter-compressor duct, initial values of α is determined by solving this equation with Cycle Design Point values of ΔP , W_{in} , T_{in} , and P_{in} . However, since inter-compressor duct was not modeled in Section 4 Aero-Thermodynamic Cycle Analysis, its α value is determined using design point pressure loss estimation mentioned in Section 8.2 Inter-Compressor and Inter-Turbine Duct

11.1.2.2. Corrections on Burner Combustion Efficiency

Per Figure 11-2 Combustor Efficiency versus Loading (H.G. Münzberg, 1977), efficiency of the burner can be correlated to its loading, which is defined as:

$$\Omega = \frac{W_{31}}{P_3^{1.8} \times e^{\frac{T_3}{300K}} \times Vol}$$

Where,

- P_3 — Burner inlet total Pressure
- W_{31} — Burner inlet mass flow rate
- T_3 — Burner inlet total temperature
- Vol — Volume of the combustor

Thus, the combustion efficiency can be calculated as (Kurzke J. , 2015):

$$\log(1 - \eta) = a + b \log(\Omega/\Omega_{des})$$

$$a = \log(1 - \eta_{des})$$

Where,

- η — Burner Efficiency; η_{des} — Design point burner efficiency
- b — A constant chosen as 1.6 by engineering experience (Kurzke J. , 2015)

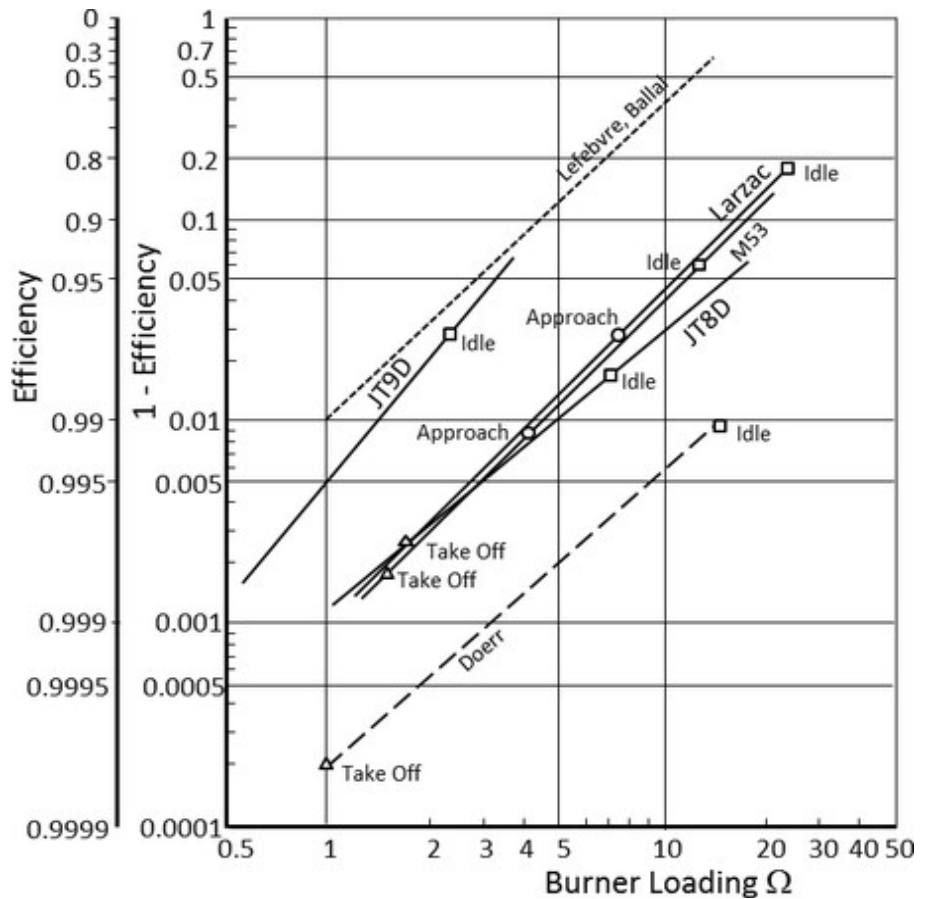


Figure 11-2 Combustor Efficiency versus Loading (H.G. Münzberg, 1977)

Station	W/lb/s			T/R			P/psia		
	T_mats	Gasturb	Raletive Error	T_mats	Gasturb	Raletive Error	T_mats	Gasturb	Raletive Error
1	13.18630141	13.221	-0.002624506	518.67	518.67	2.7879E-08	14.696	14.696	0
2	13.18630141	13.221	-0.002624506	518.67	518.67	2.7879E-08	14.3924	14.392	2.74691E-05
3	12.26326031	12.296	-0.002662629	1315.456	1318.02	-0.001945589	271.4843	273.454	-0.007203062
31	12.14062771	12.163	-0.001839373	1315.456	1318.02	-0.001945589	271.4843	273.454	-0.007203062
4	12.38393771	12.407	-0.001858813	2556.213	2565	-0.003425852	265.921	266.618	-0.002614367
41	12.38393771	12.407	-0.001858813	2556.213	2565	-0.003425852	265.921	266.618	-0.002614367
44	12.38393771	12.407	-0.001858813	1863.613	1869.6	-0.003202494	59.40692	59.657	-0.004191992
45	12.38393771	12.407	-0.001858813	1863.613	1869.6	-0.003202494	58.9491	59.197	-0.004187703
5	12.50657031	12.539	-0.002586306	1402.173	1406.11	-0.002799963	16.97939	16.945	0.002029605
6	12.50657031	12.539	-0.002586306	1402.173	1406.11	-0.002799963	16.63143	16.605	0.001591824

Figure 11-3 Cycle Design Point Model Verification

11.1.3. Steady-State Model Verification

After all modifications, a comparison between the MATLAB model and GasTurb is given in Figure 11-3 Cycle Design Point Model Verification. Satisfying results can be seen from the table with all relative error being less than 1%, which is likely caused by the numerical error. Note that the original surrogate component map used in Section 5.7 Engine Sizing is loaded into both GasTurb and MATLAB during the comparison, and component efficiencies in both models are interpolated from the map instead of using the given value in Table 4-1 Summary of Fixed Input Parameters. Several other operating points are also tested and compared, however, due to the simplicity of this document, they are not presented here.

11.1.4. Critical Off-Design Points

In order to facilitate the comparison of the WJ-25 engine performance with baseline engine, and enable the validation that design outcome meets the performance estimation made in Section 6 Cycle Summary, summary tables for several critical off-design points, including Cycle Design Point, highest COT

Table Name	Inlet Air Condition	Rating Criteria
Cycle Design Point	ISA SLS 0 Mach	PR = 18.9
Highest COT	ISA SLS 0 Mach	COT = 2,565 °R
Turbomachinery Design Point	ISA SLS 0 Mach	Spool Speed = 39,129
Takeoff Rating	ISA SLS 0 Mach	SHP = 1,600, ISA = 27 °F
Cruise Rating	10,000ft, 337 KTAS	SHP = 13,00
Test Bed Data	ISA SLS 0 Mach	No Installation Effects

Table 11-1 List of Off-Design Summary Tables

rating, Turbomachinery Design Point, cruise condition, takeoff condition, and testbed data without installation effects, are given in Table 11-2 Off-Design Summary: Cycle Design Point, Table 11-3 Off-Design Summary: Highest COT, Table 11-4 Off-Design Summary: Turbomachinery Design Point, Table 11-5 Off-Design Summary: Takeoff Rating, Table 11-6 Off-Design Summary: Cruise Rating, and Table 11-7 Off-Design Summary Table: Test Bed Data, without Installation Effects. A tabular summary of the input for each summary table is given in Table 11-1 List of Off-Design Summary Tables.

Special remarks must be made on firstly the Table 11-2 Off-Design Summary: Cycle Design Point. From the summary, when the engine reaches an overall pressure ration of 18.9:1, which is the product of two compressors' design pressure ratio, 4.2 and 4.5, the COT shows a value of 2654.986 °R, higher than the cycle design COT of 2565 °R. The reason for this increase of COT is because of an over optimistic estimation of the component efficiency, such as compressor polytropic efficiency and turbine isentropic efficiency. Thus, the real model indeed consumes more fuel to achieve the same value of pressure ratio. Inlet mass flow rate also shrinks. This is due to the inaccuracy of using external sample map when estimating the mechanical spool speed at cruise condition mentioned in Section 5.7 Engine Sizing. A direct consequence of this matter of fact is a witnessed deterioration of shaft power output. Although a higher COT contributes to engine specific power, a severer decrease of mass flow rate results in a reduction of shaft power delivered. However, the calculated value of 2654.986 °R won't cause any trouble to the user. Since both power requirement, 1600hp at takeoff and 1300 at cruise, can be met with not necessarily so high a COT of 2654.986 °R, customer expectation can still be satisfied, though the Cycle Design Point will never be achieved. Rating condition corresponding a highest COT of 2565 °R is shown in Table 11-3 Off-Design Summary: Highest COT with an overall PR of 17.3.

To demonstrate the customer that the RFP requirement of at least 20% improved fuel burn and 25% greater power output has been achieved, Table 11-7 Off-Design Summary Table: Test Bed Data, without Installation Effects is generated for comparison with the baseline engine PT6A-68B, which possesses a SLS SHP of approximately 1,250 and an SFC of roughly 0.566 lb./hr./SHP. In this summary table without installation effects a power output of 1600 SHP and an SFC of 0.437 lb./hr./SHP are realized, which corresponds a shaft power increment of 28% an SFC drop of 22.8%. However, under this set of test bed data, the WJ-25 hasn't yet been rated to its COT 2565 °R limit. Thus, the RFP requirements are fully reached.

Table 11-2 Off-Design Summary: Cycle Design Point

Cycle Design Point (PR=18.9)														
===SUMMARY OUTPUT DATA===														
MN	alt	dTamb	VTAS	N1	N2	T41	SHP	THP	ESHP	BSFC	ESFC			
0	0	0	0	41093.59326	21041	2654.986132	2087.642072	0	2087.642072	0.449675766	0.449675766			
===FLOW STATION DATA===														
		W/lb/s	ht	Tt/R	Pt/psi	FAR	Pi	Wc	Ps	Ts	R	gamt	Aera	Ma
1	Inlet	12.98697638	123.954269	518.6700145	14.696	0	0.022059391	12.98697656	14.696	518.6700145	0.06856	1.4	50.5	0
2	AC_in	12.98697638	123.954269	518.6700145	14.37181519	0	5.129127673	13.27992358	10.38679549	472.712235	0.06856	1.4	38.35870022	0.697214
24	AC_out	12.07788803	212.0074372	882.629012	73.71487502	0	0.013560672	3.141076717	61.96089393	839.8943098	0.06856	1.4	15.286917	0.504386
25	CC_in	12.07788803	212.0074372	882.629012	72.71525179	0	3.735492905	3.184257386	68.49369461	867.6744179	0.06856	1.4	20.24192531	0.293558
3	CC_out	11.95710915	321.2377785	1316.576772	271.6273071	0	0.020929909	1.030693266	265.8643434	1308.534678	0.06856	1.4	25.55443075	0.175298
4	GGT_in	12.21787639	710.1925395	2654.986132	265.9421723	0.021808552	4.20280221	1.527542219	256.6613452	2638.286649	0.06861	1.216	11.52079622	0.242091
44	GGT_out	12.21787639	508.5553453	1969.531444	63.27734662	0.021808552	0.00992727	5.529457256	59.56259562	1948.478923	0.06861	1.216	35.49304337	0.316295
45	FPT_in	12.21787639	508.5553453	1969.531444	62.64917529	0.021808552	3.627519444	5.58490007	60.3331162	1956.39677	0.06861	1.216	41.78869454	0.249327
5	FPT_out	12.21787639	387.7881463	1539.311343	17.27052777	0.021808552	0.0185834	17.91046788	15.86874758	1516.338659	0.06861	1.216	92.50119511	0.374538
6	Nozzle_in	12.33865527	387.7881463	1537.131071	16.94958264	0.02113417	1.153346669	18.41695602	16.55463064	1531.586727	0.06861	1.181	84.77614583	0.2
8	Nozzle_out	12.33865527	387.7881463	1537.131071	16.94958264	0.02113417	N/A	18.41695602	14.696	1507.529996	0.06861	1.181	84.77614583	0.465797
===TURBOMACHINERY PERFORMANCE DATA===														
Wc	PR	eff	pwr	SM	===BURNERS===									
AxiC	12.89883015	5.175941867	0.834942467	-1579.45358	5.185691074	TtOut	eff	dPnorm	Wfuel	WfuelHr	FAR			
CenC	3.070776438	3.698236623	0.87940698	-1810.97172	10.82794554	2654.986132	0.995018649	0.020929909	0.260767236	938.7620487	0.021808552			
HPT	1.528937209	4.188693566	0.904574134	3407.462605	===NOZZLES===									
FPT	5.58490007	3.627519444	0.808984908	2087.642072	PR	Cfg	Cdth	Cv	Ath	Mnth	Vact	Fg		
					1.153346669	1	0.96	0.975	81.3851	0.465796766	859.5046628	321.3771273		
===INLET===														
Inlet Fram PR														
0 0.977940609														
===DUCTS===														
Inter_Compressor dPnorm MN														
Inter_Turbine 0.00992727 0.316295														
Exit_Turbine 0.0185834 0.374538														

Table 11-3 Off-Design Summary: Highest COT

Highest COT, Tt4 = 2565R														
===SUMMARY OUTPUT DATA===														
MN	alt	dTamb	VTAS	N1	N2	T41	SHP	THP	ESHP	BSFC	ESFC			
0	0	0	0	40654.17185	21041	2565	1889.792743	0	1889.792743	0.449258165	0.449258165			
===FLOW STATION DATA===														
		W/lb/s	ht	Tt/R	Pt/psi	FAR	Pi	Wc	Ps	Ts	R	gamt	Aera	Ma
1	Inlet	12.40911579	123.954269	518.6700145	14.696	0	0.020139982	12.40911596	14.696	518.6700145	0.06856	1.4	50.5	0
2	AC_in	12.40911579	123.954269	518.6700145	14.40002282	0	4.807670503	12.66417217	10.4071817	472.712235	0.06856	1.4	38.35870022	0.697214
24	AC_out	11.54047769	207.161107	862.8545153	69.23056495	0	0.013722103	3.159717655	58.19161588	821.0772451	0.06856	1.4	15.286917	0.504386
25	CC_in	11.54047769	207.161107	862.8545153	68.28057601	0	3.733725443	3.203678866	64.3164784	848.2349653	0.06856	1.4	20.24192531	0.293558
3	CC_out	11.42507291	313.9213583	1288.219756	254.9409239	0	0.02122484	1.0379298	249.5319857	1280.350876	0.06856	1.4	25.55443075	0.175298
4	GGT_in	11.66090758	682.2353649	2565	249.5298435	0.020641853	4.188833651	1.527239411	240.8217725	2548.866517	0.06861	1.216	11.52079622	0.242091
44	GGT_out	11.66090758	487.9553701	1899.574512	59.57024419	0.020641853	0.009840888	5.505347266	56.07312183	1879.269767	0.06861	1.216	35.49304337	0.316295
45	FPT_in	11.66090758	487.9553701	1899.574512	58.98402011	0.020641853	3.477287016	5.560063224	56.80345707	1886.906376	0.06861	1.216	41.78869454	0.249327
5	FPT_out	11.66090758	373.4118558	1488.208068	16.96265503	0.020641853	0.016965207	17.11291249	15.58586365	1465.998049	0.06861	1.216	92.50119511	0.374538
6	Nozzle_in	11.77631236	373.4118558	1486.248235	16.67488007	0.02002619	1.134654333	17.56895183	16.28632908	1480.887422	0.06861	1.181	84.77614583	0.2
8	Nozzle_out	11.77631236	373.4118558	1486.248235	16.67488007	0.02002619	N/A	17.56895183	14.696	1460.947282	0.06861	1.181	84.77614583	0.437448
===TURBOMACHINERY PERFORMANCE DATA===														
Wc	PR	eff	pwr	SM	===BURNERS===									
AxiC	12.66417217	4.807670503	0.846271387	-1446.10619	11.07265976	TtOut	eff	dPnorm	Wfuel	WfuelHr	FAR			
CenC	3.203678866	3.733725443	0.880638913	-1743.18986	14.89067336	2565	0.99395346	0.02122484	0.235834672	849.0048198	0.020641853			
HPT	1.527239411	4.188833651	0.907792675	3045.056546	===NOZZLES===									
FPT	5.560063224	3.477287016	0.819411423	1889.792743	PR	Cfg	Cdth	Cv	Ath	Mnth	Vact	Fg		
					1.134654333	1	0.96	0.975	81.3851	0.437448445	796.2041375	284.1401749		
===INLET===														
Inlet Fram PR														
0 0.979860018														
===DUCTS===														
Inter_Compressor dPnorm MN														
Inter_Turbine 0.009840888 0.316295														
Exit_Turbine 0.016965207 0.374538														

Table 11-4 Off-Design Summary: Turbomachinery Design Point

Turbomachinery Design Point														
===SUMMARY OUTPUT DATA===														
MN	alt	dTamb	VTAS	N1	N2	T41	SHP	THP	ESHP	BSFC	ESFC			
0	0	0	0	39129	21041	2275.003405	1287.480178	0	1287.480178	0.457685606	0.457685606			
===FLOW STATION DATA===														
		W/lb/s	ht	Tt/R	Pt/psi	FAR	Pi	Wc	Ps	Ts	R	gamt	Aera	Ma
1	Inlet	10.40739802	123.954269	518.6700145	14.696	0	0.014166473	10.40739817	14.696	518.6700145	0.06856	1.4	50.5	0
2	AC_in	10.40739802	123.954269	518.6700145	14.48780951	0	3.780543528	10.55695296	10.47062688	472.712235	0.06856	1.4	38.35870022	0.697214
24	AC_out	9.678880163	191.1020451	797.0638533	54.77179449	0	0.014244942	3.219350624	46.03832467	758.4720034	0.06856	1.4	15.286917	0.504386
25	CC_in	9.678880163	191.1020451	797.0638533	53.99157347	0	3.722705598	3.265872791	50.85703829	783.5590102	0.06856	1.4	20.24192531	0.293558
3	CC_out	9.582091362	289.5279139	1192.957101	200.9947328	0	0.022242916	1.062531033	196.7303406	1185.670118	0.06856	1.4	25.55443075	0.175298
4	GGT_in	9.745775013	593.9400533	2275.003405	196.5240239	0.017082247	4.099915359	1.526319095	189.6657454	2260.693959	0.0686	1.28	11.52079622	0.242091
44	GGT_out	9.745775013	424.3601735	1678.907038	47.9336783	0.017082247	0.009383177	5.375792883	45.11969053	1660.96103	0.0686	1.28	35.49304337	0.316295
45	FPT_in	9.745775013	424.3601735	1678.907038	47.48390812	0.017082247	2.946637905	5.426712687	45.72848937	1667.710518	0.0686	1.28	41.78869454	0.249327
5	FPT_out	9.745775013	330.9889929	1334.610907	16.11460575	0.017082247	0.011775152	14.25698229	14.80664715	1314.693172	0.0686	1.28	92.50119511	0.374538
6	Nozzle_in	9.842563815	330.9889929	1333.217926	15.92485381	0.016630184	1.08361825	14.56253345	15.55377961	1328.409085	0.0686	1.2859	84.77614583	0.2
8	Nozzle_out	9.842563815	330.9889929	1333.217926	15.92485381	0.016630184	N/A	14.56253345	14.696	1318.858468	0.0686	1.2859	84.77614583	0.346853
===TURBOMACHINERY PERFORMANCE DATA===														
Wc	PR	eff	pwr	SM	===BURNERS===									
AxiC	10.55695296	3.780543528	0.856708571	-978.755307	17.24004044	TtOut	eff	dPnorm	Wfuel	WfuelHr	FAR			
CenC	3.265872791	3.722705598	0.881251401	-1347.86280	17.71809156	2275.003405	0.987998737	0.022242916	0.163683651	589.2611448	0.017082247			
HPT	1.526319095	4.099915359	0.908432416	2221.39418	===NOZZLES===									
FPT	5.426712687	2.946637905	0.85745767	1287.480178	PR	Cfg	Cdth	Cv	Ath	Mnth	Vact	Fg		
					1.08361825	1	0.96	0.975	81.3851	0.346853151	603.5403972	180.0169836		
===INLET===														
Inlet Fram PR														
0 0.985833527														
===DUCTS===														
Inter_Compressor dPnorm MN														
Inter_Turbine 0.009383177 0.316295														
Exit_Turbine 0.011775152 0.374538														

Table 11-5 Off-Design Summary: Takeoff Rating

Take Off ISA+27F, 1600SHP														
===SUMMARY OUTPUT DATA===														
MN	alt	dTamb	VTAS	N1	N2	T41	SHP	THP	ESHP	BSFC	ESFC			
0	0	27	0	40492.6443	21041	2484.582797	1600	0	1	600	0.443762418	0.443762418		
===FLOW STATION DATA===														
		W/lb/s	ht	Tt/R	Pt/psi	FAR	Pi	Wc	Ps	Ts	R	gamt	Aera	Ma
1	Inlet	10.50223237	130.4286147	545.670002	14.696	0	0	10.77211791	14.696	545.670002	0.06856	1.4	50.5	0
2	AC_in	10.50223237	130.4286147	545.670002	14.696	0	4.368707961	10.77211791	10.62109027	497.3198353	0.06856	1.4	38.35870022	0.697214
24	AC_out	10.50223237	212.488564	884.5900221	64.2025322	0	0.01354666	3.139453558	53.96531279	841.7603726	0.06856	1.4	15.286917	0.504386
25	CC_in	10.50223237	212.488564	884.5900221	63.33280229	0	3.604173891	3.182566709	59.65595268	869.6022021	0.06856	1.4	20.24192531	0.293558
3	CC_out	10.39721005	318.2631743	1305.059657	228.2624325	0	0.02221318	1.061820579	223.4195169	1297.087913	0.06856	1.4	25.55443075	0.175298
4	GGT_in	10.59443779	656.9465192	2484.582797	223.1919979	0.018969295	4.153712095	1.52679107	215.4030627	2468.955126	0.0686	1.256	11.52079622	0.242091
44	GGT_out	10.59443779	469.8110424	1838.499794	53.73314105	0.018969295	0.009662888	5.455330394	50.57869084	1818.847883	0.0686	1.256	35.49304337	0.316295
45	FPT_in	10.59443779	469.8110424	1838.499794	53.21392371	0.018969295	3.220759471	5.508558984	51.24667368	1826.23899	0.0686	1.256	41.78869454	0.249327
5	FPT_out	10.59443779	363.0701701	1452.177524	16.52216634	0.018969295	0.014403235	15.76791824	15.18112767	1430.505225	0.0686	1.256	92.50119511	0.374538
6	Nozzle_in	10.69946012	363.0701701	1450.733464	16.2841937	0.018433429	1.108069794	16.14890196	15.90474631	1445.500751	0.0686	1.2687	84.77614583	0.2
8	Nozzle_out	10.69946012	363.0701701	1450.733464	16.2841937	0.018433429	N/A	16.14890196	14.696	1430.692929	0.0686	1.2687	84.77614583	0.393421
===TURBOMACHINERY PERFORMANCE DATA===						===BURNERS===								
Wc	PR	eff	pwr	SM	TtOut	eff	dPnorm	Wfuel	WfuelHr	FAR				
AxiC	10.77211791	4.368707961	0.835413277	-1219.33822	3.51957022	2484.582797	0.993198814	0.02221318	0.197227741	710.0198693	0.018969295			
CenC	3.182566709	3.604173891	0.881849541	-1571.71709	18.17846792									
HPT	1.52679107	4.153712095	0.908253391	2664.826686										
FPT	5.508558984	3.220759471	0.834007812	1600										
===INLET===						===NOZZLES===								
Inlet Fram	PR					PR	Cfg	Cdth	Cv	Ath	Mnth	Vact	Fg	
0	1					1.108069794	1	0.96	0.975	81.3851	0.393420645	710.1910276	230.2692477	
===DUCTS===						===BLEEDS===								
Inter_Compressor	dPnorm	MN				from AC	Wb/Win	hscale	Pscale	W	Tt	ht	Pt	
Inter_Turbine	0.01354666	0.504386				0.07	0.855639	0.7389	0.777936103	824.3450242	197.7496003	49.27970512		
Exit_Turbine	0.009662888	0.316295				===SHAFTS===								
	0.014403235	0.374538				Nmech	trq_in	pwr_in						
						HP_Shaft	40492.6443	363.8340044	2664.826686					
						FP_Shaft	25566	322.135336	1600					

Table 11-6 Off-Design Summary: Cruise Rating

Cruise Condition: 10000ft, 337kn														
===SUMMARY OUTPUT DATA===														
MN	alt	dTamb	VTAS	N1	N2	T41	SHP	THP	ESHP	BSFC	ESFC			
0.527724402	10000	0	337	39338.29632	21041	2304.822527	1300	262.531752	1562.531752	0.415085047	0.345343742			
===FLOW STATION DATA===														
		W/lb/s	ht	Tt/R	Pt/psi	FAR	Pi	Wc	Ps	Ts	R	gamt	Aera	Ma
1	Inlet	9.332105174	121.8620664	509.9410442	12.21954558	0	0.016197712	11.12853849	10.108	509.9410442	0.06856	1.4	50.5	0.527724
2	AC_in	9.332105174	121.8620664	509.9410442	12.02161691	0	4.107546814	11.31176317	8.688260641	464.7567124	0.06856	1.4	38.35870022	0.697214
24	AC_out	8.678857812	193.0309844	804.9867467	49.37935422	0	0.01423162	3.217844929	41.50571955	766.0112899	0.06856	1.4	15.286917	0.504386
25	CC_in	8.678857812	193.0309844	804.9867467	48.67660601	0	3.726742485	3.264301224	45.85063663	791.347664	0.06856	1.4	20.24192531	0.293558
3	CC_out	8.592069234	292.5216647	1204.708598	181.4051756	0	0.022171436	1.060822391	177.5564041	1197.349832	0.06856	1.4	25.55443075	0.175298
4	GGT_in	8.741961057	602.8979775	2304.822527	177.3831624	0.01744537	4.216478908	1.526753056	171.19286	2290.325523	0.0686	1.278	11.52079622	0.242091
44	GGT_out	8.741961057	428.0456102	1691.651508	42.06902637	0.01744537	0.009875878	5.515125956	39.59932803	1673.569274	0.0686	1.278	35.49304337	0.316295
45	FPT_in	8.741961057	428.0456102	1691.651508	41.6535578	0.01744537	3.552075274	5.570135939	40.11367957	1680.369997	0.0686	1.278	41.78869454	0.249327
5	FPT_out	8.741961057	322.9406615	1303.846763	11.72654141	0.01744537	0.017479253	17.37023849	10.77474459	1284.388153	0.0686	1.278	92.50119511	0.374538
6	Nozzle_in	8.828749635	322.9406615	1302.872213	11.52157022	0.016977695	0.942880416	17.8481012	11.25309947	1298.172827	0.0686	1.2828	84.77614583	0.2
8	Nozzle_out	8.828749635	322.9406615	1302.872213	11.52157022	0.016977695	N/A	17.8481012	12.21954558	1280.058074	0.06861	1.2828	84.77614583	0.443775
===TURBOMACHINERY PERFORMANCE DATA===						===BURNERS===								
Wc	PR	eff	pwr	SM	TtOut	eff	dPnorm	Wfuel	WfuelHr	FAR				
AxiC	11.31176317	4.107546814	0.854867766	-930.187117	15.60637976	2304.822527	0.986920658	0.022171436	0.149891823	539.6105617	0.01744537			
CenC	3.264301224	3.726742485	0.881207632	-1221.67670	17.52570258									
HPT	1.526753056	4.216478908	0.909048638	2054.54335										
FPT	5.570135939	3.552075274	0.835243629	1300										
===INLET===						===NOZZLES===								
Inlet Fram	PR					PR	Cfg	Cdth	Cv	Ath	Mnth	Vact	Fg	
0	0.983802288					1.139846678	1	0.96	0.975	81.3851	0.443775081	759.0720918	203.0865315	
===DUCTS===						===BLEEDS===								
Inter_Compressor	dPnorm	MN				from AC	Wb/Win	hscale	Pscale	W	Tt	ht	Pt	
Inter_Turbine	0.01423162	0.504386				0.07	0.855639	0.7389	0.653247362	762.7276343	182.7569683	39.62483392		
Exit_Turbine	0.009875878	0.316295				===SHAFTS===								
	0.017479253	0.374538				Nmech	trq_in	pwr_in						
						HP_Shaft	39338.29632	288.7421712	2054.54335					
						FP_Shaft	25566	261.7349605	1300					

Table 11-7 Off-Design Summary Table: Test Bed Data, without Installation Effects

Test Bed Data no Installation														
===SUMMARY OUTPUT DATA===														
MN	alt	dTamb	VTAS	N1	N2	T41	SHP	THP	ESHP	BSFC	ESFC			
0	0	0	0	39548.83732	21041	2385.747538	1600	0	0	1600	0.437376191	0.437376191		
===FLOW STATION DATA===														
		W/lb/s	ht	Tt/R	Pt/psi	FAR	Pi	Wc	Ps	Ts	R	gamt	Aera	Ma
1	Inlet	10.85940588	123.954269	518.6700145	14.696	0	0	10.85940603	14.696	518.6700145	0.06856	1.4	50.5	0
2	AC_in	10.85940588	123.954269	518.6700145	14.696	0	4.431896529	10.85940603	10.62109027	472.712235	0.06856	1.4	38.35870022	0.697214
24	AC_out	10.85940588	203.1022175	846.2636132	65.13115139	0	0.013463921	3.129851428	54.74586184	805.2896332	0.06856	1.4	15.286917	0.504386
25	CC_in	10.85940588	203.1022175	846.2636132	64.25423069	0	3.596036669	3.172566616	60.52388662	831.9251667	0.06856	1.4	20.24192531	0.293558
3	CC_out	10.75081182	304.1688183	1250.267034	231.0605697	0	0.022204922	1.061623172	226.1582875	1242.629982	0.06856	1.4	25.55443075	0.175298
4	GGT_in	10.94520124	627.0847244	2385.747538	225.9298878	0.018081371	4.164080167	1.526918598	218.045406	2370.741527	0.0686	1.216	11.52079622	0.242091
44	GGT_out	10.94520124	447.3843078	1760.118904	54.25685355	0.018081371	0.009683945	5.461271011	51.07165835	1741.304814	0.0686	1.216	35.49304337	0.316295
45	FPT_in	10.94520124	447.3843078	1760.118904	53.73143319	0.018081371	3.246907198	5.514674817	51.7450515	1748.380788	0.0686	1.216	41.78869454	0.249327
5	FPT_out	10.94520124	344.0641854	1382.549407	16.54849674	0.018081371	0.014589135	15.86934899	15.20532094	1361.916239	0.0686	1.216	92.50119511	0.374538
6	Nozzle_in	11.05379529	344.0641854	1381.249846	16.30706849	0.017585762	1.109626326	16.25643165	15.92708809	1376.267757	0.06859	1.181	84.77614583	0.2
8	Nozzle_out	11.05379529	344.0641854	1381.249846	16.30706849	0.017585762	N/A	16.25643165	14.696	1361.944355	0.06859	1.181	84.77614583	0.395764
===TURBOMACHINERY PERFORMANCE DATA===						===BURNERS===								
Wc	PR	eff	pwr	SM	TtOut	eff	dPnorm	Wfuel	WfuelHr	FAR				
AxiC	10.85940603	4.431896529	0.83328285	-1216.06572	2.868885714	2385.747538	0.991851238	0.022204922	0.194389418	699.8019064	0.018081371			
CenC	3.172566616	3.596036669	0.881870694	-1552.83404	18.04618791									

11.2. Controller Design

11.2.1. Steady State Controller Design

Basic engine control concept is represented in Figure 11-4 Basic Engine Control Concept (Garg, 2013). A closed-loop control system is often adopted for aircraft engine control to obtain a better tracking ability and increase its robustness. In a typical aircraft engine control system, the pilot gives a throttle ratio command based on power or thrust requirement to the controller and the controller then computes a desired fuel flow from the difference between pilot's request and current situation. This signal is then fed to an actuator, which in this case is usually the fuel metering valve. The metered fuel flow is then injected to the combustor. The sensor measures the control variable and feeds it back to the controller to determine a new desired fuel flow. As an exact measurement of thrust or power is not practical now, shaft speed and engine pressure ratio are often used instead. (Link C.Jaw, 2009). In this proposal, shaft speed is chosen as the input signal to the controller. Moreover, the actuators and sensors are usually treated as first-order model with some time delay. In this proposal, they are considered ideal without any time delay and not covered in control logic.

In practice, the basic engine control concept which often referred to as primary control loop is far from enough. Firstly, the fact that aircraft engines are nonlinear systems and need to be in service under a wide range of operation conditions introduces lots of problems to controller design. A gain scheduling technic is usually implemented as the solution. The nonlinear models are usually firstly being linearized at several characteristic steady points, and then controllers are designed separately for these different working points whereas the controller structure remains the same but the gains change with working points. Usually, the gains implemented at different working points make up a gain schedule table for look up at different working points.

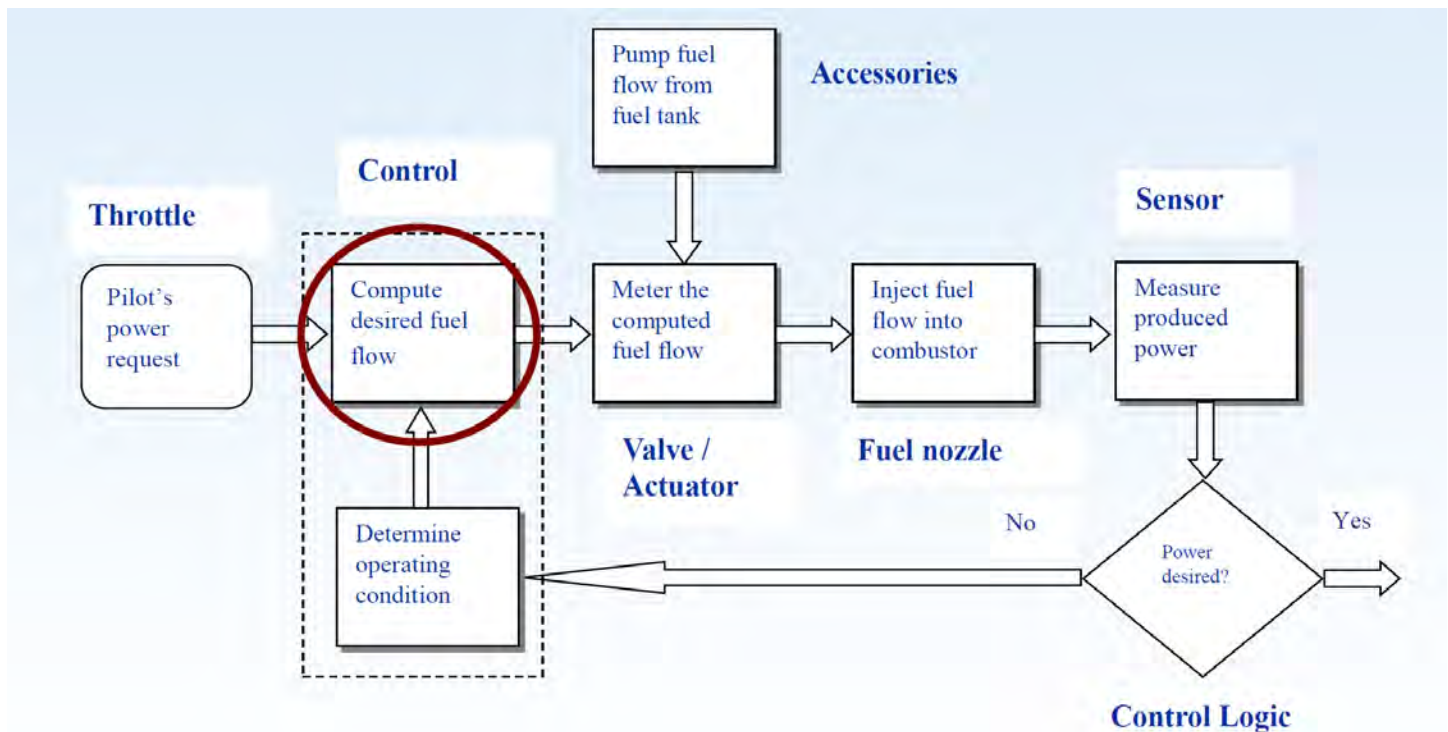


Figure 11-4 Basic Engine Control Concept (Garg, 2013)

Ideally, all the parameters required to identify an equilibrium point should be involved in the schedule variables, e.g., the state variables of the engine, ambient condition, health management parameters, etc. In practice, some of the parameters are superior to others in level of importance in defining the steady point. They are ambient conditions and the state variables of the engine. (Richter, 2012, p. 93). In the proposal, corrected gas generator turbine shaft speed is selected as the schedule variable to take engine state variable and ambient condition into consideration. The linearized block in T-MATS is employed for this purpose.

The linear model is represented as state variables here, to be specific, the descriptions are as follows:

$$\dot{x} = Ax + Bu$$

$$y = Cx + Du$$

Where in this case, x and y both represent corrected shaft speed (rpm) and u represents fuel mass flow rate (lb./s).

Corrected Shaft Speed	A	B	C	D
42089.01396	-0.799354551	18501.42962	1	0
41361.2495	-0.750759854	18939.53641	1	0
40778.47261	-1.083253954	19820.51831	1	0
40209.9343	-1.043756893	20531.12138	1	0
39559.05887	-0.937588618	21399.70272	1	0
38841.42938	-0.901315823	22427.26753	1	0
38016.12133	-0.68395126	24641.50895	1	0
36731.81055	-0.397703686	25583.43027	1	0

Table 11-8 Linearized model

To facilitate the linearization of the engine model, the high-pressure rotor moment of inertia needs to be estimated. For this purpose, the estimation approach provided by Shuangxi Yu (1998), is used, which provides an estimated high pressure rotor moment of inertia as $0.3183 \text{ slugs} \cdot \text{ft}^2$. Since the propeller is operating at synchronous speed, the FPT spool speed doesn't change during off-design, its moment of inertia is not estimated. The linearization results are shown in Table 11-8 Linearized model.

The gains of the steady state controller are demonstrated in Table 11-9 Steady State Controller Parameters.

Corrected Shaft Speed	38002.93121	38849.62518	39580.13564	40243.45457	40827.75714	41454.89012	42181.55617
Proportional Gain K_p	3.14E-05	6.92E-05	7.73E-05	8.81E-05	8.69E-05	7.09E-05	7.62E-05
Integrator Gain K_i	3.14E-05	6.18E-05	7.41E-05	9.26E-05	9.57E-05	5.65E-05	6.48E-05

Table 11-9 Steady State Controller Parameters

11.2.2. Transient Controller Design

When the engine tries to reach a higher speed, it is in the risk of crossing the surge line if the acceleration process is too violent. On the other hand, if the engine decelerates from a high speed to a lower one, it may confront combustor lean blow off due to large extraction of fuel during the deceleration. Thus, acceleration and deceleration schedules are needed to limit the fuel flow from going too high or too low. In this case, the corrected shaft speed is again chosen as the schedule variable. The results for acceleration schedule are shown in Table 11-10 Acceleration Schedule. Deceleration schedule is handled in a similar demeanor, however with combustor lean blow off limit as the constraint.

Engine Acceleration			
Corrected Shaft Speed	36731.81055	37263.86452	37650.7206
Fuel flow limit	0.11	0.13	0.15
Corrected shaft speed	38016.12133	38313.24709	38582.51427
Fuel flow limit	0.15	0.2	0.22
Corrected Shaft Speed	38841.42938	39088.07393	39326.3784
Fuel flow limit	0.24	0.26	0.29
Corrected Shaft Speed	39559.05887	39784.84183	40001.41831
Fuel flow limit	0.31	0.32	0.33

Table 11-10 Acceleration Schedule

Proportional Gain K_p	Integrator Gain K_i
0	0.000105921

Table 11-11 T4 limit controller

Moreover, due to

the material limitation, turbine entry temperature should be kept below an exact point. Thus, another controller branch need to be mounted for the temperature limitation. The limit controller should also be designed as a schedule based on corrected shaft speed. But as it only occurs when the shaft speed is relatively high, it is sufficient to use a single PI controller instead of a PI family. Controller Proportional Gain K_p and Integrator Gain K_i and shown in Table 11-11 T4 limit controller. Following this

method, limiters for inter-turbine temperature, maximum mechanical spool speed, etc. are also added, however, in the test of engine operation, none of these limiters took effect. Thus, they are left being absent from this report.

11.2.3. Control System Integration

It can be easily found that there exist four control branches, namely steady state controller, acceleration schedule, deceleration schedule, and temperature limitation, which means there would be four control signals at an individual point. Hence, selection logic has been used. To be exact, the signals from main controller, temperature limit and acceleration schedule will experience a select low block to get the lowest value from these three signals and the lowest alternative will be compared to the deceleration schedule to get a higher one, which will be the final fuel flow fed to the engine.

To solve the problem that the controller branch with an integrator inside will wind up if it hasn't been chosen, "delta controller" has been implemented here. Which means the output of the four controller branches are not real-time fuel flow but the difference between the fuel flow command and current value. Then the selection logic is implemented on these four delta outputs and the result is fed into the integrator. This method can protect the integrator from winding up and prevent sudden change of fuel flow as well. The whole control logic is shown in Figure 11-5 Control Logic. An overview of the integration of four control branches on MATLAB platform is shown in Figure 11-6 Overview of Control Blocks.

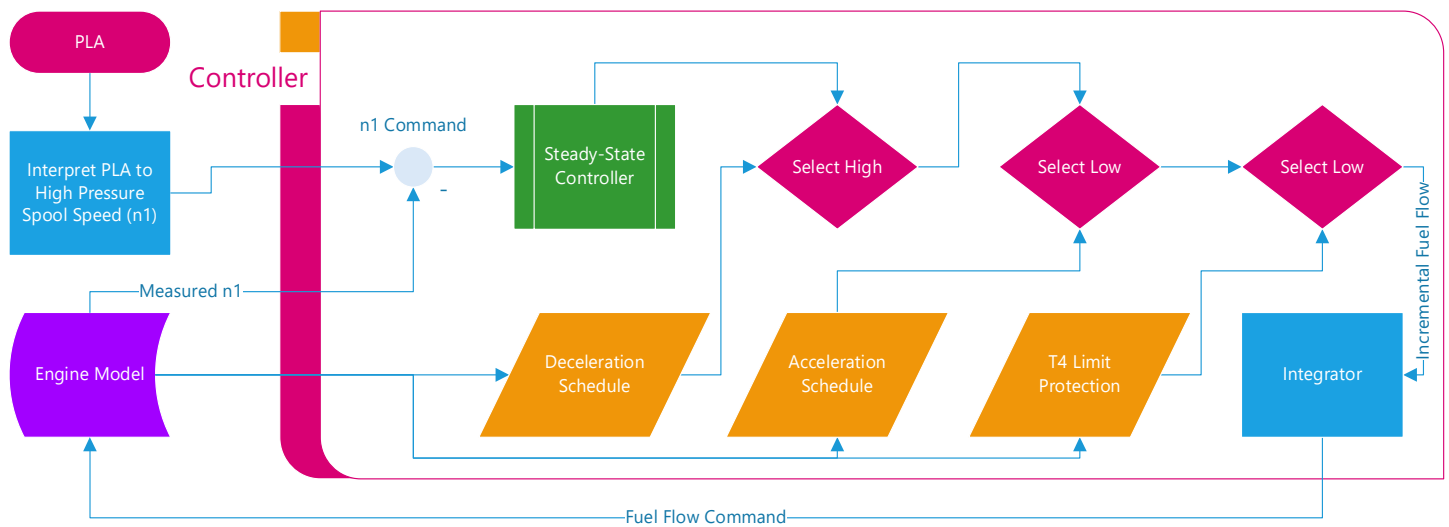


Figure 11-5 Control Logic

11.3. Transient Performance on Map

Before mission analysis, the acceleration and deceleration performance of the engine must be tested. To let the acceleration and deceleration schedule take full effect, a step signal of PLA is inputted into the MATLAB model. Since step signal represents an infinite large rate of increase for n_1 command, it can guarantee the touch of the upper boundary of acceleration schedule. A sample of acceleration and deceleration loop at ISA SLS between 37500rpm and 44000rpm high pressure spool speed is presented schematically in Figure 11-7 Acceleration and Deceleration.

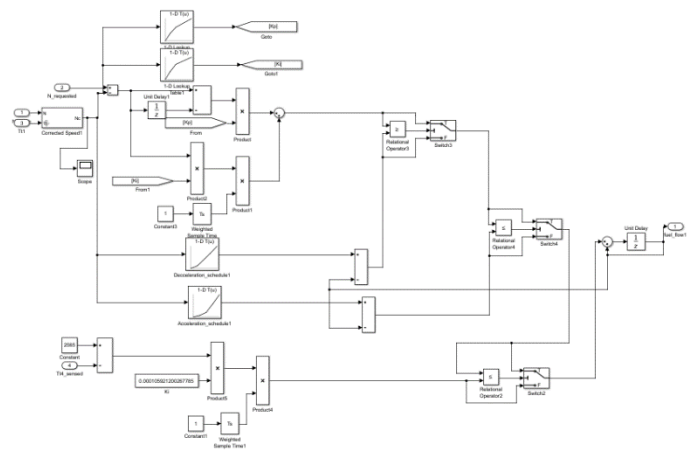


Figure 11-6 Overview of Control Blocks

From the graphical acceleration and deceleration lines, it is easy to make several conspicuous assertions. Firstly, the static off-design operation line goes away from surge on the axial compressor map when engine decelerates, which is a direct violation to the common phenomenon mentioned in standard textbooks. Reason for the increase of surge margin is probably the use of variable stator, which is well-known for its capability of avoiding surge. Secondly, all operating points on the GGT map, no matter steady state operating line or transient acceleration or deceleration, fall within a small region at the entrance to chock. This a direct validation that GGT is designed to be highly loaded with broad range of operation working under chock condition. Several discrete points shown on the left is due to the initial numerical process of firstly finding the steady 44000rpm operating point on the corrected speed line. Since transient line must both commence and terminate on steady state points, the MATLAB model is programed to first find the corresponding steady state condition, and then perform transient simulation. Thirdly, the working points on centrifugal compressor maps also collapse into a very small operating region. This is perhaps also due to the use of VSV. Since VSV affects both mass flow capability and efficiency, it tends to even out major irregularity during the operation, which in turn left the centrifugal compressor working always under a similar normalized spool speed and mass flow rate. The acceleration and deceleration schedule are both generated conservatively, as validated by the relative small distance between acceleration line and steady state line. Therefore, the engine exhibits a very slow acceleration reaction of up to 5s in accelerating from part load to 100% RPM. However, due to the demonstrative purpose of this document, further iterative refinement of the acceleration schedule will be omitted.

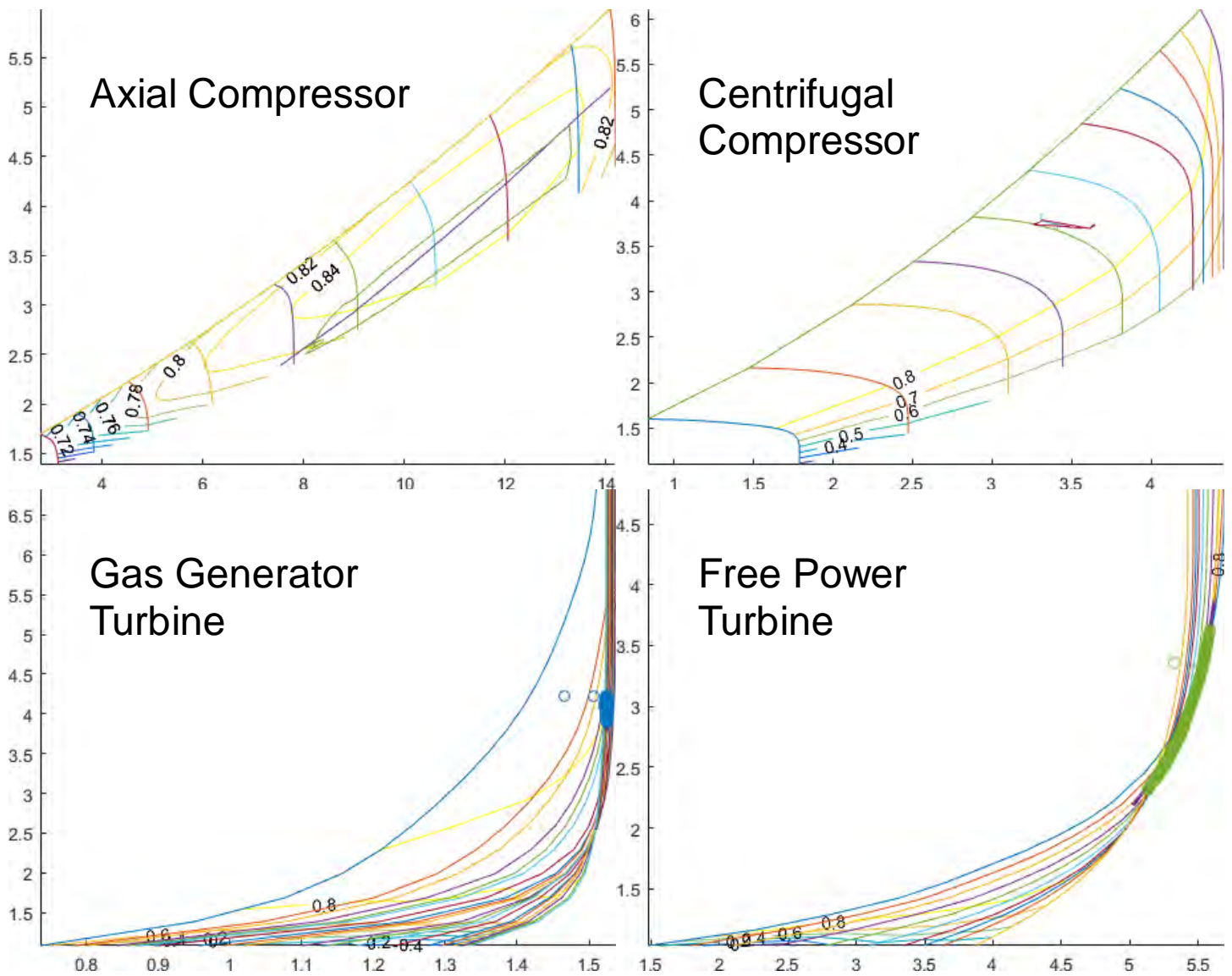


Figure 11-7 Acceleration and Deceleration

11.4. Mission Analyses

Per AIAA RFP requirements (AIAA, 2016), a typical, multi-point mission should be generated. In this case, the impact of engine improvements can be recognized by the aircraft through demonstrations of mission performance. Therefore, mission analyses in this section are first performed with the generation of mission profile from publicly available literatures, and then use the aforementioned MATLAB engine model to numerically provide mission parameters.

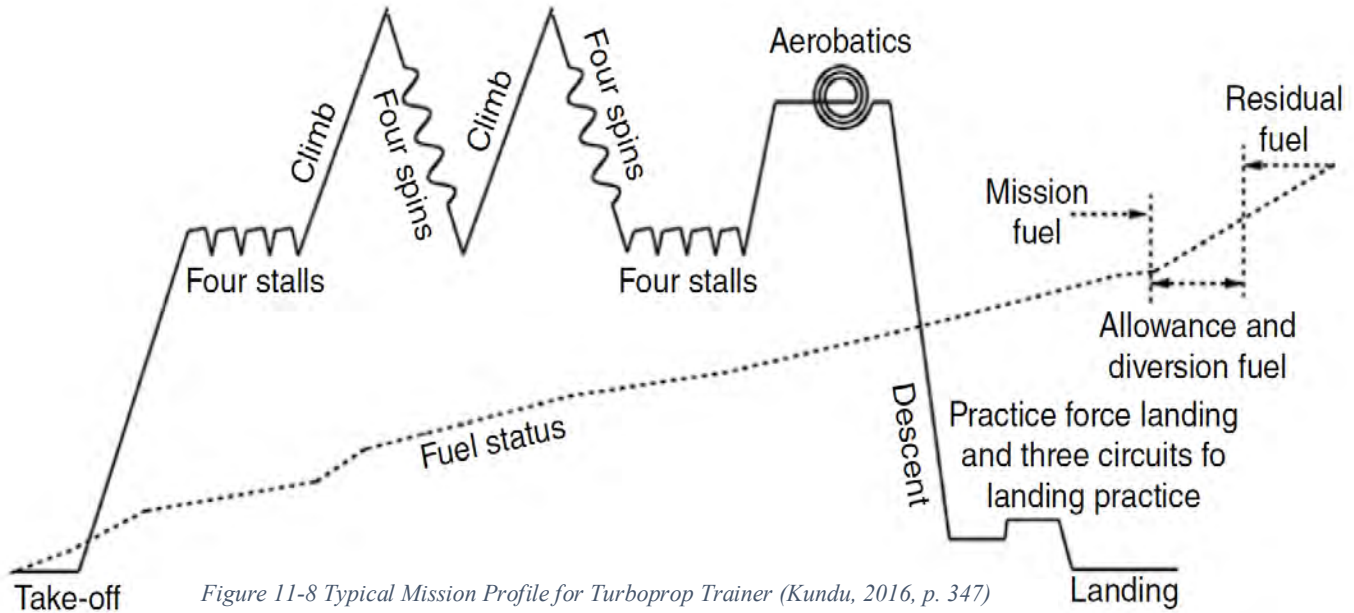


Figure 11-8 Typical Mission Profile for Turboprop Trainer (Kundu, 2016, p. 347)

11.4.1. Mission Profile

A typical mission profile for a turboprop trainer is presented in Figure 11-8 Typical Mission Profile for Turboprop Trainer. Thus, the mission profile used for simulating the performance of WJ-25 is adapted from this sample and presented in Table 11-12 Mission Profile.

TPT mission fuel and time consumed	Time (min)	Engine rating (% rpm)	Remarks
Taxi to takeoff	6.0	60% (idle)	Accelerate from 0kn-103kn
Takeoff and climb to 12000ft altitude	3.2	TO at 100% then at 95%	TAS = 220kn
Four turns/stalls	5	1minat 95% + 4minat 60%	TAS = 180kn
Climb from 10000ft to 20000ft altitude	4	95%	TAS = 220kn
Four turn spins	3.5	85%	TAS = 370kn
Climb from 10000ft to 20000ft altitude	4	95%	TAS = 220kn
Four turn spins	3.5	85%	TAS = 370kn
Four turns/stalls	5	1minat 95% + 4minat 85%	TAS = 180kn
Climb from 10000ft to 12000ft altitude	1	85%	TAS = 220kn
Aerobatics practice	6	85%	TAS = 180kn
Descent and practice force landing	7.5	2min at 95% 6min at 85%	TAS = 370kn
Three circuits for landing practice	10	Average 90%	TAS = 308kn
Approach, land return taxi	4	85%	Decelerate from 103kn-0kn
Trainee pilot allowance	2	95%	TAS = 81kn
Total time	58.7	≈60min	

Table 11-12 Mission Profile

11.4.2. Mission Analysis

The descriptive mission profile provided in Table 11-12 Mission Profile has been translated into quantitative signal inputs to the transient model shown in Figure 11-9 Mission Signal Input. The result of the test is shown in Figure 11-10 Controller Performance, Figure 11-11 Engine Performance, and Figure 11-12 Mission Fuel Consumption.

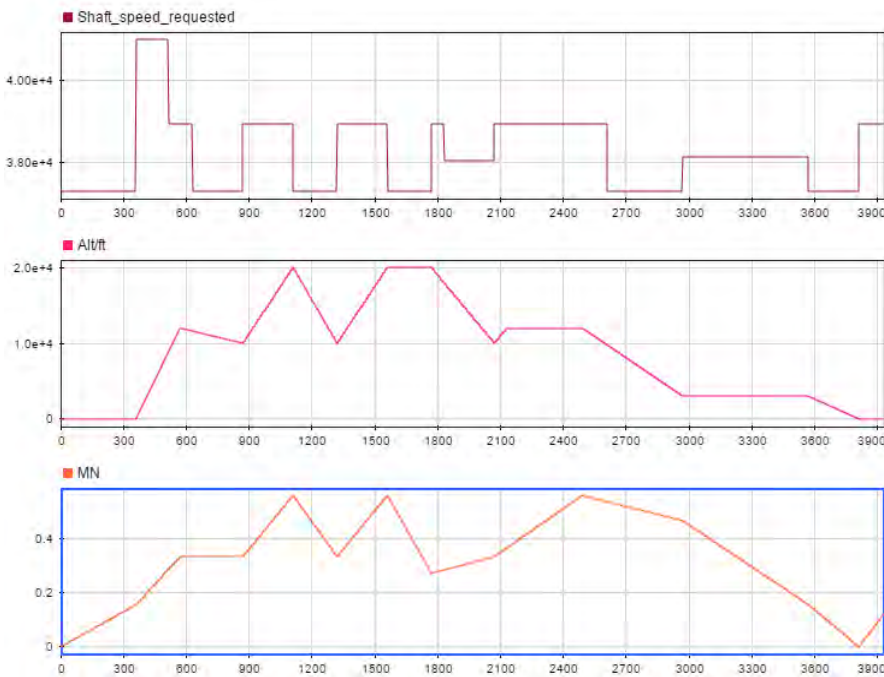


Figure 11-9 Mission Signal Input

Figure 11-10 Controller Performance conspicuously shows that the tracking ability of the controller is satisfactory with acceptable level of overshoot at some points. The mechanical shaft speed keeps under 41000rpm due to the temperature limit of the gas generator turbine nozzle.

Moreover, the amount of fuel injected into the engine changes in a relatively smooth manner to avoid damages caused by sharp fuel spike. In addition, T4 is limited under 2565°R for the whole mission profile to protect the 1st stage turbine nozzle guide vane from being overheated. In majority of time, the surge margin of axial compressor and centrifugal compressor alter between around 16% to 40%, which is enough for safety considerations of the engine in service.

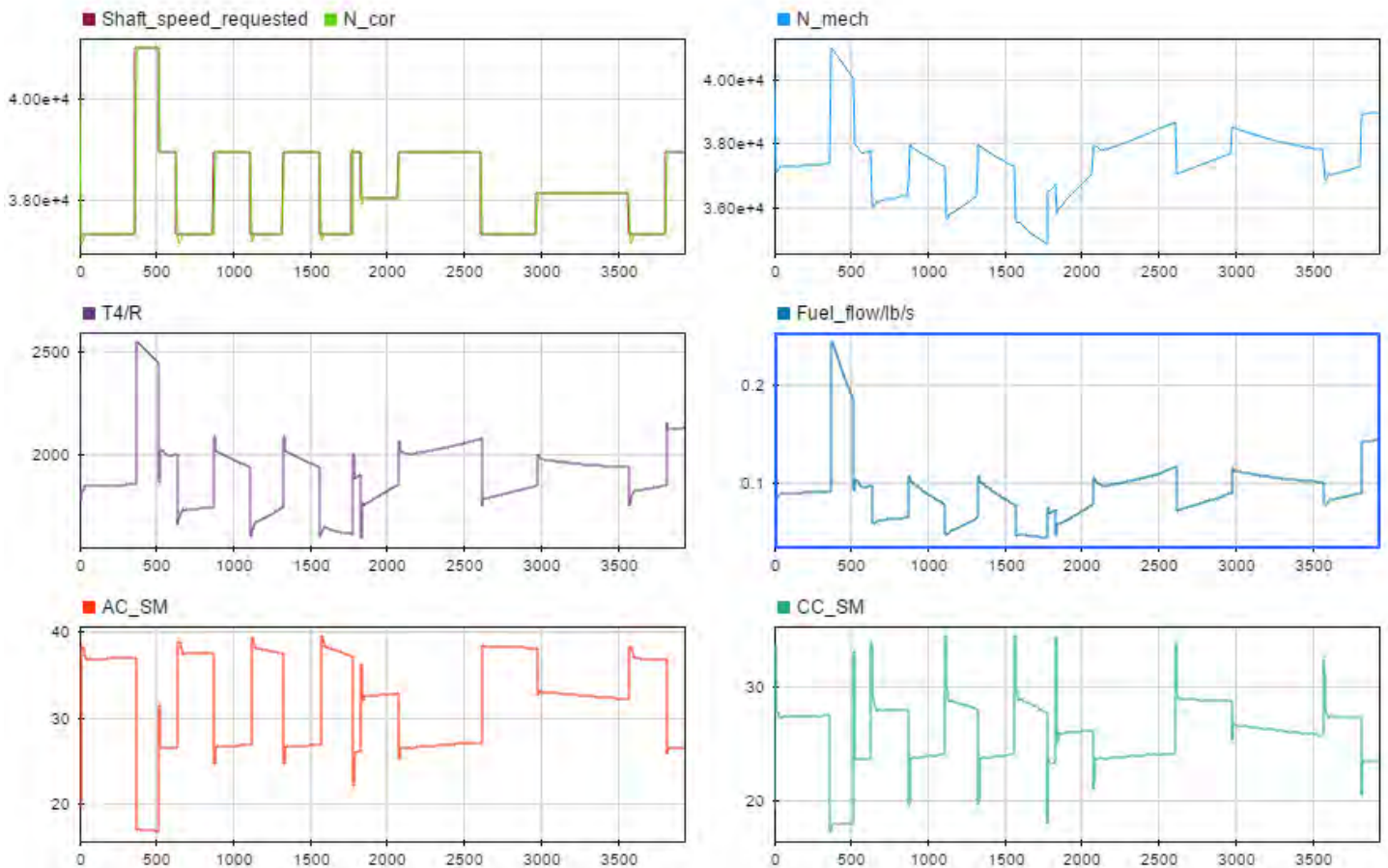


Figure 11-10 Controller Performance

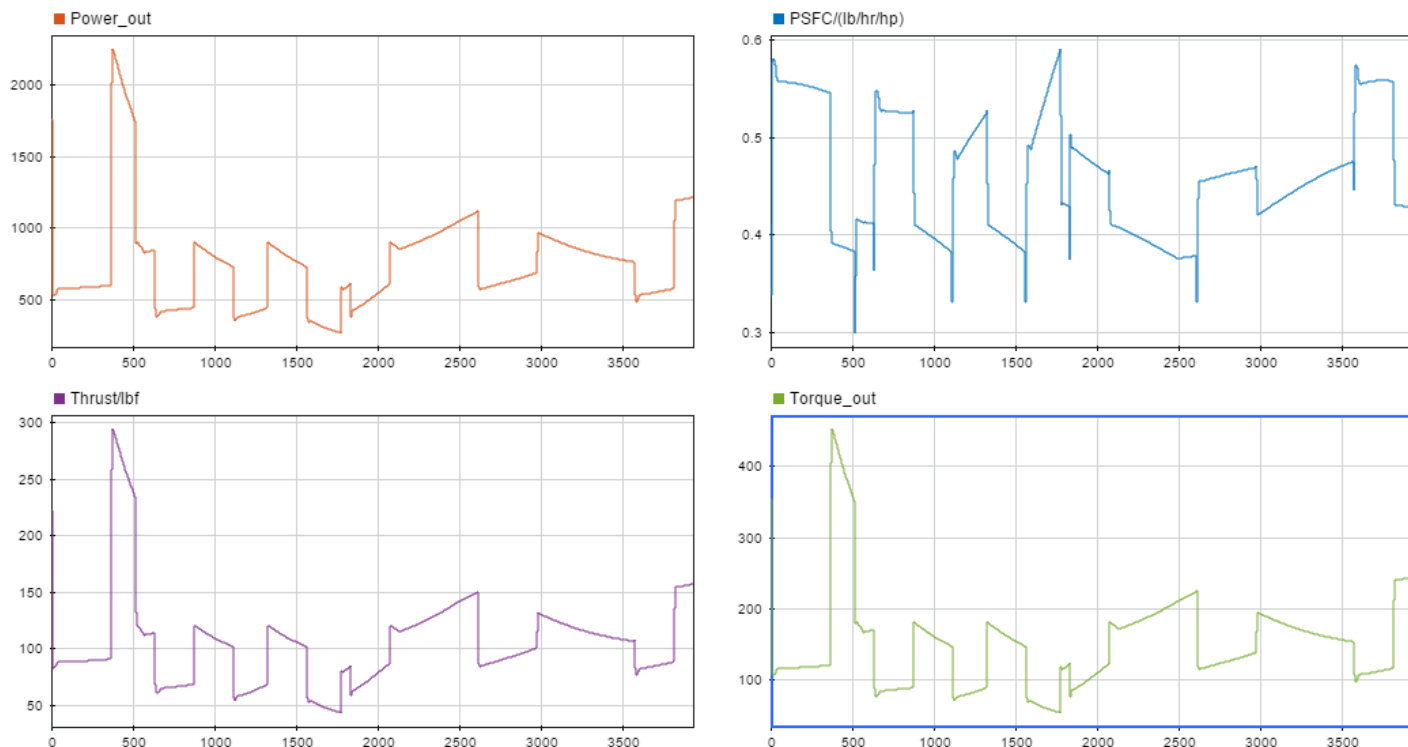


Figure 11-11 Engine Performance

In Figure 11-11 Engine Performance, critical engine performance parameters, including power output, power specific fuel consumption, residual thrust, and FPT shaft torque, are shown for the whole mission. The highest power output reaches 2200hp during the mission profile. The residue thrust changes between 45 to 290lbf, and SFC varies between 0.3 and 0.59 lb./h/hp. The improvements of the new engine over the baseline engine can be easily verified.

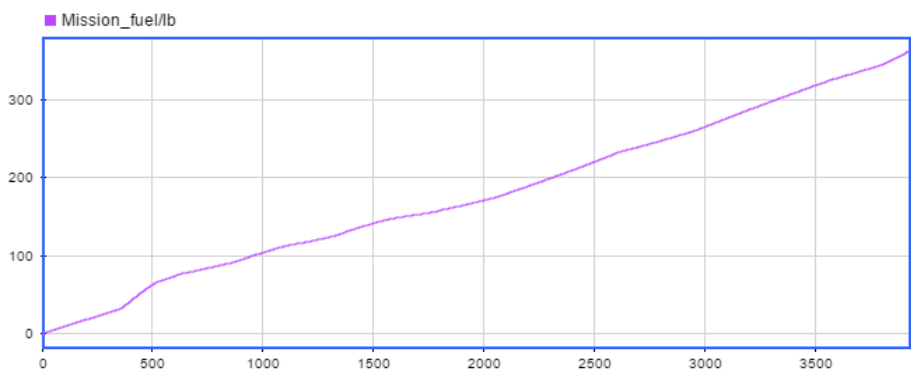


Figure 11-12 Mission Fuel Consumption

In Figure 11-12 Mission Fuel Consumption, the mission fuel burn throughout the whole profile has been presented. The exact fuel consumption values for each mission segment are demonstrated in Table 11-13 Mission Analysis. With takeoff wing loading equaling 40.5 lb./ft² and power-to-weight ratio being 0.249 hp/lb., the estimated weight fraction after each leg based on maximum take-off weight 6834 lb. (AIAA, 2016) is

also shown in Table 11-13 Mission Analysis and Figure 11-13 Weight Fraction After Each Mission.

TPT mission fuel and time consumed	Time (min)	Engine rating (% rpm)	fuel burnt(lb.)	Beta final
Taxi to takeoff	6.0	60% (idle)	32.34040919	0.995267719
Takeoff and climb to 12000ft altitude	3.2	TO at 100% then at 95%	38.35103729	0.989655919
Four turns/stalls	5	1minat 95% + 4minat 60%	53.08232864	0.981888532
Climb from 10000ft to 20000ft altitude	4	95%	59.7263735	0.973148939
Four turn spins	3.5	85%	64.82867068	0.963662742
Climb from 10000ft to 20000ft altitude	4	95%	81.10174423	0.951795352
Four turn spins	3.5	85%	74.38289302	0.940911113

Four turns/stalls	5	1minat 95% + 4minat 85%	101.3351229	0.926083029
Climb from 10000ft to 12000ft altitude	1	85%	80.35550203	0.914324834
Aerobatics practice	6	85%	138.1998837	0.894102434
Descent and practice force landing	7.5	2min at 95% 6min at 85%	122.9165386	0.876116403
Three circuits for landing practice	10	Average 90%	201.586022	0.846618887
Approach, land return taxi	4	85%	143.3256798	0.825646443
Trainee pilot allowance	2	95%	218.7012952	0.793644498

Table 11-13 Mission Analysis

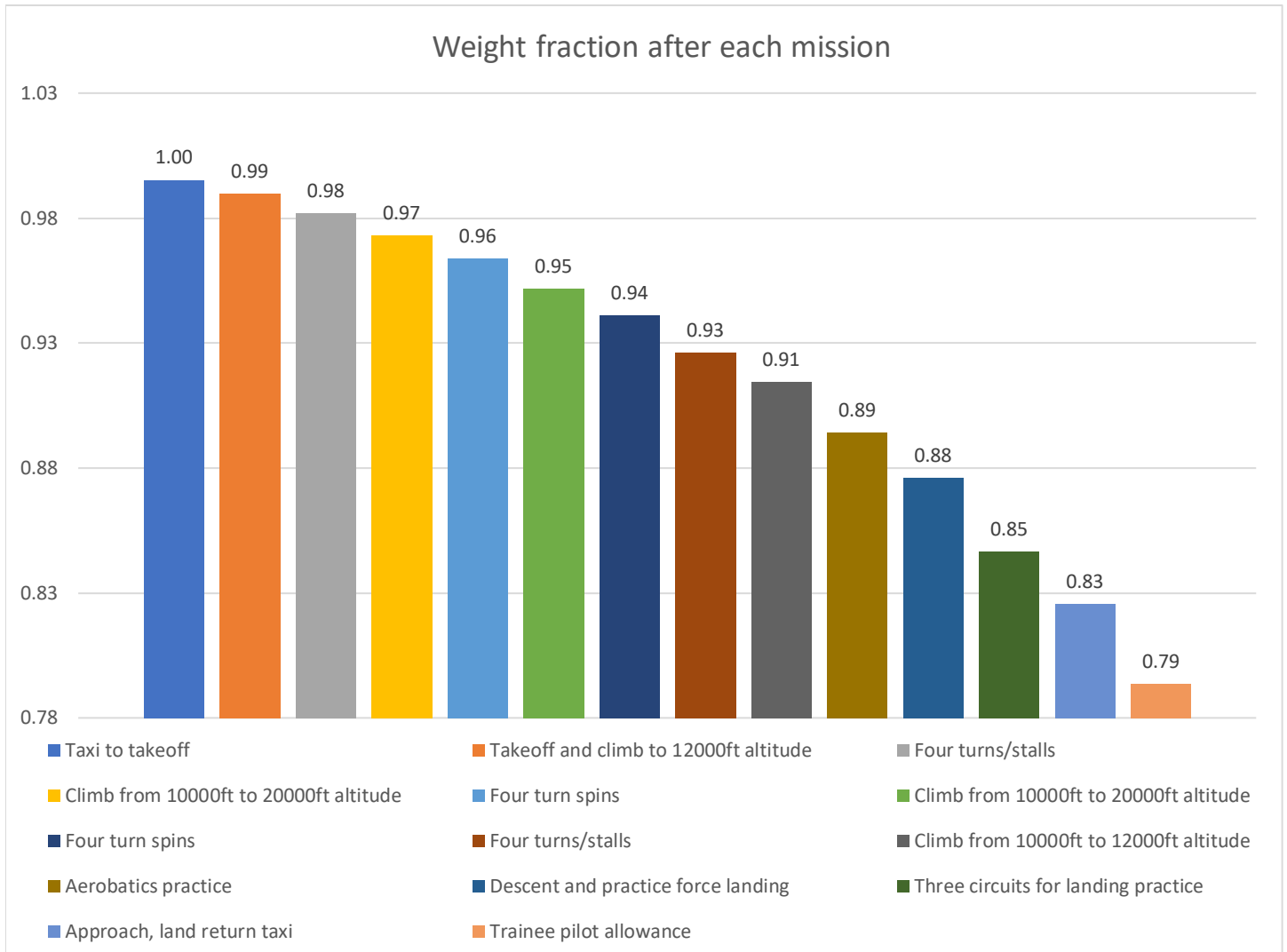


Figure 11-13 Weight Fraction After Each Mission

12. Miscellaneous Structural Issues

12.1. Bearing Supports

To support the rotating shafts inside the engine, the bearing location need to be determined. Theoretically, an individual spool can only be supported by two bearings, due to fact that it's extremely difficult to assemble three bearing concentrically when taking the issues of manufacturing uncertainties into consideration. Additionally, the two bearings on a single spool should be of different types, namely one ball bearing, which handles both axial and radial loads, and one roller bearing, which supports the shaft radially only. The reason for the impossibility of installing two ball bearings on the same shaft is because of the issue of thermal elongation. When a cold engine is heated up from starting, the shaft material also expands, and thus results in an increase of overall length of the shaft. One

characteristic difference between the ball bearing and roller bearing is that ball bearing tends to be more delicate and is more prone to failures caused by elevated environment temperature. Therefore, when determining the location of ball and roller bearings, the ball bearing should be left in an environment that is instinctually cooler.

After pondering upon all above-mentioned constraints and legacies, the final supporting architecture is determined as shown in Figure 12-1 Bearing Support Structure.

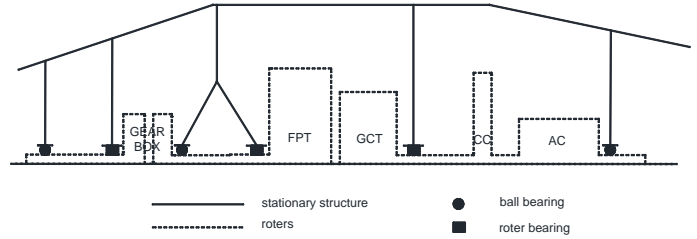


Figure 12-1 Bearing Support Structure

12.2. Main Shaft Reduction Gearbox

To accommodate the low shaft speed operation of engine propeller, the high spool speed of the FPT need to be reduced through a main shaft reduction gearbox. A planetary gear set is again used for this purpose, since the new FPT is designed with a lower spool speed of 21,041 rpm other than the 30,000rpm from the baseline engine, less stages of the planetary gear sets can be allowed, which permits a direct reduction of the engine weight. Detailed design of the gearbox cannot be conducted. Since the propeller design spool speed is not known as a prior, the gearbox reduction ratio cannot be determined.

12.3. Implementation of the Control Logic

To implement the control algorithm discussed previously in Section 11.2 Controller Design, a physical control module must be installed onto the engine. The state of art control module used in modern engines is popularly the so-call FADEC. Through the past 30 years of engine development experience, FADEC has proven the indisputable benefits of significant size and weight reduction for the same control functionality and unrestricted power lever movement (Link C.Jaw, 2009, p. 16). Therefore, solely from the perspective of engine control unit, a weight reduction of at least 5% can be promised, when updating the hydraulic controllers into an electronic counterpart.

13. 2D Engine Meridional Section View

After all the aforementioned analyses, discussions, and calculations, a 2D engine meridional section view, including a cross-section of the engine flow path, 2D geometry for the inlet, compressors, combustor, turbines, nozzle(s), and inter-component ducts, is provided in the Figure 2D Engine Meridional Section View.

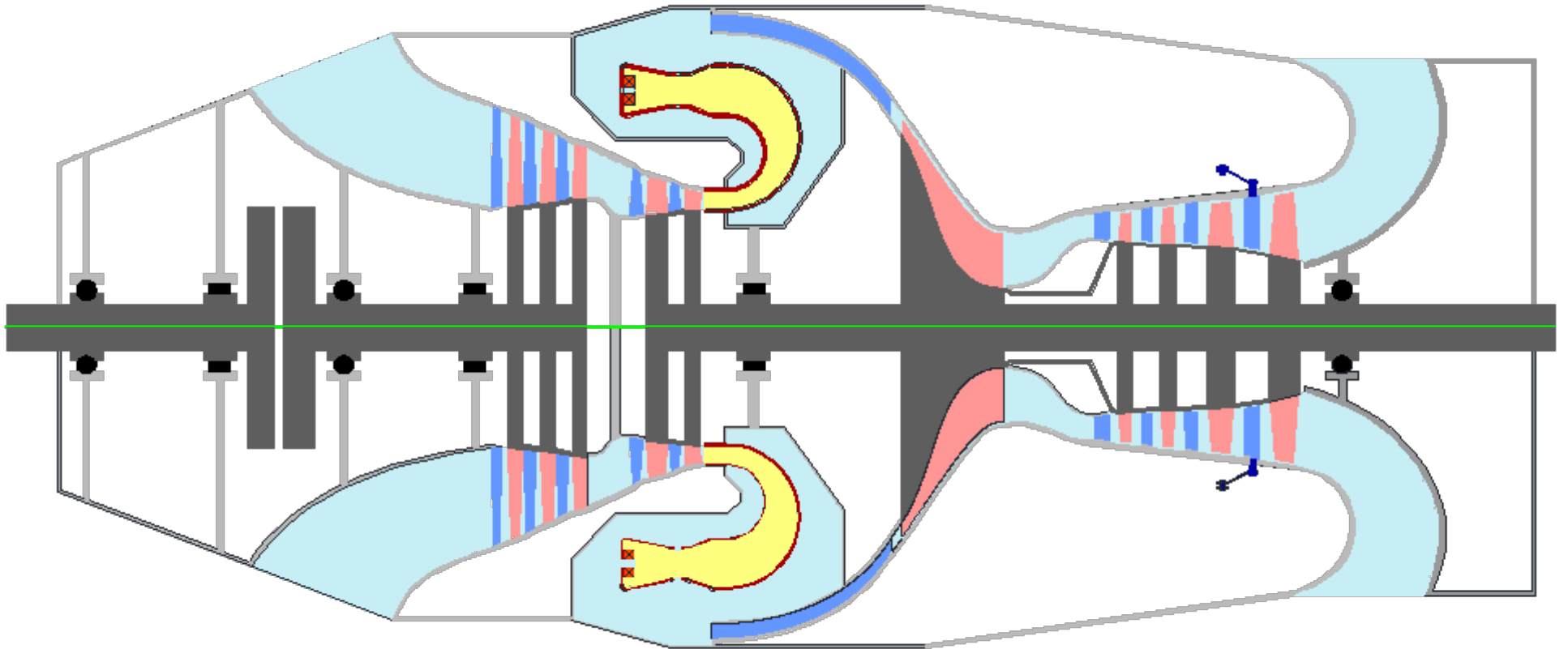


Figure 2D Engine Meridional Section View

14. References

- AIAA. (2016). *Candidate Engines for a Next Generation Single-Engine Turboprop Aircraft*. AIAA Foundation Student Design Competition 2016/17 Undergraduate Team – Engine.
- Authur H. Lefebvre, D. R. (2010). *Gas Turbine Combustion*. Boca Raton: CRC Press.
- Badger, M., Julien, A., LeBlanc, A., Moustapha, S., Prabhu, A., & Smailys, A. (1994). The PT6 Engine: 30 Years of Gas Turbine Technology Evolution. *ASME Journal of Engineering for Gas Turbine Engines and Power*, 322-330.
- Bansal, N. P. (2005). *Handbook of Ceramic Composites*. Boston: KLUWER ACADEMIC PUBLISHERS.
- BASKHARONE, E. A. (2006). *Principles of Turbomachinery in Air-Breathing Engines*. Cambridge: Cambridge University Press.
- Bullock, R. O., & Johnsen, I. A. (1965). *AERODYNAMIC DESIGN OF AXIAL-FLOW COMPRESSORS NASA-SP-36*. Cleveland: Lewis Research Center.
- Christopher O. Peterson, W. A. (2002). Performance of a Model Rich Burn-Quick Mix-Lean Burn Combustor at Elevated Temperature and Pressure. *NASA/CR--2002-211992*.
- Cumpsty, N. A. (2004). *Compressor Aerodynamics*. Malabar: Krieger Publishing Company.
- EASA. (2016). *TYPE-CERTIFICATE DATA SHEET No. EASA IM.E.038*. Longueuil: European Aviation Safety Agency.
- Europrop. (2017, 1 7). *THE TP-400 D-6*. Retrieved from Europrop International official website: <http://www.europrop-int.com/the-tp-400-d-6/>
- Gardiner, G. (2015, July 31). *Aeroengine Composites, Part 1: The CMC invasion*. Retrieved from Composites World: <http://www.compositesworld.com/articles/aeroengine-composites-part-1-the-cmc-invasion>
- Gardiner, G. (2015, August 31). *Aeroengine Composites, Part 2: CFRPs expand*. Retrieved from Composite World: <http://www.compositesworld.com/articles/aeroengine-composites-part-2-cfrps-expand>
- Garg, D. S. (2013). https://www.grc.nasa.gov/WWW/cdtb/aboutus/Fundamentals_of_Engine_Control.pdf. Retrieved from <https://www.grc.nasa.gov/>.
- GE Business & General Aviation. (2017). *GE Advanced Turboprop*. Retrieved from GE Aviation: <http://www.geaviation.com/bga/engines/advancedturboprop/>
- Glassman, J. (1972). *Computer Program for Preliminary Design Analysis of Aixel-Flow Turbines*. Cleveland: NASA Lewis Research Center.
- Glassman, J. (1992). *Users Manual for Updated Computer Code for Axial-Flow Compressor Conceptual Design*. Toledo: Lewis Research Center.

- Glassman, J. (1994). *Turbine Design and Application NASA-SP-290*. Washington, DC: Lewis Research Center.
- H.G. Münzberg, J. K. (1977). *Gasturbinen - Betriebsverhalten und Optimierung*. New York: Springer-Verlag Berlin Heidelberg.
- IPT. (2017, 19). *MTR390-E*. Retrieved from IPT official website:
http://www.itp.es/web/Sec_PL/wf_paginaPlana.aspx?IdMenu=361&Idioma=en-GB&idReg=183&idSubmenu=452&idSubSubmenu=380&idP=20&idPS=1
- ISO. (1975). *Standard Atmosphere, ISO 2533*. Geneva: International Organisation for Standardisation.
- J. Seddon, E. G. (1999). *Intake Aerodynamics*. Victoria: Blackwell Science Ltd.
- Kasper, J., & Balle, O. (2016, October 3). *Pratt & Whitney Canada PT6A*. Retrieved from FI-POWERWEB: <http://www.fi-powerweb.com/Engine/PW-CANADA-PT6A.html>
- Kundu, A. K. (2016). *Theory and Practice of Aircraft Performance*.
- Kurtz, M. (1992). *Ceramic Matrix Composites*. Bericht der DKG.
- Kurzke, J. (1992). Calculation of Installation Effects within Performance Computer Programs. In *Steady and Transient Performance Prediction of Gas Turbine Engines* (pp. 127-145). Cambridge: Specialised Printing Services Limited.
- Kurzke, J. (1995). Advanced User-friendly Gas Turbine Performance Calculations on A Personal Computer. *ASME*, 1-8.
- Kurzke, J. (1996). How to Get Component Maps for Aircraft Gas Turbine Performance Calculations. *ASME*.
- Kurzke, J. (2015). *GasTurb 12: Design and Off-Design Performance of Gas Turbines*. Aachen: GasTurb GmbH.
- L. R. Reneau, J. P. (1967). Performance and Design of Straight, Two-Dimensional Diffusers. *Journal of Basic Engineering*, 141-150.
- Link C.Jaw, J. D. (2009). *Aircraft Engine Controls: Design, System Analysis and Health Monitoring*. AIAA.
- Loftin, J. (1980). *Subsonic Aircraft: Evolution and the Matching of Size to Performance*. NASA reference publication 1060.
- Mattingly, J. D. (2002). *Aircraft Engine Design*. Reston: American Institute of Aeronautics and Astronautics.
- Mellor, A. M. (1990). *Design of Modern Turbine Combustors*. San Diego: Academic Press Inc.
- Michaux, A., Sauder, C., Camus, G., & Pailler, R. (2007). Young's modulus, thermal expansion coefficient and fracture behavior of selected Si-B-C based carbides in the 20–1200 °C temperature range as derived from the behavior of carbon fiber reinforced microcomposites. *Journal of the European Ceramic Society*, 3551-3560.
- MIL210. (1997). *Climatic Information to Determine Design and Test Requirements for Military Equipment MIL210C, Rev C*. Massachusetts: US Department of Defense.

- MIL-C-005011B. (1977). *Military Specification, Chart Standard Aircraft Characteristics and Performance, Piloted Aircraft (Fixed Wing)*. Wright-Patterson: USAF.
- MIL-DTL-5624U. (1998). *DETAIL SPECIFICATION TURBINE FUEL, AVIATION, GRADES JP-4 and JP-5*. Patuxent River: ASTM.
- Muktinutalapati, N. R. (2016). Materials for Gas Turbines - An Overview. In E. Benini, *Advances in Gas Turbine Technology* (pp. 293-314). Rijeka: Intech.
- NASA Glenn Research Center. (2014, 04 15). *T-MATS: Toolbox for the Modeling and Analysis of Thermodynamic Systems*. Retrieved from Intelligent Control and Autonomy Branch: <https://www.grc.nasa.gov/www/cdtb/software/t-mats.html>
- Norris, G. (2015, October 27). *GE Unveils CMC Production Ramp-Up Plan*. Retrieved from Aviation Week: <http://aviationweek.com/optimizing-engines-through-lifecycle/ge-unveils-cmc-production-ramp-plan>
- Philpot, M. G. (1992). Practical considerations in designing the engine cycle. *AGARD Lecture Series 183 "Steady and Transient Performance Prediction of Gas Turbine Engines"*, 26-49.
- Pilatus. (2002). *PC-21 Brochure*. Stans: Pilatus Aircraft Ltd.
- Rao, S. S. (2009). Random Search Methods. In S. S. Rao, *Engineering Optimization: Theory and Practice* (pp. 383-384). Hoboken: John Wiley & Sons, Inc.
- Richter, H. (2012). *Advanced Control of Turbofan Engines*. Springer.
- Roskam, J. (1985). *Airplane Design IV: Layout Design of Landing Gear and Systems*. Ottawa: Roskam Aviation and Engineering Corporation.
- Roskam, J. (1985). *Airplane Design Part I: Preliminary Sizing of Airplanes*. Ottawa: Roskam Aviation and Engineering Corporation.
- Roskam, J. (1985). *Airplane Design Part VI: Preliminary Calculation of Aerodynamics, Thrust, and Power Characteristics*. Ottawa: Roskam Aviation and Engineering Corporation.
- SAE. (1974). Gas Turbine Engine Performance Station Identification and Nomenclature. In Warrandale, *Aerospace Recommended Practice, ARP 755A*. Pennsylvania: Society of Automotive Engineers.
- SAE. (1974). Gas Turbine Engine Status Performance Presentation for Digital Computer Programs. In Warrandale, *Aerospace Recommended Practice, ARP 1211A*. Pennsylvania: Society of Automotive Engineers.
- SAE. (1989). Gas Turbine Engine Steady-State Performance Presentation for Digital Computer Programs. In Warrandale, *Aerospace Standard, AS681 Rev. E*. Pennsylvania: Society of Automotive Engineers.
- SAE. (1989). Gas Turbine Engine Transient Performance Presentation for Digital Computer Programs. In Warrandale, *Aerospace Recommended Practice, ARP 1257*. Pennsylvania: Society of Automotive Engineers.

- SAE. (1996). Gas Turbine Engine Interface Test Reduction Computer Programs. In Warrandale, *Aerospace Recommended Practice, ARP 1210A*. Pennsylvania: Society of Automotive Engineers.
- Saravanamuttoo, H., Rogers, G., Cohen, H., & Straznicky, P. (2009). *Gas Turbine Theory*. Harlow: Pearson Education Limited.
- Schilke, P. (2004, August). *Advanced Gas Turbine Materials and Coatings*. Retrieved from GE Energy:
https://powergen.gepower.com/content/dam/gepower-pgdp/global/en_US/documents/technical/ger/ger-3569g-advanced-gas-turbine-materials-coatings.pdf
- Serovy, G. K. (1976). Compressor and Turbine Performance Prediction. In *Modern Prediction Methods for Turbomachine Performance* (pp. 21-39). Technical Editing and Reproduction Ltd.: Munich.
- Smith, S. (1965). A Simple Correlation of Turbine Efficiency. *Journal of the Royal Aeronautical Society*, 467–70.
- SoftInWay. (n.d.). AxSTREAM® Tutorial. Burlington, MA, USA.
- Stabe, R. G., Whitney, W. J., & Moffitt, T. P. (1984). *Performance of a high-work low aspect ration turbine tested with a realistic inlet radial temperature profile*. Cleveland: NASA Lewis Research Center.
- Stewart, W. L. (1962). A Study of Axial-Flow Turbine Efficiency Characteristics in Terms of Velocity Diagram Parameters. *ASME Super alloy*. (n.d.). Retrieved from Wikipedia: <https://en.wikipedia.org/wiki/Superalloy>
- Tyner, T., & Sullivan, J. (1990). Design and Performance of a Small, High Speed Axial Compressor. *AIAA paper*, 90-1911.
- Vinayak, P. (2000). Quasi-Static and Creep Behavior of Enhanced Sic/Sic Ceramic Matrix Composites. *Master of Science in Engineering Mechanics*.
- Viswanathan, R. (2003, July). *Gas Turbine Blade Superalloy Material Property Handbook*. Retrieved from EPRI:
<http://www.epri.com/abstracts/Pages/ProductAbstract.aspx?ProductId=00000000001008477>
- Walsh, P. P., & Fletcher, P. (2004). *Gas Turbine Performance*. Oxford: Blackwell Science Ltd.
- Wood, K. (2013, January 11). *Ceramic-matrix composites heat up*. Retrieved from Composite World:
<http://www.compositesworld.com/articles/ceramic-matrix-composites-heat-up>
- Younghans, J. L., Johnson, J. E., & Csonka, S. J. (1994). A methodology to assess design uncertainty in selecting affordable gas turbine technology. *ASME Journal*.
- Авиабаза. (2017, 19). *HK-62*. Retrieved from Авиабаза: <http://www.airbase.ru/alpha/rus/n/nk/62/>
- 喻双喜. (1998). 航空发动机质量、质心及转动惯量的一种计算方法及应用. *中国航空学会重量工程专业学术会*.